UNIVERSITÀ DEGLI STUDI DI UDINE
hic sunt futura

www.uniud.it

Doctor of Philosophy in:

"ENVIRONMENTAL AND ENERGY ENGINEERING SCIENCE"

XXXIII cycle

Title of the thesis:

"EXPERIMENTAL AND THEORETICAL STUDIES TO DEVELOP SUSTAINABLE METHODS IN HOMOGENEOUS GOLD(I) AND GOLD(III) CATALYSIS"

PhD Student:
Jacopo Segato

Supervisor
Prof. Daniele Zuccaccia

Co-supervisor
Prof. Alessandro Del Zotto

Year 2021

A Matteo, Marisa e Moreno,

e ai miei nonni.

INDEX

List of abbreviations

$(Bu)_2NH_2OTf$	dibutylammonium trifluoromethanesulfonate	**NBu_4OTf**	tetrabutylammonium triflate
(Me2)(Et)(Dod)NOTf	dimethylethyldodecyl ammonium triflate	**NHC***	1,3-dimethylimidazol-2-ylidene
AE	Atom Economy	**NHC^{CH2}**	1,3-bis(2,6-di-isopropyl-phenyl)dihydroimidazol-2-ylidene
BIAN	bis(imino)acenaphtene	**OAc^-**	acetate
BMIM-OTf	1-Butyl-3-methylimidazolium triflate	**OTf^-**	trifluoromethansoulphonate
C^N^C	2,6-bis(4-$^tBuC_6H_3$)$_2$ pyridine dianion	**OTs^-**	toluensulfonate
DAD^{IPr}	diaryl-diazadien	**$P(OR)_3$**	tris(2,4-di-tert-butyl)phosphite
DFT	Density Functional Theory	**PAr^F**	tris(3,5-bis(trifluoromethyl)phenyl)phosphine
DMSO	dimethylsulfoxide	**PCy_3**	tricyclohexylphosphine
E-factor	Environmental factor	**PPh_3**	triphenylphosphine
EMY	Effective Mass Yield	**ppy**	phenylpyridine
eq.	equivalents	**P. S.**	1,8-Bis(dimethylamino)naphthalene (proton sponge)
GVL	γ-valerolactone	**RDS**	Rate Determining Step
IPr	1,3-bis(2,6-di-isopropyl-phenyl)imidazol-2-ylidene	**TFA^-**	Trifluoroacetate
JPhos	2-(di-tert-butylphosphino)biphenyl	**THT**	tetrahydrothiophene
KIE	Kinetic Isotopic Effect	**TMS**	TetraMetylSilane
L	general ligand	**TOF**	TurnOver Frequency
MIBK	methylisobutylketone	**VOS**	Volatile Organic Solvent
MS	Meyer-Schuster	**X^-**	general anion
NAC	bis(tert-butylamino)methylidene	**ε_r**	dielectric constant

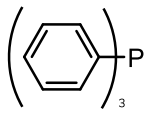

PPh_3

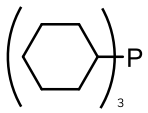

PCy_3

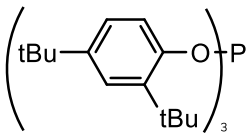

$P(OR)_3$

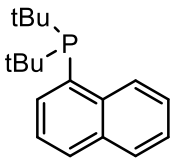

JPhos

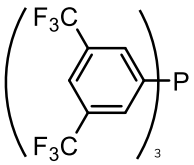

PAr^F

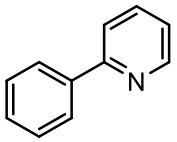

ppy

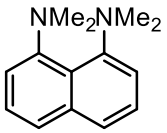

P. S.

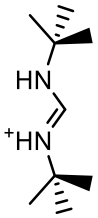

NAC

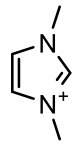

NHC*

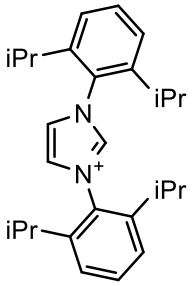

IPr

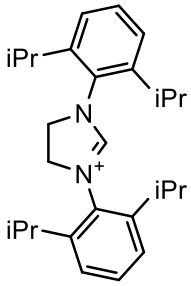

NHC^{CH2}

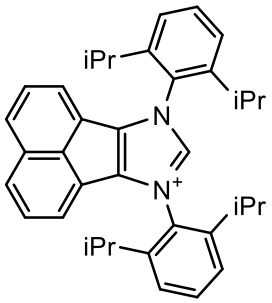

BIAN

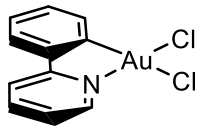

1

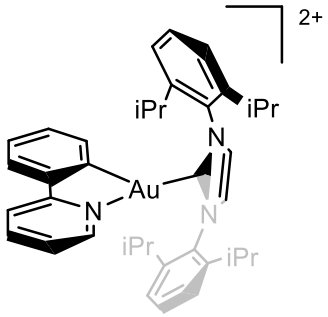

2

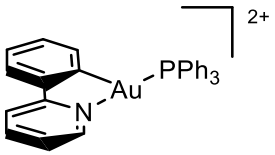

3

Abstract

Green processes have become an import topic for Chemistry in the last decade. Gold has been proved to play an important role to replace hazardous material thanks to its non-toxicity and biocompatibility. In this thesis, gold(I) complexes were employed in homogeneous catalysis for the transformations involving the activation of carbon-carbon π-systems. Important results in term of catalytic activity (TON and TOF) and green parameters (E-factor and EMY) were achieved in the hydration of alkynes in neat conditions using NBu_4OTf as the only additive. Volatile organic solvents were replaced with success by green solvents in the Meyer-Schuster rearrangement of 1-phenyl-2-propyn-1-ol and in the cyclization of propargylamide, reaching also better performances. These two studies were corroborated also by computational mechanistic investigations, unraveling the unexpected formation of a gold-oxetene intermediate for the Meyer-Schuster reaction.

Unlike gold(I), gold(III)-catalyzed reactions are still in their infancy and the vast majority of reports describe the use of inorganic salts. As done for Au(I), the development of knowledge on Au(III) catalysis and stoichiometric reactions is mandatory. Based on our studies about the hydration of alkynes catlyzed by L-Au-X complexes, a $[Au^{III}\text{-(ppy)-IPr}]^{2+}$ catalyst was engineered to promote this kind of reaction, while maintaining its stability. Structure, reactivity and catalytic properties have been addressed in this thesis by means of multinuclear solution NMR and computational (DFT) studies, with an important focus on the preequilibrium step.

NMR spectroscopy combined with DFT calculation has proved successful for the comprehension of reaction mechanisms and to better understand the chemical structure of the catalytic species, thus allowing the development of sustainable homogeneous gold catalysis.

Summary

In the last few years, the interest for the employment of gold in homogeneous catalysis has greatly increased. Numerous transformations involving the activation of carbon-carbon π-systems towards the nucleophilic attack of a large variety of nucleophiles have been studied from ~~a~~ mechanistic and kinetic point of view. In particular, a copiously information about the ligand and counterion effects in homogeneous gold(I) catalysis are present in the literature. The mechanistic understanding of all the single steps in the nucleophilic addition to a co-ordinate alkyne, when gold(I) complexes are used as the catalysts, provided the development of new [L-Au-X] catalysts for those reactions. On the other hand, mechanistic proposals for reactions involving Au(III) catalysts most often lack reliability and few computational and experimental evidences are given, so a "trial and error" approach in the development of new gold(III) catalysts is still present, and the outcome is often unpredictable and unsatisfactory. Finally, most of the gold-catalyzed transformations proceed under unsustainable conditions, and protocols describing the use of low catalyst loadings, room/lower temperature, solvent-/silver-free conditions and recyclable catalysts are limited. Therefore, the design of new, efficient, and sustainable processes represents a fundamental challenge in the future of gold-based catalysis.

In chapter 2.1.1, the results of the study of the hydration of alkynes are presented and discussed. A green and sustainable protocol for this reaction promoted by NHC gold catalysts, in solvent-, silver-, and acid-free conditions at room temperature has been further developed starting from a previous work done in the research group. The activity of the [L-Au-X] catalysts by changing the nature of the ligand L (from phosphine to NAC and NHC) has been studied. The in-situ generation of the pre-catalyst, using silver salts as chloride scavenger, did not appear as a good strategy, owing to the negative influence of silver on the reaction. A screening of ionic additives was also made and the best conditions were used for the hydration of deactivated diphenylacetylene.

In chapter 2.1.2, the results of the investigation on the Meyer-Schuster (MS) rearrangement, catalyzed by IPr-Au-X, that can deliver α,β-unsaturated carbonyl compounds in complete atom economy fashion, are presented. Despite all the experimental advances on the gold-catalyzed MS rearrangement, unfortunately a green development and a deep and complete understanding of the catalytic mechanism is still lacking. We propose here a commonly accepted mechanism for gold(I)-catalyzed alkyne reactions showing that it accounts for the formation of an unprecedented gold-

oxetene intermediate via 4-endo-dig cyclization. This mechanism fully rationalizes the experimental reactivity which is highly dependent on both anion and solvent effects.

The counterion and solvents effects are fully rationalized in the cyclization of the N-(prop-2-yn-yl)benzamide to 2-phenyl-5-vinylidene-2-oxazoline in a wide set of neoteric solvents promoted by IPr-Au-X catalysts. In most of these solvents the activity is comparable of even better than that observed in traditional VOS. The main results are depicted in chapter 2.1.3, where kinetic experiments and DFT calculations seem to indicate that both the characteristic of the solvent and counterion should be taken into account.

In chapter 2.2.1, we focused our attention on the hydration of alkynes in γ-valerolactone (GVL), under acid-free conditions promoted by [**2**-Cl]Cl and [**3**-Cl]OTf complexes. The solution structure, reactivity, and catalytic properties of [**2**-Cl]Cl and [**3**-Cl]OTf were established by means of multinuclear NMR and computational (DFT) studies. The overall catalytic and kinetic investigation, supported by computational results, confirmed that the preequilibrium step of the reaction mechanism is the RDS: water or counterion substitution by 3-hexyne in the first co-ordination sphere of Au(III) is the key step of the whole process.

The coordination ability of **2** towards different anionic and neutral X ligands is computationally (DFT) investigated in chapter 2.2.2 to shed light on unexpected experimental observations on its catalytic activity in the alkyne hydration reaction. The coordination ability trend towards Cl^-, OTf^-, BF_4^-, 3-hexyne, 2-butyne and H_2O has been studied for all the systems. Also the effect of the ancillary ligand substitution has shown to play and important rule during the catalysis. In conclusion, even if [**2**-alkyne]$^{2+}$ appears to be a more favourable complex, the stabilization of the [**2**-H_2O]$^{2+}$ complex was rationalized including within a microsolvation model.

This deep study on counterion, ligand and solvent effects in homogeneous gold(I) and gold(III) catalysis, based on both experimental and computational studies, allowed us to develop not only a sustainable methodology for homogeneous gold catalysis, but also opened new directions to better understand and rationalize the mechanism in homogeneous gold catalysis.

1. Introduction

1.1 General features

1.1.1 History

There is not a precise date about the first use of gold. It is a unique metal which differs from the others in various physical and chemical properties. In its purest form is a bright, reddish-yellow, soft and malleable metal. Bits of natural gold, used by Palaeolithic Man about 40,000 B.C., were found in Spain during archaeological digs.[1] High value such as power, beauty and cultural elite, have been associating to gold by humans and since it is widely spread all over the world, it has been perceived in the same way throughout different population everywhere.[2] Gold artefacts, dating back to 4th Millennium B.C., have been discovered in the Varna Necropolis (Bulgaria)[3] and at the Nahal Qana cave cemetery (Occupied Palestinian Territories).[4] Gold played a key role in ancient Egypt culture in the religious cult as it was considered the "flesh of the gods".[5] Artisans made amulets, death masks (**Figure 1.1a**), diadems, ornamental weapons, vessels, and funeral art out of gold to adorn the tombs of pharaohs.[6] The Minoan civilization (or just Minoan) became very expert in modelling and transformation of the metal already 1800 years ago.[7] One the most splendid example date from this period is the Master of the Animals pendant (**Figure 1.1b**). The earliest worked gold recovered from the Americas is a gold necklace (**Figure 1.1c**), dated 2155 to 1936 B.C. in Jiskairumoko archaeological site (Peru).[8]

a. b. c.

Figure 1.1: a. *Mask of Tutankhamun (1323 B.C. Valley of the Kings - Egypt).*[9] ***b.*** *Minoan 'Master of the Animals' Pendant (18-17th century BC). Provenance: Aegina (British Museum, London).*[10] ***c.*** *Gold necklace recovered from Jiskairumoko (2155 to 1936 B.C – Peru).*[8]

Nowadays, gold in its metallic forms finds application in different fields like: jewellery or gold alloys, where the carat (kt) is the unit of measure for the purity degree: 24 kt = 999.9 grams of gold in 1000 grams of alloy; monetary use, before as exchange currency, now as gold reserve held by the central bank; in medicine due to its chemical inertial, not-toxicity and biocompatibility for restorative

dentistry (crowns and bridges); in the electronic devices, especially for the coating of electrical connectors; astronautic, for the spacesuit visors because it shields the solar light; cuisine as decorative ingredient.

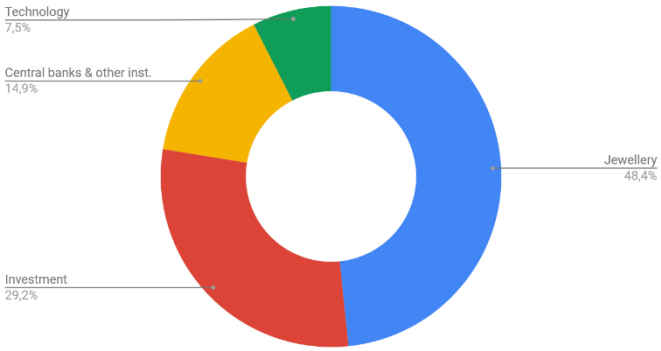

Initially, the reactivity of gold was linked only to recovery and purification process. Using strong acid condition, such as the aqua regia which form a solution of tetrachloroauric acid ($HAuCl_4$), or under alkaline in presence of sodium or potassium cyanide ($Au(CN)_2^-$ and $Au(CN)_4^-$), leading the wrong idea of the non-reactivity of gold in chemistry. Only in the 20th-century, gold complexes were introduced for the treatment of rheumatoid arthritis, culminating in the introduction of Auranofin in 1985. New medical uses of gold complexes are nowadays focused on anticancer and antimicrobial properties.[11]

1.1.2 Physical and chemical properties

Gold, a group 11 element, is the heaviest transition metal[12] with atomic number 79 and with an electron configuration [Xe] $4f^{14}\ 5d^{10}\ 6s^1$ in its ground state. The lowest electrochemical potential and the highest electronegativity, compared to the other metals, confirm the noble character of gold.

The different behaviours between gold and the other two elements of the group 11, silver and copper, are due to the relativistic effects which reach a maximum with this metal. The large number of protons in the nuclei cause the velocity of electrons approaching that of light, and they must be treated according to Einstein's theories of relativity, especially for those in the *s* orbitals. The concept of the simultaneous *s*-orbital contraction and *d*-orbital expansion, can leads to a good explanation of the valence electrons behaviours.[13]

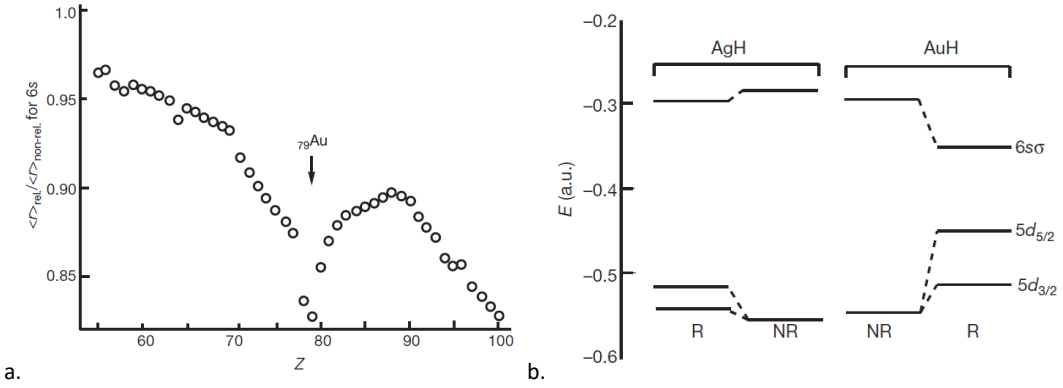

Figure 1.2: a. *Calculated relativistic contraction of the 6s orbital.* ***b.*** *Relativistic and nonrelativistic Hartree-Fock one-center expansion calculations of the valence orbital energies for AgH and AuH molecules. The nonrelativistic ones are very similar, while the relativistic ones are not.*

Accepting those assumptions, we can explain:

a. The yellowish colour attributed to the transition from the 5*d* band to the 6*s* (Fermi level) at 517 nm (2.4 eV) with strong absorption in the blue-violet region.
b. The reduced atomic and ionic radii; especially it is noticeable that Au^+ is much smaller than the analogous silver cation in the presence of the same coordination sphere.
c. The access to higher oxidation state +3, thanks to the proximity of the 5*d* and 6*s* valence orbitals and their hybridization.
d. The aurophilicity, that is the behaviour of a gold atom in a complex to approach others gold metal centres. Depending on the nature of the ligands and counter-ions, this interaction has an energy that is comparable to those of hydrogen bonding.

Gold presents different oxidation number: -1, 0, +1, +2, +3 and +5. There are few examples of -1, +2 and +5 oxidation state (CsAu, $Au(SbF_6)_2$, Au_2F_{10} are just some examples of those rare states) but the chemistry is mainly dominated by Au(I) and Au(III).

Gold (I)

Gold(I) is quite stable and it has an electronic configuration $5d^{10}$ $6s^0$ with two sites of coordination which lead to the linear geometry of the type [L-Au-X].[14] The atomic orbitals (AOs) of the metal

involved in the bond's formation are the $5d_{z2}$, the 6*s* and the $6p_z$. The other AOs have non-bonding character, but the d_{xz} and d_{yz} can interact with the π-acid ligands. The relativistic effects decrease the 6*s* orbital energy and increase that of the $5d_{z2}$ orbital, approaching them energetically and facilitating their combination, favouring the molecular orbital typical of the linear complexes.

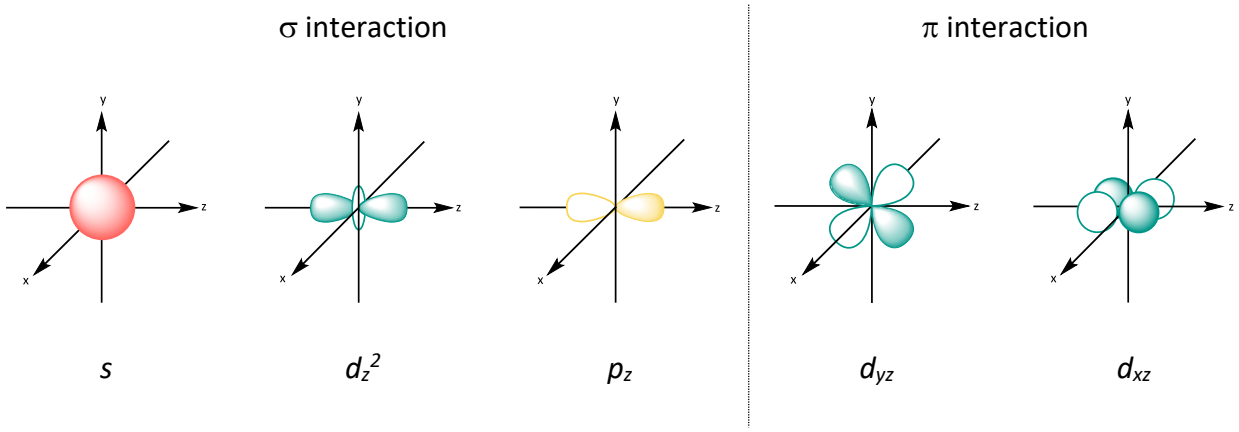

***Figure 1.3**: atomic orbitals involved in Au(I) bonds.*

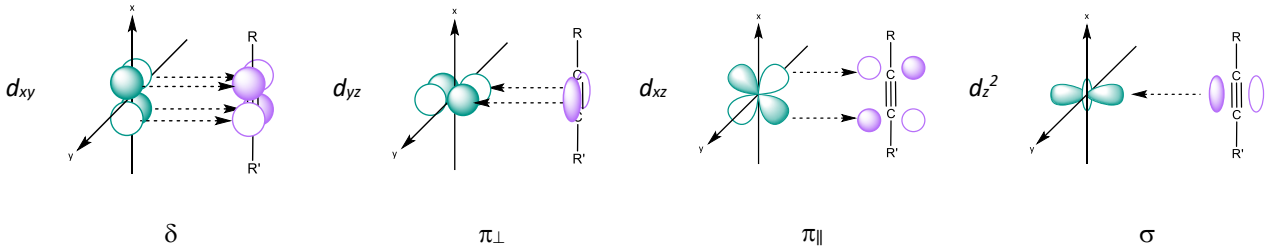

***Figure 1.4:** Qualitative orbital interaction between the gold metal center and the alkyne.*

According to the *hard and soft acid and base theory* of Pearson,[15] Au(I) favours ligands such as carbenes (C), phosphines (P), thiolates and thioethers (S) and selenates (Se), because of its soft-metal nature.[16] In this electronic configuration, gold can coordinate also ligand containing a double or triple bond (**Figure 1.4**). These interactions are dominate by the symmetric bond L→Au σ-donation and the Au→L $\pi_\parallel^*$-backdonation. The orthogonal L→Au $\pi_\perp$-donation can also occur, and this minor interaction is stronger for the alkynes complexes in which the ligand serves as a four-electron donor. A weak interaction is represented by Au→L back-donation having δ symmetry between the occupied d_{xy} orbitals and the empty $\pi_\perp^*$ of the alkyne.

Gold(I) complexes finds different application in medicine. The gold drug Auranofin (**Figure 1.5a**) is used to treat the rheumatoid arthritis, reducing some symptoms, such as swelling and pain in the joints.[17] In monkey trials, the drug has shown to reduce the viral reservoir of HIV that lies latent in the body's T-cells.[18] Latest studies in cell culture have shown that Auranofin may inhibit replication of SARS-CoV-2.[19] Another gold-base drugs used for the immunosuppressive anti-rheumatic effects is the sodium aurothiomalate (**Figure 1.5b**).

Thanks to the proximity between the 5*d* and 6*s* level, the gold complexes prove to have good luminescent abilities,[20,21] and in combination with other metal can be used also as theranostic agents (combine diagnostic and therapeutic capabilities into a single agent, **Figure 1.5d**).[22]

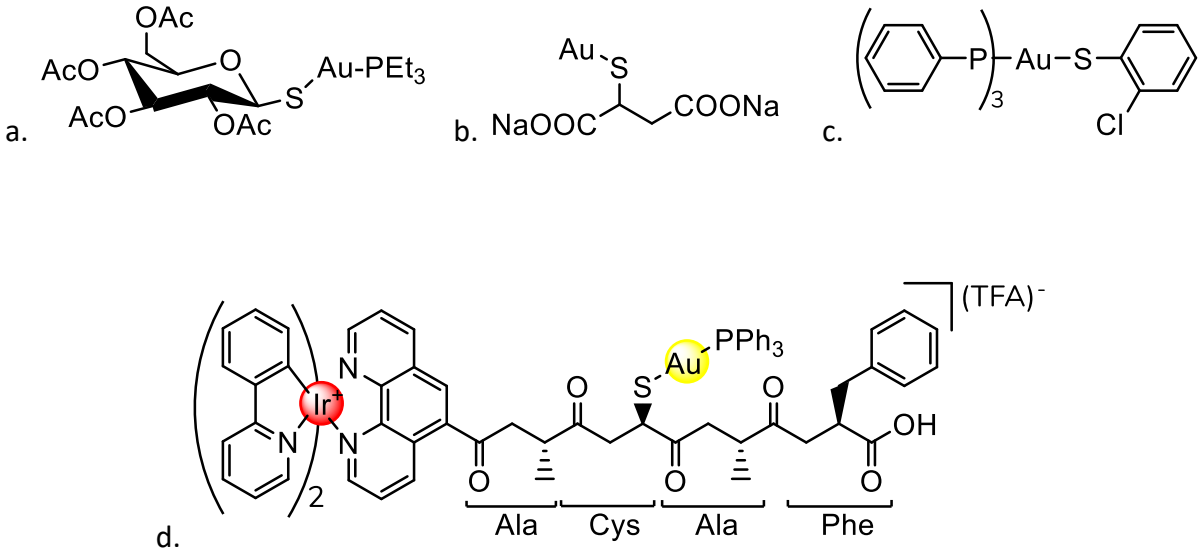

Figure 1.5: a. *Auranofin;* ***b.*** *sodium aurothiomalate;* ***c.*** *[triphenylphosphine] gold(I)-2-chlorobenzenethiolate;* ***d.*** *luminescent bimetallic peptide as potential theranostic agents.*

Gold (III)

Gold(III) complexes have a $5d^8$ electronic configuration with a square planar geometry and a coordination number of 4, the same as Pt(II) whose reactivity is almost similar. The AOs involved in the σ interactions are those which belong to the x and y axis: 6*s* and $5d_{z^2}$, that combine themselves to form one MO, $5d_{x^2-y^2}$, $6p_x$ and $6p_y$. The electrons can occupy the non-bonding orbitals d_{xy}, d_{yz}, d_{xz} and the combined MO sd_{z^2}. The d_{xy} orbitals can give interaction π with the ligands.

Unlike gold(I), Au(III) has a more acidic behavior, thus being able to form stable complexes also with C, N and O-donor ligands. Au(III) is easily reduced by phosphine and sulphates due to its high redox potential.

Owing to the fact that gold(III) is isoelectronic and isostructural to platinum(II), Au(III) compounds look very attractive for cancer treatment. Bindoli et al.[23] in their study on the thioredoxin reductase, explained the mechanism of action of anticancer gold compounds as an effective druggable target, due to the presence of selenol and thiol groups of the protein.

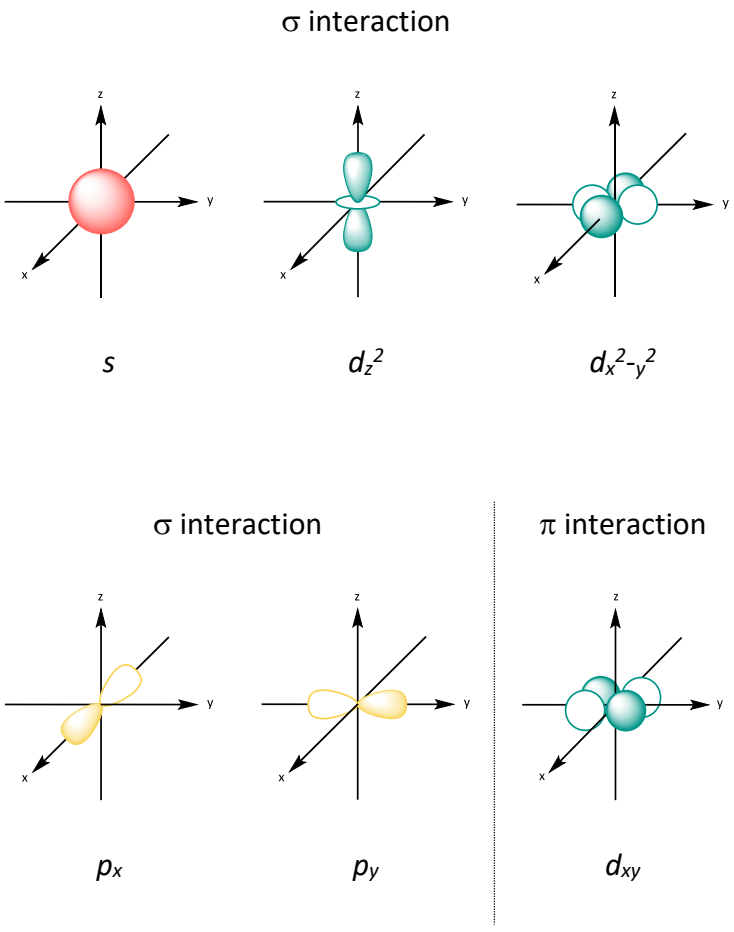

Figure 1.6: *atomic orbitals involved in Au(III) bonds*

Luminescence gold(III) compounds are very rare, probably due to the low *d-d* energy and the electrophilicity of the metal. Zhu et al. proved that the introduction of strong σ-donating alkynyl ligands (**Figure 1.7**) enhances the luminescence properties of gold(III) compounds by increasing the

splitting of the *d–d* states.[24] Their compounds displayed an intense luminescence at 468-611 nm in solution at room temperature, on a excitation at $\lambda \geq 360$ nm.

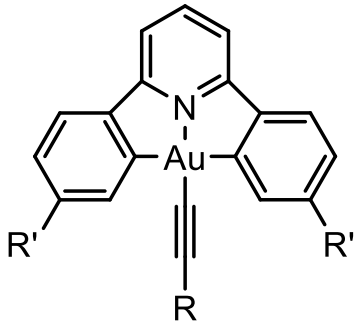

R' = H; R = C_6H_5

C_6H_4-Cl-p

C_6H_4-OCH_3-p

C_6H_6-NH_2-p

R' = tBu; R = C_6H_5

Figure 1.7: *gold(III) complex with σ-donating alkynyl ligands.*

Luminescent gold(III) complexes can have use as light-emitting device[25] or in reaction such as light-induced oxidative C-H bond functionalization.[26]

In the next chapter the use of gold in catalysis is examined and discussed.

1.2 Catalysis

1.2.1 Heterogeneous catalysis

Although gold had received great interest already in ancient times thanks to the alchemists, nowadays there is renewed interest in it, confirmed by the exponential increase in the number of publications.[27] As shown in **Figure 1.8**, the use of gold in catalysis in its various forms has aroused great attention.

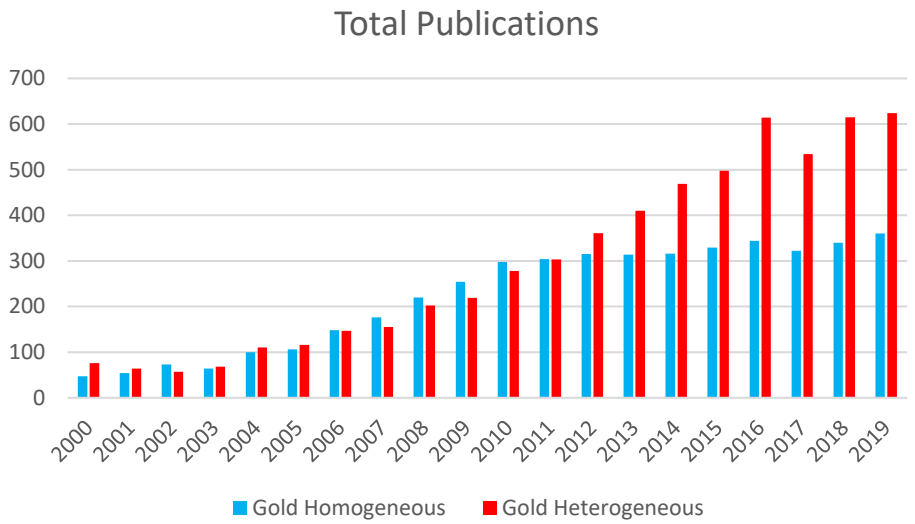

Figure 1.8: *Publication concerning homogeneous and heterogeneous gold catalysis on Web of Science.*

The first uses of gold as catalysts date back to the 1970s, when Bond and Sermon hydrogenated and isomerized olefins using gold catalysts supported on silica and alumina.[28,29]

Nowadays, gold has a huge industrial importance,[30] especially in heterogeneous catalysis. Two of the most used industrial applications are the synthesis of vinyl chloride from the hydrochlorination of ethylene and the oxidation of carbon monoxide at low temperature (**Scheme 1.1**).

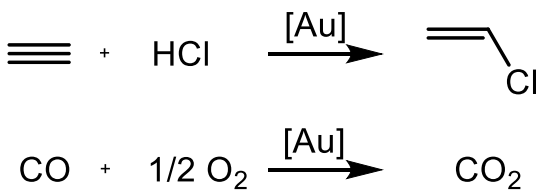

Scheme 1.1: *heterogeneous gold catalysis in industrial applications.*

Aqueous solutions of tetrachloroauric acid can be easily reduced by various agents under different conditions and parameters.[31] One of the most used agent is the citrate,[32] which produces monodisperse colloidal gold, also called gold nanospheres. The diameters could vary from 2 nm to 100 nm, with an absorption peak that ranged from 510 to 550 nm, which confers the typical ruby colour of gold-nanoparticles (Au-NPs). Various other forms of Au-NPs can be obtained such as nanorods, nanoshells and nanocages.

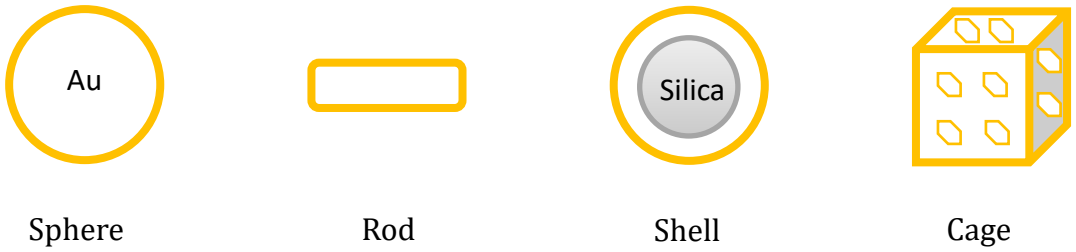

Figure 1.9: *Schematic representation of various types Au nanomaterials.*

In a recent review, Carabineiro[33] described the various methods of synthesis of heterogeneous catalysts where Au-NPs are involved and their application in oxidation reactions of alcohols (aliphatic, aromatic, cycloalcohols, diols, polyalcohols, aminoalcohols) and alkanes.

Gold nanoparticles can be combined with other metals to increase its catalytic performance. In this context Nieuwenhuys and coworkers[34] employed Au-NPs with MgO and MnO_x supported on alumina for the CO and hydrogen oxidation.

1.2.2 Homogeneous catalysis

Gold (I)

As described above, gold(I) complexes can activate the C-C multiple bonds (alkenes, alkynes, allenes, etc.), acting as a Lewis acid. The catalytic cycle is almost the same for different substrate-nucleophile couple, and it can be represented in a similar pathway, proceeding through an inner-sphere or outer-sphere mechanism (**Scheme 1.2**).[35]

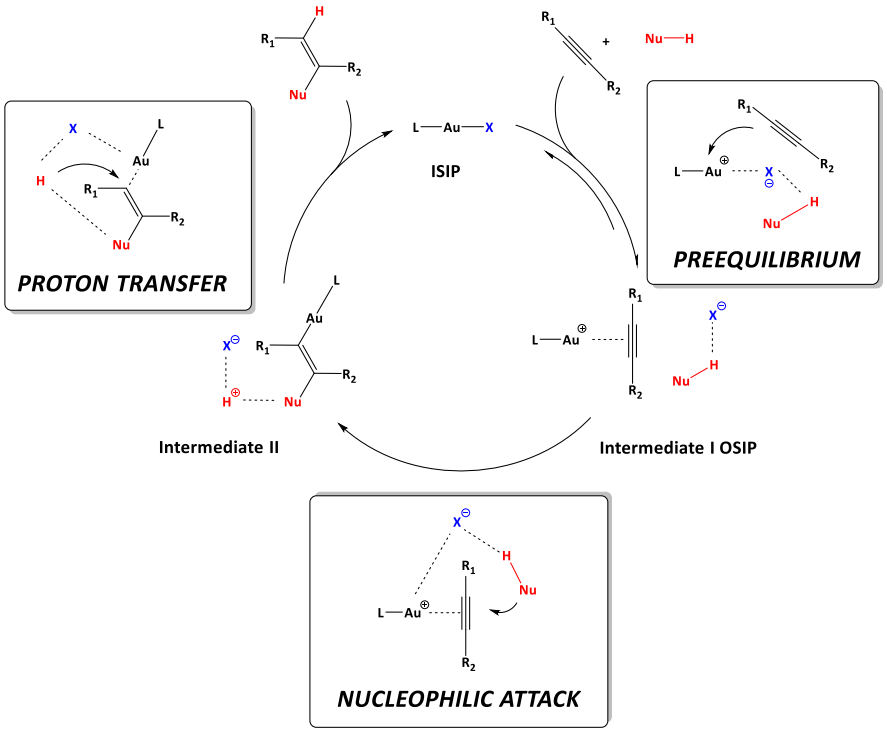

Scheme 1.2: *General mechanism for homogeneous Au(I) catalysis.*

L-Au-X represents a general gold(I) catalyst, where L is a neutral ligand (phosphine, carbene, etc.) and X^- is an anion (triflate, tosylate, trifluoroacetate, tetrafluoroborate, etc.). The cycle is composed by three main steps:

1- The pre-equilibrium: the substrate coordinates to the metal replacing X and generating a η^2 complex (intermediate I).
2- The nucleophilic attack: gold complex activates the substrate acting like a Lewis acid.
3- The proton transfer: the product is released when the proto-deauration does occur, with regeneration of the catalyst.

In 1998, Teles et al.[36] investigated the activity of gold(I) complexes bearing different phosphorous-containing ligands in the methoxylation of 1-propyne.

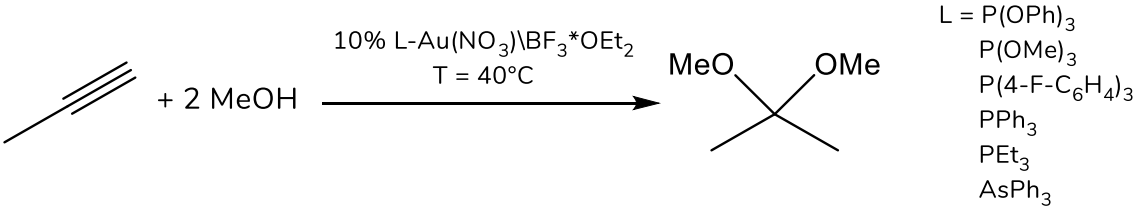

Scheme 1.3: *methoxylation of 1-propyne*

The results showed that the activity was inversely correlated to the Lewis basicity of the ligand, in fact, higher value of turnover frequency (TOF) was obtained with the most electron-poor ligands. Hammond and coworkers[37] in 2012 tested different phosphino-gold(I) complexes in different reactions, and proved that there is not a ligand which works better than others, but a better understanding of the ligand behavior allows to design the best ligand for each specific reaction.

In 2003 the first use of a nitrogen heterocyclic carbene (NHC) as ligand for gold(I) for the hydration reaction was reported by Herrmann and coworkers.[38] As the chloride species of this catalyst was inactive, the acetate ion was successfully employed. The presence of a Lewis acid was necessary to increase the activity of this reaction. Nolan and co-workers[39] performed the hydration of alkynes at 120°C in methanol/water or dioxane/water mixtures. In this reaction different NHCs were employed. Several silver salts were also tested, and the best result was achieved using silver hexafluoroantimonate.

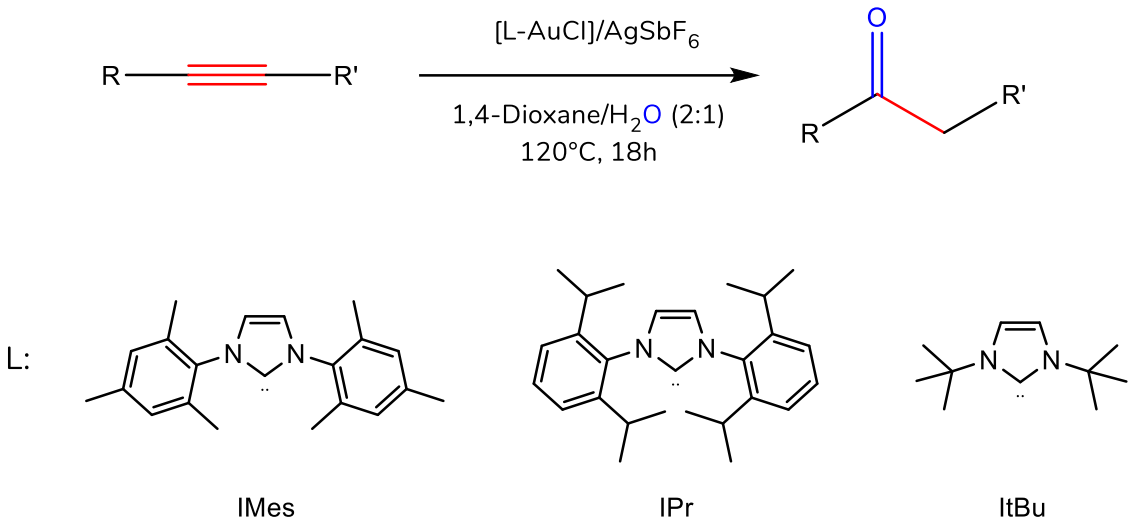

Scheme 1.4: *hydration of alkyne with different ligands.*

Catalyst loading between 0.1 and 0.001%, with respect to the substrate, were reached when the IPr ligand was used. This is indeed an appreciable result since for gold homogeneous catalysis the typical loading is from 5 to 1%. However, silver can act as co-catalyst, proving active participation in the reaction.[40,41] Shi and co-workers studied the "silver effect" on gold(I) catalysis.[42]

Gold complexes are also active for the addition of other heteroatoms to unsaturated substrates.[43] Tanaka and co-workers[44] developed the hydroamination reaction of alkynes (**Scheme 1.5**) using the catalyst proposed by Teles, in acidic conditions to promote the reaction.

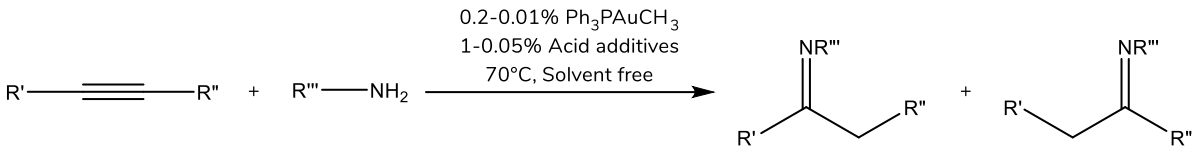

Scheme 1.5: *intramolecular hydroamination of alkyne.*

Nolan, Brouwer and He[45] have employed different silver salts, showing how anions can give different activity in the hydroamination reaction.

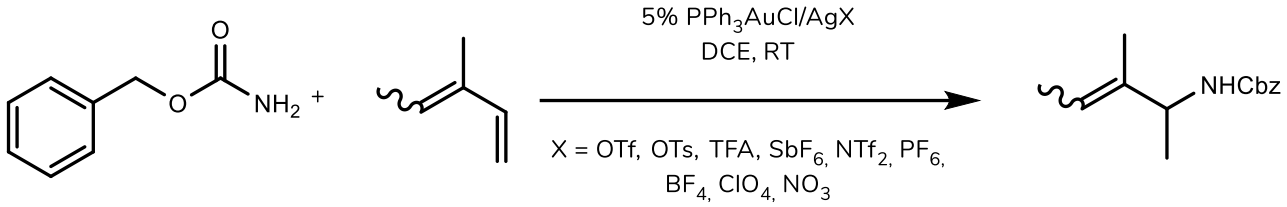

Scheme 1.6: *hydroamination of 1,3-dienes.*

Using lower coordinating anions, such as OTf^- or ClO_4^-, a full conversion was achieved, while no formation of any products was observed with the other anions (Cl^-, OTs^-, NO_3^- and CF_3COO^-) due to their high affinity to gold. Measurement of the coordination abilities of these anions[46,47] confirmed the order found by Brouwer and He.

The anion effect in the alkoxylation of alkynes by IPr-Au(I) catalyst was studied in 2014 by Zuccaccia and co-workers.[48] The coordination ability and the basicity of the anion have a notable impact on the catalytic performance of the gold complex, and the commonly used non-coordinative anions (such as SbF_6^- and BF_4^-) may not be the right choice in some cases.

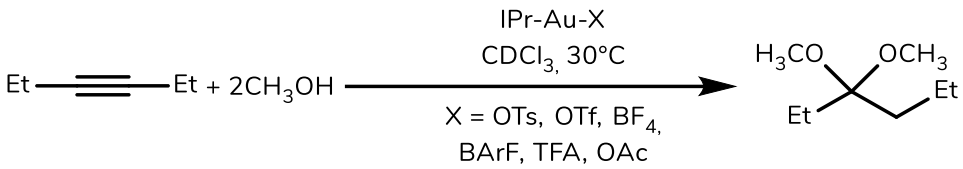

Scheme 1.7: *reaction of alkoxylation of 3-hexyne.*

The tosylate anion (OTs^-) gives the right balance between basicity and coordination ability in this reaction. The preequilibrium (**Scheme 1.2**) is shifted towards the OSIP, the nucleophilic attack is promoted by the OTs^- basicity and the deactivation to gold-methoxide is prevented. The study was then extended to other ligands and the cycloisomerization of N-(prop-2-ynyl)benzamide was also investigated.[49,50] Weakly coordinating anions generate a more electrophilic gold centre with consequent stronger metal-π system interaction. On the other hand, more coordinating anions can

positively affect late-stage catalytic event such as the protodeauration and formation of ISIP. Furthermore, basic anions can interact through hydrogen bond with the reaction partner, determining optimal structural geometries, thus controlling chemo-, regio-, or stereo-selectivity. The important role played by the anion in homogeneous gold catalysis is summarized in a review by Bandini e Jia.[51]

A screening of the reactivity of various gold catalysts with different ligands was conducted by Hashmi and co-workers.[52] The counterion strongly affects the catalytic activity more than the ligand does. It was pointed out that no perfect catalyst exists for a specific reaction, and the counterion influence is still underestimated in homogeneous gold catalysis.

Gold (III)

The catalytic activity of gold(III) complexes is not as well studied as that of gold(I) species, which has many reported examples.[53–63] Typically the use of inorganic gold(III) salts, such as $AuCl_3$ or $HAuCl_4$ is reported, which promote different type of reactions: hydroamination,[64] intramolecular hydroarylation,[65,66] oxidation,[67] rearrangements,[68] and C-C bond cyclizations.[69,70] The number of papers where an organometallic Au(III) complex is used as catalyst, are however increasing;[71–85] Limbach and co-workers,[71] after having studied the electrochemical stability of gold(I) and gold(III) species bearing a N-heterocycle carbene, applied these complexes as catalysts in the cycloisomerization of ω-alkynylfuran to give 4-isobenzofuranol (**Scheme 1.8**). The Au(III) complex showed a good activity (TON was 112 after 1 h, with a catalyst loading of 0.25 mol %).

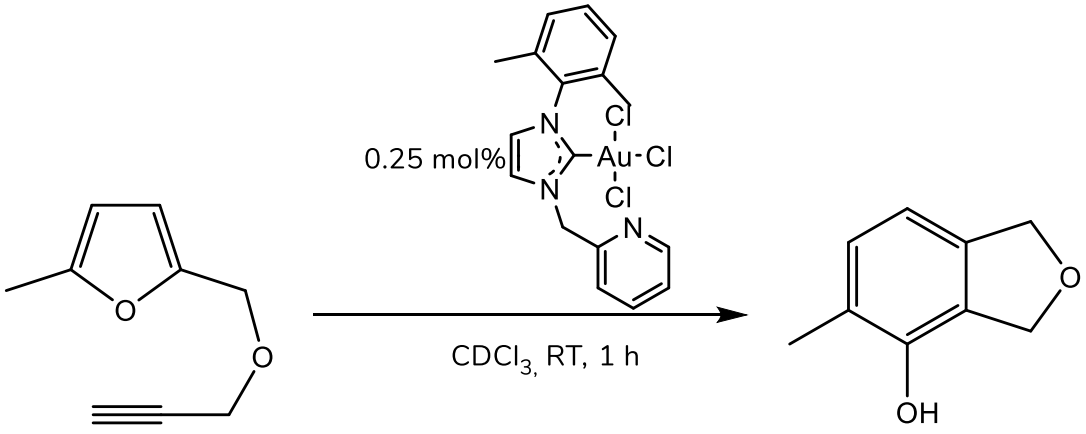

Scheme 1.8: *isomerization of ω-alkynylfuran to 4-isobenzofuranol.*

Lee and co-workers[78] employed gold(III)-oxo complexes for the intramolecular hydroamination reaction reaching a 70 % yield after 16 h with a catalyst loading of 5 mol%.

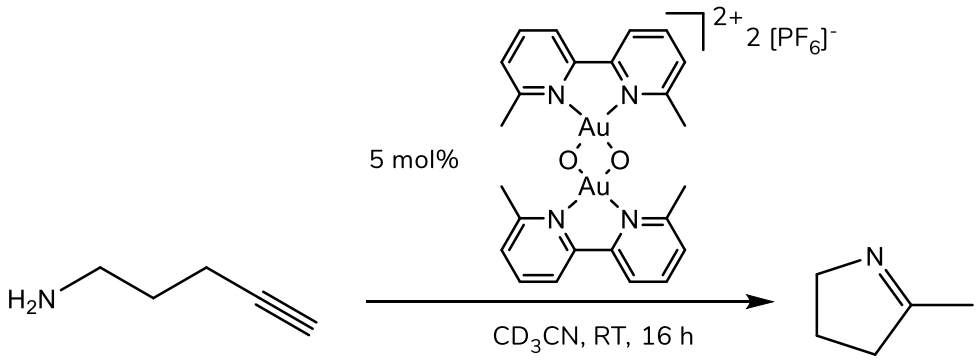

Scheme 1.9: *intra-hydroamination.*

Likewise gold(I), an important application of gold(III) is the C-C coupling reaction. Different examples are present in the literature. For example, Gimeno and co-workers[80] applied a gold(III) complex for the synthesis of indolizine. The reaction proceeds without the use of solvent at 60 °C, with a catalyst loading of 0.5 mol% and a complete conversion was reached within 5 h. This synthesis represents an example of tricomponent reaction catalysed by gold(III).

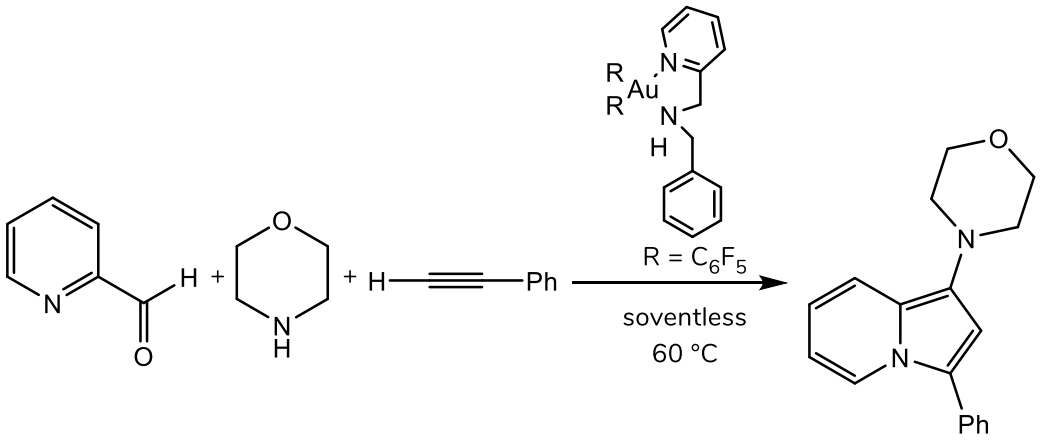

Scheme 1.10: tricomponent for C-C coupling reaction.

However, the mechanistic proposal lacks reliability and the experimental and computational evidence are frequently limited.[86–93] Mechanistic studies, stability of the Au(III) species, identification of the effective catalytic species and intermediates and assessment of the importance

and role of the ancillary ligands are issues that must be explored in the coming years. Erdélyi, Fiksdahl and Pápai[94] in a very recent paper established the mechanism of the alkoxycyclization of a 1,6-enyne by combining computational (DFT) investigation, NMR spectroscopy and single-crystal X-ray crystallography, focusing on the role of the ligand, counterion, and solvent.

There are different examples of hydration of alkynes in the literature.[95–99] Schwerdtfeger and co-workers[100] in 2010 proposed for the first time the complete mechanism of the nucleophilic attack of water to propyne promoted by $AuCl_3$. This expands and complements the work by Teles et al.[36] who proposed a possible mechanism on the basis of the experimental data.

1.2.3 Catalysis and Green Chemistry

The safeguard of the environment led the USA and Europe in the 90s to setup several laws to limit and regulate the industrial emissions. The design of new chemical processes, not only focusing on hazardous products but also designed to reduce the waste, pushed the scientific community to give rise to 12 principles called of Green Chemistry.[101–104]

The waste prevention is the main goal of these principles. It is easier to setup an experiment with no production of waste rather than treat or clean it. A measure of waste production is the E-factor, introduced by Sheldon,[102] which relates the weight of waste to the weight of the desired product.

Table 1.1: *The 12 principles of Green Chemistry.*

1- Prevent Waste	7- Use of Renewable Feedstocks
2- Atom Economy	8- Reduce Derivatives
3- Less Hazardous Synthesis	9- Catalytic rather Stoichiometric Reagents
4- Design Benign Chemical	10- Design for degradation
5- Benign Solvent & Auxiliaries	11- Real-Time Analysis for pollution Prevention
6- Design for Energy Efficiency	12- Inherently Safer Chemistry

Engineering the synthesis means to use innocuous substances or with low toxicity whenever possible, such as using solventless systems, water, supercritical fluids, ionic liquids,[105] or solvents arising from natural sources (agricultural crops, i.e., ethyl lactate).[106] In this contest, the Effective Mass Yield (EMY) parameter, introduced by Hudlicky et al.,[107] helps to evaluate how safe and environmental friendly is a process. Catalyzed reactions are to prefer to stoichiometric ones because of the energy efficiency and a good design of the synthetic method must provide in the

product as much starting material as possible. Trost[101] introduced the atom economy (AE) as parameter to evaluate and maximize the incorporation of all materials used in a given process into the final product.

$$\textbf{E-factor} = \frac{\text{waste mass}}{\text{desired product mass}} \qquad \textbf{EMY} = \frac{\text{desired product mass}}{\text{non-benign reagents mass}} \times 100 \qquad \textbf{AE} = \frac{\text{desired product mass}}{\text{all products mass}}$$

In a green process, the use of a catalyst is highly desirable and, as we will see later, often it helps to observe several of the principles. Thus, prevention of waste, atom economy, less hazardous synthesis, reduced derivates, and energy efficiency process can be easily designed. Turnover number (TON) and turnover frequency (TOF) are useful tools to understand and compare the potential of a catalytic system.

$$\textbf{TON} = \frac{\text{moles of products}}{\text{moles of catalyst}} \qquad \textbf{TOF} = \frac{\text{TON}}{\text{time}}$$

In this green context, gold can play an important role to replace all those reactions which use hazardous material thanks to its non-toxicity and biocompatibility. For its electronic similarities to mercury, it was possible to replace the Hg-salts with gold in industrial processes.[108] Nowadays, protocols describing room or low temperature reactions, acid and silver-free conditions, with the use of green solvents or even solvent-free conditions are limited.[109–118] In the gold-based catalysis the design of efficient, new sustainable process represents an important challenge.

An environmentally friendly method to form a carbon−oxygen bond is the hydration of alkynes,[119,120] because this reaction satisfies both carbon efficiency and atom economy rules. Toxic mercury salts were initially used as catalysts for the alkyne hydration.[121]

Afterward the introduction of gold(I) catalyst by Teles et al.,[36] Tanaka and co-workers extended this work to several internal and terminal alkynes using also different acids (**Table 1.2**).[122] Once optimized the conditions, they obtained 1000 and 1000 h^{-1} TON and TOF, respectively, using PPh_3-Au^+ as the catalyst.[123] The E-factor and EMY values were 22 and 5, respectively. Nolan was able to reduce the catalyst loading up to 10 ppm optimizing the reaction conditions using an NHC ligand

instead of phosphine.[39] By a green point of view, the process is less sustainable because of the temperature of 120 °C and the use of 1,4-dioxane in the presence of silver salts. The E-factor and EMY values were 8 and 15. Hu and Wu[124] performed the hydration at room temperature, under silver and acid free condition (E-factor: 17; EMY: 10). Under neat condition and using $KB(C_6F_5)_4$ as ionic additive, they were able to reach an appreciable EMY value of 67. Unfortunately, the TON and TOF values were both very low (**Table 1.2**).

***Table 1.2**: principal parameter in hydration of alkynes.*

	Tanaka[122]	Nolan[39]	Wu[124]		Li[125]		Zuccaccia[126,127]	
Solvent	MeOH	Dioxane	MeOH	***neat***	MeOH	MeOH[a]	***neat***	**GVL**
TON	**1000**	**84000**	20	11	200	1200	**5000**	990
TOF (h^{-1})	**1000**	**4500**	1	0.5	10	10	500	283
T (°C)	70	120	**RT**	**RT**	120	120	**RT**	120
Ag^+ additive	**NO**	YES	**NO**	**NO**	**NO**	**NO**	**NO**	**NO**
H^+ additive	YES	**NO**	**NO**	**NO**	**NO**	**NO**	**NO**	**NO**
Catalyst reuse	NO	NO	NO	NO	**YES**	**YES**	**YES**	NO
E-factor	22	8	17	5	**2**	**2**	**0.03**	2.6
EMY	5	15	10	67	34	35	**97**	28

[a]After 6 recycles

AuNHC@porous organic polymers were used by Li in order to recycle the catalyst.[125] The system resulted poorly sustainable due to the high temperature and large amount of solvent used to separate the product, but it showed moderate activity (TON was in the range 10^2-10^3) and very low value of E-factor.

In 2016 Zuccaccia and co-workers[126] developed a sustainable and highly efficient methodology for the hydration of alkynes. They worked under silver- and acid-free conditions without solvent, at room/mild temperature with suitable ionic additives. The study further highlighted the pivotal role of the anion in gold(I) catalysis. Once optimized the conditions, with a IPr-Au-X catalyst, they were able to reach high values of TON and TOF (10^4 and 10^3 h^{-1}, respectively) reducing the catalyst loading

up to 0.01 mol% at room or mild temperature. Also the green parameters E-factor and EMY (0.03-0.06 and 94-97) were the best reported for those type of reactions using a gold-based catalyst.

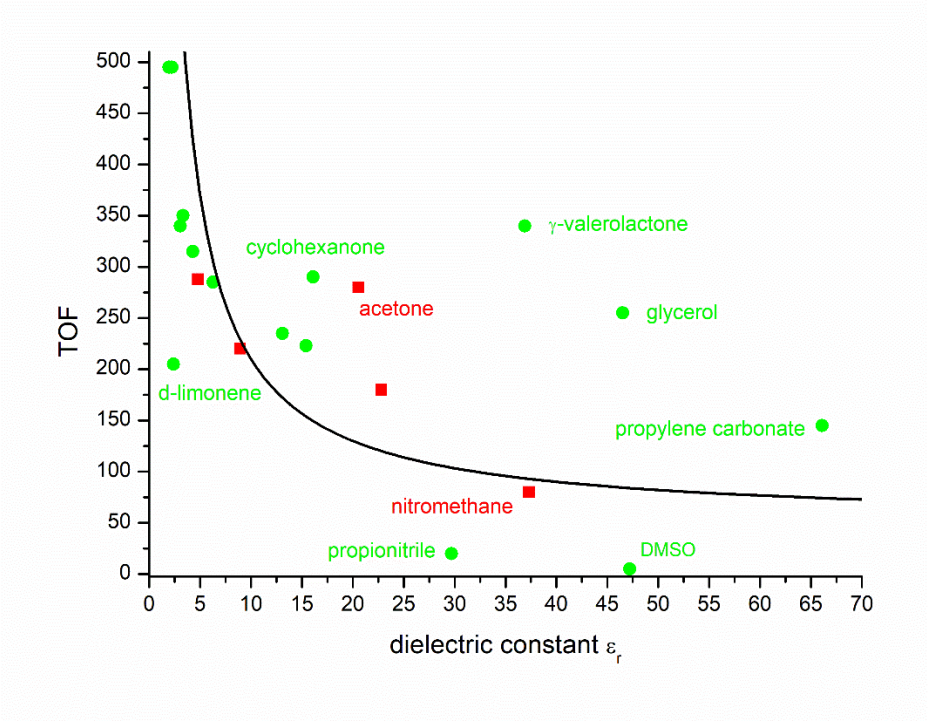

Figure 1.10: *TOF vs. dielectric constant for green solvents (green; in the order from left to right: perfluoro-decalin, p-cymene, D-limonene, propionic acid, ethyl palmitate, anisole, isopropyl acetate, MIBK, ethyl lactate, cyclohexanone, propionitrile, γ-valerolactone, DMSO, glycerol, and propylene carbonate) and VOSs (red; in the order from left to right: chloroform, dichloromethane, acetone, 3-nitrotoluene, and nitromethane).*

According to the 12 principles of green chemistry (**Table 1.1**), the use of solvents with sustainable functionality (green solvents) seems to be a step towards new and sustainable gold catalyzed reactions. Replacing the volatile organic solvents (VOS) with green solvents is a key topic in organic chemistry.[128–130] In this direction, Zuccaccia and co-workers[127] developed the hydration and methoxylation of alkynes in different green solvents obtaining both good performance (TON: 990; TOF: 283 h^{-1}) and optimal green parameters (**Table 1.2**. E-factor: 2.6; EMY: 28) in the case of γ-valeroactone (GVL). The role of the solvent has been underlined by the fact that the activity (in terms of TOF) is inversely correlated to the polarity of the solvent (**Figure 1.10**). The equilibrium between free ion/ion pair is shifted towards the former when the dielectric constant increases.

2. Results and discussion

2.1 Green solvents

2.1.1 Hydration of alkynes

The hydration of alkynes is an important environmentally friendly reaction in organic chemistry. We used gold(I) catalyst for a complete screening on alkynes hydration reaction in neat condition, without adding acids or silver salts and operating at low or mild temperature. Once optimized, the protocol was applied to 3-hexyne and diphenylacetylene. The compounds L-Au-X [L= IPr, BIAN, NHC^{CH2}, NAC, JPhos, PCy_3, PAr^F, PPh_3, $P(OR)_3$ (R = tris(2,4-di-*tert*-butylphenyl)phosphite); X^- = Cl^-, OTf^-, OTs^-] were synthesized according to literature procedures (see Experimental Section) or generated in situ during the catalytic tests (**Table 1.3**).

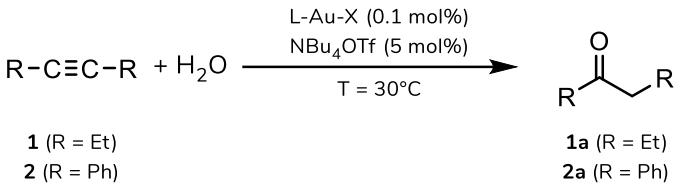

Figure 1.11: *Hydration of 3-hexyne and diphenylacetylene*

Previous studies on the nucleophilic addition to a carbon–carbon unsaturated bond promoted by gold(I) complexes allowed us to understand the ligand effects in the different steps of the catalytic cycle.[37] The stereo-electronic structure of the ligand modulates the acidic character of the metal fragment in the catalytic cycle and affects the stability of the postulated intermediates.[53,131]

The choice of different ligands L in L-Au-X complexes were done with the purpose of varying their stereo-electronic character. They were used to promote the catalysis in the hydration of 3-hexyne to form 3-hexanone and of diphenylacetylene to form 1,2-diphenylethanone (**Table 1.3** and **Table 1.4**) in solvent- and acid-free conditions in order to complete and extend our previous investigation.[126] The role played by silver salts (**Table 1.3**) and ionic additives other than NBu_4OTf (Experimental Section, **Table 3.2**) on the catalytic performances has been evaluated.

Table 1.3: *L-Au-X (0.1 mol%) catalyzed hydration of 3-hexyne at 30 °C in the presence of NBu_4OTf*[a,b]

Entry	L[c]	X^-	AgOTf (mol%)	Conv. (%)[d]	Time[e] (h) (TOF[f])
1[g]	IPr	OTf^-	-	>99	2 (495)
2	IPr	Cl^-	0.1	70	2 (350)
3	BIAN	Cl^-	0.1	76	2 (380)
4	NHC^{CH2}	Cl^-	0.1	76	2 (380)
5	NAC	Cl^-	0.1	0	24
6	JPhos	Cl^-	0.1	75	4 (188)
7	PCy_3	Cl^-	0.1	0	24
8	PAr^F	Cl^-	0.1	0	24
9	PPh_3	Cl^-	0.1	0	24
10	$P(OR)_3$	Cl^-	0.1	0	24
11	IPr	OTs^-	-	>99	3.5 (285)
12	BIAN	OTs^-	-	>99	4 (248)
13	NHC^{CH2}	OTs^-	-	98	8 (122)
14	NAC	OTs^-	-	9	24 (4)
15	JPhos	OTs^-	-	74	5 (148)
16	PCy_3	OTs^-	-	6	24 (3)
17	PAr^F	OTs^-	-	0	24
18	PPh_3	OTs^-	-	3	24 (1)
19	$P(OR)_3$	OTs^-	-	17	24 (7)
20	BIAN	OTf^-	-	>99	2 (495)
21	NHC^{CH2}	OTf^-	-	>99	4 (248)

[a] Catalytic conditions: 3-hexyne (1.75 mmol, 200 µL), 5 mol% NBu_4OTf (0.087 mmol, 34.3 mg), H_2O (1.92 mmol, 35 µL), L-Au-X (0.00175 mmol) and AgOTf (0.00175 mmol, 0,45 mg) when indicated. [b] mol% = (moles of catalyst / moles of alkyne) x 100. [c] see text. [d] Determined by ^1H NMR; averaged value of three measurements. [e] Time necessary to reach the reported conversion. [f] TOF = ($n_{product}$ / $n_{catalyst}$) / t(h) at the reported conversion. [g] from reference [126].

A standard catalytic run was by mixing the alkyne, water (1.1 equivalents), the catalyst (from 0.1 to 0.01 mol% with respect to the alkyne), silver triflate (when the chloride catalyst were used) and an additive (up to 5 mol% with respect to the alkyne) in a range of temperature from 30 to 120 °C (**Table 1.3** and **Table 1.4**). The complex IPr-Au-OTf has been included in **Table 1.3** to compare the catalytic results with previous data obtained by our group.[126] NMR spectroscopy was used to monitor the catalytic process (see **Table 3.1**). For each run the TOF value [TOF (h^{-1}) = (number of

mole of product)/mole of catalyst)/elapsed time, (**Table 1.3** and **Table 1.4**)] was calculated to evaluate the catalytic activity in different conditions.

At first, the L-gold-chloride complexes were tested in the presence of one equivalent of AgOTf (**Table 1.3,** entries 2-10). The catalysts bearing NAC, PCy_3, PAr^F, PPh_3 and $P(OR)_3$ ligands showed no conversion after 24 h (**Table 1.3,** entries 5 and 7-10). On the other hand, significant but not quantitative conversion (around 75%) of 3-hexyne into 3-hexanone was reached within 2 h using IPr, BIAN and NHC^{CH2} ligands (**Table 1.3**, entries 2-4 **Figure 1.12**), or 4 h using JPhos (**Table 1.3,** entry 6). Prolonging the reaction time to 24 h the conversion did not increase.

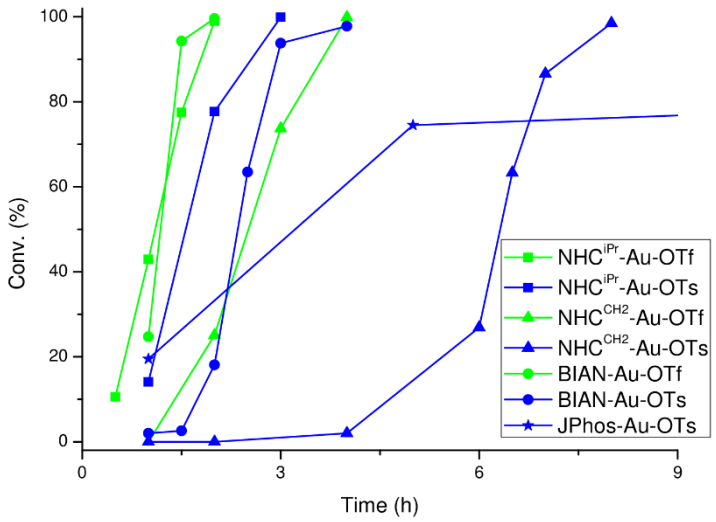

Figure 1.12: *Hydration of 3-hexyne with 0.1 mol% of L-Au-X in the presence of 5 mol% NBu_4OTf.*

The TOF obtained using the IPr-Au-Cl and AgOTf system is 350 h^{-1}, a notably lower value with respect to that reported in silver-free condition (495 h^{-1}, see **Table 1.3** entry 1 vs. entry 2).

As mentioned above, for the complexes containing PCy_3, PAr^F, $P(OR)_3$, PPh_3, and NAC ligands (**Table 1.3** entries 5 and 7-10) the formation of any product was not observed within 24 h. For a better comprehension of the gold stability, we studied the hydration reaction promoted by PPh_3-Au-Cl/AgOTf (**Table 1.3** entry 9) by ^{31}P NMR spectroscopy. At the end of the reaction the spectra were collected (see Experimental Section for details) and the signal at δ 41.9 ppm typical of $[(PPh_3)_2Au]OTf$ was observed.[47,132–134] This result clearly indicates that a decomposition of the catalyst takes place,

also confirmed by the formation of a film of gold on the walls of the reaction vessel. Decomposition of phosphine-based gold catalyst is frequently documented in the literature.[135,136]

A decomposition process seems to be present also for the more stable complex bearing the IPr ligand and promoted by the silver salt in neat- and acid-free conditions. Therefore, even prolonging the reaction time to 24 h (**Table 3.1**) no quantitative conversion into 3-hexanone (**Table 1.3** entry 1 vs. entry 2) was observed. The presence of silver additives in gold catalysis is still debated for both beneficial and detrimental effects.[137]

For the purpose of compare the different ligands and to avoid the silver-induced decomposition of the gold catalyst, L-Au-OTs catalysts has been employed because L-Au-OTf complexes are not stable and isolable with all the ligands here utilized.[46,138] With exception of JPhos-Au-OTs, which gave a conversion of 74 % after 5 h with a TOF of 148 h^{-1} (**Table 1.3** entry 15), the decomposition or deactivation of catalysts containing phosphine was observed, even in silver-free conditions (**Table 1.3** entries 16-19). With the JPhos-Au-Cl/AgOTf system (**Table 1.3** entry 6) a similar result has been obtained.[139] IPr-Au-OTf evidences better catalytic activity when compared to IPr-Au-OTs (**Table 1.3** entry 1 vs. entry 11). A complete conversion of 3-hexyne was observed after 2 h using IPr-Au-OTf and 3.5 h with IPr-Au-OTs species (see also **Figure 1.12**). An explanation of this difference could be found in the OTs^- coordinating ability higher than that of OTf^- toward the gold fragment. In our previous work we reported that in neat conditions OTs^- inhibits the hydration of 3-hexyne.[126] It is plausible that the presence of an excess of NBu_4OTf slowly converted the non-active form IPr-Au-OTs into the more active IPr-Au-OTf during the catalysis.

Keeping in mind that: a) phosphine-based gold catalysts showed very low activity, b) silver salts deactivate the catalyst, and c) L-Au-OTf species showed the higher catalytic activity, we decided to extend the investigation to other gold catalyst containing NHC ligands and OTf^- as the counterion. Therefore, BIAN-Au-OTf and NHC^{CH2}-Au-OTf were employed for the catalysis and compared with IPr-Au-OTf. BIAN-Au-OTf (**Table 1.3** entry 20), showed the same quantitative conversion of 3-hexyne as IPr-Au-OTf (**Table 1.3** entry 1) in 2 h. NHC^{CH2}-Au-OTf promoted the complete formation of 3-hexanone twice the reaction time (**Table 1.3** entry 21).

These results demonstrated that the best performances are obtained when there is an NHC type ligand in L-Au-X complexes, while the use of silver salts must be avoided.

For what concerns the ionic additives, our group has demonstrated that the rate of the reaction can be improved in the presence of NBu_4OTf, because it acts as PTC (phase transfer catalysts).[140] Otherwise, NH_4OTf does not show any appreciable effect and [BMIM]OTf even stops the reaction.[126]

Different ammonium triflate salts, in terms of different number and length of alkyl chains, were deeply investigated to understand the effectiveness during the catalysis. We added 5 mol% of Bn_3NHOTf, Bu_2NH_2OTf, $Me_2(Et)(Dec)NOTf$, $(Cy)NH_3OTf$, Aliquat-OTf in the catalytic process of IPr-Au-OTf (see Experimental Section for details). We found that NBu_4OTf is the most effective additive (**Table 3.2**), as previously observed.[126]

We decided to apply the best combination system (IPr-Au-OTf/NBu_4OTf 5 mol% solvent-, silver-, and acid-free) in the hydration of diphenylacetylene. To afford 1,2-diphenylethanone the temperature must be increased above the diphenylacetylene melting point (62 °C). Hydration of diphenylacetylene is frequently studied in the literature in the presence of solvent and additives such as silver salts and acids.[141–145] In **Table 1.4** and **Figure 1.13** the most salient results are summarized. Despite this, the optimization is far from being achieved from a greener point of view.

Table 1.4: *IPr-Au-OTf catalyzed hydration of diphenylacetylene*[a]

entry	Loading (mol%)[b]	T (°C)	Anion (X)	Conv.[c] (%)	Time[d] (h) (TOF[e])
1	0.1	65	OTf^-	82	8 (102)
2	0.05	80	OTf^-	42	8 (105)
3	0.05	120	OTf^-	94	4 (470)
4	0.025	120	OTf^-	85	8 (435)
5	0.01	120	OTf^-	27	5 (560)
6[f]	0.05	120	OTf^-	88	8 (220)
7	0.05	120	OTs^-	7	8 (17)

[a] Catalysis conditions: diphenylacetylene (1.75 mmol, 312 mg), 5 mol% NBu_4OTf (0.087 mmol, 34.3 mg) and H_2O (1.92 mmol, 35 µL). [b] (moles of catalyst / moles of alkyne) x 100. [c] Determined by ^1H NMR; average value of three measurements. [d] Time necessary to reach the reported conversion. [e] TOF = ($n_{product}$ / $n_{catalyst}$) / t(h) at the reported conversion. [f] with D_2O instead of H_2O.

Diphenylacetylene, 1.1 equiv of H_2O, NBu_4OTf (5 mol%) and IPr-Au-OTf (from 0.01 mol% to 0.1 mol% with respect to diphenylacetylene) were mixed at the desired temperature. A high conversion of diphenylacetylene was obtained in 8 h using 0.1% mol of catalyst at 65 °C (**Table 1.4** entry 1). Both temperature and catalyst loading were varied to optimize the reaction conditions (**Figure 1.12**). Increasing the temperature to 120 °C and reducing the catalyst amount to 0.05 mol% led a yield of 94% of 1,2-diphenylethanone (**Table 1.4** entry 3). A reduction of IPr-Au-OTf concentration to 0.025 mol% and 0.01 mol% resulted in a progressive drop in conversion (**Table 1.4** entries 4 and 5). The highest TOF was reached at 120 °C with a catalyst loading of 0.01 mol% (560 h^{-1}, **Table 1.5** entry 5), while the highest TON (3400) was obtained with 0.025 mol% of IPr-Au-OTf at the same temperature. These catalytic conditions led to a very high EMY value (77) as well as to an excellent E-factor value (0.03).

The comparison of the catalytic parameters obtained by us with the best ones reported to date in the literature (see **Table 1.5**) highlights the excellent results obtained by applying our protocol. Tanaka and coworkers studied the catalytic hydration of diphenylacetylene promoted by phosphine gold complexes in 2002.[36] A TON of 53 in 5 h was obtained in methanol under strongly acidic conditions at 70 °C with an E-factor of 6 and EMY values of 10. In 2009 NHC gold(I) complexes were introduced by Nolan and co-workers.[39] In a 1,4-dioxane/water 2:1 mixture the catalyst loading was reduced to 0.1 mol%, the temperature was increased to 120 °C, in acid-free condition. A maximum TON and TOF of 770 and 42 h^{-1} were achieved, respectively. On the other hand, the EMY value obtained (13) was still low. The same group attained TON of 400 and TOF of 67 h^{-1} by employing as catalysts dimeric $(NHC\text{-}Au)_2SO_4$ complexes at 80 °C.[146] E-factor and EMY values did not improved, despite these conditions. We studied also this reaction using γ-valerolactone (GVL) as the solvent.[127] With a catalyst loading of 0.1 mol% a maximum TOF of 283 h^{-1} was reached. However, a marked improvement of E-factor (2.6) and EMY (28) values was reached. However, both are still very far from being acceptable in terms of effective green catalysis.

Table 1.5: *Main parameters for hydration of diphenylacetylene in 1,2-diphenylethanone*

	Tanaka[36]	Nolan[39]	Nolan[146]	Zuccaccia[127]	This work
Solvent	MeOH/H_2O (2:1)	Dioxane/H_2O (2:1)	MeOH/H_2O (2:1)	γ-valerolactone	-
TON	80	***770***	***400***	***990***	***3400***
TOF (h^{-1})	80	43	67	283	***435***
T (°C)	***70***	120	***80***	120	120
Ag^+ additives	***NO***	YES	***NO***	***NO***	***NO***
Other additives	H_2SO_4	NO	***NO***	***NO***	NBu_4OTf
E-factor	6	4.8	5	2.6	***0.3***
EMY[a]	10	13	10	28	***77***

[a] EMY= Effective mass yield

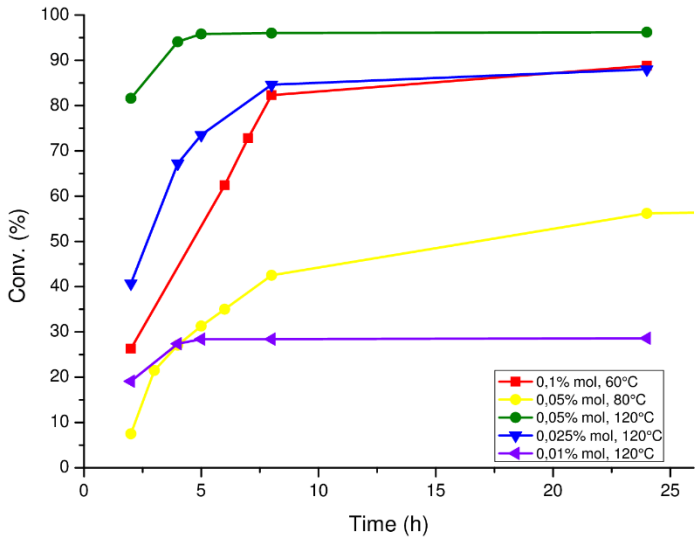

Figure 1.13: *Hydration of diphenylacetylene with different loadings of IPr-Au-OTf, in the presence of 5 mol% NBu_4OTf, at different temperatures.*

For the purpose of shed some light on the reaction mechanism, we quantify the KIE value by conducting some experiments using D_2O instead of H_2O in these aprotic and apolar conditions at high temperature (**Table 1.4** entry 6). In the solvent- and silver-free hydration of 3-hexyne, the addition of 5 mol% of NBu_4OTf resulted in a neat change of the KIE value from 3.8 to 2.5.[126] These KIE values point out that the turnover-limiting step is the proton transfer. We observed a small reduction of TOF using D_2O instead of H_2O, which changed from 470 to 433 h^{-1} (see Experimental

Section, compare in **Table 3.3** entries 3 and 6), and the KIE was 1.2. Diphenylacetylene is much less reactive with respect to internal aliphatic alkynes, therefore it is plausible that the RDS might be the nucleophilic attack.

As far as the role of the counterion in the pre-equilibrium step is concerned, when OTs^- is employed instead of OTf^-, the higher co-ordinating ability the former towards cationic gold fragments shifts the pre-equilibrium step towards the non-active inner sphere ion pair (**Table 1.3**).[126] In the present work this difference is confirmed, as the conversion of 94 % (4 h), shown by IPr-Au-OTf (**Table 1.4** entry 3), drops to 7 % (8 h) when IPr-Au-OTs is employed as the catalyst (**Table 1.4** entry 7). We can deduce that the counterion effect is the same as that observed for the hydration of 3-hexyne, notwithstanding the temperature has been raised to 120 °C. Thus, when OTs^- is involved the equilibrium is strongly shifted towards the precatalyst.

2.1.2 Meyer-Shuster rearrangement

Transformations of propargyl alcohols catalyzed by gold became very popular since these species contain both a nucleophilic hydroxy group and a potentially electrophilic alkyne moiety which can be efficiently activate by gold, due to its soft Lewis acid nature. To this day, several transformations of these substrates have been reported catalyzed by gold.[147] Among the others, the Meyer-Schuster (MS) rearrangement is one of the most popular, because it can deliver α,β-unsaturated carbonyl compounds in complete atom economy.[148,149] Gold complexes allow to carry out this rearrangement with high yields and in mild experimental conditions.[147] Unfortunately, a deep and complete understanding of the catalytic mechanism is still lacking, despite all the experimental advances on the gold-catalyzed MS rearrangement. During the years, a large variety of mechanisms have been proposed on the basis of experimental results.[150–153] As an example, Marion et al. suggested an unusual gold-hydroxy complex as the active catalytic species on the NHC-gold(I)-catalyzed MS rearrangement of propargylic acetates.[154] All the proposed mechanisms share two common features: 1) they take into account the presence of either water or alcohols as the solvent; 2) the role of the counterion is completely neglected. However, the counterion effect has been shown to be crucial for understanding the reactivity in similar gold catalyzed processes.[48,51,52,126,155–159] Experimental proof (**Table 1.6** and **Figure 1.14**) for both a solvent and a counterion effect is given here for the rearrangement of 1-phenyl-2-propyn-1-ol to cinnamaldehyde at 50˚C catalyzed by IPr-Au-X (X^- = Cl^-, BF_4^-, OTf^-, OTs^-, TFA^-) (for details see **Figure 3.5** and **4.6** and **Table 3.5** and **4.6** in the Experimental Section). Substitution of volatile organic solvents (VOS) with green solvents or performing the reaction in neat conditions is a key topic in organic synthesis, but it is not common in gold catalysis.[127] Here, VOS and green solvents, with different polarity and with the presence of particular functional groups, have been tested. The results are summarized in **Table 1.6** and **Figure 1.14**.

The complex IPr-Au-OTf was inactive in DMSO, with no formation of the product also after 24 h (**Table 1.6**, entry 17). This can be related to the remarkable coordination ability of this solvent towards gold.[127] On the other hand, high or even quantitative formation of cinnamaldehyde was reached within 1-24 h using other solvents or neat conditions (**Table 1.6** and **Figure 1.14**).

Table 1.6: *Meyer-Schuster rearrangement of 1-phenyl-2-propyn-1-ol to cinnamaldehyde at 50°C.*[a]

Entry	Solvent	Catalytic system	Conv.[b] (%)	TOF[c] (h^{-1})	ε_r[d]
	VOS				
1	Chloroform	IPr-Au-OTf	75	300	4.81
2	Dichloromethane	IPr-Au-OTf	12	53	8.93
3	Acetone	IPr-Au-OTf	13	50	21
	Green				
4	p-Cymene	IPr-Au-OTf	91	394	2.24
5	p-Cymene[e]	IPr-Au-Cl/ AgOTs	11	44	2.24
6	p-Cymene[f]	IPr-Au-Cl/ AgTFA	0.4	2	2.24
7	p-Cymene[g]	IPr-Au-Cl/$AgBF_4$	7	28	2.24
8	p-Cymene[h]	IPr-Au-Cl/AgOTf	30	115	2.24
9	p-Cymene[i]	IPr-Au-OTf/HOTf	100	400	2.24
10	p-Cymene[j]	IPr-Au-OTf/HOTs	93	371	2.24
11	p-Cymene[k]	IPr-Au-OTf/P.S.	0	0	2.24
12	Limonene	IPr-Au-OTf	67	246	2.4
13	Anisole	IPr-Au-OTf	85	368	4.3
14	Ethyl Lactate	IPr-Au-OTf	24	106	15.4
15	Furfuryl alcohol	IPr-Au-OTf	37	161	16.9
16	γ-Valerolactone	IPr-Au-OTf	23	105	36.9
17	DMSO	IPr-Au-OTf	0	0	46.7
18	Methyl levulinate	IPr-Au-OTf	17	74	-
19	-[l]	IPr-Au-OTf	74	296	-

[a]Catalysis conditions: IPr-Au-OTf (0.0025 mmol, 1.8 mg), 1-phenyl-2-propyn-1-ol (0.5 mmol, 61 µL), solvent (200 µL). [b]Determined by ^{1}H NMR; average value of three measurements after 30 minutes. [c]TOF = ($mol_{product}/mol_{catalyst}$)/t calculated after 30 minutes. [d]ε_r = dielectric constant. [e]IPr-Au-Cl (0.0025 mmol, 1.6 mg), 1.1 eq AgOTs. [f]IPr-Au-Cl (0.0025 mmol, 1.6 mg), 1.1 eq AgTFA. [g]IPr-Au-Cl (0.0025 mmol, 1.6 mg), 1.1 eq $AgBF_4$. [h]IPr-Au-Cl (0.0025 mmol, 1.6 mg), 1.1 eq AgOTf. [i]IPr-Au-OTf (0.0025 mmol, 1.8 mg), 10 mol% (respect to substrate) HOTf. [j]IPr-Au-OTf (0.0025 mmol, 1.8 mg), 10 mol% (respect to substrate) HOTs. [k]IPr-Au-OTf (0.0025 mmol, 1.8 mg), 10 mol% (respect to substrate) proton sponge (1,8-Bis(dimethylamino)naphthalene). [l]no solvent was used.

In the case of VOS, high conversion of 1-phenyl-2-propyn-1-ol into cinnamaldehyde was reached in 0.5 h in chloroform (**Table 1.6**, entry 1) without formation of side products. In dichloromethane and acetone (**Table 1.6**, entries 2 and 3, **Figure 1.14**) much less efficiently IPr-Au-OTf promoted the formation of the reaction product in rather low yield (12-13 % after 0.5 h).

Higher conversions were generally achieved using neoteric solvents (**Table 1.6**, **Figure 1.14**). Using low-polarity solvent such as p-cymene, limonene, and anisole (**Table 1.6**, entries 4, 12 and 13, respectively) high conversion was obtained after 0.5 h, while an about half conversion was reached using ethyl lactate, furfuryl alcohol and γ-valerolactone (**Table 1.6**, entries 14, 15 and 16, respectively). The reaction slowly proceeded in methyl levulinate (**Table 1.6**, entry 18).

The catalysis was conducted in p-cymene with IPr-Au-Cl/AgX (X = BF_4^-, OTf^-, OTs^-, TFA^-) as the catalytic system to understand the importance of the counterion. The efficiency is strongly dependent on the counterion: conversion of 30 %, 11 %, 7 % and 0.4 % were observed after 30 min for OTf^-, OTs^-, BF_4^-, TFA^-, respectively (**Table 1.6**, entries 5-8).

Comparing the conversion given by IPr-Au-OTf (**Table 1.6**, entry 4) and the one generated in situ (IPr-Cl + AgOTf) (**Table 1.6**, entry 8), a neat decrease is observed in the latter case. This may suggest a negative effect of the silver ion,[160] but the presence of an induction time connected to the activation of the catalyst cannot be excluded.

Examining the TOF value [TOF (h^{-1}) = moles of product/moles of catalyst/time, **Table 1.6**)] allows for a deep comparison of the catalytic activity of gold catalyst in different solvents. The calculated TOFs range from 0 h^{-1} (DMSO) to 394 h^{-1} (p-cymene) (**Table 1.6**, entries 17-4). A general trend can be observed: the value decreases when the polarity of the solvent increases (**Table 1.6**, **Figure 1.14**) as also observed in the gold catalyzed methoxylation of 3-hexyne.[127]

Furthermore, in p-cymene the catalyst efficiency strongly depends on the counterion, according to the following order: $OTf^- > OTs^- > BF_4^- > TFA^-$ (**Table 1.6**, compare entries 4-7). This finding, combined with the observed trend of TOF *vs* ε_r, suggests a role of the anion during the catalysis.

We also investigated the effect of the addition of acids and bases. The addition of triflic acid (HOTf) and *p*-toluenesulfonic acid (HOTs) does not alter the reaction rate and the TOF values remain around 371-400 h^{-1} (compare in **Table 1.6** entries 4, 9, and 10) also indicating that, in acidic condition, the rate does not depend on the counterion. On the other hand, the catalysis is completely stopped when the proton sponge (P.S.) 1,8-bis(dimetilammino)naftalene (**Table 1.6**, entry 11) is added to the catalytic mixture. A possible explanation can be found in the formation of a stable σ-bonded gold-alkynyl complex, with abstraction of the acidic hydrogen of the terminal alkyne by P.S. (see below).

Finally, an intermediate catalytic performance is observed when the reaction is run in γ-valerolactone, a commonly employed green solvent,[157] despite its high dielectric constant, and also

when the reaction is run in neat conditions (**Table 1.6**, entries 16 and 19), thus indicating that a green version of the reaction is feasible.

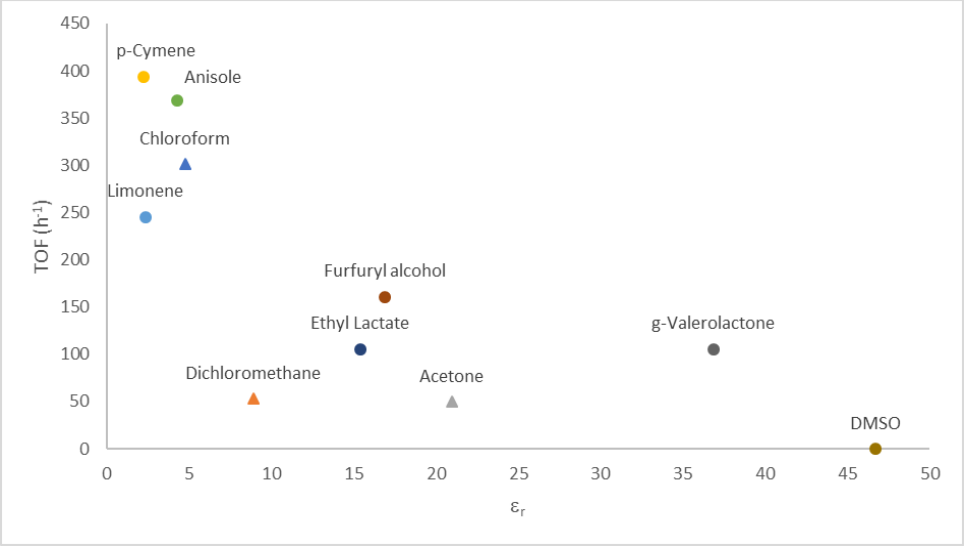

Figure 1.14: *TOF vs dielectric constant for IPr-Au-OTf catalyzed Meyer-Schuster rearrangement of 1-phenyl-2-propyn-1-ol to cinnamaldehyde at 50 °C (selected values from* ***Table 1.6****).*

Motivated by the lack of a general mechanistic comprehension,[131,161] a computational study has been carried out to both rationalize the experimental outcome and give further insights into the yet elusive mechanism of the gold-catalyzed MS rearrangement. An accepted mechanism for gold(I) catalysis of alkyne substrates consists of: 1) a pre-equilibrium step; 2) a nucleophilic attack step with formation of an organogold intermediate; and 3) a protodeauration step. An essential counterion effect has been previously found by some of us in each step of this reaction mechanism.[158]

With the intention of explaining the counterion-dependent reactivity observed for this MS rearrangement, the gold-catalyzed intramolecular nucleophilic attack has been considered in our study, where the complex [NHC*-Au-X] (NHC*= 1,3-dimethylimidazol-2-ylidene, X^-= OTf^-, OTs^-, BF_4^-) is used as model. This step has been found to be the rate-determining one (RDS) in similar reactions.[9] The schematic representation of the mechanism is shown in **Scheme 1.11**. The geometries of the stationary points and transition states have been optimized at the DFT level including relativistic effects (BP86/ZORA/D3). Single-point energy calculations have been performed at both DFT (B2PLYP/CPCM) and DLPNO-CCSD(T)[162,163] levels (see the Experimental Section for computational details). All the optimized geometries are reported in **Figure 3.23-4.25**.

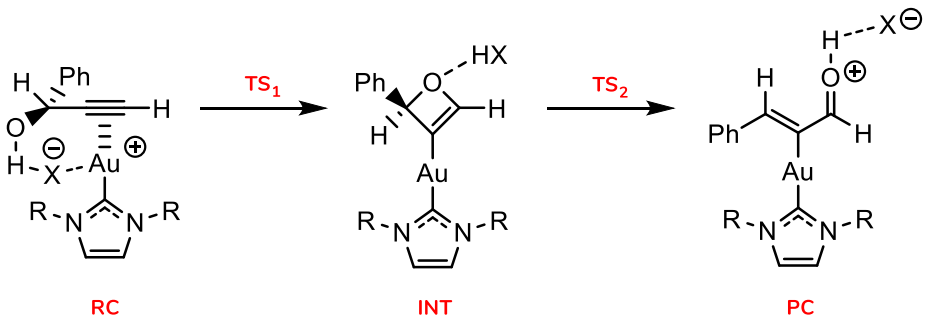

***Scheme 1.11**: DFT mechanism of the intramolecular nucleophilic attack in 1-phenyl-2-propyn-1-ol rearrangement catalysed by the [Au-NHC*]$^+$ complex and assisted by three different counterions (X$^-$= OTf$^-$, OTs$^-$ and BF$_4^-$).*

Based on the well-known gold ability to activate triple bonds, the investigation started by considering the cationic [Au-NHC*]$^+$ fragment coordinated to the alkyne moiety as our reactant complex, RC. In principle, we expect the RC to directly convert into the product complex (PC), i.e. a gold-aldehyde species, that should yield the cinnamaldehyde and regenerate the catalyst through the protodeauration step. Unexpectedly, we find that, independently from the nature of the counterion, cyclization a gold-oxetene intermediate (INT) is formed via 4-*endo*-dig, which subsequently undergoes electrocyclic ring opening and yields the expected PC (**Scheme 1.11**). The proposed mechanism is able to completely rationalize the observed reactivity. As represented in **Scheme 1.11**, the role of the counterion in this reaction is key. It behaves as a hydrogen-bond acceptor, by increasing the nucleophilicity of the attacking hydroxy group, and as a template, helping the hydroxy to assume its reactive position through simultaneous interaction with the OH hydrogen and the gold center. Furthermore, it acts as a "proton shuttle", by transferring the proton from the intermediate to generate the PC. Clearly, the different basicity behavior and coordination ability of the counterions reflect in a very different reactivity, with reaction yields and TOF values highly depending on it (**Table 1.6**). In particular, the anion is known to act as catalyst deactivator, by either its strong coordinating and/or basicity power, in the pre-equilibrium step of the reaction.[158] Preliminary calculations have been performed for this step by comparing the strongest coordinating/basic OTf$^-$, OTs$^-$ and TFA$^-$ anions which have allowed us to immediately rationalize the poorest efficiency of TFA$^-$. The results (**Figure 3.26** in the Experimental Section) show that a stable σ-bonded gold-alkynyl complex is formed through abstraction of the acidic hydrogen of the terminal alkyne by TFA$^-$ with a low energy barrier (5.0 kcal/mol) while the expected gold-alkyne complex is obtained for OTf$^-$ and OTs$^-$. Formation of the σ-complex, due to the strongest basicity of TFA$^-$ in the

anion series and to its bidentate nature, prevents the π activation of the triple bond and is consistent with the experimentally observed lowest efficiency of TFA^-. Therefore, only OTf^-, OTs^- and BF_4^- anions have been compared in the nucleophilic attack step, starting from a suitable RC conformation where the anion occupies a vicinal position to the attacking OH group. The calculated energy profiles highlight substantial differences, as reported in **Figure 1.15**.

For the OTf^--assisted intramolecular attack (from **Figure 1.15**), the lowest activation barrier is calculated (32.6 kcal/mol), whereas, when the OTs^- and BF_4^- anions are involved, the barriers are higher (34.3 and 36.9 kcal/mol, respectively), in full agreement with the experimentally observed reactivity trend.

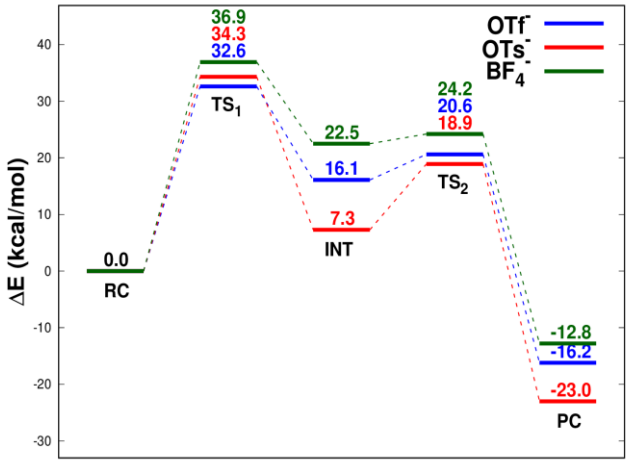

Figure 1.15: *Energy profiles (BP86/ZORA/D3//B2PLYP/CPCM, see Experimental Section for details) for the intramolecular nucleophilic attack in the 1-phenyl-2-propyn-1-ol rearrangement catalyzed by the [Au(I)-NHC*]⁺ complex and assisted by three different counterions (X^- = OTf^- , in blue; OTs^-, in red; and BF_4^-, in green). Energy values refer to the corresponding reactant complex RC taken as zero.*

Enthalpy and Gibbs free energy profiles computed at the BP86/ZORA/D3//BP86/ZORA/D3 levels are also reported in **Figure 3.26-4.28**, showing that electronic energy $\Delta E^{\#}$ can be considered as a good approximation to $\Delta G^{\#}$. Reaction profiles calculated using different computational setups (BP86/ZORA//B2PLYP, BP86/ZORA/D3//B2PLYP and BP86/ZORA/D3//DLPNO-CCSD(T)) are compared in **Figure 3.30-4.32**, showing that they are quantitatively similar. Interestingly, the results of these test calculations fully validate the accuracy of a computational protocol based on BP86 optimization geometry and B2PLYP single point energy calculations suggested by us for similar gold-catalyzed reactions.[164] Finally, the importance of solvent (p-cymene) inclusion to exactly match the experimental trend is demonstrated, since in gas phase almost identical barriers are calculated for OTs^- and OTf^- (31.5 vs. 31.6 kcal/mol at BP86/ZORA/D3//B2PLYP level, and 32.2 and 32.6 kcal/mol at

BP86/ZORA/D3//DLPNO-CCSD(T) level, respectively). Notably, all the calculated reaction energy profiles (**Figure 3.27-4.32**) are qualitatively similar to those depicted in **Figure 1.15**. A rationalization for OTf^- favoring the intramolecular nucleophilic attack can be reached by analyzing the three TS1 structures.

In all the TS1 structures, the anion features a bridging position between the OH and the Au center. By comparing the hydroxy O-H distances (**Figure 3.23-4.25** in the Experimental Section), we can observe that they match the hydrogen-bond acceptor ability of the three anions (1.021 for OTs^-, 1.016 for OTf^- and 1.001 Å for BF_4^-), but they do not correlate with the activation energy barrier trend. Based on the anion basicity strength, the best nucleophile activator OTs^- should give the lowest barrier. Instead, the X-Au distances in the RC structures (2.847 for X = OTs^-; 2.955 for X = OTf^-; 2.976 Å for X = BF_4^-) are consistent with the anion coordinating ability trend (OTs^- > OTf^- > BF_4^-). Based on the anion coordinating strength, the best CC triple bond de-activator OTs^- should give the highest barrier. However, as previously reported by some of us, the extent of alkyne slippage (i.e. the $\eta^2 \rightarrow \eta^1$ deformation occurring at the alkyne coordination to gold) can be considered as a reactivity index. A larger alkyne slippage corresponds to a more electrophilic terminal carbon atom (C1) and therefore to a lower activation barrier for the nucleophilic attack.[50,127,165] In the TS1 structures the Au-C1 distances (2.919 Å for X = OTf^-; 2.876 Å for X = OTs^-; 2.817 Å for X = BF_4^-) show that for the OTf^- anion-assisted attack, the largest $\eta^2 \rightarrow \eta^1$ deformation occurs, resulting in a more electrophilic C1 carbon atom and, as a consequence, in the lowest activation barrier. These findings suggest that the activation of the nucleophilic hydroxy group should be counteracted by a de-activation of the electrophilic character of the CC triple bond through interaction with the gold center. Thus, the activation energy barrier appears to arise as a balance between the anion hydrogen-acceptor ability and the anion affinity towards gold (extent of alkyne slippage), which is ultimately responsible for the observed (and calculated) catalyst efficiency trend.

Preferential coordination of gold-carbene fragment to propargylic hydroxyl group with formation of a gold-hydroxo species similar to that proposed as the catalytically active species in ref. 154 has been also calculated. Although this species is 11.4 kcal/mol more stable than RC, the nucleophilic attack requires a much higher activation barrier (65.3 kcal/mol) (**Figure 3.33**) than that from RC (31.2 kcal/mol) (at BP86/ZORA//B2PLYP level, **Figure 3.30**). No reaction intermediate is formed in this case.

The mechanism proposed here (**Scheme 1.11**) is peculiar. We find that the 4-*endo*-dig cyclizations and the ring opening of 4-endo products are feasible, although they are commonly kinetically very unfavorable.[55,166] To the best of our knowledge, evidence of gold-catalyzed synthesis of oxetenes and of the presence of gold-oxetene intermediates has been only reported few times[167–170] and never in gold-catalyzed MS rearrangement.

In order to isolate and characterize the predicted gold-oxetene adduct, a stoichiometric reaction between 1-phenyl-2-propyn-1-ol and IPr-Au-OTf in the presence of a 3-fold excess of 1,8-bis(dimetilammino)naftalene in $CDCl_3$ was performed. Unfortunately, the abstraction of the acidic hydrogen of the terminal alkyne was accomplished with formation of a stable σ-bonded gold-alkynyl complex (see Experimental Section for details). The internal alkynes 3-hexyn-2-ol and 1,3-diphenyl-2-propyn-1-ol were used in an attempt to observe the oxetene intermediate in NMR tube. Formation of the oxetene intermediate (see Experimental Section) was not observed, despite we have changed the temperature (up to -50°C), the base (bis(dimetilammino)naftalene and potassium carbonate), the solvent ($CDCl_3$ and CD_3OD), and the gold complex (IPr-Au-OTf and IPr-Au-TFA). Failure to isolate the oxetene intermediate is however still consistent with the computationally proposed mechanism, since this species is predicted to very easily undergo electrocyclic ring opening (conversion from INT to PC requires an activation barrier of 4.5 kcal/mol, see **Figure 1.15**).

In order to better understand the experimental conditions which may affect the mechanism, in **Figure 1.16** the gas-phase profile for the OTf^--assisted nucleophilic attack is compared with those accounting for 1) the use of more polar solvents and 2) the presence of traces of acid.

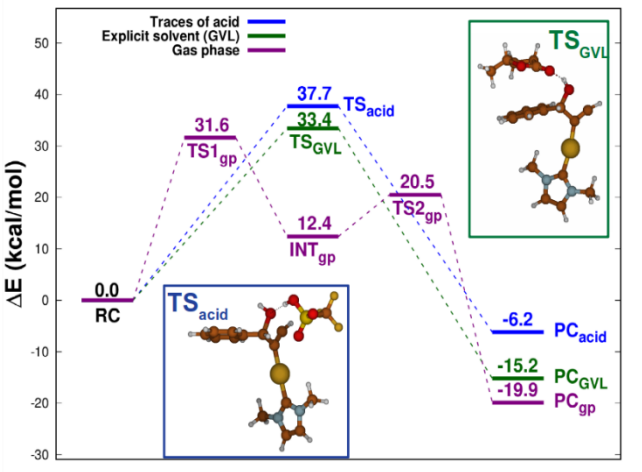

Figure 1.16: *Energy profiles (BP86/ZORA/D3//B2PLYP) of the intramolecular nucleophilic attack of the 1-phenyl-2-propyn-1-ol catalyzed by the [Au(I)-NHC*]$^+$ complex in three different conditions: gas phase (OTf^-) (violet line), in the*

presence of explicit traces of acid (HOTf) (blue line) and with an explicit molecule of polar solvent (γ-valerolactone) replacing the anion (green line). The structure of the transition states is shown for the acid (TS_{acid}) and polar solvent (TS_{GVL}) conditions. Energy values refer to the corresponding reactant complex RC taken as zero.

Possible traces of acid in solution are accounted for by protonating the OTf^- anion. As shown in **Figure 1.16**, with the HOTf species assisting the attack, no intermediate is formed since HOTf cannot behave as a proton-shuttle. As a result, the reaction proceeds via TS_{acid} to the PC_{acid}, with the latter being thermodynamically less stable with respect to the OTf^- assisted attack (-6.2 vs. -19.9 kcal/mol respectively) and with a slightly higher activation barrier (37.7 kcal/mol), consistently with the experimental findings. This result shows that for the formation of the oxetene intermediate to occur, the anion hydrogen bond-acceptor ability is essential. As previously pointed out, the role of the anion in gold-catalyzed processes can be heavily modified by the polarity of the solvent.[127] In the case of low-polarity p-cymene, the presence of a catalytically active ion pair is reasonable (i.e. [IPr-Au(I)-(1-phenyl-2-propyn-1-ol)]$^+X^-$), with the counterion playing an active role in the reaction. By increasing the polarity of the solvent, we expect that active free ions are predominant species in solution (i.e. [IPr-Au(I)-(1-phenyl-2-propyn-1-ol)]$^+$ + X^-), with the counterion losing its fundamental role. As shown in **Figure 1.16**, when the anion is replaced with an explicit molecule of a neoteric polar solvent (i.e. GVL), a reactivity change is observed. The structure of the TS_{GVL} suggests that GVL is not able to substitute the role of the OTf^- in accepting the proton from the substrate hydroxyl group, resulting in a one-step intramolecular nucleophilic attack without formation of the intermediate and in a slightly higher activation energy barrier (33.4 kcal/mol).

2.1.3 Cyclization of propargylamide

The alkoxylation and hydration of alkynes were investigated by some of us[127] in a wide set of neoteric solvents using IPr-Au-OTf as catalyst and we found that polarity and functionalities present in the solvent influence the three steps of the reaction pathway (pre-equilibrium, nucleophilic attack, and protodeauration). Previously, also the counterion and ligand effects have been studied for the cycloisomerization of N-propargylcarboxamides,[49] founding out that the most efficient L-Au-X catalyst arises from balanced contributions of the properties of L and X^- together.

Building on this state of the art, the activity of IPr-Au-X (X^- = BF_4^-, OTf^- OTs^-, TFA^-) catalysts has been investigated in the cycloisomerization of N-(prop-2-yn-yl)benzamide to 2-phenyl-5-vinylidene-2-oxazoline (**Scheme 1.12**) conducted in green solvents. Most of these solvents are comparable or better solvents with respect to traditional VOS. Kinetic experiments coupled with DFT calculations have allowed us to shed light on the mechanism of cycloisomerization in green conditions. The results presented here show that the anion properties, both coordination ability and basicity (hydrogen-bond acceptor power), should have a great impact on its "proton shuttle ability".

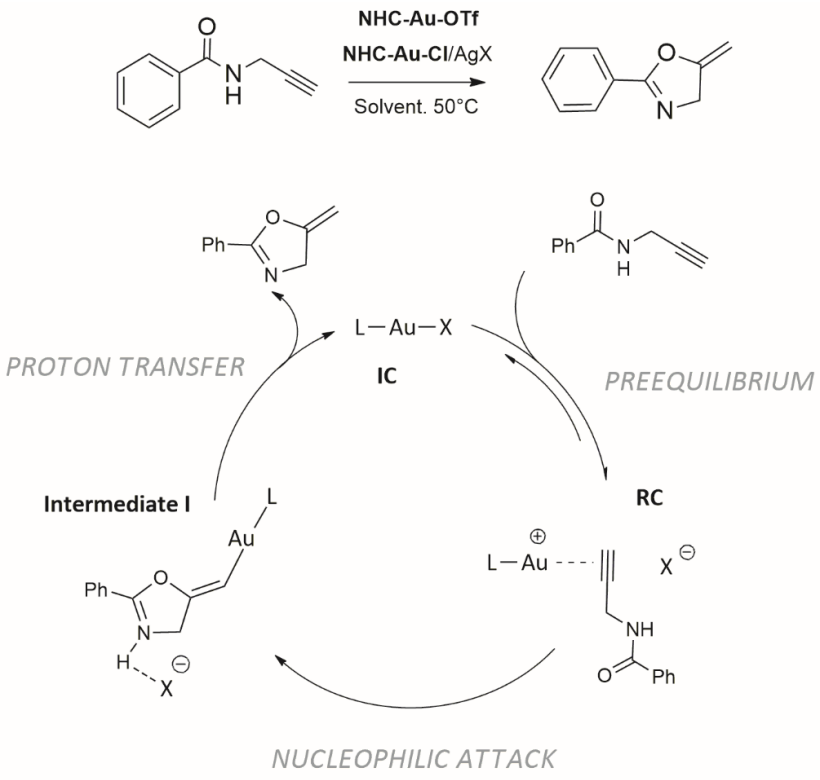

Scheme 1.12: *Cycloisomerization of N-(prop-2-yn-yl)benzamide to 2-phenyl-5-vinylidene-2-oxazoline.*

Gold complexes were synthesized according to literature procedures (see Experimental Section for details). All complexes IPr-Au-X (**Scheme 1.12**, X^- = BF_4^-, OTf^-, OTs^-, TFA^-) have been tested as

catalysts in the cycloisomerization of N-(prop-2-yn-yl)benzamide to 2-phenyl-5-vinylidene-2-oxazoline (**Scheme 1.12** and **Table 1.7**). Isolated IPr-Au-OTf was directly employed, whereas in all other cases the catalyst was prepared *in situ* in an NMR tube by mixing equimolar amounts of the precursor IPr-Au-Cl and the appropriate silver salt (**Scheme 1.12** and **Table 1.7**). Interestingly, all the solvents were used as delivered without further purification.

Table 1.7: *IPr-Au-X catalysed N-(2-Propynyl)benzamide isomerization at 50°C.*[a]

Entry	Solvent	Conv.[b] %	TOF[c](h^{-1})	ε_r[d]
	VOS			
1	Chloroform	90	354	4.81
2	Dichloromethane	89	406	8.93
3	Acetone[e]	10	43	21
4	3-Nitrotoluene	65	281	22.2
5	Nitromethane	67	274	35.87
	Green			
6	Cyclohexanone	47	206	2.02
7	p-Cymene	15	63	2.24
8	Limonene[e]	11	50	2.4
9a	Propionic acid	94	431	3.35
9b	Propionic acid[f]	16.7	65	3.35
9c	Propionic acid[g]	39.6	154	3.35
9d	Propionic acid[h]	90.9	354	3.35
10	Cyrene	23	94	3.4
11	Anisole[e]	13	56	4.3
12	Isopropyl acetate	49	223	6.3
13	MIBK	62	250	13.1
14	Ethyl Lactate	73	317	15.4
15	Furfuryl alcohol	39	148	16.85
16	Propionitrile[e]	12	50	27.7
17	γ-Valerolactone	47	192	36.9
18	DMSO	5	21	46.7
19	Propylene carbonate	49	180	64
20	BMIM-OTf	28	120	-
21	Methyl levulinate	21	90	-

[a]Catalysis conditions: IPr-Au-OTf (0.0025 mmol, 1.8 mg), N-(2-Propynyl)benzamide (0.5 mmol, 79.6 mg), solvent (200 µL). [b]Determined by 1H NMR; average value of three measurements after 30 minutes. [c]TOF = ($mol_{product}/mol_{catalyst}$)/t calculated after 30 minutes. [d]ε_r = dielectric constant. [e]slightly or not soluble. [f]IPr-Au-Cl (0.0025 mmol, 1.6 mg), 1.1 eq AgOTs. [g]IPr-Au-Cl (0.0025 mmol, 1.6 mg), 1.1 eq AgTFA. [h]IPr-Au-Cl (0.0025 mmol, 1.6 mg), 1.1 eq $AgBF_4$.

A typical catalytic run was performed by dissolving N-(prop-2-ynyl)benzamide (0.5 mM) in the presence of 0.5 mol% of IPr-Au-OTf (or 1:1 L-Au-Cl/AgX) at 50 °C in the appropriate solvent (0.2 mL). The progress of the reaction was monitored by NMR spectroscopy (see Experimental Section for details).

Most reactions reached more than 90% of conversion within 8 h (see **Table 3.8**) except those run in acetone, limonene, anisole and proprionitrile (**Table 1.7**, entries 3, 8, 11, and 16) in which N-(prop-2-ynyl)benzamide resulted slightly soluble or even insoluble, and in dimethyl sulfoxide (**Table 1.7**, entry 18) due to its strong coordination capability, as previously observed.

In order to compare the catalytic activity in different solvent, the values of the initial turnover frequency, TOF (**Table 1.7**) were calculated. Chloroform and dichloromethane showed the best performance among the volatile organic solvents (VOS) giving a TOF of 354 and 406 h^{-1}, respectively (**Table 1.7**, entries 1 and 2). Less efficiently, IPr-Au-OTf promoted the formation of the reaction product with a very similar TOF of 281 and 274 h^{-1} in the higher polar solvents 3-nitrotoluene and nitromethane (**Table 1.7**, entries 4 and 5). Finally, the very low value of 43 h^{-1} was obtained in acetone (**Table 1.7**, entry 3).

Turning into green solvents, very different catalytic performances were observed, and although the green solvents showed, on average, slower conversion with respect to VOS, propionic acid resulted to be the best among all solvents with a TOF of 431 h^{-1} (**Table 1.7**, entry 9). Medium TOF values in the range 150-300 h^{-1} were obtained in cyclohexanone, isopropyl acetate, MIBK, ethyl lactate, furfuryl alcohol, γ-valerolactone, and propylene carbonate (**Table 1.7**), while lower catalytic performances (TOFs in the range 90 - 150 h^{-1}) were observed for p-cymene, BMIM-OTf and methyl levulinate (**Table 1.7**). Finally, limonene, cyrene, anisole, propionitrile and DMSO gave the worst catalytic performances (TOFs below 90 h^{-1}) owing to coordination of the solvent to the metal fragment (propionitrile in addition to DMSO) or low solubility of the starting material.

These results confirm our previous results concerning the hydration and alkoxylation of alkynes: a sustainable production of chemicals with homogeneous gold catalysts in neoteric solvents is reachable[171] and exploration of the use of gold catalysts in other nucleophilic addition reactions on substrates with unsaturated bonds (especially alkynes) in neoteric solvents is mandatory.

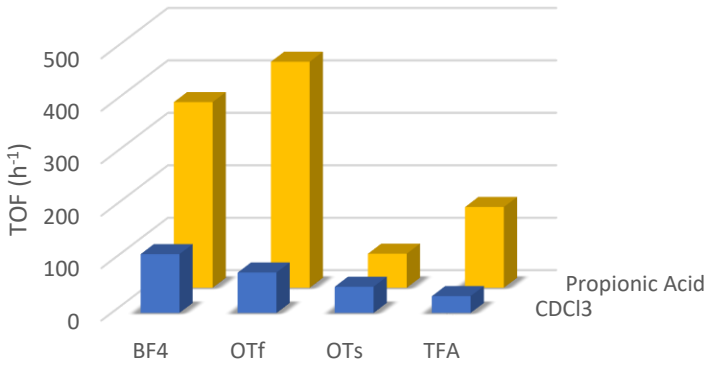

Figure 1.17: *TOF values for the cycloisomerization of N-(prop-2-yn-yl)benzamide to 2-phenyl-5-vinylidene-2-oxazoline catalyzed by IPr-Au-X (X^- = BF_4^-, OTf^-, OTs^-, and TFA^-) in $CDCl_3$[49] and propionic acid.*

In order to verify the importance of the acid-base nature and hydrogen-bond acceptor powers of the counterion in this reaction we have just considered (**Figure 1.17**) the catalytic properties of IPr-Au-X (X^- = BF_4^-, OTf^-, OTs^-, and TFA^-) in $CDCl_3$.[49] The catalyst activity is related to the basic strength of the anion and the performances of the catalysts decrease (**Figure 1.17**) gradually with increasing basicity and hydrogen-bond acceptor power of X^- (basic strength: BF_4^- < OTf^- < OTs^- < TFA^-). The plausible scenario for IPr-Au-X is that too basic anions with higher hydrogen-bond acceptor power (OTs^- and TFA^-) do not easily release the proton to gold thus slowing down the reaction rate. In addition, the higher coordination ability of TFA^- versus the IPr-Au^+ fragment probably favours the formation of the precatalyst IPr-Au-TFA during the catalysis.

In the case of propionic acid, OTf^- shows the best performance followed by BF_4^-. OTs^- exhibited the lower activity according to the previous study. On the other hand, the most basic anion TFA^- shows better results probably due to the acid environment that is able to protonate TFA^- disfavouring the formation of IPr-Au-TFA.

Summarizing, the experimental catalytic activity trend found here for the cyclization of propargylamides, namely, TFA^- < OTs^- < OTf^- < BF_4^-, shows that the performances of the catalysts increase gradually with decreasing coordinating ability and hydrogen-bond acceptor power of X^- (basicity and coordinating strength: BF_4^- < OTf^- < OTs^- < TFA^-), with TFA^- being by far the worst counterion. Thus, the results presented here show that the anion properties, both coordination ability and basicity (hydrogen-bond acceptor power), should have a great impact on its "proton shuttle ability". To elucidate the gold(I) catalytic activity in the cyclization of propargylamide, the

NHC*-Au-X (NHC* = 1,3-dimethylimidazol-2-ylidene; X^- = BF_4^-, OTf^-, OTs^-) complexes have been considered as catalysts and N-(prop-2-ynyl)benzamide as the substrate for the calculations (**Scheme 1.12**). The calculated reaction energy profiles for the nucleophilic attack step are shown in **Figure 1.18**.

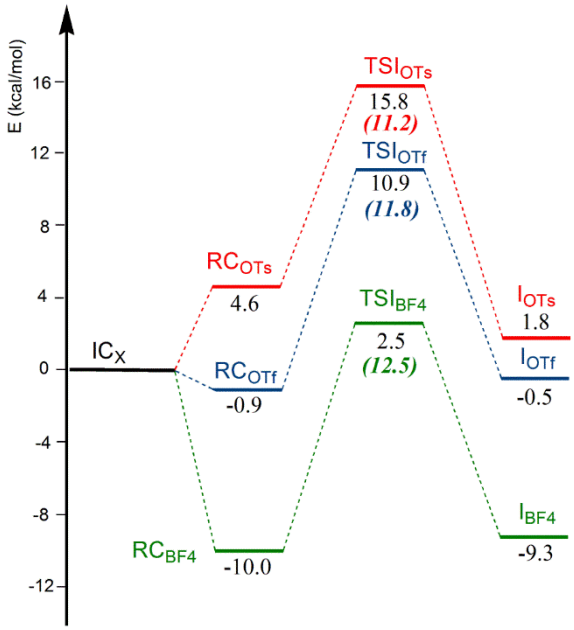

Figure 1.18: *Energy profiles for the nucleophilic attack step of the cycloisomerization of N-propargylcarboxamides reaction mechanism catalysed by NHC-*Au-X (X^- = BF_4^-, OTf^-, and OTs^-). Energy values (kcal/mol) refer to the corresponding IC_X taken as zero.*

The NHC*-Au-X initial complex (IC), with the N-(prop-2-ynyl)benzamide in the second coordination sphere, has been considered as zero energy reference structure for all the three anions. The displacement of the coordinated anion has been calculated to be a thermodynamically favourable process for BF_4^- (-10.0 kcal/mol) and OTf^- (-0.9 kcal/mol), leading to the corresponding reactant complexes RC_{BF4} and RC_{OTf}, where N-(prop-2-ynyl)benzamide is coordinated to gold and the anion is in the second coordination sphere weakly interacting with the NH moiety of the substrate through a hydrogen bond. The OTs^- replacement with the substrate is instead an endergonic process, yielding a destabilized RC_{OTs} (4.6 kcal/mol) through a calculated energy barrier of 11.8 kcal/mol and a tri-coordinated transition state where both N-(prop-2-ynyl)benzamide and OTs^- are bound to gold (see **Figure 3.34**). The optimized geometries of all species are shown in **Figure 3.35-4.37**. In all the RC complexes the counterion X^- is placed above gold, weakly interacting with the metal centre with at least one basic atom (Au···O = 2.903/3.579 Å for OTs^-, Au···O = 3.046/3.731 Å for OTf^-, and Au···F = 3.028/3.839 Å for BF_4^-) and forming a hydrogen bond with substrate NH group (NH···O = 1.789 Å

for OTs^-, NH···O = 1.808 Å for OTf^-, and NH···F = 1.757 Å for BF_4^-). Starting from these RC adducts, the oxygen atom of the substrate CO group intramolecular nucleophilic attack to one carbon atom of the activated triple bond can easily occur, with relativity low energy barriers (12.5, 11.8 and 11.2 kcal/mol for BF_4^-, OTf^- and OTs^-, respectively) (**Figure 1.18**). The nucleophilic attack energy barrier trend is consistent with the partial slippage away from the symmetrical η^2 coordination of the triple bond to gold favoring the charge transfer from the nucleophile to the distorted π system. In particular, the Au-C bond distances in the transition state (TSI) structures, which are depicted in **Figure 1.19**, can be related to the nucleophilic attack activation barrier.[50,165]

TSI geometry shows that the Au-C1 and Au-C2 bond distances are significantly different in all the cases, with the Au-C1 (with C1 representing the carbon atom undergoing the nucleophilic attack) amounting to 2.676 Å for OTs^-, 2.647 Å for OTf^- and 2.584 Å for BF_4^-. These values show that for the OTs^- anion-assisted attack, the largest $\eta^2 \rightarrow \eta^1$ deformation occurs, resulting in a more electrophilic C1 carbon atom and, consequently, in the lowest activation barrier.

By comparing the N-H distances (**Figure 1.19**), we note that they do not match the hydrogen-bond acceptor ability trend of the three anions (1.036 Å for OTs^-, 1.038 Å for OTf^-, and 1.029 Å for BF_4^-). Analogously, the X-Au distances do not follow the anion coordinating ability trend (Au···O = 3.146 Å for OTs^-, Au···O = 3.392 Å for OTf^-, and Au···F = 3.393 Å for BF_4^-). Thus, the activation energy barrier appears to arise as a balance between the anion hydrogen-bond acceptors and coordinating abilities (extent of alkyne slippage), suggesting an impact of the most coordinating and basic anion in enhancing the electrophilicity of the triple bond C atom.

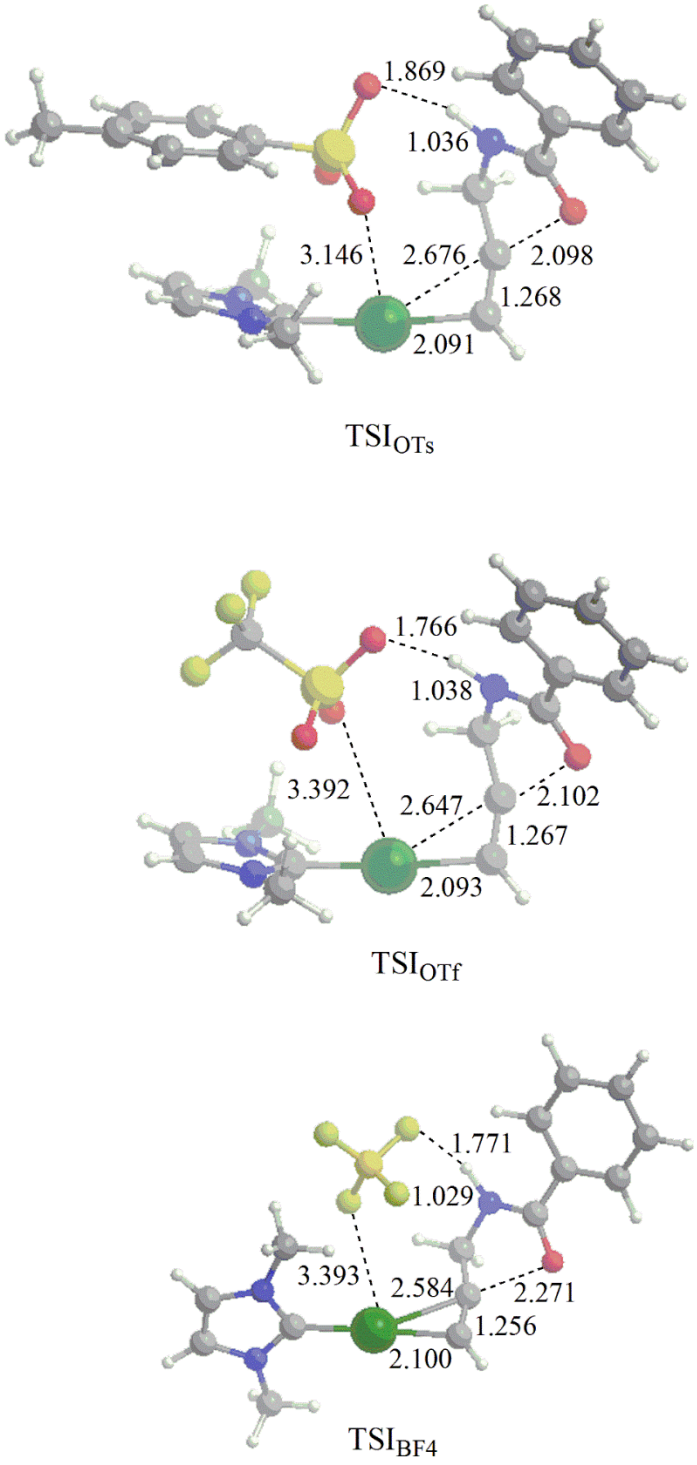

Figure 1.19: *Transition state (TSI) geometries for the nucleophilic attack step of the cycloisomerization of N-propargylcarboxamides reaction mechanism catalyzed by NHC*-Au-X (X^- = BF_4^-, OTf^-, and OTs^-). Bond lengths are in Å.*

Formation of the vinyl gold complex (intermediate I) from this step is a slightly endergonic process for OTf^- and BF_4^-, whereas it is exergonic for OTs^- (**Figure 1.18**). In the intermediate I, the acidic NH hydrogen should be transferred to the C2 carbon atom coordinated to Au by the anion, acting as

proton shuttle. To calculate the overall path starting from NH proton detachment, due to the very large number of different conformations involved, molecular dynamics simulations would be needed, which are beyond the scope of this work.

However, we started our analysis of the protodeauration step with a reactant complex consisting of a protonated anion HX interacting with the de-protonated substrate (RCII, see **Figure 3.38**) and the transition state for the final proton transfer from the anion to C2 (TSII) has been located here, which allows to completely rationalize the experimental findings.

Note that in the TSII structure for BF_4^- ($TSII_{BF4}$ in **Figure 1.21**), an incipient HF molecule is formed, as expected on the basis of BF_4^- instability to H^+ with respect to the HF elimination. For this reason, an additional water molecule has been included in the calculations to explore the protodeauration step for this anion (BF_4^-/H_2O). Energy profiles for the protodeauration step are shown in **Figure 1.20**.

The energy barrier calculated from RCII follows the trend BF_4^-/H_2O < OTf^- < OTs^- (1.3, 3.0 and 11.8 kcal/mol, respectively). However, for comparison with the nucleophilic attack step, the energy barrier should be calculated from the IC_X structure as reference since selection of any configuration of the RCII complex would be arbitrary.

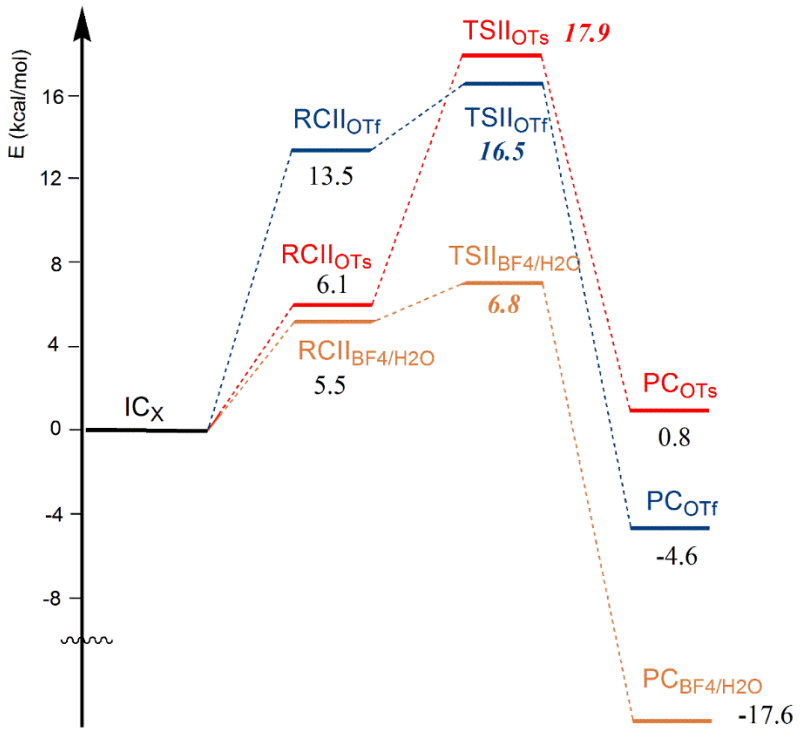

***Figure 1.20**: Energy profiles for the protodeauration step of the cycloisomerization of N-propargylcarboxamides reaction mechanism catalyzed by NHC*-Au-X (X^- = BF_4^-/H_2O, OTf^-, and OTs^-). Energy values (kcal/mol) refer to corresponding IC_X taken as zero.*

As it can be seen, this step requires a higher energy barrier than that of the nucleophilic attack step for all the three anions, in full agreement with the experimental observations (a calculation of the transition state TSI for the nucleophilic attack step including one additional water molecule shows that the energy barrier decreases from 12.5 for BF_4^- to 6.3 kcal/mol for BF_4^-/H_2O). The geometries of TSII are compared in **Figure 1.21**, whereas PC structures are reported in **Figure 3.39**.

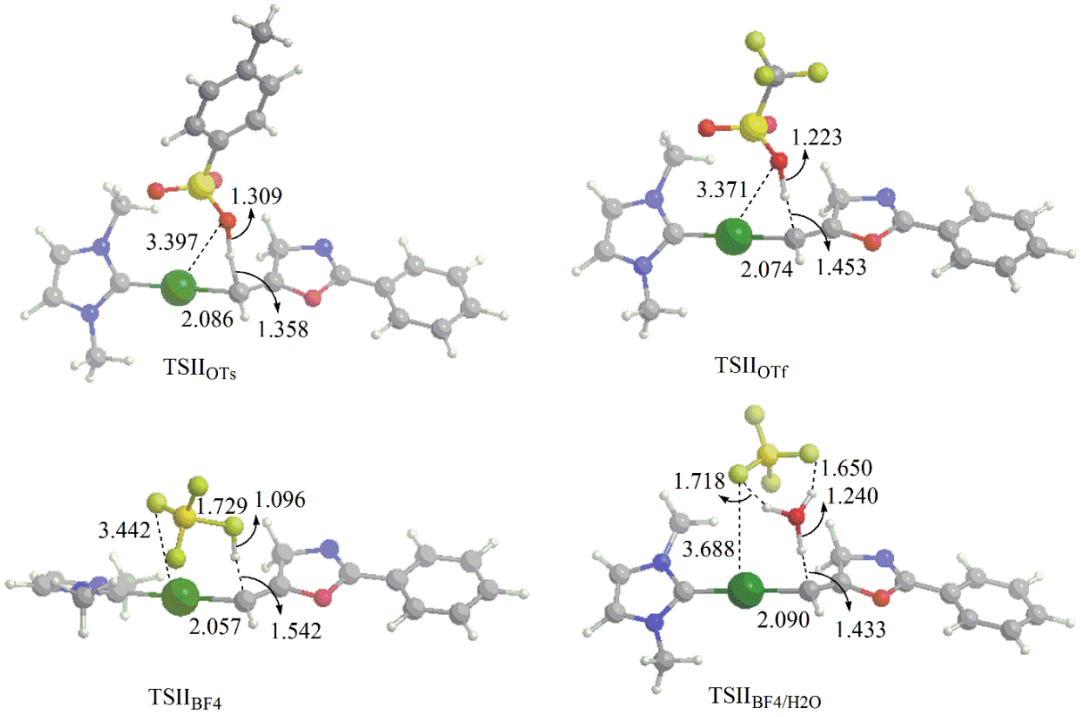

Figure 1.21: *Transition state (TSII) geometries for the protodeauration step of the cycloisomerization of N-propargylcarboxamides reaction mechanism catalyzed by NHC*-Au-X (X^- = BF_4^-,BF_4^-/H_2O, OTf^-, and OTs^-). Bond lengths are in Å.*

The protodeauration energy barrier trend exactly matches both that of the catalytic performances, namely BF_4^-/H_2O (6.8) > OTf^- (16.5 kcal/mol) > OTs^- (17.9 kcal/mol) and that of the anion basicity and hydrogen-bond acceptor power (BF_4^- < OTf^- < OTs^-), thus suggesting an impact of the anion in controlling the reaction rate through releasing of the proton to C2 atom bond to gold. Interestingly, inspection of the TSII structures in **Figure 1.21** reveals that neither the coordinating ability trend (Au···O = 3.397 Å for OTs^-, Au···O = 3.371 Å for OTf^-, and Au···F = 3.688 Å for BF_4^-/H_2O) nor the hydrogen-bond acceptor power (O···H = 1.309, H···C = 1.358 Å for OTs^-, O···H = 1.223, H···C = 1.453 Å for OTf^-, and O···H = 1.240, H···C = 1.433 Å for BF_4^-/H_2O) separately are able to account for the energy barrier trend, which rather arises from a balance between them. Overall, these results suggest that too basic anions with higher hydrogen-bond acceptor power (OTs^-) do not easily transfer the proton thus slowing the reaction rate, consistently with experimental findings.

2.2 Gold (III)

2.2.1 Hydration of alkynes

In this chapter we investigated the structure, catalytic properties and reactivity of [**2**-Cl]Cl and [**3**-Cl]OTf complexes in γ-valerolactone, under acid-free conditions, by means of solution NMR spectroscopic and computational (DFT) techniques.

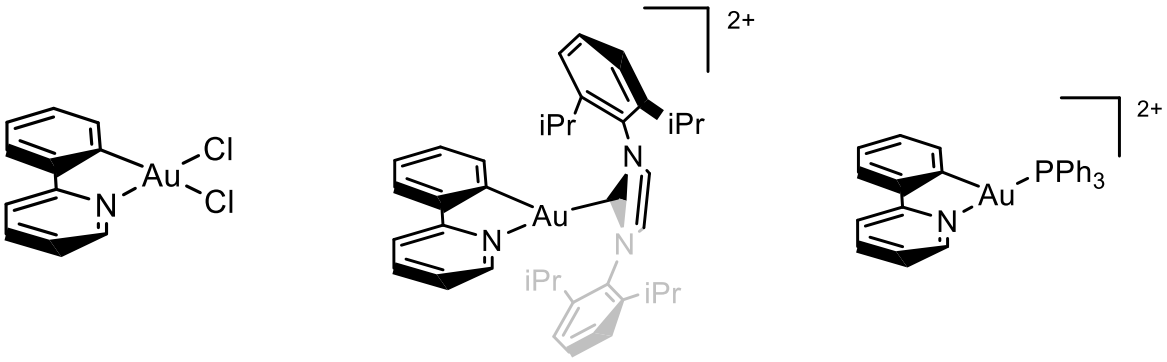

1 **2** **3**

The precursor compound (ppy)-Au-Cl_2 (**1**) was synthesized according to the literature[172] (see Experimental Section). From the reaction of **1** with a slightly excess of IPr·HCl and four equivalents of $KHCO_3$, complex [**2**-Cl]Cl was obtained in acetonitrile overnight, at room temperature, in air, and without the purification of the solvent or drying the salt, according to our previously reported procedure (see Experimental Section for details).[173] High yield and purity of the desired product has been given with this simple one-pot reaction, avoiding oxidative addition of diazonium salt by photoredox catalysis[174] that requires moisture- and air-free conditions or the use of silver salts.[175] Slight modifications of the literature procedures[176] led to the synthesis of the complex [**3**-Cl]OTf.

Elemental analysis and NMR spectroscopy were employed to analyze complexes [**2**-Cl]Cl and [**3**-Cl]OTf. All proton and carbon resonances were unequivocally assigned (see Experimental Section) from ^{1}H, ^{13}C, ^{1}H-^{1}H COSY, ^{1}H-^{1}H NOESY, ^{1}H-^{13}C HSQC, and ^{1}H-^{13}C HMBC NMR experiments.

The most important resonances for complex [**2**-Cl]Cl, of its ^{1}H, ^{13}C and ^{15}N NMR spectra, belonging to both ppy and IPr ligands and the most important NOE signals are shown in **Figure 1.22**.

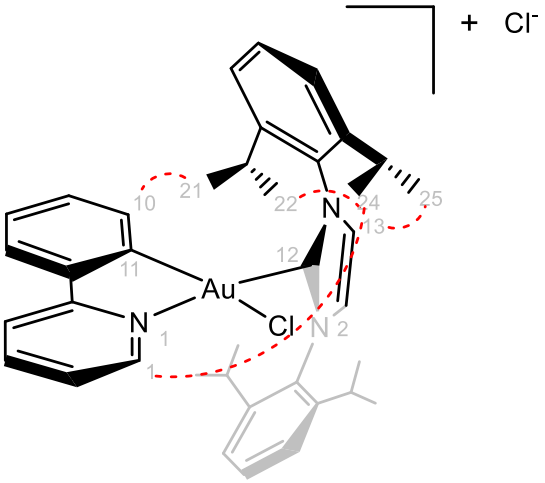

Selected δ (ppm)	
H1	9.27
H10	6.96
H13	7.88
H21	0.70
H22	1.23
H24	1.43
H25	1.09
C11	143.2
C12	149.2
N1	-147.7
N2	-189.8

Figure 1.22: *Numbering and chemical shift of the most relevant resonances of complex [**2**-Cl]Cl and the most important NOE signal for structure elucidation (in red).*

It is evident from these configurations of signals, that both ligands are coordinated to the metal center with IPr trans to the N atom of ppy, and that ligands are perpendicular one to each other, as such a configuration around the metal center leading to four different signals for the methyl groups of the isopropyl fragments of IPr (**Figure 1.22**).

Complexes [**2**-Cl]Cl and [**3**-Cl]OTf were employed as catalysts in the hydration of 3-hexyne to 3-hexanone. A standard catalytic run was performed by mixing the alkyne and 1.1 equivalents of H_2O in 400 µL of GVL, and in the presence of 1 mol% [**2**-Cl]Cl (or [**3**-Cl]OTf) and 2 mol% AgX (X^- = BF_4^-, OTf^-, SbF_6^-, and TFA^-) as the catalytic system at 50 °C. NMR spectroscopy was used to monitoring the progress of the reaction (see Experimental Section). The TOF value was calculated for each run to evaluate the catalytic activity in different conditions.

Table 1.8: *Complexes [2-Cl]Cl and [3-Cl]OTf (1 mol%) catalyzed hydration of 3-hexyne at 50 °C in GVL.*[a,b]

Entry	Complex	Additive	Conv. (%)[c]	TOF[d]
1	**1**	AgOTf	-	-
2	[**2**-Cl]Cl	-	-	-
3	[**3**-Cl]OTf	-	-	-
4	[**3**-Cl]OTf	AgOTf	58	14
5	[**2**-Cl]Cl	AgOTf	49	12
6	[**2**-Cl]Cl	AgTFA	4	1
7	[**2**-Cl]Cl	$AgSbF_6$	60	15
8	[**2**-Cl]Cl	AgOTs	20	5
9	[**2**-Cl]Cl	$AgBF_4$	44	11
10	[**2**-Cl]Cl	AgOAc	2	1
11[e]	[**2**-Cl]Cl	AgOTf	46	12
12[f]	[**2**-Cl]Cl	AgOTf	58	15

[a] Catalytic conditions: 3-hexyne (0.88 mmol, 100 µL), H_2O (1.00 mmol, 18 µL), [**2**-Cl]Cl or **2** (0.0088 mmol) and AgX (0.0166 mmol) in γ-valerolactone (400 µL). [b] mol% = (moles of catalyst / moles of alkyne) x 100. [c] Determined by ^1H NMR after 4h; averaged value of three measurements. [d] TOF = ($n_{product}$ / $n_{catalyst}$) / t(h) at 4h of conversion. [e] D_2O instead of H_2O (1.10 mmol, 20 µL). [f] in the presence of HOTf (0.043 mmol, 3.8 µL).

No conversion after 24 h (entries 1-3, **Table 1.8**) has been shown by the precursor **1** (activated by AgOTf) as well as [**2**-Cl]Cl and [**3**-Cl]OTf (without addition of the silver salt) at 50 °C. Trace amounts of product were observed after 24 h (entries 6 and 10, **Table 1.8**) with [**2**-Cl]Cl in combination with AgTFA and AgOAc. Conversely, with [**2**-Cl]Cl in the presence of AgOTf, $AgSbF_6$, AgOTs, and $AgBF_4$, (entries 5, 7, 8, and 9, respectively in **Table 1.8** are the conversions after 4 h) quantitative (> 95%) transformation of 3-hexyne into 3-hexanone was reached within 24 h. Also complex [**3**-Cl]OTf, in combination with AgOTf as halide scavenger, promoted the complete formation of 3-hexanone (entry 4 **Table 1.8**: 58% of conversion after 4 h).

The TOF value [TOF (h^{-1}) = ($n_{product}$) / $n_{catalyst}$) / 4h, **Table 1.8**] was calculated to compare the catalytic activity in different conditions. The values obtained for [**2**-Cl]Cl using $AgBF_4$, $AgSbF_6$ and AgOTf, and [**3**-Cl]OTf using AgOTf, are in the range 11-15 h^{-1}. Similar TOFs are reported in the literature for both inorganic salts or organometallic complexes of gold(III), although reflux of methanol/water mixture and use of acidic conditions were frequently employed.[100,118,177–180] When [**2**-Cl]Cl is used in

combination with AgOTs (**Table 1.8** entry 8) about half value of TOF is obtained. This result, jointly with the poor activity of the AgTFA and AgOAc catalytic system (**Table 1.8** entries 6 and 10), suggests a precise role of the anion during the reaction, as already observed for gold(I) catalysis.[181,182]

In the catalytic behavior of [**2**-Cl]Cl the counterion effect suggests that the coordination of the substrate could be the key step and high conversion into ketone has been found only in the case of low and intermediate strength co-ordinating anions (SbF_6^-, BF_4^-, OTf^-, and OTs^-) whereas, if anions with stronger co-ordinating properties (TFA^-, Cl^-, and OAc^-) are employed, poor or no catalytic activity has been observed.

Before starting the study of the mechanism, we were interested in the stability in solution of the catalytic systems employed in the hydration reaction. Therefore, complex [**3**-Cl]OTf and AgOTf were mixed with 10 equivalents of 3-hexyne and water in acetone-d_6. The characteristic broad signal at 43.46 ppm in the ^{31}P-NMR spectrum (see Experimental Section for details) disappeared immediately and the contemporary formation of several sharp signals, indicated the formation of different PPh_3-containing compounds. In particular, the signals at 45.00 ppm and 25 ppm related to the well-known $[PPh_3\text{-Au-}PPh_3]^+$ cation and $O{=}PPh_3$, respectively, were observed.[132,133,183] Complex [**3**-Cl]OTf was not further considered for the mechanistic study because of its clear decomposition with formation of gold(I) new species which are able to catalyze the reaction.

A sample was prepared by mixing the complex [**2**-Cl]Cl, 1.2 equivalents of $AgBF_4$ and 10-fold amount of water in acetone-d_6, in order to study the stability of [**2**-Cl]Cl in catalytic conditions (**Table 1.9** solution A). As can be observed in **Table 1.9** (see Experimental Section for details) the ^{1}H, ^{13}C-DEPT and ^{1}H-^{15}N HMBC NMR spectra were quite similar to those of complex [**2**-Cl]Cl in deuterated acetone. The spectra indicate that phenylpyridine is still chelated to Au. In particular, H1 is at 8.69 ppm, C11 at 143.2 ppm, and N1 at -147.7 ppm.[184]

For the IPr ligand the resonances of the four doublets in the aliphatic region belonging to the methyl groups are at 0.94, 1.33, 1.46, 1.13 ppm, C12 is at 150.3 ppm and that of N2 is at -190.0 ppm (**Table 1.9**). These patterns assess the simultaneous coordination of the N1 and C11 of ppy and C12 of IPr (Experimental Section and **Figure 1.22**), confirming the integrity of the structure of the gold(III) complex before starting the catalysis. Then, 10 equivalents of 3-hexyne were added to the mixture and the catalysis started. ^{1}H, ^{13}C-DEPT and ^{1}H-^{15}N HMBC NMR spectra were again recorded at 30% of conversion (**Table 1.9** solution B). As a matter of fact, the spectra are similar to those previously recorded (solution A) (see Experimental Section for details).

The complex [**2**-H_2O]$(BF_4)_2$ was prepared in-situ in an NMR tube in order to deeply understand the nature of gold(III) species in solution during the catalysis. All proton and carbon resonances belonging to the different fragments were unequivocally assigned (see Experimental Section) from ^1H, ^{13}C, ^1H-^1H COSY, ^1H-^1H NOESY, ^1H-^{13}C HSQC, and ^1H-^{13}C HMBC NMR spectra recorded in CD_2Cl_2. Selected chemical shifts match with those observed for solution A (**Table 1.9**). In particular, the coordination of water to gold (replacing inner the Cl^- ion) shifted the proton resonance of H1 from 9.27 ppm to 8.75 ppm and for the resonances of carbons C11 and C12 from 143.2 and 149.2 to 143.05 and 150.6 ppm, respectively (**Figure 1.22** and **Table 1.9**). Finally, in the ^1H-^1H NOESY spectrum an intense NOE between the signal of H1 and that of water at 1.76 ppm can be observed. From these patterns of signals, it seems clear that the predominant complex present in solution during the catalysis is the water adduct [**2**-H_2O]$^{2+}$.

***Table 1.9**: Selected ^1H, ^{13}C, ^{15}N chemical shift (ppm) of 1, 3 and solutions A and B (see text) in acetone-d_6*

	1	**3**[a]	**A**	**B**
H1	9.28	8.75	8.72	8.72
H13	8.58	7.71	8.31	8.32
H21	0.76	0.94	0.92	0.93
H22	1.23	1.33	1.26	1.25
H24	1.49	1.46	1.45	1.46
H25	1.15	1.13	1.11	[b]
C11	143.2	143.1	143.0	143.3
C12	149.2	150.6	150.3	150.2
N1	-147.7		-144.1	-144.2
N2	-189.8		-190.0	-190.0

[a] Recorded in CD_2Cl_2. [b] Superimposed with signals of both substrate and reaction product.

The stronger Au-IPr bond (with respect to the Au-PPh_3 one)[185–187] allows the metal to maintain its +3 oxidation state during the entire catalytic cycle, avoiding the reduction to Au(I) and/or to Au(0) nanoparticles. To confirm the absence of Au(I) catalyst in solution, the [IPr-Au-Cl]/AgOTf system was examined as catalyst for the hydration of 3-hexyne in the same exact conditions employed for [**2**-Cl]Cl and higher TOF of 115 h^{-1} was obtained (see Experimental Section for details).

During the hydration reaction, two of the three coordination sites in [**2**-Cl]Cl are occupied by ppy and IPr ligands, and only one site is accessible for the substrate/nucleophile species. Therefore, presumably a possible mechanism for the gold(III) catalyst can be similar to that accepted for Au(I) (**Scheme 1.13**) for the hydration of alkynes. The metal fragment acts as a Lewis acid by coordinating 3-hexyne, which consequently undergoes a nucleophilic attack by water, with the formation of an organogold intermediate. The gold–carbon bond is typically split by a proton (protodeauration), leading to the vinyl alcohol and regenerate the catalyst. In the end, keto-enol tautomerization provides the desired product. To better understand the reaction mechanism, we decided to analyze the influence of acid additives and the kinetic isotopic effect (KIE) for the evaluation of the rate determining step, the order of reaction with respect to catalyst, alkyne and nucleophile and, finally, the effect of the temperature.

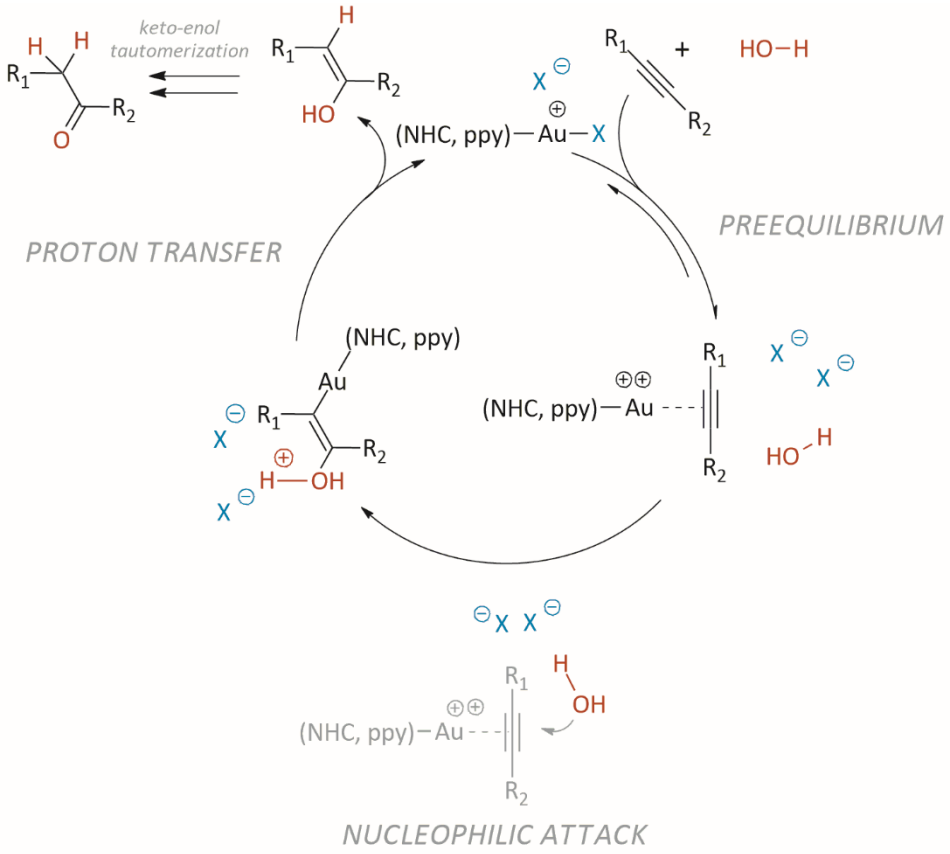

Scheme 1.13: *Proposed mechanism for the alkyne hydration reaction catalyzed by complex [**2**-Cl]Cl.*

D_2O was used instead of H_2O (entry 11, **Table 1.8**) to calculate the KIE. Similar values of TOF (compare entries 5 and 11 in **Table 1.8**) indicated that KIE is close to one, thus suggesting that the

proton transfer is not the RDS. This is confirmed also by the addition of trifluoromethanesulfonic acid (5% mol with respect to 3-hexyne; entry 12, **Table 1.8**) that only slightly accelerates the progress of the reaction. The H^+ ions therefore do not play an active role during the catalysis and, more importantly, the acidic environment does not poison the catalyst. In part these first findings disagree with those reported in the literature: the addition of acid generally increases the reaction rate[100,118,177–180] and, moreover, the acidic condition could favored the protonation of the gold-carbon bond of the cyclometalated ligand.[188]

In the presence of identical amounts of 3-hexyne and H_2O, when the loading of [**2**-Cl]Cl was increased from 0.2 to 2% (entries 1-5, **Table 1.10**) an increasing of the conversion (after one hour) was observed.[189] In particular, it can be observed (**Figure 1.23**) a linear growth of the conversion with catalyst concentration. As the case of the methoxylation of alkynes promoted by IPr-gold complexes[48] this trend suggests a 1st order dependence on the catalyst. Furthermore, giving an almost constant value of TOF (entries 1-5, **Table 1.10**), it can be asserted that only one gold atom is involved in the reaction.

Table 1.10: *Hydration of 3-hexyne at 50 °C in GVL catalyzed by **1**[a]*

Entry	Conc. (%)	Conv. (%)[b,c]	TOF[d] (h^{-1})
1	0.2	3	13
2	0.5	7	14
3	1.0	13	13
4	1.5	19	13
5	2.0	24	12

[a] Catalytic conditions: 3-hexyne (0.88 mmol, 100 µL), H_2O (1.00 mmol, 18 µL) in GVL (400 µL). [b] mol% = (moles of [**2**-Cl]Cl / moles of alkyne) x 100. [c] Determined by ^1H NMR after 1h; averaged value of three measurements. [d] TOF = ($n_{product}$ / $n_{catalyst}$) / 1 h.

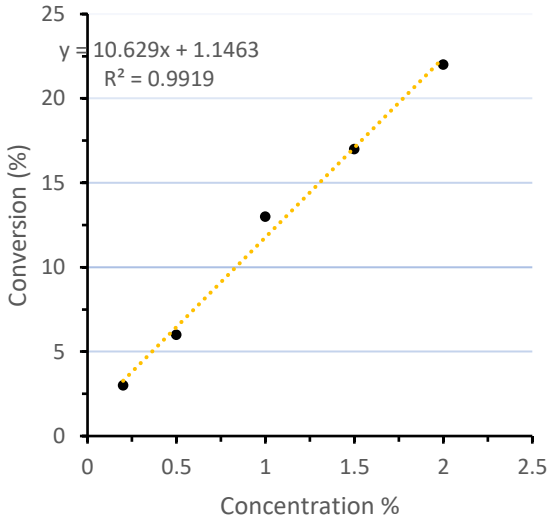

Figure 1.23: *Substrate conversion after one hour of hydration of 3-hexyne vs. concentration of [**2**-Cl]Cl.*

*Table 1.11: Hydration of 3-hexyne at 50 °C in GVL catalysed by [**2**-Cl]Cl* [a]

Entry	3-hexyne (µL)	Water (µL)	Conv. (%)[b]	Time[c] (h) (TOF[d])
1	50	18	91	4(11)
2	100	18	93	8(12)
3	200	18	44	8(11)
4	100	36	87	8(11)
5	100	54	87	8(11)

[a] Catalytic conditions: [**2**-Cl]Cl (0.0088 mmol) and AgOTf (0.0166 mmol) in GVL (amount necessary to reach a final volume of 518 µL). [b] Determined by ^{1}H NMR; average value of three measurements. [c] Time necessary to reach the reported conversion. [d] TOF = ($n_{product}$ / $n_{catalyst}$) / t(h) at the reported conversion.

Subsequently, the effect of alkyne and water concentration on the reaction rate (the results are collected in **Table 1.11**) was determined. A standard catalytic run was performed by maintaining constant both the loading of the catalyst (0.0088 mmol) and the final volume (518 µL). The volume of 3-hexyne (50, 100 and 200 µL, entries 1-3, **Table 1.11**) and water (18, 36, 54 µL, entries 1, 4, and 5, **Table 1.11**) were varied. About the same value of TOF was obtained (around 11-12 h^{-1}) suggesting a pseudo-zero order reaction with respect to both reagents. In the gold(I) catalyzed addition of a nucleophile to an unsaturated bond,[48,181,182,190,191] a pseudo-zero order reaction with respect to the substrate is frequently observed, contrarily a pseudo first-order reaction with respect to the nucleophile is observed when the RDS is the nucleophilic attack.[48,181,182,190,191]

In the past the hydration of alkynes promoted by gold(III) has not been deeply studied (see the Introduction) and the activation energy (E_a) has not been experimentally evaluated yet. For the hydration of 3-hexyne, catalyzed by [**2**-Cl]Cl/AgOTf, the measurement of the activation parameters was obtained by conducting the catalysis in the temperature range between 313-393 K, and by monitoring the reaction through in situ ^{1}H NMR spectroscopy. The results are collected in **Table 1.12** and **Figure 1.24**.

The activation energy (E_a) was obtained from the slope of the plot of ln(TOF/T) against 1/T (**Figure 1.24**) on the basis of the Arrhenius equation: $\ln(TOF/T) = \ln(A) - E_a/RT$. From the **Figure 1.24**, we determined the activation energy equal to 46.6 kJ mol^{-1} (11.1 kcal mol^{-1}). In the alkoxylation of 3-hexyne catalyzed by [NHC-Au-OTf][191] we obtained a higher value of activation enthalpy (16.7-18.1 kcal mol^{-1}) and, furthermore, a much higher activation energy value (15.2 kcal mol^{-1}) was reported

by Nevado and co-workers[192] in their studies on the gold(I)-catalyzed oxidative coupling of arylsilanes and arenes.

Table 1.12: *Complex [**2**-Cl]Cl catalyzed hydration of 3-hexyne in GVL[a,b] at different temperatures.*

Entry	Temp. (K)	Time (min)[c]	TOF[d] (h^{-1})
1	313	396	8
2	323	205	14
3	338	92	30
4	353	28	57
5	393	12	252

[a] Catalytic conditions: 3-hexyne (0.88 mmol, 100 µL), H_2O (1.00 mmol, 18 µL), [**2**-Cl]Cl (0.0088 mmol, 9.1 mg) and AgOTf (0.0166 mmol) in GLV (400 µL). [b] mol% = (moles of catalyst / moles of alkyne) x 100. [c] Time necessary to reach 50% conversion, determined by ^{1}H NMR; averaged value of three measurements. [d] TOF = ($n_{product}$ / $n_{catalyst}$) / t(h) elapsed, at the reported conversion.

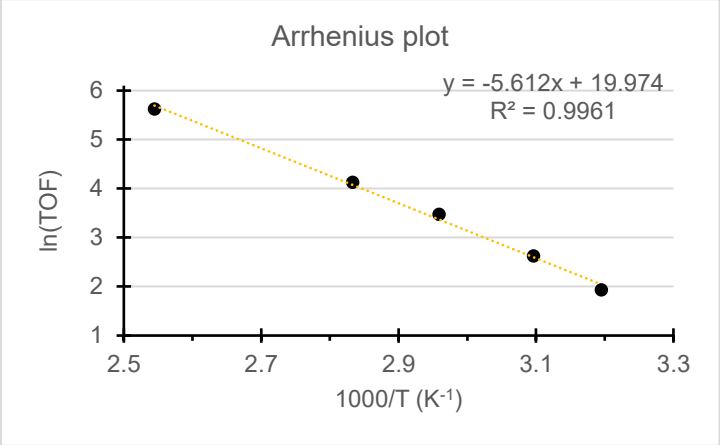

Figure 1.24: *Arrhenius plot at 50% of conversion of hydration of 3-hexyne catalyzed by [**2**-Cl]Cl.*

It can be reasonably argued that of the whole mechanistic investigated, only one gold atom is involved in the rate determining step of the reaction. The nucleophilic attack or the protodeauration are excluded to be the RDS. DFT calculations have been performed (see Computational Details in the Experimental Section) to shed light on these intriguing results.

The nucleophilic attack step is commonly known to be the RDS for gold(I)-catalyzed alkyne hydration and alkoxylation reactions,[126,127,157,158] and we started our study by examining this step. For the triple CC bond, we found the larger σ donation and smaller π back-donation in Au(III)-alkyne system, compared to the Au(I) ones, and this result leads to a more effective activation towards nucleophilic

attacks combined with a greater CC polarization.[193] For the calculations the [(ppy)-Au-NHC*-OTf]OTf (NHC* = 1,3-dimethylimidazol-2-ylidene) was considered as model for catalyst [**2**-Cl]Cl, 2-butyne and water have been chosen as substrate and nucleophile respectively. A low energy barrier of 5.6 kcal/mol (at BP86/B2PLYP level) was calculated. The starting complex for the study of the nucleophilic attack process, is the reactant complex RC, where 2-butyne is coordinated to gold in trans position with respect to the C atom of the ppy ligand. The inner triflate passes in the second sphere such as the other OTf^- and the water molecule. In **Figure 1.25** the optimized geometry is shown. The two OTf^- anion are placed one above the ppy-Au plane, with a week interaction with the metal (Au···O = 2.821 Å), and the other forms a hydrogen bond with the water. The oxygen atom of water is at about 3.1 Å distance from the closest carbon atom of the coordinated alkyne. We considered the above conformation because it bears some analogy to the gold(I) RC complexes,[157,158] nevertheless, different positions of the triflates are possible. Interestingly, the bond distances between the gold and the two alkynic carbons are significantly different (Au-C1 = 2.477Å and Au-C2 = 2.353 Å). C1 is the carbon placed at the same side of the OTf^- anion while and C2 is the 2-butyne carbon atom at the opposite side. It is known that the consequences of the alkyne coordination to gold center are the lengthening of the triple bond (1.234 Å in RC), and the alkyne distortion from linearity. A larger distortion is observed at C2 in RC with a CH_3-C2-C1 bond angle of 162.5° whereas the CH_3-C1-C2 bond angle is 169.1°. Compared to the corresponding RC for [IPr-Au(I)]$^+$ with the OTf^- anion:[158] i) the nucleophile is activated by the water bearing one anion for an outer-sphere addition and ii) although in gold(I) species a single anion is able to perform both the roles, acting as template, here the anion just weakly interacting with gold.

The nucleophilic attack activation barrier can be related to the Au-C bond distance depending on the carbon atom undergoing the nucleophilic attack.[50] In fact, the charge transfer from the nucleophile to the distorted π system is favored by the partial slippage from the symmetrical η^2 coordination of alkyne to gold and, in particular, to the carbon atom of the triple bond farther away from gold.[165] For this reason, the nucleophilic attack of water has been calculated both for C1 and C2, since different Au-C1 and Au-C2 bond distances were observed. The two profiles are compared in **Figure 1.25**. A lower activation energy barrier is calculated for C1 with respect to that for the water attack towards C2 (C1: 5.6 vs. C2: 7.8 kcal/mol). In the absence of the second counterion the lowest barrier from RC amounts to 5.6 kcal/mol is in agreement with the value calculated in ref. [193]. The transition states evolve to the vinyl gold intermediates PC_{C1} and PC_{C2}, which are more stable than RC by 5.9 and 5.2 kcal/mol, respectively (**Figure 1.26**). Main geometrical parameters of all

nucleophilic attack transition states and products with optimized geometries are reported in **Figure 1.25**.

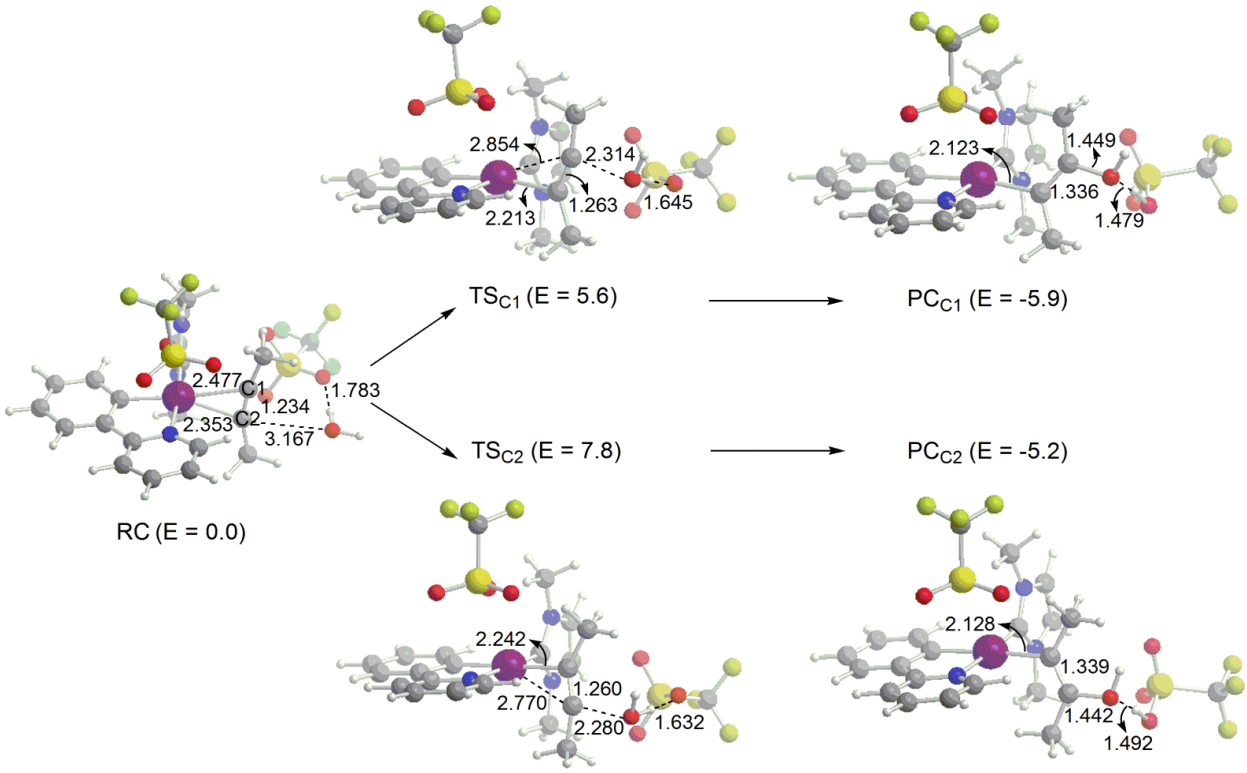

Figure 1.25: *Reactant complex RC, transition state TS and product complex PC for the water nucleophilic attack towards 2-butyne C1 and C2 carbon atoms. Energies values (kcal/mol) refer to corresponding RC taken as zero. Bond lengths are in angstroms.*

The gold-carbon bond distances can be considered as a reactivity index related to the nucleophilic attack activation barrier. Weak interaction of the anion with gold on the same side of the 2-butyne C atom could have a role in the partial slippage away from the symmetrical η^2 alkyne coordination to gold. In the absence of both the anions, the geometry optimization of the reactant complex shows that the two Au-C1 and Au-C2 bond distances within $RC_{noanion}$ (2.477 and 2.475 Å) are only slightly different (**Figure 3.40** in the Experimental Section) confirming that the anion above the ppy-Au plane should be responsible for their different values in the RC structure in **Figure 1.25**.

Confirming what found in in ref. 193, gold(III) species are generally much more efficient in the triple bond activation than gold(I) species to the point that the nucleophilic attack for the investigated reaction was not the rate determining step. Moreover, inclusion of the second counterion seems to affect only slightly the nucleophilic attack process.

The pre-equilibrium step was then considered, beginning by looking for the most stable species formed by the di-cationic gold catalyst [(ppy)-Au-NHC*]$^{2+}$, the 2-butyne substrate, the H_2O nucleophile and the two OTf^- anions. For the study of this process, the initial complex IC were: the [(ppy)-Au-NHC*-OTf]OTf complex where one OTf^- anion is directly coordinated to gold, and water and 2-butyne (and the second anion) are in the second coordination sphere. In **Figure 1.26** the optimized geometry is shown. The substitution of the anion by the alkyne is the first step of the catalysis, leading to the reactant complex RC previously analyzed. The optimized geometry of the species where the anion is replaced by water (IC_{H2O}) is shown in **Figure 1.26**. Due to the interaction with the anion, the water (OTf···HOH distance 1.481 Å) coordinated to gold shows one elongated O-H distance (1.046 vs. 0.993 Å) in the IC_{H2O} species, leading to a coordinated incipient "OH" group (**Figure 1.26**). This species could be responsible for catalyst deactivation, making the alkyne substitution difficult. Indeed, the anion substitution by the water molecule is thermodynamically favored (-3.6 kcal/mol). Then, the coordination of 2-butyne to the metal center requires the displacement of the water. The calculated transition state for this process is also shown in **Figure 1.26**.

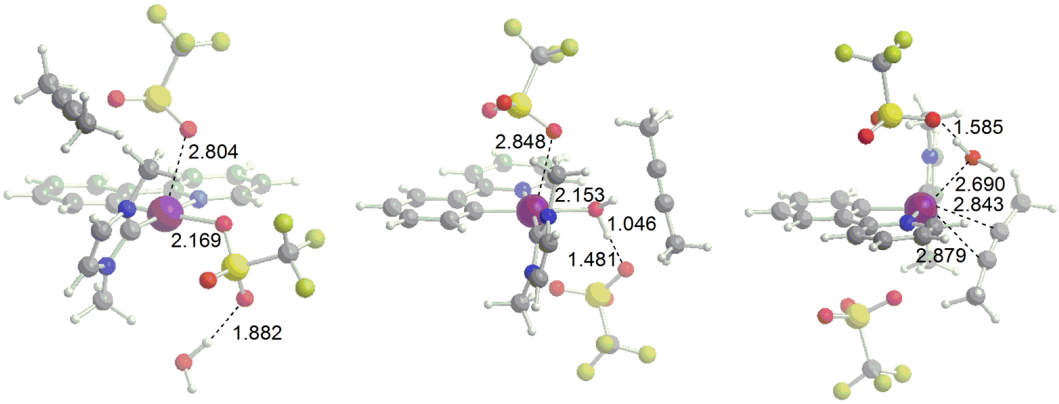

Figure 1.26: *Optimized geometries of the initial complex IC, water adduct IC_{H2O}, and transition state for the water substitution by 2-butyne process (pre-equilibrium step) TS. Distances are in angstroms. Energy values (kcal/mol) refer to IC taken as zero.*

An activation barrier energy of 19.6 kcal/mole has been calculated for the pre-equilibrium. The structure of gold is penta-coordinate in the transition state, with water and 2-butyne in the inner sphere and the triflate, initially above the gold-phenylpyridine plane, moves away from the metal center, forming a hydrogen bond with the water molecule. The pre-equilibrium and the nucleophilic attack step reaction energy profile (red line) are summarized in **Figure 1.27**.

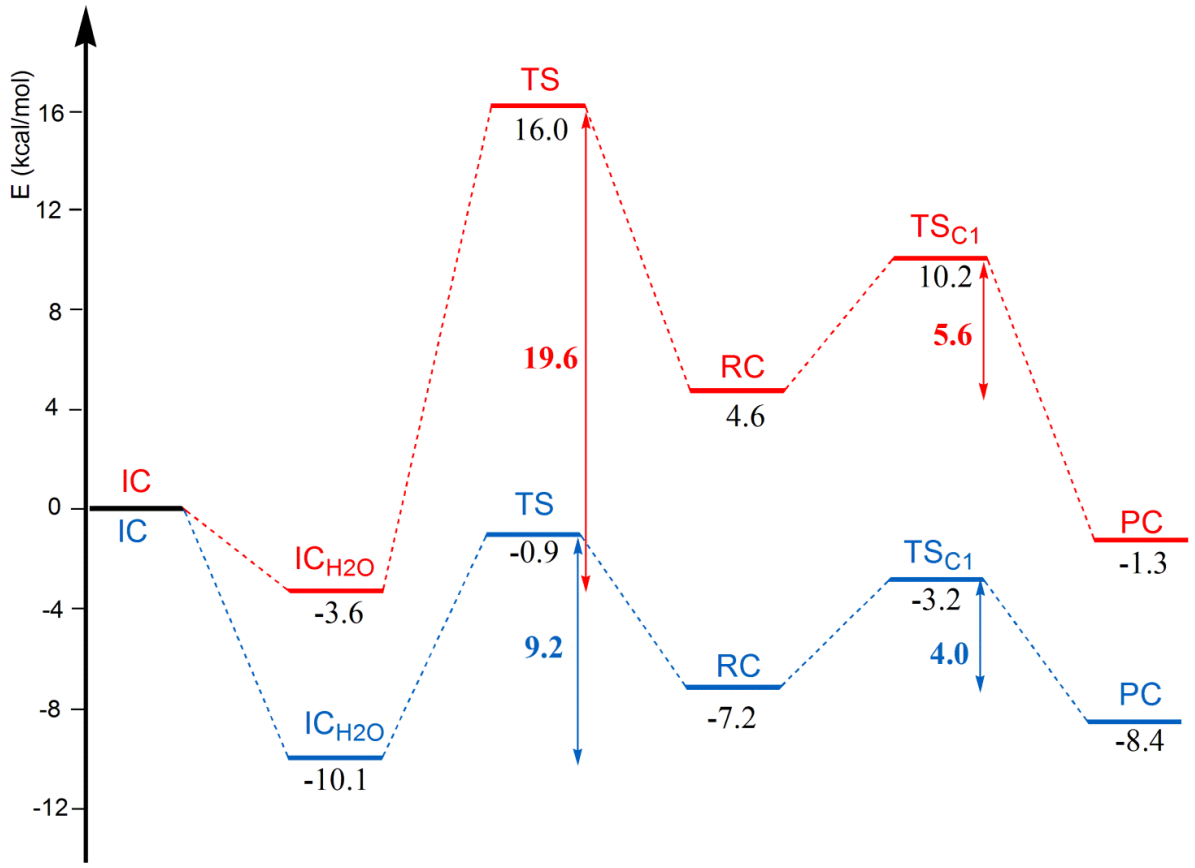

Figure 1.27: *Reaction energy profiles for the pre-equilibrium and nucleophilic attack steps calculated at BP86/B2PLYP level of theory in gas phase (red line) and at BP86+D/COSMO level including solvent (blue line). Energy values refer to corresponding IC taken as zero.*

The involvement of both the alkyne and the water clearly indicate that the pre-equilibrium is the rate-determining step, and it is fully consistent with the experimental results.

The activation energy obtained experimentally (11.1 kcal/mol) is almost half compared to the calculated one (19.6 kcal/mol). The solvent can influence this activation barrier and, therefore, COSMO single point calculation was carried out on IC_{H2O} and TS structures. Nitromethane was used as solvent since its dielectric constant is very close to that of GVL ($\varepsilon_{\text{nitromethane}} = 37.3$, $\varepsilon_{\gamma\text{-valerolactone}} = 36.9$) which is not available in ADF program package. In addition, we observed that inclusion of solvent in conjunction with B2PLYP functional in ORCA is not feasible, therefore we compared first the gas phase BP86 and BP86 including dispersion correction (BP86+D) energies as a preliminary test for the dispersion effect (which is already included in the B2PLYP functional). A value of 22.8 kcal/mol was found for gas phase BP86 activation energy barrier, whereas gas phase BP86+D value is 15.8 kcal/mol. So, consistently with the BP86/B2PLYP result (19.6 kcal/mol), the inclusion of dispersion decreases the barrier. After that, we performed BP86+D/COSMO single point calculations

to get an estimate of the combined dispersion and solvent effects on the pre-equilibrium barrier which give a value of 9.2 kcal/mol. As result of this, solvent inclusion further decreases the pre-equilibrium BP86+D activation energy barrier by 6.6 kcal/mol. Thus, the solvent effect largely improves in agreement with experiment (9.2 vs. 11.1 kcal/mol). Also, for the nucleophilic attack step we performed BP86+D/COSMO single point calculations and in **Figure 1.27** (blue line) the overall reaction profile is shown. Remarkably, the inclusion of the solvent largely stabilizes the IC_{H2O} complex with respect to IC (-10.1 kcal/mol) and slightly decreases the nucleophilic attack energy barrier (4.0 kcal/mol). In conclusion, the water disfavors the reaction as well as the high reactivity of Au(III)-alkyne make it difficult to isolate and characterize. In agreement with the experimental evidence, the large stability of the IC_{H2O} complex makes the water adduct with gold the predominant species for the whole catalysis.

2.2.2 Preequilibrium study

Compared to Au(I),[53–63] catalysis by Au(III) is far less developed and much more challenging. Au(III) easily tends to reduce to Au(I) or Au(0) if electron-rich species are present in the reaction environment.[86–93] On the other hand, the ligands that completely stabilize the charge of the metal generate a catalytically non-active complex.[194] A theoretical study by some of us on the alkyne activation with Au(III) complexes with different pincer ligands has shown that the Au(III)-alkyne complexes very efficiently activate the alkyne triple bond to the point that the nucleophilic attack step could cease to be the rate determining step (RDS) of the reaction, at variance with Au(I)-alkyne complexes.[193] Then, other steps of the catalytic cycle, particularly the pre-equilibrium, were suggested to be a key step for the reaction. The mechanism of the hydration of 3-hexyne catalyzed by [**2**-Cl]Cl in γ-valerolactone (GVL) as the solvent has been investigated (chapter 2.2.1) by some of us both experimentally (NMR) and computationally (DFT), demonstrating that the pre-equilibrium step is effectively the RDS.

The aim of this chapter is exactly to computationally investigate the coordination ability of catalytic Au(III) complexes and its dependence on the ancillary ligands on the basis of the experimental results acquired by studying the alkyne hydration reaction.

Experimental results on the coordination ability of 2

The catalytic activity of [**2**-Cl]Cl in the hydration of alkyne (3-hexyne) have shown a not completely satisfactory efficiency of this complex.[193]

The reactivity of [**2**-Cl]Cl towards the addition of $AgBF_4$ or AgOTf in different solvents, in the presence of 3-hexyne or water was studied, in order to characterize and isolate the reaction intermediates of the pre-equilibrium step of the hydration reaction mechanism, namely the complexes [**2**-(3-hexyne)]$^{2+}$, [**2**-H_2O]$^{2+}$, [**2**-OTf]$^{+}$, and [**2**-BF_4]$^{+}$, The starting complex (or pre-catalyst) [**2**-Cl]Cl coordinates the chloride ions in the first and second coordination shells. To coordinate and activate the 3-hexyne substrate, the Cl^- must be removed. Experimentally, this step requires the addition of silver salts, and therefore AgOTf and $AgBF_4$ were used to remove the Cl^- ions in different conditions (**Scheme 1.14**).

By reacting in a NMR tube [**2**-Cl]Cl with 2 equivalents of $AgBF_4$ in non-anhydrous CD_2Cl_2 were generated [**2**-H_2O]$(BF_4)_2$ and [**2**-BF_4]BF_4 complexes (see Experimental section for details). From ^{1}H, ^{13}C, ^{1}H-COSY, ^{1}H-NOESY, ^{1}H,^{13}C-HSQC NMR, and ^{1}H,^{13}C-HMBC NMR spectroscopies all proton and

carbon resonances belonging to the different fragments of both complexes were assigned (see Experimental section). The two complexes are present in about equal amount (52% of [**2**-BF_4]BF_4) and monitoring the chemical exchange between the two resonances of proton H1 (**Scheme 1.14**) by qualitative ^{1}H-EXSY NMR experiments allowed to extract the rate constant (k_{obs}) for their interconversion, k_{obs} was found to be 1.0 s^{-1}.

10 equiv. of 3-hexyne were added to the CD_2Cl_2 solution containing [**2**-H_2O]$(BF_4)_2$ and [**2**-BF_4]BF_4, in order to synthesize the complex [**2**-(3-hexyne)]$(BF_4)_2$, but no variations of the resonances belonging to both complexes were observed, indicating that no formation of the desired product did occur. On the contrary, the addition of 5 equiv. of water quantitatively shifted the [**2**-H_2O]$(BF_4)_2$/[**2**-BF_4]BF_4 equilibrium towards the former.

Following the same procedure, we decided to try to synthesize [**2**-H_2O]$(OTf)_2$ and [**2**-OTf]OTf complexes, but the formation of [**2**-Cl]OTf was obtained (**Scheme 1.14**). The addition of 4 equiv. of AgOTf to a solution of [**2**-Cl]Cl in acetone at 50 °C overnight gave the formation of a mixture of [**2**-Cl]OTf, [**2**-OTf]OTf, and [**2**-H_2O]OTf in 0.22, 0.70, 0.08 ratio (see Experimental Section for details). Also in this case, the addition of 10 equiv. of 3-hexyne to a CD_2Cl_2 solution of the mixture did not change its composition, while the addition of water gave the formation of a mixture of [**2**-Cl]OTf and **2**-H_2O]OTf.

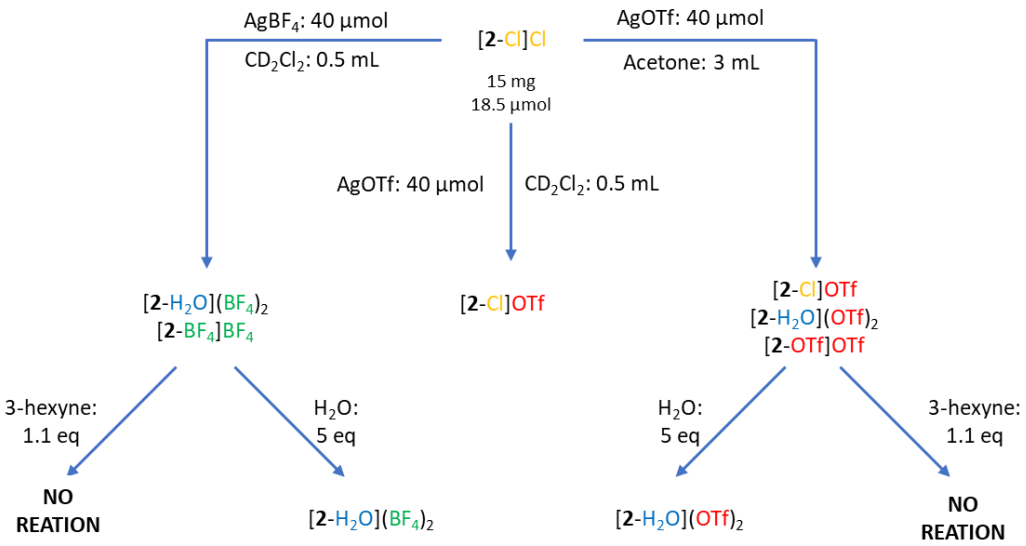

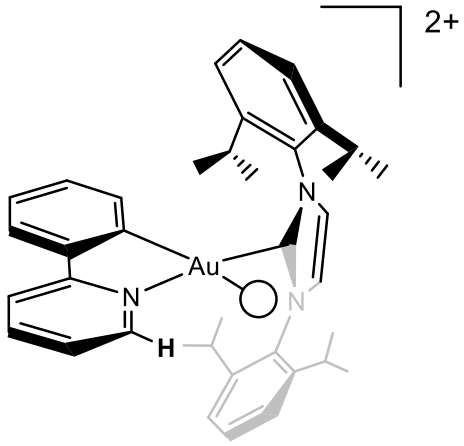

Scheme 1.14: *The reactions studied in this work.*

In summary, 3-hexyne does not coordinate to the **2** fragment when BF_4^-, OTf^- or water are present into the mixture. In addition, BF_4^- and OTf^- showed the same coordinating ability towards **2** and slightly less than water. To date, only the water-containing species [**2**-H_2O]BF_4 can be isolated and characterized, consistently with the highly reactive character of the catalyst-substrate complex during the catalysis.[193]

These results contrast with what found for the $[IPr\text{-}Au]^+$ fragment, where 3-hexyne and OTf^- are more coordinating than water and BF_4^-.[48,50,126,127,158] As a partial confirmation, Glorius and coworkers have isolated a similar compound, [**3**-BF_4]$^+$, in which the BF_4^- ion is coordinated in the inner sphere instead of water.[174]

These experimental counterintuitive results and challenges have been addressed computationally in an attempt to rationalize them and, consequently, to optimize the catalytic efficiency of this type of Au(III) complexes.

As mentioned, the coordination ability of the gold(III) monocationic/bicationic fragments towards the counterion, alkyne or nucleophile has an impact on the pre-equilibrium step of the catalytic cycle, favouring it or deactivating the catalyst, as demonstrated for a gold(I) monocationic fragment.[48,50,126,127,158]

On the basis of the above reported experimental data, the coordinating ability of the **2** fragment towards Cl^-, BF_4^-, OTf^-, H_2O, 3-hexyne, and 2-butyne has been computationally studied. Moreover, the effect of the ancillary ligand modelling, namely, replacing of IPr with NHC* (NHC* = 1,3-dimethylimidazol-2-ylidene), and of the pincer ligand substitution, namely, replacing of

phenylpyridine (ppy) and IPr with (C^N^C) (C^N^C = 2,6-bis(4-^{t}BuC$_6$H$_3$)$_2$ pyridine dianion) and of IPr with Cl^-, on Au(III) coordination ability has been investigated. Although in computational studies the ancillary ligands are commonly simplified, a simplified model of the ligand could be no longer acceptable when one explores the energetics of ion pair dissociation, which are strongly governed by steric factors. The effects of dispersion and solvent inclusion in the calculations are also explicitly estimated. In order to highlight differences and similarities between the gold +1/+3 oxidation states, all the results are compared with those obtained for the $[IPr\text{-}Au]^+$ fragment. Finally, the pre-equilibrium step has been studied by evaluating the activation energy for the H_2O substitution by 2-butyne in $[\mathbf{2}\text{-}H_2O]^{2+}$ and $[IPr\text{-}Au\text{-}H_2O]^+$ complexes under modelled experimental conditions, namely, in the presence of explicit GVL and H_2O molecules as the solvents.

Coordination ability of the 2 fragment

The bonding energies of X (X = Cl^-, BF_4^-, OTf^-, H_2O, 2-butyne and 3-hexyne) have been evaluated in order to study the coordination ability of the **2** fragment. We have performed calculations of electronic energy change (ΔE) for the following reactions:

$\mathbf{2} + X \rightarrow [\mathbf{2}\text{-}X]^{+/2+}$ (1)

$[(ppy)\text{-}Au\text{-}NHC^*]^{2+} + X \rightarrow [(ppy)\text{-}Au\text{-}NHC^*\text{-}X]^{+/2+}$ (2)

$[NHC^*\text{-}Au]^+ + X \rightarrow [NHC^*\text{-}AuX]^{0/+}$ (3)

In reaction (1) the experimental complex is taken into account, denoted as “Au(III) real”, whereas in reaction (2) the IPr ligand is simplified by replacing the two isopropylphenyl moieties by methyl groups (NHC* = 1,3-dimethylimidazol-2-ylidene), denoted as “Au(III) model”, as commonly done in computational studies. Finally, in reaction (3), the corresponding simplified Au(I) complex, denoted as “Au(I)” is examined, for comparison. A test calculation of the bonding ΔH and ΔG values has been performed showing that the bonding ΔE values are good/reasonable approximation to ΔH/ΔG values. The results are reported in the Experimental Section (**Table 3.15**).

As the X ligands are concerned, we selected all the experimentally employed species. In addition to 3-hexyne, also 2-butyne was examined, which is however usually considered as a model alkyne in computational investigations. The results are summarized in **Table 1.13**.

Table 1.13: *X (X = Cl^-, OTf^-, BF_4^-, 3-hexyne, 2-butyne, and H_2O) bonding energies (ΔE in kcal/mol) to* ***2*** *(Au(III) real), $[(ppy)\text{-}Au\text{-}NHC^*]^{2+}$ (Au(III) model) and $[NHC^*\text{-}Au]^+$ (Au(I)).*

ΔE	Cl^-	OTf^-	BF_4^-	3-hexyne	2-butyne	H_2O
Au(III) real	-202.3	-158.5	-153.6	-30.0	-25.8	-21.5
Au(III) model	-225.0	-187.5	-176.5	-44.9	-39.2	-28.4
Au(I)	-157.0	-120.2	-110.1	-52.0	-50.2	-36.6

The bonding energies span a range of -21.5/-202.3 kcal/mol for the real catalyst and of -28.4/-225.0 kcal/mol for the model one. For Au(I) complexes the bonding energies are calculated between -36.6 and -157.0 kcal/mol. The overall energetic trend in all the different systems can be readily visualized in **Figure 1.28**.

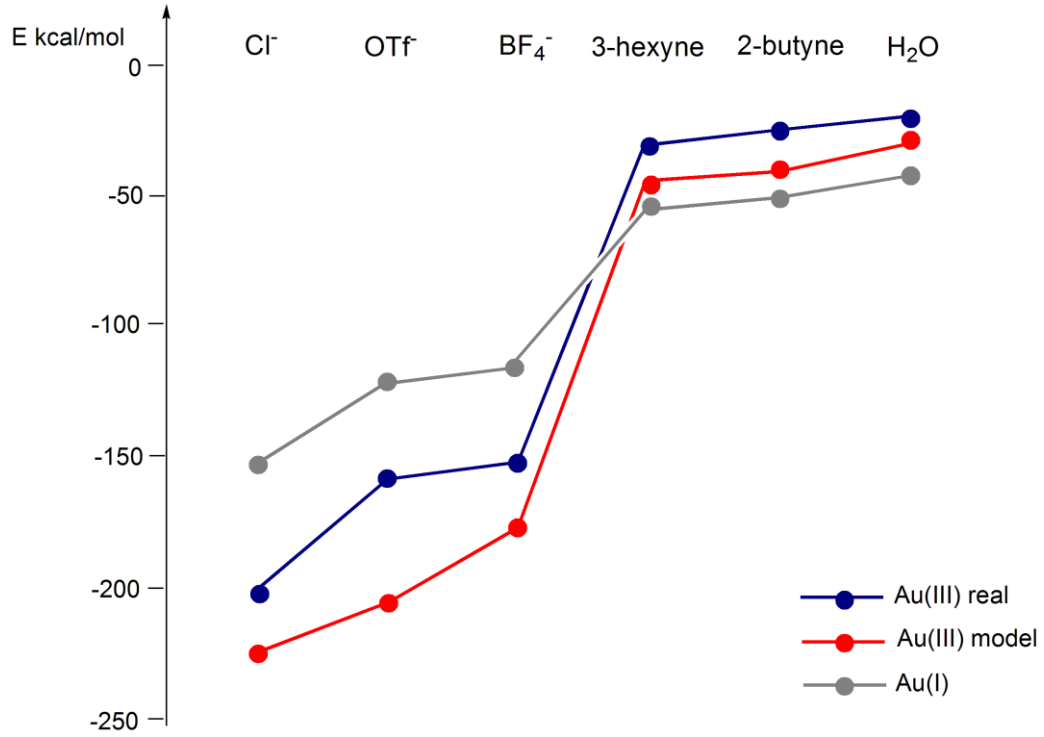

Figure 1.28: *Bonding energy trend for real and model Au(III)X and for Au(I)X (X = Cl^-, OTf^-, BF_4^-, 3-hexyne, 2-butyne and H_2O) complexes. Plotted data are taken from* **Table 1.13**.

As a general trend, the anionic ligands exhibit the largest bonding interactions compared to the neutral ones. In particular, Au(III)Cl shows the highest bonding energy, following the Au(III)Cl > Au(III)OTf > Au(III)BF_4 order. Note that the Cl^- strongest coordination ability is in full agreement with the difficulty experimentally encountered when attempts are made to remove the chlorine from the first coordination shell of the Au(III) complex. By contrast, removal of Cl^- from L-Au-Cl by AgX is easier.[48,50,126,127,158]

Bonding energies of neutral ligands are lower, with the minimum value calculated for H_2O, in the order Au(III)3-hexyne > Au(III)2-butyne > Au(III)H_2O. This energetic trend is the same for all the systems, Au(III) real, Au(III) model and Au(I) complexes.

However, the bonding energies along the Au(III) real complex series are always lower than the corresponding ones in the Au(III) model complex series. Interestingly, the Au(III) model systems, which should simulate the real ones, show a different stabilization depending on the X ligand. For instance, H_2O has a larger bonding energy in the Au(III) model complex by 6.9 kcal/mol, whereas 2-butyne and 3-hexyne have larger ΔE by 13.4 and 14.9 kcal/mol, respectively, with respect to the Au(III) real complex. This difference is even more pronounced for the anionic X ligands: Au(III)OTf model complex is stabilized by 29.0 kcal/mol with respect to the real one, whereas Au(III)BF_4 and Au(III)Cl model species are stabilized by 22.9 and 22.7 kcal/mol, respectively. This finding, showing a different energy gap between the model and the real systems, would suggest that replacing IPr by NHC* could be not quantitatively safe for all the X ligands, although qualitatively the same trend is reproduced. We will analyze this issue in detail later on.

On the other hand, the difference in ΔE values between Au(III) model and Au(I) systems is approximately constant within each ligand subset. For instance, for the neutral X ligand series, the bonding energies are larger for Au(I) than for Au(III) model by 7.1/11.0 kcal/mol, and for the anionic X they are larger for Au(III) model than for Au(I) by 66.4/68.0 kcal/mol. From these results we can surmise that Au(III) model and Au(I) systems can be directly compared. From **Table 1.13** and **Figure 1.28** we can also see that Au(III) interacts more strongly with anionic X than Au(I) does, as one should expect. Au(I) instead shows a larger bonding interaction with neutral X ligands: Au(III)X complexes bonding energy values range from -28.4 kcal/mol to -44.9 kcal/mol (or from -21.5 to -30.0 kcal/mol for the Au(III)X real complexes) vs. the corresponding Au(I) ones ranging from -36.6 to -52.0 kcal/mol.

By taking the Au(III)/Au(I)-H_2O bonding energy as zero reference point and plotting the bonding energies of all the complexes, we can separately analyze the different system series, namely Au(III) real, Au(III) model and Au(I), as shown in **Figure 1.29**.

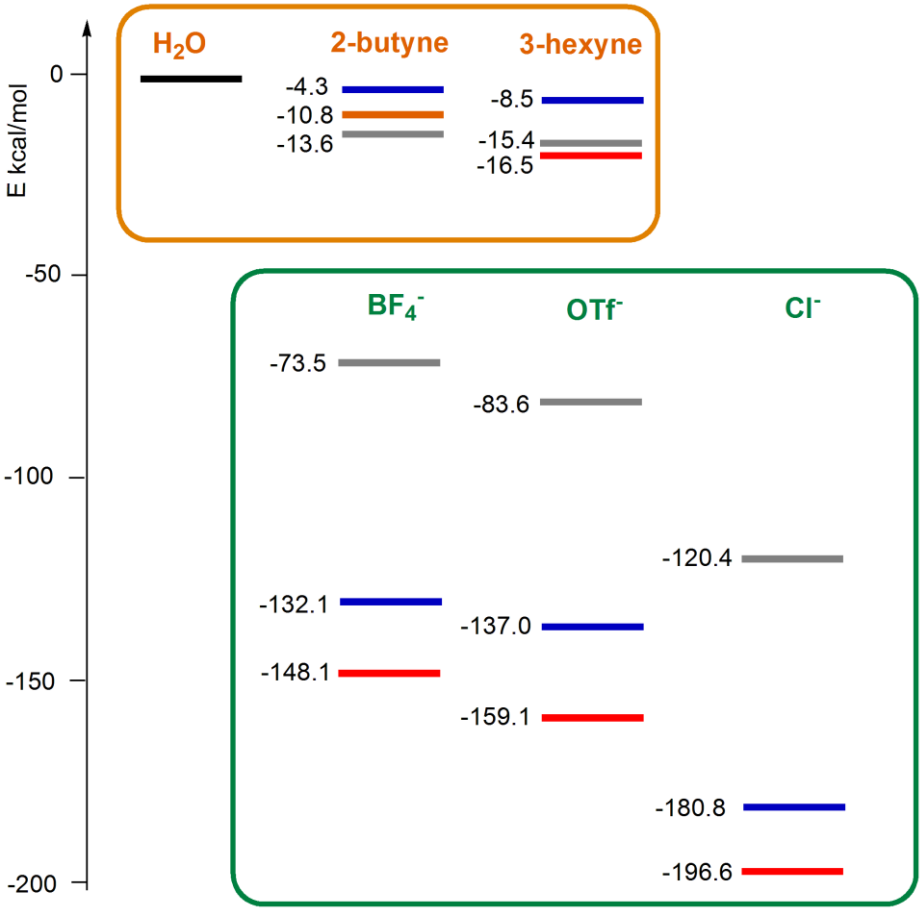

Figure 1.29: *Bonding energy trend for Au(III)X real complexes (blue lines), Au(III)X model complexes (red lines) and Au(I)X complexes (grey lines) (X = H_2O, 2-butyne, 3-hexyne, BF_4^-, OTf^- and Cl^-). For each series the bonding energy with X = H_2O is taken as zero reference value. Plotted data are taken from* ***Table 1.13****.*

Based on **Figure 1.29**, we can roughly divide the ligands into two groups: anionic and neutral ligands. The energy gap between the two groups is larger for Au(III) than for Au(I) complexes. The difference between Au-BF_4 and Au-(3-hexyne), which represents the energetic gap between strong and weak ligands, is 123.6 kcal/mol for the Au(III) real, 131.6 kcal/mol for the Au(III) model and 58.1 kcal/mol for the Au(I) system series, respectively. Within the same ligand group, the energy gap between the complexes is also different by moving from one system series to another: it is similar for Au(III) model and Au(I) series and decreases for the Au(III) real one, where alkynes coordinate to the

complex only slightly stronger than water, and OTf^- and BF_4^- show very similar coordination strength. These findings suggest that the Au(III) real system would be less selective than Au(III) model and Au(I) systems towards the different ligands belonging to the same group.

In the following, the coordination ability of Au(III) and Au(I) catalyst complexes is analyzed in detail and the results are discussed separately for anionic and neutral ligand groups.

Anionic ligands (X = Cl^-, OTf^-, BF_4^-)

The optimized structures of the [**2**-X]$^+$ real and [(ppy)-Au-NHC*-X]$^+$ model complexes (X = Cl^-, OTf^-, BF_4^-) are compared in **Figure 1.30**.

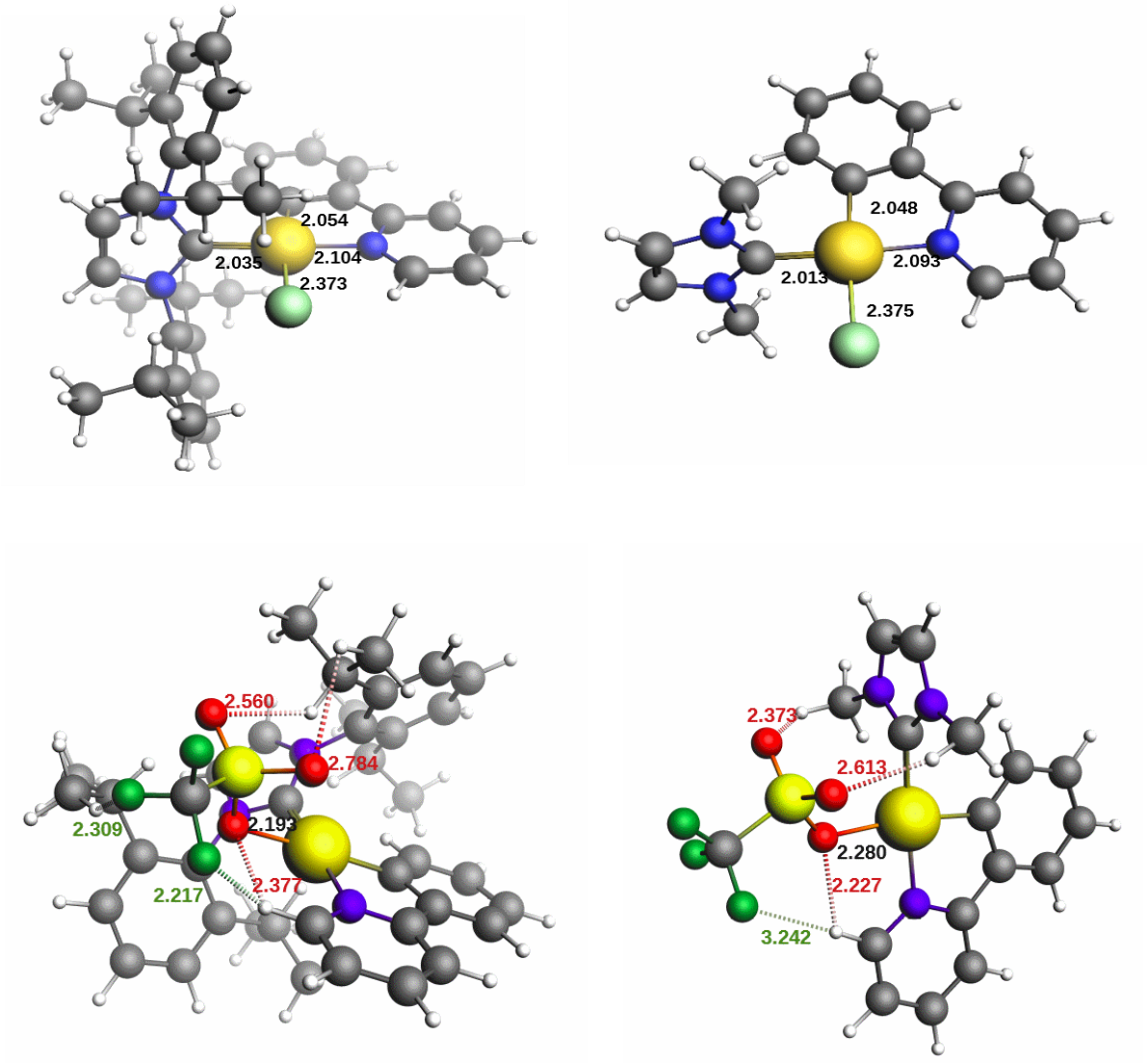

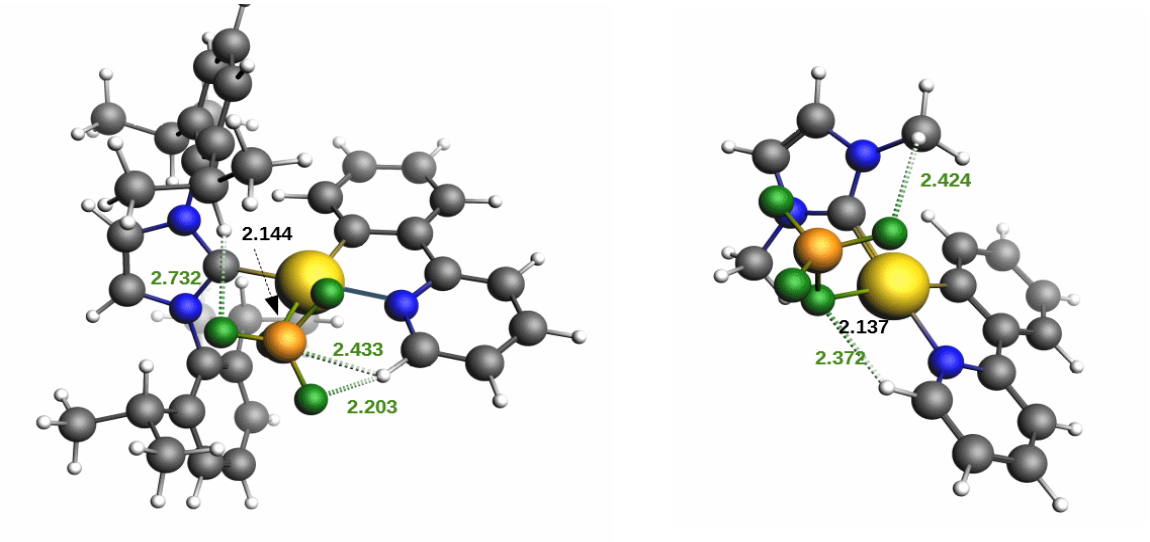

Figure 1.30: *Optimized structures of: top) Au(III)Cl real and Au(III)Cl model complexes; middle) Au(III)OTf real and Au(III)OTf model complexes; and bottom) Au(III)BF_4 real and Au(III)BF_4 model complexes. Bond distances are in Å.*

The most relevant structural variation from the real to the model Au(III)Cl complex concerns the shortening of the Au(III)-IPr(NHC) bond distance from 2.035 to 2.013 Å. The model complex is stabilized by 22.7 kcal/mol with respect to the real one.

On comparing the coordination ability of BF_4^- and OTf^- to the metal center, a difference of only 4.9 kcal/mol is calculated in the Au(III) real complex, with OTf^- being more coordinating. This relatively low value is unexpected on the basis of the commonly recognized, both theoretically and experimentally, higher coordination ability of OTf^- compared to BF_4^-. However, this finding nicely explains the experimentally observed similar coordination ability of BF_4^- and OTf^- towards the **2** fragment, which is only slightly shifted in favour of the triflate ion. Interestingly, in the Au(III) model complex such an energy difference increases to 11.0 kcal/mol. We can surmise that the higher steric hindrance in real complex due to the two isopropylphenyl groups of IPr is responsible for a larger destabilization of the Au(III)-OTf bond than the Au(III)-BF_4 one caused by the larger size and less "spherical" symmetry of OTf^- compared to BF_4^-. As a consequence, the coordination ability of OTf^- decreases in the Au(III) real complex, although it remains slightly more coordinating than BF_4^-.

However, the decreasing contribution of the steric hindrance to the OTf^- bonding energy could be counteracted by an additional effect due to the IPr and ppy ligands. To understand this effect, we need to look closer at the geometries of the species shown in **Figure 1.30**. The hydrogens of the

isopropylphenyl groups of IPr and of the ppy pyridine ring, which are close to the BF_4^- and OTf^- ligands, can interact with their highly electronegative (fluorine and oxygen) atoms by establishing long-range noncovalent bonds that can contribute to the overall bonding energy. In particular, in the Au(III)OTf real complex (**Figure 1.30**, middle), the ppy pyridine hydrogen can be found at a 2.217 Å distance from a OTf^- fluorine atom and at 2.377 Å distance from the OTf^- oxygen atom bound to Au. In addition, a OTf^- fluorine atom is positioned at 2.309 Å from a IPr isopropyl hydrogen atom and a OTf^- oxygen at 2.560 Å from a IPr isopropyl hydrogen atom. Similar interactions can be found in the Au(III)BF_4 real complex, where the corresponding distances with BF_4^- fluorine atoms are longer (**Figure 1.30**, bottom), except for the ppy pyridine hydrogen that can be found at a 2.203 Å distance from a BF_4^- fluorine atom. In the corresponding Au(III)OTf model complex, the ppy pyridine hydrogen can be found at a longer 3.242 Å distance from a OTf^- fluorine atom and at a shorter 2.277 Å distance from the OTf^- oxygen atom bound to Au. Two oxygen atoms of OTf^- move towards the two methyl groups of the NHC* ligand, at 2.373 and 2.613 Å distance, respectively, with no interaction between NHC* and fluorine atoms. For the Au(III)BF_4 model complex, the ppy pyridine hydrogen can be found at a much longer 3.164 Å distance from a BF_4^- fluorine atom and at a shorter 2.372 Å distance from the BF_4^- fluorine atom bound to Au. Only one fluorine atom is placed at a relatively short distance of 2.424 Å from the hydrogen of one methyl group of NHC*. Thus, in general, the coordinated anion reorients with respect to IPr, and fewer hydrogen bond interactions can be established with NHC* than with IPr.

Considering the BF_4^- and OTf^- coordination in the Au(I) complex, the difference between their bonding energies is -10.1 kcal/mol, similar to that between their bonding energies in the Au(III) model complex (-11.0 kcal/mol). Thus, the Au(I) and Au(III) model systems seem to similarly interact with the two anions. This is a surprising result on the basis of the two-charge unit difference between the two metal centres. Taking into account the linearity of the Au(I) complex and the absence of steric hindrance, which is also not greatly pronounced in the Au(III) model system, then probably the most important contribution to the OTf^- bonding energy in the Au(III) real system is the destabilizing steric effect of IPr.

Dispersion and solvation effects

The dispersion contribution for properly describing the noncovalent interactions, such as those playing a role in the anion-ligand interactions in the Au(III) real complexes, deserves a more detailed analysis.

Actually, the bonding energies in **Table 1.13** have been calculated using the B2PLYP functional which already includes dispersion. The dispersion effect on the bonding energy can be explicitly estimated by comparing the BP86 calculated bonding energies with those obtained by BP86 plus the Grimme dispersion correction (BP86-D3) for the Au(III) real and model systems. The results are reported in **Table 1.14**.

Table 1.14: X (X = Cl^-, BF_4^-, OTf^-) bonding energies (kcal/mol) to **2** (Au(III) real) and [(ppy)-Au(III)- NHC*]$^{2+}$ (Au(III) model) complexes calculated at the BP86 (ΔE(BP86)), BP86 including the Grimme dispersion correction (ΔE(BP86-D3)) and BP86 including both the Grimme dispersion correction and solvent (ΔE(BP86-D3) solv) levels. Corresponding values calculated at the B2PLYP level are also shown in parentheses for comparison. Energy differences (ΔE OTf^-/BF_4^-) between coordination ability of OTf^- and BF_4^- for Au(III) real and Au(III) model at each level of theory are reported.

	ΔE (BP86)	ΔE (BP86-D3)	ΔE (BP86)	ΔE (BP86-D3)	ΔE (BP86-D3) solv	
	Au(III) real		Au(III) model		Au(III) real	Au(III) model
$[Au(III)Cl]^+$	-190.0	-196.8 (-202.3)	-214.0	-220.8 (-225.0)	-53.3	-60.2
$[Au(III)BF_4]^+$	-142.4	-150.7 (-153.6)	-167.0	-175.7 (-176.5)	-22.8	-32.6
$[Au(III)OTf]^+$	-140.2	-156.2 (-158.5)	-173.0	-185.8 (-187.5)	-33.0	-46.0
ΔE OTf^-/BF_4^-	2.2	-5.5 (-4.9)	-6.0	-10.1 (-11.0)	-10.2	-13.4

From BP86 calculations an energy difference between the BF_4^- and OTf^- Au(III) real systems of 2.2 kcal/mol is obtained with Au(III)BF_4 being more stable than Au(III)OTf. This result is completely different from that found at the B2PLYP level. Inclusion of Grimme D3 dispersion correction in the BP86 calculations gives an energy difference of -5.5 kcal/mol, with Au(III)OTf as the most stable complex. This result is close to that obtained with B2PLYP calculations (-4.9 kcal/mol) and shows the importance of the van der Waals dispersion forces in the anion coordination. These long-range interactions are thus demonstrated to play an important role in these large dimension systems where high polarization of the ligands fragments is expected.[195,196]

Looking at the Au(III)BF_4^- and Au(III)OTf^- model complexes, the energy difference between them is -6.0 kcal/mol at BP86 level, with Au(III)OTf^- as the most stable complex. This value increases when the Grimme D3 dispersion correction is included in the calculations (-10.1 kcal/mol), getting closer to the B2PLYP's one (-11.0 kcal/mol). The contribution of the dispersion forces to the bonding energy is generally lower for the Au(III) model systems, in agreement with the smaller number of non-covalent interactions arising when NHC* replaces IPr. Note that for Au(III)Cl, contribution of

dispersion has the same value in both model and real complex (6.8 kcal/mol), as expected on the basis of the lacking of any interaction between Cl^- and both NHC* and IPr. We can conclude that increasing the dimension of the ligands L and X the contribution of the dispersion forces to the total energy becomes increasingly relevant.

Solvation is also expected to have an impact on the bonding energies through modulation of dispersion interactions. In **Table 1.14** values calculated at BP86-D3 level by including dichloromethane as solvent are shown. A general decrease of the bonding energies can be observed, although the trend of the gas phase BP86-D3 values (i.e. Au(III)Cl > Au(III)OTf > Au(III)BF_4) is retained for both Au(III) real and model complexes. Interestingly, the energy difference between Au(III)BF_4^- and Au(III)OTf^- real complexes increases to -10.2 kcal/mol, with Au(III)OTf^- as the most stable complex, as well as that between corresponding model complexes (-13.4 kcal/mol). Thus the dichloromethane effect appears to be beneficial for stabilizing the Au(III)OTf^- (both real and model) complex.

Neutral ligands (X = H_2O, 2-butyne and 3-hexyne)

Among the neutral ligands, H_2O exhibits the smallest calculated bonding energy in all the Au(III) real, Au(III) model and Au(I) complexes (**Table 1.13**, **Figure 1.28** and **Figure 1.29**). On the basis of these results, water could be considered the weakest ligand in the series, in strong disagreement with the experiment. Indeed, in the reaction environment, only the [**2**-H_2O]$^{2+}$ complex could be experimentally isolated and characterized, which would suggest H_2O as the strongest ligand between the neutral species. In particular, [**2**-(3-hexyne)]$^{2+}$ could not be isolated. To rationalize these intriguing results we first compare the optimized structures of the [**2**-(H_2O)]$^{2+}$ real and [(ppy)-Au-NHC*-H_2O]$^{2+}$ model complexes depicted in **Figure 1.31** (top), with those of the [**2**-(3-hexyne)]$^{2+}$ and [**2**-(2-butyne)]$^{2+}$ real and [(ppy)-Au-NHC*-(3-hexyne)]$^{2+}$ and [(ppy)-Au-NHC*-(2-butyne)]$^{2+}$ model complexes (**Figure 1.31**, middle and bottom).

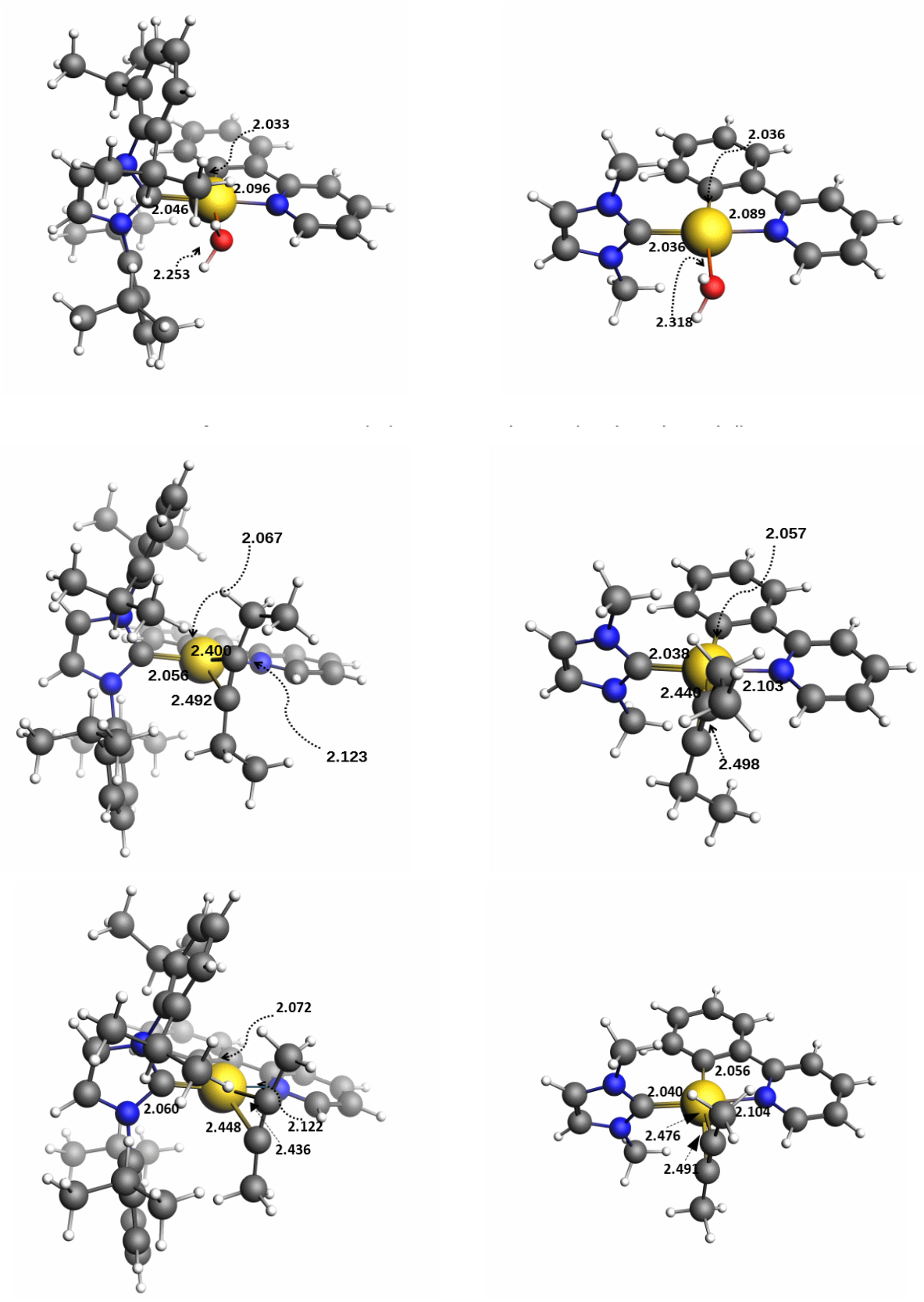

Figure 1.31: *Optimized structures of: top) Au(III)H_2O real and Au(III)H_2O model complexes; middle) Au(III)3-hexyne real and Au(III)3-hexyne model complexes; and bottom) Au(III)2-butyne real and Au(III)2-butyne model complexes. Bond distances are in Å.*

By comparing the Au(III)H_2O real and model geometries we can observe only slightly different bond distances. The most relevant structural variation from the Au(III) real to the model complex concerns the shortening of the Au(III)-IPr(NHC) bond distance from 2.046 to 2.036 Å and the increase of the H_2O-Au distance from 2.253 (real) to 2.318 (model) Å. The model complex is stabilized by 6.9 kcal/mol with respect to the real one. Note that H_2O is oriented to form a hydrogen bond with the long-range noncovalent bonds of ppy pyridine ring in both complexes (H_2O-H(ppy) distance 2.308 and 2.407 Å in Au(III) real and model complexes, respectively). On the other hand, alkyne coordination shows large structural differences between the Au(III) real and Au(III) model complexes. In particular, the Au-IPr and Au-ppy distances are significantly elongated in the real complex for both 2-butyne and 3-hexyne, whereas the two alkyne C≡C distances from Au are shortened (to 2.448 and 2.436 Å for 2-butyne, and to 2.400 and 2.492 Å for 3-hexyne, respectively). Notably, in the real complex the 2-butyne C≡C coordination is more "symmetric" (η^2–like) than that of 3-hexyne. In addition, hydrogen bonds are formed between a carbon atom of the IPr phenyl ring and the hydrogen atom of the CH_3 (2-butyne) or CH_2 group (3-hexyne). Interestingly, the model complex is stabilized by 13.4 and 14.9 kcal/mol with respect to the real one for 2-butyne and 3-hexyne, respectively (**Table 1.13**). In the model complexes the C≡C distances from gold are 2.491 and 2.476 Å for 2-butyne 2.440 and 2.498 Å for 3-hexyne, which compared to the real ones, result larger. In particular, 2-butyne experiences the largest elongation and removal from the η^2 coordination mode. The larger bonding energy calculated for the alkynes with the model complex with respect to the real one could be then attributed to the decreasing of the NHC steric hindrance.

As a balance between the steric effects due to the IPr ligand and the stabilizing effects of hydrogen bonds between alkyne and IPr and ppy, both the alkynes are found to be more strongly coordinating to Au than water, with 3-hexyne having the highest bonding energy (see **Table 1.13**). This finding suggests that the gold(III) complex under study would be more π-philic than oxophilic, at variance with common assumption in the literature that gold(III) catalysts do have a strong oxophilic nature, whereas gold(I) catalysts do not.[81,197–199]

Looking at the Au(I) complexes geometries depicted in **Figure 1.32**, we generally observe shorter Au-OH_2, 2-butyne C≡C, and 3-hexyne C≡C bond distances (2.145, 2.219 and 2.220 Å, respectively) with respect to the corresponding Au(III) real and model complexes in a η^2 coordination mode, associated with higher bonding energies (**Table 1.13**). This result indicates that steric effects are very important for water and alkyne coordination. In particular, the bonding distances between the

two alkyne carbon atoms and Au(I) are equal, and the bonding energy difference between 2-butyne and 3-hexyne is only 1.8 kcal/mol, thus showing that the absence of steric hindrance makes the coordination ability of the two ligands almost identical.

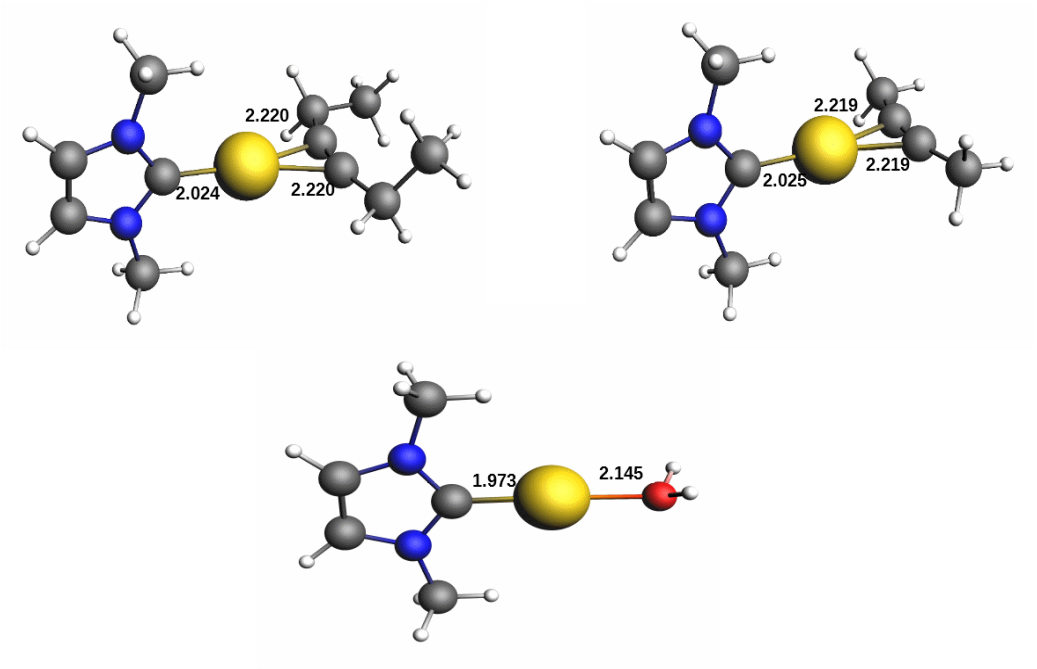

Figure 1.32: *Optimized structures of: bottom) Au(I)H2O; top) Au(I)3-hexyne (left) and Au(I)2-butyne (right) complexes. Bond distances are in Å.*

In the Au(III) real and Au(III) model systems the steric hindrance, which is reflected in larger structural modifications on going from the real to the model system and in longer bonding distances compared to the Au(I) ones, increases the bonding energy difference between the two alkyne ligands. However, the larger size 3-hexyne coordinates better than 2-butyne (ΔE -30.0 vs. -25.8 kcal/mol or -44.9 vs. -39.2 kcal/mol, respectively, see **Table 1.13**), so again the steric hindrance should not be the only effect that contributes to the selectivity of the metal towards the considered neutral ligands.

On comparing the bonding energy of Au(III) real, Au(III) model and Au(I) complexes with water and alkynes, we observe that Au(III) model and Au(I) complexes shows similar values of bonding energy difference between H_2O and alkynes, which are -10.8/-13.6 for 2-butyne and -16.5/-15.4 kcal/mol for 3-hexyne, respectively. These differences for the Au(III) real and Au(III) model complexes decrease in the Au(III) real complex from -10.8 to -4.3 kcal/mol for 2-butyne and from -16.5 to -8.5 kcal/mol for 3-hexyne.

In conclusion, Au(III) model and Au(I) complexes seem to behave similarly in the coordination trend of the neutral ligands, although Au(I) complex coordinates all the three neutral ligands more strongly than Au(III).

Dispersion and solvation effects

To further analyse the selectivity of the metal towards the considered neutral ligands, the effect of noncovalent interactions between H_2O, 2-butyne and 3-hexyne with IPr(NHC) and ppy ligands has been explicitly evaluated by comparing BP86 and BP86-D3 bonding energies. The results are shown in **Table 1.15**.

Table 1.15: *X (X = H_2O, 3-hexyne, 2-butyne) bonding energies (kcal/mol) to **2** (Au(III) real) and [(ppy)-Au-NHC*]$^{2+}$ (Au(III) model) complexes calculated at the BP86 (ΔE(BP86)), BP86 including the Grimme dispersion correction (ΔE(BP86-D3)) and BP86 including both the Grimme dispersion correction and solvent (ΔE(BP86-D3 solv)) levels. Corresponding values calculated at the B2PLYP level are also shown in parentheses for comparison. Energy differences between coordination ability of H_2O and 3-hexyne (ΔE H_2O/3-hexyne) and of H_2O and 2-butyne (ΔE H_2O/2-butyne) for Au(III) real and Au(III) model at each level of theory are reported.*

	ΔE (BP86)	ΔE (BP86-D3)	ΔE (BP86)	ΔE (BP86-D3)	ΔE (BP86-D3) solv	
	Au(III) real		Au(III) model		Au(III) real	Au(III) model
[Au(III)H_2O]$^{2+}$	-14.8	-19.0 (-21.5)	-20.7	-25.5 (-28.4)	-12.5	-20.9
[Au(III)3-hexyne]$^{2+}$	-10.4	-34.4 (-30.0)	-30.0	-47.2 (-44.9)	-27.9	-32.8
ΔE H_2O/3-hexyne	4.4	-15.4 (-8.5)	-9.3	-21.7 (-16.5)	-15.4	-11.9
[Au(III)2-butyne]$^{2+}$	-9.6	-29.3 (-25.8)	-28.0	-41.9 (-39.2)	-25.1	-31.3
ΔE H_2O/2-butyne	5.2	-10.3 (-4.3)	-7.3	-16.4 (-10.8)	-12.6	-10.4

Interestingly, for the Au(III) real complex the BP86 bonding energy is lower for both 2-butyne and 3-hexyne than for H_2O, with a bonding energy difference of 5.2 and 4.4 kcal/mol, respectively. Inclusion of Grimme dispersion correction changes the result: the BP86-D3 bonding energy is higher for both 2-butyne and 3-hexyne than for H_2O, with a bonding energy difference of -10.3 and -15.4 kcal/mol, respectively (-4.3 and -8.5 kcal/mol at B2PLYP level, respectively). For the Au(III) alkyne model complexes, the dispersion contribution to the bonding energy is generally lower than that calculated for the corresponding Au(III) real complexes, whereas is nearly negligible for Au(III)H_2O model (compare bonding energies at BP86 and BP86-D3 values in **Table 1.15**). These results show

again that the dispersion contribution is more relevant for the larger size ligand (IPr vs. NHC*). Overall, this analysis shows the crucial contribution of the dispersion forces to the total bonding energy also for neutral ligands. In addition, these results also demonstrate that dispersion forces are responsible for the bonding energy difference between the two alkynes, making 3-hexyne more coordinating than 2-butyne.

Inclusion of solvent effect generally lowers the bonding energies for both Au(III) real and Au(III) model complexes, although the energy differences between H_2O and alkynes are only slightly affected for Au(III) real complexes (compare BP86-D3 and BP86-D3 solv ΔE H_2O/3-hexyne and ΔE H_2O/2-butyne values in **Table 1.15**). Instead, the latter are significantly reduced for the Au(III) model complexes (from -21.7 to -11.9 kcal/mol for 3-hexyne and from -16.4 to -10.4 kcal/mol for 2-butyne). The same general trend of the gas phase BP86-D3 values (i.e. Au(III)3-hexyne > Au(III)2-butyne > Au(III)H_2O) is found for both Au(III) real and model complexes. It is worth noting that dichloromethane further lowers the bonding energy of Au(III)H_2O real and model complexes from -19.0 to -12.5 kcal/mol and from -25.5 to -20.9 kcal/mol, respectively.

Ligand effect on the coordination ability

To shed light into the above intriguing results for neutral ligands, where H_2O results a weaker coordinating ligand than alkynes, the ancillary ligand influence on the Au(III) coordination ability is now analyzed.

To be independent of any ancillary ligand interaction with X, in our analysis we selected the bis-cyclometalated $[(C\hat{}N\hat{}C)\text{-}Au]^+$ (C^N^C = 2,6-bis(4-^{t}BuC_6H_3)$_2$ pyridine dianion) and the monocyclometalated $[(ppy)\text{-}Au\text{-}Cl]^+$ Au(III) complexes. In particular, alkyne complexes with $[(C\hat{}N\hat{}C)Au(III)]^+$ have been experimentally observed and characterized by Bochmann et al with different internal alkynes.[188,200] Theoretical studies on the $[(C\hat{}N\hat{}C)\text{-}Au(III)]^+$ alkyne and carbonyl complexes have also been performed previously by some of us.[201,202] Instead, the $[(ppy)\text{-}Au\text{-}Cl]^+$ complex, where a Cl^- replaces the IPr (or NHC*) ligands in our reference complex, allows for a direct comparison with **2**, where the X interactions with IPr (or NHC*) are switched off. The optimized structures of $[(C\hat{}N\hat{}C)AuX]^+$ and $[(ppy)AuClX]^+$ (X = H_2O, 2-butyne, 3-hexyne) are shown in **Figure 1.33**.

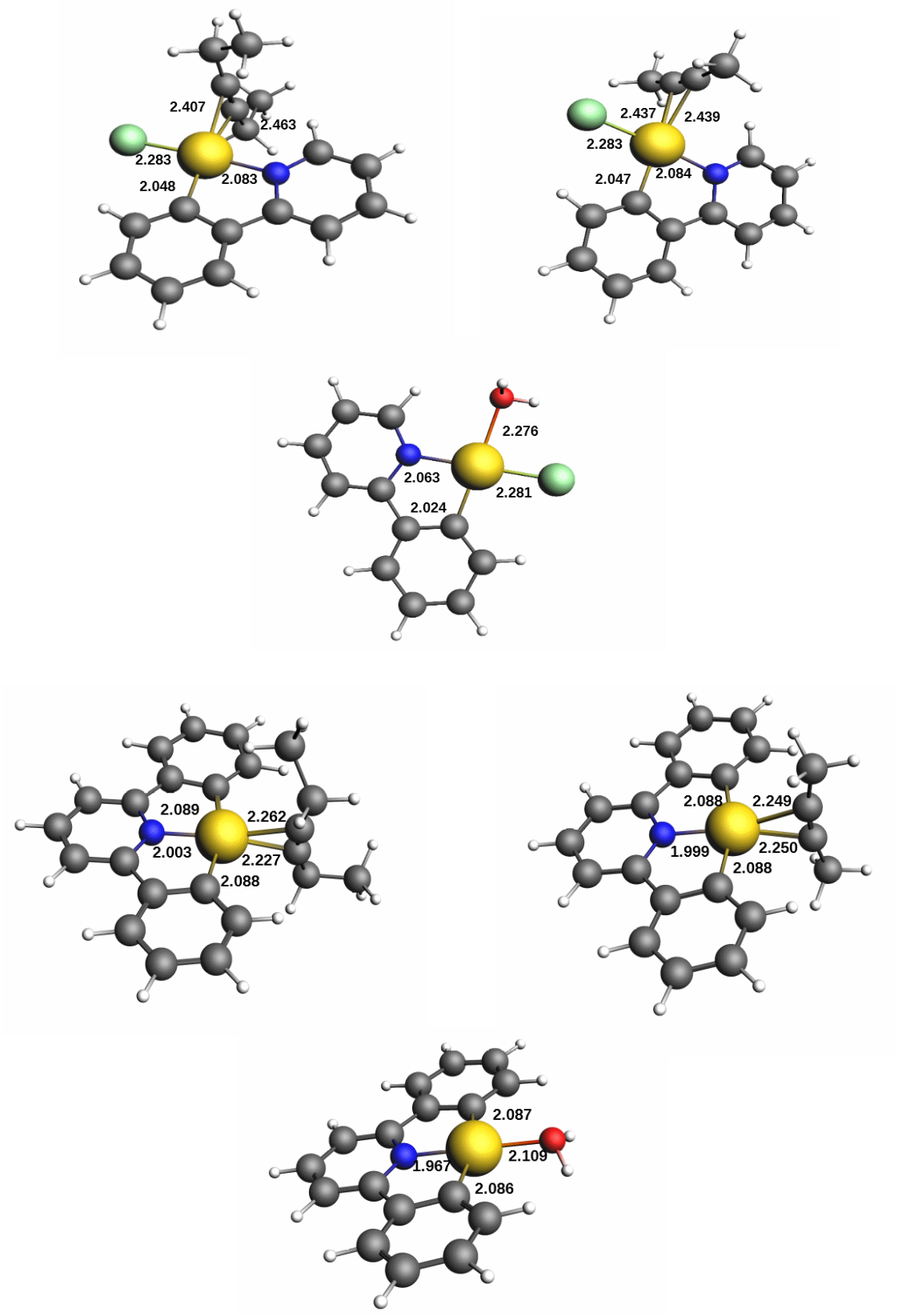

Figure 1.33: *Optimized structures of: upper panel bottom) [(ppy)-Au-Cl-(H_2O)]$^+$; top) [(ppy)-Au-Cl-(3-hexyne)]$^+$ (left) and [(ppy)-Au-Cl-(2-butyne)]$^+$ (right) complexes; lower panel: bottom) [(C^N^C)-Au-(H_2O)]$^+$; top) [(C^N^C)-Au-(3-hexyne)]$^+$ (left) and [(C^N^C)-Au-(2-butyne)]$^+$ (right) complexes. Bond distances are in Å.*

Analogously to **2**, the bonding energies of X (X = H_2O, 2-butyne, 3-hexyne) have been calculated for the following reactions:

$[(C\hat{}N\hat{}C)Au]^+ + X \rightarrow [(C\hat{}N\hat{}C)AuX]^+$ (4)

$[(ppy)AuCl]^+ + X \rightarrow [(ppy)AuClX]^+$ (5)

The results are shown in **Table 1.16**, where data for Au(III) real, Au(III) model and Au(I) complexes are also reported for comparison.

Table 1.16: *X (X = H2O, 3-hexyne, 2-butyne) bonding energies (ΔE in kcal/mol) to $[(ppy)AuCl]^+$, $[(C\hat{}N\hat{}C)Au]^+$, **2** (Au(III) real), $[(ppy)\text{-}Au\text{-}NHC^*]^{2+}$ (Au(III) model) and $[NHC^*\text{-}Au]^+$ (Au(I)) in all the complexes.*

ΔE	$[(ppy)AuCl]^+$	$[(C\hat{}N\hat{}C)Au]^+$	Au(III) real	Au(III) model	Au(I)
H_2O	-26.6	-42.9	-21.5	-28.4	-36.6
3-hexyne	-36.3	-64.7	-30.0	-44.9	-52.0
2-butyne	-33.5	-61.1	-25.8	-39.2	-50.2

The overall energetic trend in all the systems can be readily visualized in **Figure 1.34**.

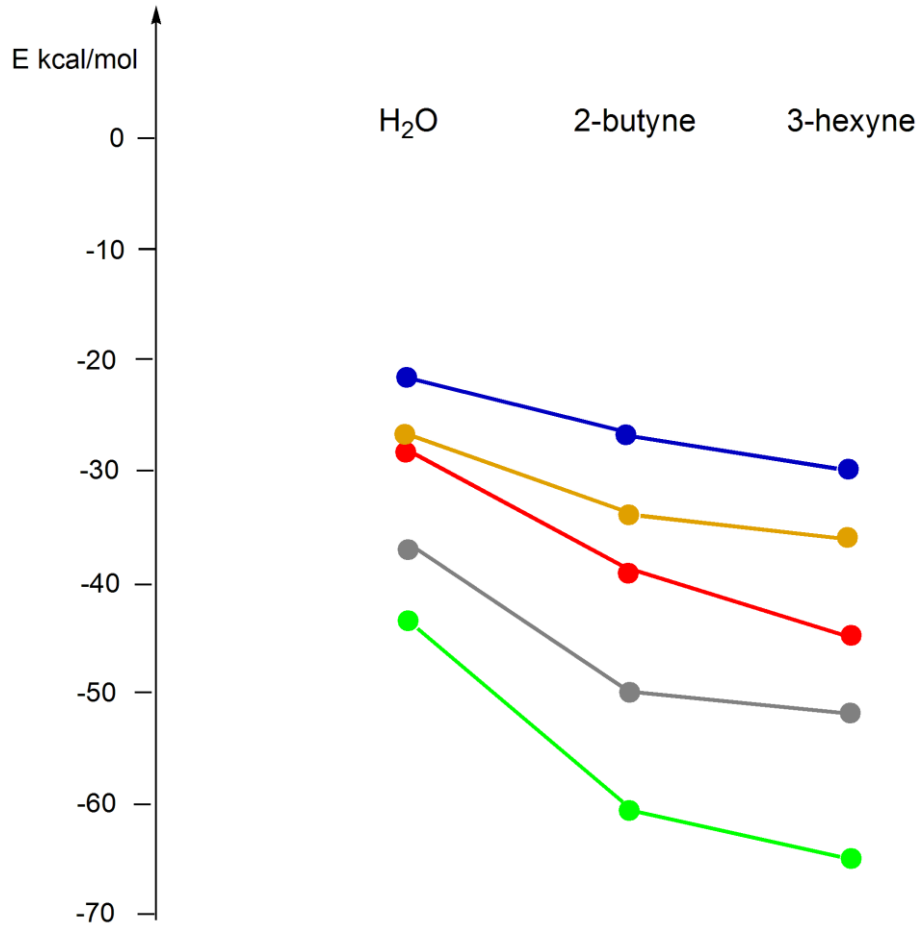

Figure 1.34: *Bonding energy trend for [(ppy)-Au-Cl-X]⁺ (orange line), [(C^N^C)-Au-X]⁺ (green line) [Au(III)X]²⁺ real (blue line), [Au(III)X]²⁺ model (red line) and [Au(I)X]⁺ (grey line) complexes (X = H₂O, 3-hexyne, 2-butyne). Plotted data are taken from* ***Table 1.13*** *and* ***Table 1.16****.*

From **Table 1.16** and **Figure 1.34** we can observe that: i) the coordination ability of Au(III) is quantitatively strongly affected by the ligands; ii) the coordination ability trend is the same for all the complexes, namely ΔE (3-hexyne) > ΔE (2-butyne) > ΔE (H_2O). In particular, for a given X (X = H_2O, 3-hexyne, 2-butyne), the coordination ability follows the trend [(C^N^C)-Au]⁺ > Au(I) > Au(III) model > [(ppy)-Au-Cl]⁺ > Au(III) real. Notably, only Au(III) in [(C^N^C)-Au]⁺ can coordinate alkynes better than the Au(I) complex. In addition, these results suggest that Au(III) coordination ability does not depend on the charge of the complex: for example, [(C^N^C)-Au]⁺ coordinates to X more strongly than Au(III) model with 2+ charge which, in turn, coordinates to X more strongly than [(ppy)-Au-Cl]⁺. Again, these findings seem not to support a commonly encountered postulate in the literature, according to which Au(III) species are more oxophilic in nature whereas Au(I) species show a more π-philic property,[81,202] since, within the considered auxiliary ligands set, both Au(III)

and Au(I) show a stronger coordination ability towards alkynes than water. In other words, Au(III) seems to be not more oxophilic than Au(I), at least in gas phase. Finally, on comparing Au(III) model, $[(ppy)\text{-}Au\text{-}Cl]^+$ and Au(III) real, replacing of IPr with NHC or Cl^- has a beneficial effect on coordination ability, thus indicating a sizable role of IPr interactions with X.

Solvation effect

Bonding energies of $[(ppy)AuCl]^+$, $[(C\text{^}N\text{^}C)Au]^+$, Au(III) real, Au(III) model and Au(I) with X = H_2O, 3-hexyne and 2-butyne have been also calculated at BP86-D3 solv level of theory to analyze the solvent effect. Results are collected in **Table 1.17**.

Table 1.17: *X (X = H_2O, 3-hexyne, 2-butyne) bonding energies (ΔE in kcal/mol) to $[(ppy)\text{-}Au\text{-}Cl]^+$, $[(C\text{^}N\text{^}C)\text{-}Au]^+$, **2** (Au(III) real), $[(ppy)\text{-}Au\text{-}NHC^*]^{2+}$ (Au(III) model) and $[(NHC)\text{-}Au]^+$ (Au(I)) calculated at the BP86-D3 solv level of theory in all the complexes.*

	ΔE (BP86-D3) solv				
	$[(ppy)\text{-}Au\text{-}Cl]^+$	$[(C\text{^}N\text{^}C)\text{-}Au]^+$	Au(III) real	Au(III) model	Au(I)
H_2O	-19.2	-36.3	-12.5	-20.9	-28.2
3-hexyne	-29.0	-56.8	-27.9	-32.8	-42.5
2-butyne	-27.5	-53.9	-25.1	-31.3	-41.5

As observed in the previous sections, inclusion of solvent generally lowers the bonding energies. However, all the above observations referring to the gas phase also apply to the solvent data of **Table 1.17**. Note that even inclusion of dichloromethane suggests that Au(III) is not more oxophilic than Au(I), i.e. bonding energies with H_2O are always lower than those with alkynes for all the considered ligands.

Substitution of H_2O with the substrate: the pre-equilibrium step

From the above study, water clearly emerges as the weakest ligand in the whole series. All the studied Au(III) complexes are important species in catalytic alkyne nucleophilic addition reaction.

The first step of the reaction mechanism is represented by the pre-equilibrium, where the substrate (alkyne) replaces the anion in the initial complex, binds to the gold center, and is activated for the nucleophilic attack. However, in the alkyne hydration reaction, where H_2O is the nucleophile, the anion substitution by the water molecule, i.e. formation of the water adduct from the corresponding initial complex, has been shown to be both thermodynamically and kinetically favored with respect to the formation of alkyne complex, in agreement with the experimental evidence, in our previous work. [193] Therefore, starting from the experimentally isolated and characterized [**2**-H_2O]$^{2+}$, it is interesting to explore the pre-equilibrium step consisting of H_2O substitution by the alkyne.

To understand the reason why [**2-**(3-hexyne)]$^{2+}$ is not experimentally observed, the experimental conditions of the alkyne hydration reaction need to be modelled. In a reaction environment where anionic ligands are not close to the Au(III) catalytic complex (for instance, using highly polar solvents or very weakly coordinating anions) the present species can be additional water, alkyne and/or high polarity solvent molecules. To model such reaction conditions, calculations of the initial complex (IC) and reactant complex (RC) using the Au(III) model complex and 2-butyne have been performed in an attempt to study the pre-equilibrium step of the hydration reaction mechanism. The initial complex is represented by the Au(III)-H_2O model complex with 2-butyne in the second coordination sphere, whereas the reactant complex is the Au(III)-2-butyne model complex with H_2O in the second coordination sphere.

A preliminary calculation of the energy difference between IC and RC when the water and 2-butyne molecules are both present in close proximity to the Au(III) complex shows that 2-butyne coordinates to Au(III) more strongly than H_2O (ΔE=-2.2 kcal/mol). This value confirms once again the finding that water, in the gas phase condition, is a weaker ligand than alkyne.

To account for the experimental conditions, the same IC and RC calculations have been performed including: i) an additional water molecule to model traces of water or water solvent effect; ii) a GVL molecule to model the polar aprotic solvent effect. The results are summarised in **Figure 1.35**, where the energy profiles for the pre-equilibrium step have been shown.

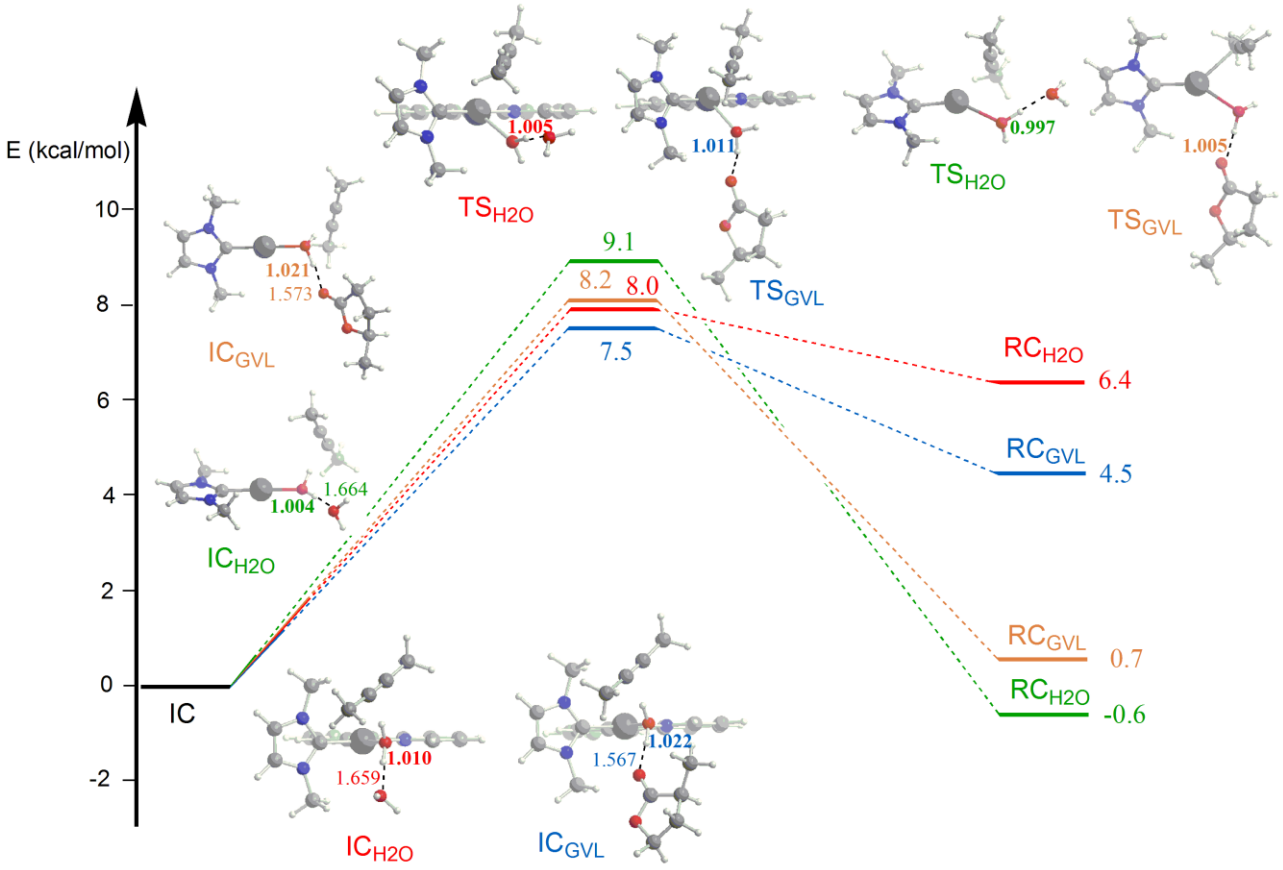

Figure 1.35: *Energy profile for the pre-equilibrium step of the 2-butyne hydration reaction catalyzed by [(ppy)-Au-NHC*]$^{2+}$ and [NHC*-Au]$^{+}$ complexes in water (Au(III) red line, Au(I) green line) and in GVL (Au(III) blue line, Au(I) orange line) as solvent. Optimized structures of IC, TS and RC with relevant distances (in Å) are shown. IC has been taken as zero reference energy for all profiles.*

Interestingly, in both cases IC is more stable than RC, thus indicating that water is a stronger ligand than 2-butyne in these experimental conditions. It is remarkable that the IC stabilization is due to an explicit interaction of the coordinated H_2O with a solvent molecule, namely only microsolvation can account for "oxophilicity" of gold(III) which could not be found using an implicit solvent model (COSMO calculations). Transition state calculations for the IC → RC process show that the activation energy barrier is 8.0 kcal/mol for H_2O and 7.5 kcal/mol for GVL. However, the reverse process RC → IC requires only 1.6 kcal/mol for H_2O and 3.0 kcal/mol for GVL, explaining why it is not possible to experimentally isolate the alkyne complex: anytime the complex binds to the alkyne, its substitution with the H_2O in the first coordination shell is nearly instantaneous.

These results can be explained by assuming that the presence of a polar molecule (H_2O or GVL) which is able to establish a hydrogen interaction with water in IC_{H2O} or IC_{GVL} polarizes the water O-H bond, increasing the partial negative charge on the oxygen atom which becomes more

coordinating toward the metal center. The lower activation energy barrier obtained when the solvent is GVL, compared to water, suggests that the "activation" of the O-H bond is prevalently caused by the hydrogen bond strength. Indeed, in TS_{GVL} structure, the water O-H distance involved in GVL hydrogen bond is 1.011 Å, whereas in TS_{H2O} structure the corresponding O-H distance is 1.005 Å, thus indicating that GVL is more efficient in "activating" H_2O to an incipient "OH^-". Notably, in IC_{GVL} the water O-H distance is also larger than that in IC_{H2O} (1.022 Å vs. 1.010 Å, respectively), predicting a larger stabilization of IC_{GVL} compared to IC_{H2O}.

A comparison with the $[NHC^*\text{-}Au]^+$ fragment, whose energy profiles for the pre-equilibrium step of the 2-butyne hydration reaction in the same modelled experimental conditions are also reported in **Figure 1.35**, shows that the most noticeable difference relies on the equally stable IC and RC. Therefore, in the Au(I) case, water is as strong as 2-butyne as ligand, and an equilibrium between the two species is suggested. The partial negative charge on the oxygen atom of the water O-H bond induced by microsolvation appears to be less stabilized by gold +1 charge than +3, as one could expect.

This study fully supports the findings on the alkyne activation with Au(III) complexes and on the importance of the pre-equilibrium step in Au(III)-catalyzed alkyne hydration reaction reported in previous works by some of us.[203,204] The Au(III)-alkyne complexes were found to very efficiently activate the alkyne triple bond to the point that the pre-equilibrium becomes the rate-determining step of the Au(III)-catalyzed alkyne hydration reaction. In addition, it advises that the experimental conditions of the pre-equilibrium step are crucial in Au(III) catalysis. To experimentally isolate and characterize the considered $[\mathbf{2}\text{-(alkyne)}]^{2+}$ complex, an anhydrous environment is required together with the utilization of very non-coordinating anion,[205] which means that alkyne hydration reaction is not a suitable process to reach this goal. Other Au(III)-catalyzed reactions, such as hydroarylation of alkynes, Meyer-Schuster rearrangement of propalgyl alcohols or even alkoxylation of alkynes, could be more appropriate for this target.

3. Conclusion and perspectives

The main focus of this thesis was an extension of the previous studies on the catalytic activity of the gold(I) L-Au-X systems in green conditions, from both experimental and theoretical point of view. The knowledge previously acquired allowed us to investigate successfully the chemistry of gold(III) catalysts in green media.

At first, 3-hexyne and diphenylacetylene were used as substrates in the reaction promoted by L-Au-X complexes in the presence of NBu_4OTf as an additive, in acid- and solvent-free conditions. The effect of the neutral ligands L was firstly investigated. During the catalysis the decomposition of the phosphorous-based ligand, with the exception of JPhos, was observed by ^{31}P NMR spectroscopy. On the other hand, NHC based ligands, thanks to their high stability, showed superior performances. However, the use of silver salts promoted the decomposition even when NHC ligands were employed. Combining all these findings, we were able to develop a green methodology for the hydration of diphenylacetylene. The catalyst loading was reduced for the first time to 0.01 mol%, obtaining the highest values of TON (3400) and TOF (435 h^{-1}) reported to date, and very good values of EMY (77) and E-factor (0.03). These results suggest that a sustainable production of ketones from alkynes using gold-based catalysts is achievable.

The commonly accepted mechanism for the gold(I) catalyzed alkyne reactions (a sequence of pre-equilibrium, nucleophilic attack and protodeauration steps) can also explain the Meyer-Schuster rearrangement of 1-phenyl-2-propyn-1-ol in p-cymene as the solvent. Using the gold catalyst, the studied mechanism showed the formation of an unprecedented gold-oxetene intermediate via unprecedented 4-*endo*-dig cyclization. The experimental reactivity, which is highly dependent on both anion and solvent effects, is fully rationalizes by this mechanism. The theoretical calculations give insights into the experimental conditions that may modify the mechanism and favor/disfavour the formation of the intermediate, such as the presence of traces of acid (that may alter the activity of the counterion) and the nature of the solvent (low-polarity solvents should favor the formation and the stabilization of the gold-oxetene intermediate due to the anion effect). The use of green solvents in gold catalysis, instead of the traditional VOS, is further consolidated.

We extended our previous work on the cycloisomerization of N-propargylcarboxamides catalyzed by IPr-Au-X complexes in green solvents from an experimental and theoretical point of view. At first, we investigated the effect of the solvent employed establishing that the reaction proceeds very well in most of the alternative solvents employed, such as cyclohexanone, isopropyl acetate, MIBK, ethyl lactate, furfuryl alcohol, γ-valerolactone, and propylene carbonate. TOFs are comparable or even

better with respect to those obtained using VOS. On the other hand, when the reaction is performed in DMSO or propionitrile the TOFs are much lower, owing to the presence of a coordinating functional group (>S=O and -C≡N, respectively) that, upon coordination to the metal center, affords inactive IPr-Au(solvent)OTf species. We also observed that the use of propionic acid resulted in a speed up of the reaction, according to the view that protodeauration is the RDS.

Secondarily, we found, according to our previous work, that the activity of the catalyst in propionic acid (in terms of TOF) seems to be inversely correlated to the coordinating ability and hydrogen-bond acceptor power of X^- (basic and coordinating strength: BF_4^- < OTf^- < OTs^- < TFA^-), with TFA^- being by far the worst counterion. Such a behaviour is consistent with the active role of the counterion in all the three steps of the reaction pathway (pre-equilibrium, nucleophilic attack and protodeauration). DFT calculations reinforce these peculiar experimental kinetic findings showing an excellent agreement, and the suggested mechanism fully rationalizes the experimental reactivity, which is highly dependent on both anion and solvent. These results are indeed remarkable and suggest that a sustainable production of 2-phenyl-5-vinylidene-2-oxazoline promoted by gold catalysts can be pursued if both solvent and counterion effects are carefully taken into account.

The structure, reactivity and catalytic properties of two Au(III) complexes, [**2**-Cl]Cl and [**3**-Cl]OTf, in the hydration of alkynes in γ-valerolactone, under acid-free conditions, have been addressed in this thesis by means of multinuclear solution NMR and computational (DFT) studies. Complex [**2**-Cl]Cl retains its square planar structure and no reduction to Au(I) and/or Au(0) nanoparticles was observed during the catalysis. On the other hand, deactivation of [**3**-Cl]OTf does occur with the formation of Au(I) species, detected by ^{31}P NMR spectroscopy.

Experimental studies, corroborated by DFT calculations, clearly and unequivocally indicate that the RDS of the reaction is the pre-equilibrium step. Such a conclusion arises from: KIE is very close to 1; the addition of acid has no effect on the reaction rate; pseudo zero order was obtained for both 3-hexyne and water. As matter of fact, the entrance in the first coordination sphere of 3-hexyne is the key step of the whole process, with an experimental activation enthalpy of 11.1 kcal/mol. The subsequent nucleophilic attack and the intermolecular proton transfer proceed with lower activation barrier.

As a support of previous results, low and intermediate strength coordinating anions (BF_4^-, SbF_6^-, and OTf^-) facilitate the coordination of the unsaturated substrate, while the stronger coordinating anions (OAc^-, Cl^-) shown poor or no catalytic activity. The description of the mechanism of the hydration

reported in this thesis appears therefore to be of high significance to corroborate the lack of experimental basis in the mechanistic studies of Au(III) catalysis. The importance of the synergistic approach arising from the combination of deep experimental investigations and computational studies have been highlighted. NMR spectroscopy studies and DFT calculations gave detailed information on the reaction mechanism and on the role of both counterion and neutral ligand in gold(III) chemistry.

The coordination ability of Au(III) is computationally (DFT) investigated to shed light on unexpected experimental observations on its catalytic activity in the alkyne hydration reaction. For all the examined complexes the coordination ability towards gold fragment is Cl^- > OTf^- > BF_4^- > 3-hexyne > 2-butyne > H_2O. Due to the steric hindrance/dispersion interaction balance between ligand and IPr, the Au(III) real complex is found to be less selective towards the different ligands, with OTf^- and BF_4^- showing very similar coordination strength, in agreement with the experimentally observed equilibrium. Inclusion of solvent within the implicit solvent model provides qualitatively analogous results, suggesting that Au(III) is not more "oxophilic" than Au(I), inconsistently with the experimental evidence that only the [**2**-H_2O]$^{2+}$ complex could be isolated and characterized, whereas [**2**-(3-hexyne)]$^{2+}$ could not be identified. Remarkably, a stabilization of the [**2**-H_2O]$^{2+}$ complex with respect to [**2**-alkyne]$^{2+}$ can be achieved within a microsolvation model, which reconciles theory with experiment.

Although gold(III) catalysis is still in its infancy, it started to appear an important tool for chemists, able to promote the isomerization, hydration, hydroamination, C-C coupling, and cycloisomerization reactions. On the other side, sustainable and green protocols for the reactions mentioned above are not still fully developed. In fact, silver additives, acids, solvents, high temperature and high catalyst loading are commonly used in homogeneous gold(III) catalysis. NMR spectroscopy combined with DFT calculation has been shown to be a winning combination to study reaction mechanism and to better understand the chemical structure of the catalysis species promoting the development of sustainable homogeneous gold(III) catalysis.

4. Experimental Section

4.1 General procedures and materials

$NaAuCl_4 \cdot 2H_2O$, tetrahydrothiophene (THT), tert-butylamine, paraformaldehyde, glyoxal 40%, chlorotrimethylsilane, 2,6-diisopropylphenylamine, formic acid, acetic acid, trifluoromethanesulfonic acid (HOTf), p-toluensulfonic acid (HOTs), 1,8-Bis(dimethylamino)naphthalene (proton sponge), acenaphthenequinone, methoxy(methyl)chloride, triphenylphosphine (PPh_3), tricyclohexylphosphine (PCy_3), (2-biphenyl)di-tert-butylphosphine (JPhos), tris(3,5-bis(trifluoromethyl)phenyl)phosphine (PAr^F), tris(2,4-di-tert-butyl)phosphite [$P(OR)_3$], silver trifluoromethansoulphonate (AgOTf), silver p-toluensulfonate (AgOTs), silver tetrafluoroborate ($AgBF_4$), silver hexafluoroantimonate (V) ($AgSbF_6$), silver acetate (AgOAc), silver trifluoroacetate (AgTFA), sodium tetrakis[3,5-bis(trifluoromethyl)phenyl]borate ($NaBAr^F$), ammonium chloride, triethyl orthoformate, dibutylammonium trifluoromethanesulfonate (NH_2Bu_2OTf), Aliquat336, dimethylethyldodecyl ammonium triflate (Me2)(Et)(Dod)NOTf, 3-hexyne, diphenylacetylene, 1-phenyl-2propyn-1-ol, 3-hexyn-2-ol, 1,3-diphenyl-2-propyn-1-ol, and all the solvents were purchased from Ricci Chimica, Strem Chemicals, and Sigma Aldrich and used without further purification. All manipulations of moisture-sensitive materials were performed in flamed Schlenk glassware on a Schlenk line, interfaced to a high vacuum pump. All the new compounds were characterized in solution by ^1H, ^{13}C, ^{19}F, and ^{31}P NMR spectroscopies. All the spectra were measured on Bruker AC-200 or Bruker AVANCE III HD 400 MHz spectrometer. Referencing is relative to TMS (^1H and ^{13}C), CH_3NO_2 (^{15}N), CCl_3F (^{19}F), and 85% H_3PO_4 (^{31}P). The elemental analyses were carried out with a Carlo Erba 1106 elemental analyzer.

4.2 Synthesis and characterization

4.2.1 Carbene ligands

1,3-Bis(2,6-diisopropylphenyl)imidazolium chloride (IPr·HCl)

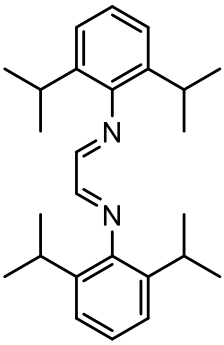

i) glyoxal-bis-(2,6-diisopropylphenyl)imine.

The diaryl-diazadien (DAD^{IPr}) was prepared following the procedure reported in the literature.[206] A mixture of n-propanol (20 mL), water (50 mL) and a 40% aqueous solution of glyoxal (18.15 g, corresponding of 0.125 mol of glyoxal) was added to a solution of freshly distilled 2,6-diisopropylphenylamine (49.25 g, 0.28 mol) in 200 mL of n-propanol at room temperature. The solution was stirred at 70°C for 1 h, and then 200 mL of water was added. The white precipitate was filtered and dried under vacuum (yield 95.1 g, 90.8%).

DAD^{IPr}: ^{1}H NMR (200 MHz, $CDCl_3$, 298 K): δ (ppm) 8.11 (s, 2H), 7.25-7.1 (m, 12H), 2.94 (sept, 4H, $^3J_{HH}$ = 6.9 Hz), 1.21 (d, 24H, $^3J_{HH}$ = 6.9 Hz).

ii) Preparation of 1,3-bis-(2,6-diisopropylphenyl)imidazolium chloride

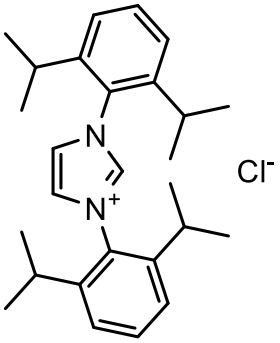

IPr·HCl was prepared following the procedure reported in the literature.[207] A 500 mL round bottom flask containing 240 mL of fresh distilled ethyl acetate was heated at 70°C. DAD^{IPr} (1.0 g, 26.55 mmol) and paraformaldehyde (0.797 g, 26.55 mmol) were added under magnetic stirring. A solution of freshly distilled chlorotrimethylsilane (3.37 ml, 26.55 mmol) in 5 mL of dry EtOAc was added over a period of 45 minutes under vigorous stirring, and the resulting yellow wassuspension stirred for other 2 h. The solution was cooled down to 10°C in an ice-bath and the suspension was filtered and washed with EtOAc and tBuOMe. The white solid was dried under vacuum (yield 78%).

^{1}H NMR (400 MHz, DMSO-d_6, 298 K): δ (ppm) 10.29 (s, 1H), 8.60 (s, 2H), 7.70 (t, 2H, $^3J_{HH}$ = 7.8 Hz), 7.54 (d, 4H, $^3J_{HH}$ = 7.8 Hz), 2.37 (p, 4H, $^3J_{HH}$ = 6.8 Hz), 1.27 (d, 12H, $^3J_{HH}$ = 6.8 Hz), 1.17 (d, 12H, $^3J_{HH}$ = 6.7 Hz).

1,3-Bis-(2,6-diisopropylphenyl)-4,5-dehydroimidazolium chloride (NHC^{CH2}·HCl)

i) N,N'-bis(2,6-diisopropylphenylamino)-1,2-ethandiamin dihydrochloride

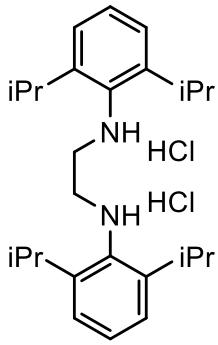

This compound was prepared starting from DAD^{IPr} and following the procedure reported in the literature.[206] In a 250 mL round bottom flask containing DAD^{IPr} (3.92 g, 0.01 mol) in a mixture of MeOH/THF (100 mL) was slowly added $NaBH_4$ (3.78 g, 0.1 mol) cooled with an ice bath. After 1.5 h the reaction (turning white from yellow) was quenched using an aqueous solution of NH_4Cl. The diamine was extracted using diethyl ether (3 x 50 mL). The organic phase was washed with distilled water (3 x 50 mL) then dried using $MgSO_4$. The solvent evaporated by reduced pressure giving a white powder (3.6 g, 97%).

^{1}H NMR (200 MHz, $CDCl_3$, 298 K): δ (ppm) 7.40-7.25 (m, 6H), 3.72 (s, 4H), 3.58 (sept, 4H, $^3J_{HH}$ = 6.6 Hz), 1.24 (d, 24H, $^3J_{HH}$ = 6.6 Hz). ^{13}C {^{1}H} NMR (200 MHz, $CDCl_3$, 298 K): δ (ppm) 151.0, 142.7, 127.1, 124.8, 50.6, 27.2, 24.4. Anal. Calc. for $C_{26}H_{40}N_2$ (380.61): C, 82.05; H, 10.59; N, 7.36. Found: C, 82.72; H, 10.23; N, 7.88.

ii) 1,3-Bis-(2,6-diisopropylphenyl)imidazolinium chloride

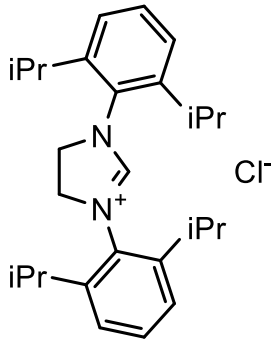

NHC^{CH2}·HCl was prepared following the procedure reported in the literature.[206] In a Schlenk tube a mixture of N,N'-bis(2,6-diisopropylphenylamino)ethanediamine dihydrochloride (8 g, 19.2 mmol), triethyl orthoformate (100 mL) and two drops of 96 % formic acid was refluxed for 45 h. The solid formed on cooling was collected by filtration and washed with EtOAc. The solid was dried under vacuum (yield 4.82 g, 59%).

^{1}H NMR (200 MHz, DMSO-d_6, 298 K): δ (ppm) 9.63 (s, 1H), 7.6-7.3 (m, 6H), 4.41 (s, 4H), 3.09 (sept, 4H, $^3J_{HH}$ = 6.9 Hz), 1.36 (d, 12H, $^3J_{HH}$ = 6.6 Hz), 1.25 (d, 12H, $^3J_{HH}$ = 6.6 Hz). ^{13}C {^{1}H} NMR (200 MHz, DMSO-d_6, 298 K): δ (ppm) 160.0 144.0, 131.0, 129.8, 124.7, 53.7, 28.3, 25.0, 23.3. Anal. Calc. for $C_{27}H_{39}ClN_2$ (427.06): C, 75.93; H, 9.20; Cl, 8.30; N, 6.56. Found: C, 76.05; H, 9.02; N, 6.68.

7,9-bis(2,6-diisopropylphenyl)-7H-acenaphtho[1,2-d]imidazol-9-ium chloride (BIAN)

i) Bis[N,N'-(2,6-diisopropylphenyl)imino]acenaphthene

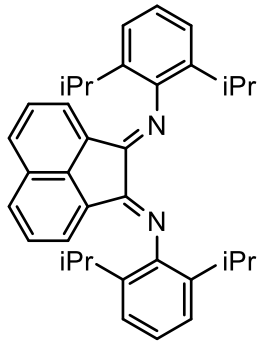

This compound was prepared using a modified method present in literature.[208] Acenaphthenequinone (7.0 g, 38.4 mmol) was suspended in acetonitrile (150mL) and heated under reflux for 60 min. Acetic acid (65 mL) was then added, and heating was continued until acenaphthenequinone had completely dissolved. To this hot solution was added freshly distilled 2,6-diisopropylphenylaniline (16.0 g, 89.9 mmol) over a period of 30 min with the help of a dropping funnel. The solution was heated under reflux for a further 5 h and then cooled to room temperature. The resulting orange-yellow solid was filtered, washed with pentane (3 x 20 mL), and dried under vacuum (yield 18.1 g, 94%).

^{1}H NMR (200 MHz, CD_2Cl_2, 298 K): δ (ppm) 7.88 (d, 2H), 7.36-7.26 (m, 8H), 6.63 (d, 2H), 3.03 (sept, 4H $^{3}J_{HH}$ = 7.1 Hz), 1.23 (d, 24 h, $^{3}J_{HH}$ = 6.9 Hz). ^{13}C {^{1}H} NMR (200 MHz, CD_2Cl_2, 298 K): δ (ppm) 161.1, 148.0, 141.2, 135.5, 131.6, 130.0, 129.2, 128.3, 124.6, 123.9, 123.5, 29.1, 23.2, 23.1. Anal. Calc. for $C_{36}H_{40}N_2$ (500.72): C, 86.35; H, 8.05; N, 5.59. Found: C, 86.71; H, 7.98; N, 5.72.

ii) 7,9-bis(2,6-diisopropylphenyl)-7H-acenaphtho[1,2-d]imidazol-9-ium chloride

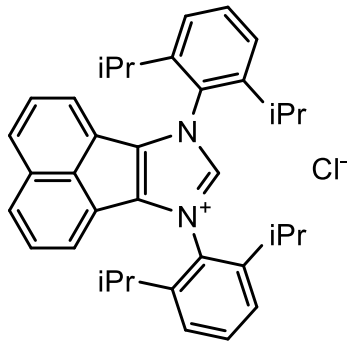

BIAN·HCl was prepared using a modified method present in the literature.[209] In an argon-flushed Schlenk tube were added Bis[N,N'-(2,6-diisopropylphenyl)imino]acenaphthene (484 mg, 0.97 mmol) and methoxy(methyl)chloride (1.5 mL, 19.4 mmol). The reaction mixture was stirred overnight at reflux. After cooling down the temperature, 10 mL of diethylether was added with the formation of a yellow precipitate. The resulting solid was collected by filtration, washed with diethylether (3 x 3 mL) and then with pentane (3 x 3 mL). The bright-yellow product was dried under vacuum (yield 493 mg, 92.5%).

^{1}H NMR (200 MHz, CD_2Cl_2, 298 K): δ (ppm) 12.11 (bs, 1H), 8.02 (d, 2H, $^{3}J_{HH}$ = 8.3 Hz), 7.68 (t, 2H, $^{3}J_{HH}$ = 8.3 Hz), 7.62 (t, 2H, $^{3}J_{HH}$ = 8.3 Hz), 7.58 (d, 2H, $^{3}J_{HH}$ = 7.7 Hz), 7.21 (d, 2H, $^{3}J_{HH}$ = 7.1 Hz), 2.27 (sept, 4H, $^{3}J_{HH}$ = 6.9 Hz), 1.40 (d, 12H, $^{3}J_{HH}$ = 6.8 Hz), 1.16 (d, 12H, $^{3}J_{HH}$ = 6.8 Hz). ^{13}C {^{1}H} NMR (200 MHz, CD_2Cl_2, 298 K): δ (ppm) 145.4, 142.5, 138.1, 132.7, 130.8, 130.4, 129.4, 128.7, 125.4, 123.4, 123.4,

29.7, 24.8, 23.5. Anal. Calc. for $C_{37}H_{41}ClN_2$ (549.19) C, 80.92; H, 7.52; Cl, 6.46; N, 5.10. Found: C, 81.11; H, 7.21; N, 5.30.

4.2.2 Gold(I) complexes

Chloro(tetrahydrothiophene)gold(I) (THT-Au-Cl)

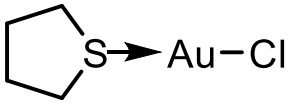

THT-Au-Cl was prepared according to a literature procedure.[210] Tetrahydrothiophen (0.47 mL, 5.3 mmol) was added dropwise to a solution of $NaAuCl_4 \cdot 2H_2O$ in 20 mL of H_2O/EtOH 1:1 and the mixture was stirred for 15 minutes. The precipitate was collected by filtration, washed with water (2 x 10 mL) and dried under vacuum (yield 95%).

^{1}H NMR (400 MHz, $CDCl_3$, 298 K): δ (ppm) 3.44 (bs, 4H), 2.21 (bs, 4H).

General synthesis for phosphine gold(I) chloride complexes.

The synthesis follows a modified procedure reported in literature.[211] Starting from THT-Au-Cl (1 eq.) was dissolved in 5mL of CH_2Cl_2, and 1.1 eq of relative phosphine was then added. The reaction mixture was stirred in the dark (using aluminium foil) for 1 hour (or more if necessary). The reaction mixture was dried under reduced pressure and then re-dissolved with a minimum amount of DCM. n-Pentane (4 mL) was added with formation of a solid which was filtered off, washed with of n-pentane (3x2 mL) and then dried under vacuum.

Chloro(triphenylphosphine)gold(I) (PPh_3-Au-Cl)

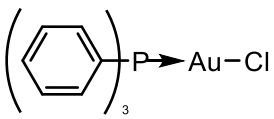

(Yield 87%). ^{1}H NMR (200 MHz, CD_2Cl_2, 298 K): δ (ppm) 7.56-7.24 (m, 15H). ^{13}C {^{1}H} NMR (200 MHz, CD_2Cl_2, 298K): δ(ppm) 134.2, 132.2, 129.3, 128.5. ^{31}P {^{1}H} NMR (200 MHz, CD_2Cl_2, 298K): δ (ppm) 33.8. Anal. Calc. for $C_{18}H_{15}AuClP$ (494.71): C, 43.70; H, 3.06; Au, 39.81; Cl, 7.17; P, 6.26. Found: C, 43.61; H, 3.11.

Chloro(tricyclohexylphosphine)gold(I) (Cy_3-Au-Cl)

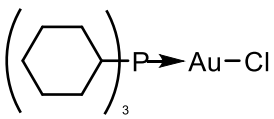

(Yield 90%). ^{1}H NMR (200 MHz, $CDCl_3$, 298 K): δ (ppm) 2.01-1.61 (m, 18H), 1.50-1.35 (m, 6H), 1.32-1.15 (m, 9H). ^{13}C {^{1}H} NMR (200 MHz, $CDCl_3$, 298K): δ (ppm) 33.4, 33.1, 30.7, 27.4, 26.9, 25.8. ^{31}P {^{1}H} NMR (200 MHz, $CDCl_3$, 298K): δ (ppm) 54.01. Anal. Calc. for $C_{18}H_{33}AuClP$ (515.85): C, 42.16; H, 6.49; Au, 38.41; Cl, 6.91; P, 6.04. Found: C, 42.20; H, 6.41.

Chloro(tris(2,4-di-tert-butylphenyl)phosphito)gold(I) (P(OR)$_3$-Au-Cl)

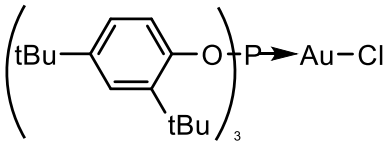

(Yield 75%). ^{1}H NMR (200 MHz, $CDCl_3$, 298 K): δ (ppm) 7.52-7.46 (m, 2H), 1.71 (d, 1H, $^{3}J_{HH}$ = 8.5 Hz,), 1.46 (s, 9H), 1.31 (s, 9H). ^{13}C {^{1}H} NMR (200 MHz, $CDCl_3$, 298K): δ (ppm) 148.28, 147.38, 139.31, 125.51, 124.30, 119.37 (d, *J* = 8.6 Hz), 35.23, 34.80, 31.52, 30.69. ^{31}P {^{1}H} NMR (200 MHz, $CDCl_3$, 298K): δ (ppm) 101.42. Anal. Calc. for $C_{42}H_{63}AuClO_3P$ (879.34): C, 57.37; H, 7.22; Au, 22.40; Cl, 4.03; O, 5.46; P, 3.52. Found: C, 57.42; H, 7.18.

Chloro(Tris[3,5-bis(trifluoromethyl)phenyl]phosphine)gold(I) (PAr^F-Au-Cl)

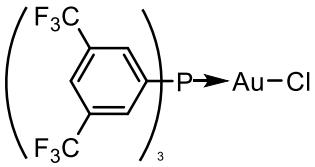

(Yield 92%). ^{1}H NMR (200 MHz, CD_2Cl_2, 298 K): δ (ppm) 8.18 (s, 3H), 7.94 (d, 6H, $^{3}J_{CP}$ = 13.5 Hz). ^{13}C {^{1}H} NMR (200 MHz, CD_2Cl_2, 298 K): δ(ppm) 134.29 (dq, $^{2}J_{CP}$ = 15.3 Hz, $^{3}J_{CF}$ = 3.3 Hz), 133.34 (dq, $^{2}J_{CF}$ = 34.7 Hz, $^{3}J_{CP}$ = 12.8 Hz), 128.62, 128.41 (d, $^{1}J_{CP}$ = 67.6 Hz), 125.27 (q, $^{1}J_{CF}$ = 273 Hz), 122.3 (q, $^{1}J_{CP}$ = 273.7 Hz). ^{19}F NMR (200 MHz, CD_2Cl_2, 298 K): δ (ppm) -63.38. ^{31}P {^{1}H} NMR (200 MHz, CD_2Cl_2, 298 K): δ (ppm) 35.77. Anal. Calc. for $C_{24}H_9AuClF_{18}P$ (902.69): C, 31.93; H, 1.00; Au, 21.82; Cl, 3.93; F, 37.88; P, 3.43. Found: C, 32.05; H, 0.98.

Chloro[(1,1'-biphenyl-2-yl)di-tert-butylphosphine]gold(I) (JPhos-Au-Cl)

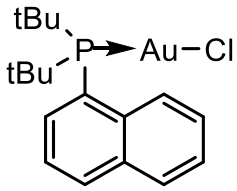

(Yield 91%). ^{1}H NMR (200 MHz, CD_2Cl_2, 298 K): δ (ppm) 7.89 (t, 1H, $^{3}J_{HH}$ =7.2 Hz), 7.50 (m, 3H), 7.38 (t, 2H, $^{3}J_{HH}$ = 7.5 Hz), 7.28 (m, 1H), 7.14 (d, 2H, $^{3}J_{HH}$ = 7.3 Hz), 1.40 (d, 18H, $^{3}J_{HH}$ = 15.6). ^{13}C {^{1}H} NMR (200 MHz, CD_2Cl_2, 298 K): δ(ppm) 149.6, 142.0, 133.3, 132.7, 132.6, 130.0, 128.8, 128.0, 127.4, 126.2, 37.4, 37.0, 30.2, 30.2. ^{31}P {^{1}H} NMR (200 MHz, CD_2Cl_2, 298 K): δ (ppm) 60.5. Anal. Calc. for $C_{18}H_{25}AuClP$ (504.78): C, 42.83; H, 4.99; Au, 39.02; Cl, 7.02; P, 6.14. Found: C, 42.91; H, 4.83.

Chloro[bis(tert-butylamino)methylidene]gold(I) (NAC-Au-Cl)

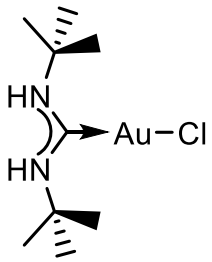

NAC was prepared according to a literature procedure.[212] Tert-butylamine (69.3 µL, 0.66 mmol) was added to a solution of tert-buthylisocyano gold(I) chloride (173 mg, 0.55 mmol) in 4 mL of dichloromethane. The mixture was stirred at room temperature and protect from the light for 3 days. Dichloromethane was added to the mixture (that results milky) until it became limpid. The solution was filtered on a Silica pad and concentrated to minimum volume. The white solid precipitated by addition of pentane was filtered and dried under vacuum (yield 154 mg, 72.6%).

^{1}H NMR (200 MHz, CD_2Cl_2, 298 K): δ (ppm) rotamer A: 6.77 (bs, 2H), 1.59 (s, 18H), rotamer B: 6.37 (bs, 2H), 6.13 (bs, 2H), 1.60 (s, 9H), 1.40 (s, 9H). ^{13}C {^{1}H} NMR (200 MHz, CD_2Cl_2, 298 K): δ (ppm) 189.31, 53.24, 31.48. Anal. Calc. for $C_9H_{20}AuClN_2$ (388.69): C, 27.81; H, 5.19; Au, 50.67; Cl, 9.12; N, 7.21. Found: C, 27.79; H, 5.22; N, 7.18.

Chloro[1,3-bis(2,6-diisopropylphenyl)imidazol-2-ylidene]gold(I) (IPr-Au-Cl)

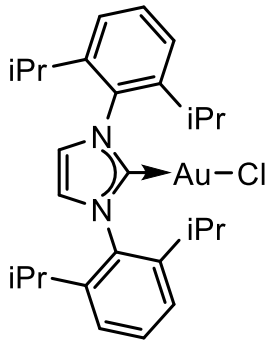

IPr-Au-Cl was prepared according to a literature procedure.[213] In a Schlenk tube containing 18 mL of a DCM:MeOH (5:1) mixture were added IPr·HCl (212.1 mg, 0.5 mmol), $KHCO_3$ (150 mg, 1.5 mmol), and THT-Au-Cl (160 mg, 0.5 mmol). The tube was covered with an aluminium sheet and the mixture was stirred at room temperature for 3 days. The reaction mixture was filtered on a Celite® pad and dried under vacuum. The solid was recrystallized from DCM/ pentane. The resulting white powder was filtered and washed (3x2 mL) with pentane and then dried under vacuum (yield 91%).

^{1}H NMR (400 MHz, $CDCl_3$, 298 K): δ (ppm) = 7.52 (t, 2H, $^{3}J_{HH}$ = 7.8 Hz), 7.31 (d, 4H, $^{3}J_{HH}$ = 7.8 Hz), 7.19 (s, 2H), 2.58 (p, 4H, $^{3}J_{HH}$ = 6.9 Hz), 1.37 (d, 12H, $^{3}J_{HH}$ = 6.9 Hz), 1.24 (d, 12H, $^{3}J_{HH}$ = 6.9 Hz). ^{13}C {^{1}H} NMR (400 MHz, $CDCl_3$, 298 K): δ (ppm) 175.3, 145.5, 133.9, 130.7, 124.2, 123.0, 28.8, 24.5, 24.0. Anal. Calc. for $C_{27}H_{36}AuClN_2$ (621.01): C, 76.29; H, 8.77; Cl, 8.34; N, 6.59. Found: C, 76.35; H, 8.65; N, 6.45.

Chloro[1,3-bis(2,6-diisopropylphenyl)-4,5-dihydroimidazolium]gold(I) (NHC^{CH2}-Au-Cl)

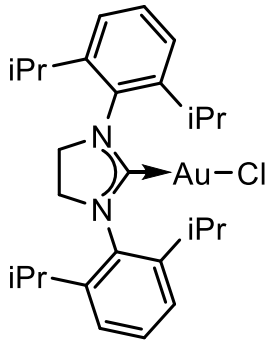

NHC^{CH2}-Au-Cl was prepared using a modified method present in the literature.[209] In Schlenk tube containing 30 mL of dichloromethane were added NHC^{CH2}·HCl (51 mg, 0.079 mmol) and THT-Au-Cl (25 mg, 0.078 mmol). The reaction mixture was stirred for 12 hours at room temperature in the dark. The solvent was removed under reduced pressure and the compound was dissolved in a minimum amount of DCM. Pentane was added resulting in the formation of a yellow solid the solid, which was filtered off, washed with pentane (3 x 3 mL), and dried under vacuum (yield 51 mg, 86%).

^{1}H NMR (200 MHz, CD_2Cl_2, 298 K): δ (ppm) 7.53-7.35 (m, 2H), 7.25-7.22 (m, 4H), 4.05 (d, 4H, $^{3}J_{HH}$ = 7.4 Hz), 3.08-3.02 (m, 4H), 1.41 (d, 12H, $^{3}J_{HH}$ = 6.9 Hz), 1.33 (d, 12H, $^{3}J_{HH}$ = 6.9 Hz). ^{13}C {^{1}H} NMR (200 MHz, CD_2Cl_2, 298K): δ (ppm) 196.0, 146.5, 134.0, 130.0, 124.7, 53.8, 28.9, 25.4, 24.0. Anal. Calc. for

$C_{27}H_{38}AuClN_2$ (623.02): C, 52.05; H, 6.15; Au, 31.61; Cl, 5.69; N, 4.50. Found: C, 52.21; H, 6.01; N, 4.78.

Chloride(BIAN)gold(I) (BIAN-Au-Cl)

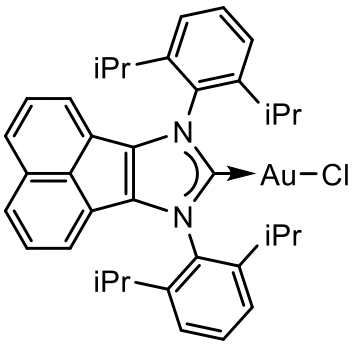

BIAN-Au-Cl was prepared using a modified method present in the literature.[209] In Schlenk tube containing 30 mL of dichloromethane were added BIAN-Cl (51 mg, 0.079 mmol) and THT-Au-Cl (25 mg, 0.078 mmol). The reaction mixture was stirred for 12 hours at room temperature in the dark. The solvent was removed under reduced pressure, the residue was dissolved in a minimum amount of DCM and re-precipitated with pentane. The yellow solid was filtered and washed with pentane (3 x 3 mL) and dried under vacuum (yield 51 mg, 86%).

^{1}H NMR (200 MHz, CD_2Cl_2, 298 K): δ (ppm) 7.84 (d, 2H, $^3J_{HH}$ = 8.4 Hz), 7.68 (t, 2H, $^3J_{HH}$ = 7.8 Hz), 7.46 (dd, 2H, $^3J_{HH}$ = 8.4 Hz, $^4J_{HH}$ = 7.0 Hz), 7.45 (d, 4H, $^3J_{HH}$ = 7.9 Hz), 7.03 (d, 2H, $^3J_{HH}$ = 7.1 Hz), 2.83 (sept, 4H, $^3J_{HH}$ = 7.2 Hz), 1.38 (d, 12H, $^3J_{HH}$ = 6.9 Hz), 1.21 (d, 12H, $^3J_{HH}$ = 6.9 Hz). ^{13}C {^{1}H} NMR (200 MHz, CD_2Cl_2, 297 K): δ (ppm) 175.6, 146.1, 138.4, 133.1, 131.3, 130.5, 129.0, 128.2, 125.6, 125.0, 121.7, 29.3, 24.59, 23.91. Anal. Calc. for $C_{37}H_{40}AuClN_2$ (745.15) C, 59.64; H, 5.41; Au, 26.43; Cl, 4.76; N, 3.76. Found: C, 59.7; H, 5.47; N, 3.72.

General synthesis of P-Au-OTs (P = PPh_3, JPhos, PCy_3, PAr^F, $P(OR)_3$)

A general catalyst of the type R_3P-Au-Cl (0.11 mmol) was dissolved in 5mL of CH_2Cl_2. Subsequently, 1.1 eq (0.12 mmol) of AgOTs was added, leading to the precipitation of AgCl. The reaction mixture was stirred overnight, and then dried. After the addition of 2 mL of fresh dichloromethane, the mixture was filtered on a Celite® pad the solid was washed with CH_2Cl_2 (3x1 mL). The solution was concentrated under vacuum and then n-pentane (4mL) was added, resulting in the formation of a precipitate. The resulting solid was filtered off, washed with 3x2 mL of n-pentane, and then dried under vacuum to afford the product as a white powder.

PPh_3-Au-OTs

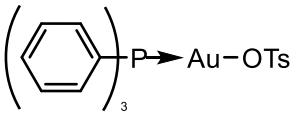

(Yield 78%). ^{1}H NMR (200 MHz, $CDCl_3$, 298 K): δ (ppm) 7.9-7.1 (m, 19H), 2.41 (s, 3H). ^{13}C {^{1}H} NMR (200 MHz, $CDCl_3$, 298 K): δ (ppm) 141.7, 139.2, 134.1, 132.2, 129.4 129.0, 127.6, 126.5, 53.3. ^{31}P {^{1}H} NMR (81 MHz, $CDCl_3$,

298K): δ (ppm) 27.9. Anal. Calc. for $C_{25}H_{23}AuO_3PS$ (631.45): C, 47.55; H, 3.67; Au, 31.19; O, 7.60; P, 4.91; S, 5.08. Found: C, 47.19; H, 3.28; S, 4.99.

PCy_3-Au-OTs

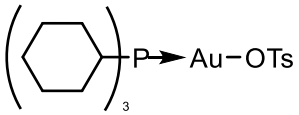

(Yield 75%). ^{1}H NMR (200 MHz, $CDCl_3$, 298 K): δ (ppm) 7.88 (d, 2H, $^3J_{HH}$ =8.2Hz), 7.21 (d, 2H, $^3J_{HH}$ = 8.0Hz), 2.37 (s, 3H), 2.01-1.61 (m, 18H), 1.50-1.35 (m, 6H), 1.32-1.15 (m, 9H). ^{13}C {^{1}H} NMR (200 MHz, $CDCl_3$, 298K): δ(ppm) 141.7, 139.0, 128.9, 126.4, 39.6, 33.1, 30.7, 27.4, 26.9, 25.8, 21.3. ^{31}P {^{1}H} NMR (200 MHz, $CDCl_3$, 298K): δ (ppm) 54.01. Anal. Calc. for $C_{25}H_{40}AuO_3PS$ (648.59): C, 46.30; H, 6.22; Au, 30.37; O, 7.40; P, 4.78; S, 4.94. Found: C, 46.76; H, 6.11; S, 4.63.

$P(OR)_3$-Au-OTs

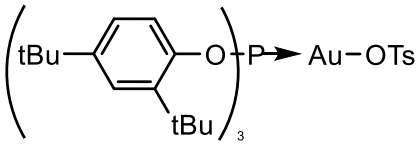

(Yield 63%). ^{1}H NMR (200 MHz, $CDCl_3$, 298 K): δ (ppm) 7.88 (d, 2H, $^3J_{HH}$ =8.1Hz), 7.52-7.46 (m, 6H), 7.21 (d, 2H, $^3J_{HH}$ = 8.1Hz), 7.15 (m, 3H, $^3J_{HH}$ = 8.5 Hz), 2.36 (s, 3H), 1.465 (s, 27H), 1.311 (s, 27H). ^{13}C {^{1}H} NMR (200 MHz, $CDCl_3$, 298K): δ(ppm) 148.3, 147.3, 141.7, 139.3, 129.0, 126.3, 125.51, 124.30, 119.37 (d, J = 8.6 Hz), 35.23, 34.80, 31.52, 30.69, 21.3. ^{31}P {^{1}H} NMR (200 MHz, $CDCl_3$, 298K): δ (ppm) 93.2. Anal. Calc. for $C_{49}H_{70}AuO_6PS$ (1015.08): C, 57.98; H, 6.95; Au, 19.40; O, 9.46; P, 3.05; S, 3.16. Found: C, 58.15 H, 6.72; S, 3.01.

PAr^F-Au-OTs

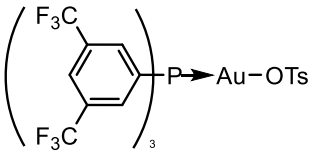

(Yield 72%). ^{1}H NMR (200 MHz, $CDCl_3$, 298 K): δ (ppm) 8.22 (s, 3H), 7.97 (d, 6H, J_{HP} = 13.5 Hz), 7.85 (d, 2H, $^3J_{HH}$ = 7.3 Hz), 7.26 (d, 2H, $^3J_{HH}$ = 7.4 Hz), 2.40 (s, 3H). ^{13}C {^{1}H} NMR (50 MHz, $CDCl_3$, 298K): δ (ppm) 142.02, 139.26, 134.53 (m), 133.61 (m), 129.21, 128.86 (d, $^1J_{CP}$ = 64.8 Hz), 127.79 (m), 126.38, 122.03 (m), 21.40. ^{19}F NMR (188 MHz, $CDCl_3$, 298K): δ (ppm) -63.88 (s, CF_3). ^{31}P {^{1}H} NMR (81 MHz, $CDCl_3$, 298K): δ (ppm) 32.45 (s, P). Anal. Calc. For $C_{31}H_{16}AuF_{18}O_3PS$ (1038.43): C, 35.86; H, 1.55; Au, 18.97; F, 32.93; O, 4.62; P, 2.98; S, 3.09. Found: C, 35.90; H, 1.58.

JPhos-Au-OTs

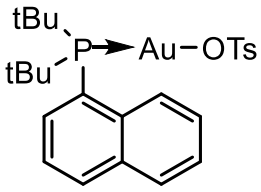

(Yield 75%). ^{1}H NMR (200 MHz, $CDCl_3$, 298 K): δ (ppm) 7.88 (d, 2H, $^3J_{HH}$ = 8.2 Hz), 7.58 (t, 3H, $^3J_{HH}$ = 7.3 Hz), 7.48-7.56 (m, 2H), 7.45 (t, 1H, $^3J_{HH}$ = 7.7 Hz), 7.32 (t, 1H, $^3J_{HH}$ = 5.4 Hz), 7.21 (d, 2H, $^3J_{HH}$ = 8.0 Hz), 7.14 (d, 2H, $^3J_{HH}$ = 7.4 Hz),

2.37 (s, 3H), 1.43 (d, 18H, $^{3}J_{HH}$ = 15.5 Hz). ^{13}C {^{1}H} NMR (200 MHz, $CDCl_3$, 298 K): δ (ppm) 133.6, 133.3, 130.7, 129.5, 128.8, 128.4, 126.9, 37.9, 21.0. ^{31}P {^{1}H} NMR (200 MHz, $CDCl_3$, 298 K): δ (ppm) 56.8. Anal. Calc. for $C_{25}H_{32}AuO_3PS$ (640.53): C, 46.88; H, 5.04; Au, 30.75; O, 7.49; P, 4.84; S, 5.01. Found: C, 47.01; H, 4.90; S, 4.17.

General synthesis for NHC-anion exchange using silver salts

The NHC-Au-Cl complex (0.11 mmol) was dissolved in 5 mL of CH_2Cl_2, then 1.1 eq. (0.12 mmol) of AgX (X = OTf^- or OTs^-) was added leading to the precipitation of AgCl. The reaction mixture was stirred in the dark (using aluminium foil) overnight. The reaction mixture was dried under reduced pressure and re-dissolved with a minimum amount of DCM, filtered on Celite® pad, concentrated under vacuum. The addition of n-pentane (4mL) resulted in the formation of a precipitate which was filtered off, washed with 3x2 mL of n-pentane and then dried under vacuum.

IPr-Au-OTf

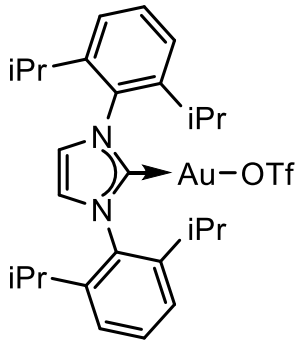

(Yield 85.1%). ^{1}H NMR (200 MHz, CD_2Cl_2, 298 K): δ (ppm) 7.58 (t, 2H, $^{3}J_{HH}$ = 7.8 Hz), 7.37 (d, 4H, $^{3}J_{HH}$ = 7.7 Hz), 7.28 (s, 2H), 2.56 (sept, 4H, $^{3}J_{HH}$ = 6.9 Hz), 1.35 (d, 12H, $^{3}J_{HH}$ = 6.8 Hz), 1.24 (d, 12H, $^{3}J_{HH}$ = 6.8 Hz). ^{13}C {^{1}H} NMR (200 MHz, CD_2Cl_2, 298 K): δ (ppm) 166.0, 162.1, 146.4, 134.4, 131.2, 124.8, 124.3, 116.50, 29.4, 24. ^{19}F NMR (200 MHz, CD_2Cl_2, 298 K): δ (ppm) -73.89 (s, CF_3). Anal. Calc. for $C_{38}H_{26}AuF_3N_2O_3S$ (734.62) C, 45.78; H, 4.94; Au, 26.81; F, 7.76; N, 3.81; O, 6.53; S, 4.36. Found: C, 45.99; H, 4.81; N, 3.92; S, 4.21.

IPr-Au-OTs

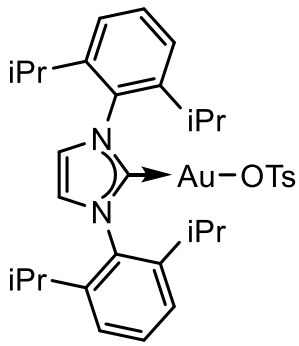

(Yield 90%). ^{1}H NMR (200 MHz, CD_2Cl_2, 298 K): δ (ppm) 7.55 (t, 2H, $^{3}J_{HH}$ = 7.8 Hz), 7.39 (d, 4H, $^{3}J_{HH}$ = 7.7 Hz), 7.31 (d, 2H, $^{3}J_{HH}$ = 7.7 Hz), 7.21 (s, 2H), 6.98 (d, 2H, $^{3}J_{HH}$ = 7.4 Hz), 2.47 (sept, 4H, $^{3}J_{HH}$ = 6.8 Hz), 2.32 (s, 3H), 1.29 (d, 12H, $^{3}J_{HH}$ = 6.8 Hz), 1.21 (d, 12H, $^{3}J_{HH}$ = 6.8 Hz). ^{13}C {^{1}H} NMR (200 MHz, CD_2Cl_2, 298 K): δ (ppm) 164.5, 145.7, 133.8, 131.1, 128.8, 126.4, 124.6, 123.6, 123.2, 29.05, 24.3, 21.6, 21.6. Anal. Calc. for $C_{34}H_{44}AuN_2O_3S$ (757.76): C, 53.89; H, 5.85; Au, 25.99; N, 3.70; O, 6.33; S. 4.23. Found: C, 53.91; H, 5.84; N, 3.6.

NHC^{CH2}-Au-OTf

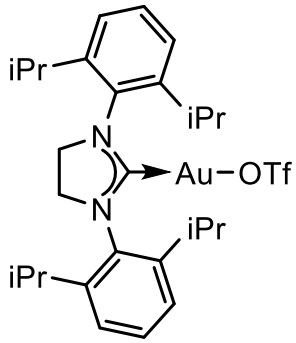

(Yield 95%). ^{1}H NMR (200 MHz, CD_2Cl_2, 298 K): δ (ppm) 7.53-7.35 (m, 2H), 7.25-7.22 (m, 4H), 4.05 (d, 4H, $^{3}J_{HH}$ = 7.4 Hz), 3.08-3.02 (m, 4H), 1.41 (d, 12H, $^{3}J_{HH}$ = 6.9 Hz), 1.33 (d, 12H, $^{3}J_{HH}$ = 6.9 Hz). ^{13}C {^{1}H} NMR (200 MHz, CD_2Cl_2, 298K): δ (ppm) 196.0, 146.5, 134.0, 130.0, 124.7, 53.8, 28.9, 25.4, 24.0. ^{19}F NMR (200 MHz, $CDCl_3$, 298 K): δ (ppm) -78.22. Anal. Calc. for $C_{28}H_{38}AuF_3N_2O_3S$ (736.64): C, 45.65; H, 5.20; Au, 26.74; F, 7.74; N, 3.80; O, 6.52; S. 4.35. Found: C, 49.47; H, 5.06; N, 3.92; S, 4.13.

NHC^{CH2}-Au-OTs

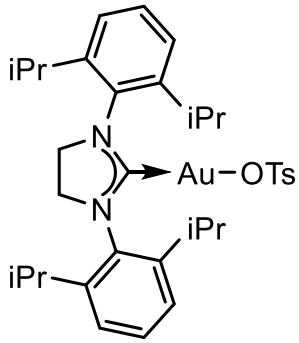

(Yield 94%). ^{1}H NMR (200 MHz, CD_2Cl_2, 298 K): δ (ppm) 7.88 (d, 2H, $^{3}J_{HH}$ = 8.2Hz), 7.53-7.35 (m, 2H), 7.25-7.22 (m, 2H), 4.05 (d, 4H, $^{3}J_{HH}$ = 7.4 Hz), 3.08-3.02 (m, 4H), 2.37 (s, 3H), 1.41 (d, 12H, $^{3}J_{HH}$ = 6.9 Hz), 1.33 (d, 12H, $^{3}J_{HH}$ = 6.9 Hz). ^{13}C {^{1}H} NMR (200 MHz, CD_2Cl_2, 298K): δ (ppm) 196.0, 146.5, 141.7, 139.0, 134.0, 130.0, 128.9, 126.4, 124.7, 53.8, 28.9, 25.4, 24.0, 21.3. Anal. Calc. for $C_{34}H_{45}AuN_2O_3S$ (758.76): C, 53.82; H, 5.98; Au, 25.96; N, 3.69; O, 6.33; S. 4.23. Found: C, 54.03; H, 5.55; N, 3.82; S, 4.10.

BIAN-Au-OTf

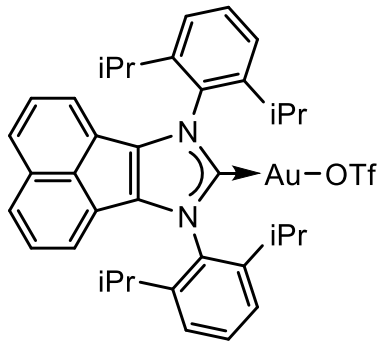

(Yield 91%). ^{1}H NMR (200 MHz, CD_2Cl_2, 298 K): δ (ppm) 7.84 (d, 2H, $^{3}J_{HH}$ = 8.4 Hz), 7.68 (t, 2H, $^{3}J_{HH}$ = 7.8 Hz), 7.46 (dd, 2H, $^{3}J_{HH}$ = 8.4 Hz, $^{4}J_{HH}$ = 7.0 Hz), 7.45 (d, 4H, $^{3}J_{HH}$ = 7.9 Hz), 7.03 (d, 2H, $^{3}J_{HH}$ = 7.1 Hz), 2.83 (sept, 4H, $^{3}J_{HH}$ = 7.2 Hz), 1.38 (d, 12H, $^{3}J_{HH}$ = 6.9 Hz), 1.21 (d, 12H, $^{3}J_{HH}$ = 6.9 Hz). ^{13}C {^{1}H} NMR (200 MHz, CD_2Cl_2, 298 K): δ (ppm) 175.6, 146.1, 165.8, 138.4, 133.1, 131.3, 130.5, 129.0, 128.2, 125.6, 125.0, 121.7, 29.3, 24.59, 23.91. Anal. Calc. for $C_{38}H_{40}AuF_3N_2O_3S$ (858.76) C, 53.15; H, 4.69; Au, 22.94; F, 6.64; N, 3.26; O, 5.59; S, 3.73. Found: C, 60.08; H, 5.24; N, 3.24; S, 3.43.

BIAN-Au-OTs

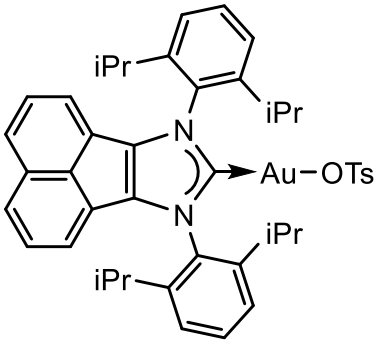

(Yield 96%). ^{1}H NMR (200 MHz, CD_2Cl_2, 298 K): δ (ppm) 7.84 (m, 4H), 7.68 (t, 2H, $^{3}J_{HH}$ = 7.8 Hz), 7.46 (dd, 2H, $^{3}J_{HH}$ = 8.4 Hz, $^{4}J_{HH}$ = 7.0 Hz), 7.45 (d, 4H, $^{3}J_{HH}$ = 7.9 Hz), 7.21 (d, 2H, $^{3}J_{HH}$ = 8.0Hz), 7.03 (d, 2H, $^{3}J_{HH}$ = 7.1 Hz), 2.83 (sept, 4H, $^{3}J_{HH}$ = 7.2 Hz), 2.37 (s, 3H), 1.38 (d, 12H, $^{3}J_{HH}$ = 6.9 Hz), 1.21 (d, 12H, $^{3}J_{HH}$ = 6.9 Hz). ^{13}C {^{1}H} NMR (200 MHz, CD_2Cl_2, 298 K): δ (ppm) 175.6, 146.1, 141.7, 139.0, 138.4, 133.1, 131.3, 130.5, 129.0, 128.9, 128.2, 126.4, 125.6, 125.0, 121.7, 29.3, 24.59, 23.91, 21.3. Anal. Calc. for $C_{44}H_{47}AuN_2O_3S$ (880.89) C, 59.99; H, 5.38; Au, 22.36; N, 3.18; O, 5.45; S, 3.64. Found: C, 60.08; H, 5.24; N, 3.24; S, 3.43.

4.2.3 Gold(III) complexes

1 Dichloro(phenylpyridin)gold(III) [(ppy)-Au-Cl_2]

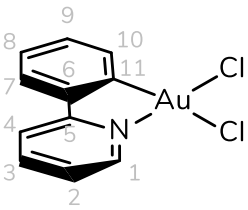

The complex (ppy)-Au-Cl_2 (**1**) was prepared according to aliterature procedure.[172] 1 mmol of $NaAuCl_4 \cdot 2H_2O$ was dissolved in 8 mL of water in a Schlenk flask. A solution obtaining by dissolving 0.99 mmol of 2-phenylpyridine (ppy) in 1.6 mL of acetonitrile was dropwise added under vigorous agitation. A bright yellow powder was instantly formed. After 4 h, the solid was filtered and dried under pressure. Finally, the complex was put in an oven at 165°C for 12 h during which time the cyclometallation occurred. The complex was used without any other purification (yield 76%). The assignment of all ^{1}H, ^{13}C was made by means of bidimensional experiments such as ^{1}H-^{1}H COSY, ^{1}H-^{13}C HSQC, and ^{1}H-^{13}C HMBC.

^{1}H NMR (400 MHz, DMSO-d_6, 298 K) δ(ppm): 9.54 (d, 1H, $^{3}J_{HH}$ = 6.0 Hz, H_1), 8.44 – 8.37 (m, 2H, H3-4), 7.97 (dd, 1H, $^{3}J_{HH}$ = 7.7, $^{4}J_{HH}$ = 1.7 Hz, H7), 7.83 (dd, 1H, $^{3}J_{HH}$ = 8.1, $^{4}J_{HH}$ = 1.1 Hz, H10), 7.78 (td, 1H $^{3}J_{HH}$ = 5.9, $^{4}J_{HH}$ = 3.3 Hz, H2), 7.48 (td, 1H, $^{3}J_{HH}$ = 7.5, $^{4}J_{HH}$ = 1.2 Hz, H8), 7.39 (td, 1H, $^{3}J_{HH}$ = 8.9, $^{4}J_{HH}$ = 7.4, H9). ^{13}C {^{1}H} NMR (101 MHz, DMSO-d_6, 298 K): δ(ppm) 164.46 (C5), 152.76 (C6), 148.53 (C1), 144.45(C4), 143.46 (C11), 132.13 (C9), 130.52 (C10), 129.82 (C8), 127.21 (C7), 125.80 (C2), 122.66 (C3). Anal. Calc. for $C_{11}H_8AuNCl_2$ (MW: 422.06 g·mol^{-1}) C, 31.30; H, 1.91; Au, 46.67; N, 3.32; Cl, 16.80. Found: C, 31.4; H, 1.9; N 3.2.

[2-Cl]Cl [(ppy)-Au-IPr-Cl]Cl

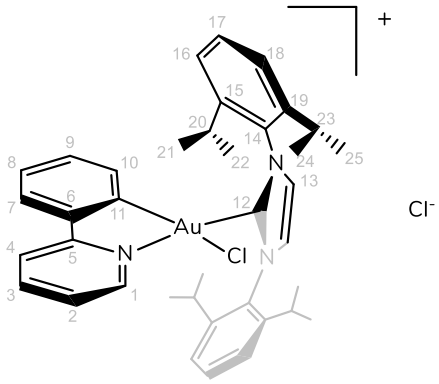

In a Schlenk flask 1 eq. (0.25 mmol) of IPr·HCl, 1.1 equiv. (116.1 mg, 0.275mmol) of **1** and 4 equiv. (100.1 mg, 1 mmol) of $KHCO_3$ were dissolved in 10 mL of acetonitrile and stirred at room temperature overnight. The solvent was then removed under vacuum. The residue was dissolved in CH_2Cl_2 and filtered through a paddle of Celite®. The volume of the solution was reduced and then complex wasprecipitated with n-pentane. The white microcrystalline product was collected by filtration, washed with n-pentane (2 x 2 mL), and dried under vacuum. Yield of 94%. NMR and elemental analysis data are in accordance with those reported in the literature.

^{1}H NMR (400 MHz, $CDCl_3$, 298 K): δ(ppm) 9.28 (dd, 1H, $^3J_{HH}$ = 6.1 Hz, $^4J_{HH}$ = 1.6 Hz, H1), 8.43 (dd, 1H, $^3J_{HH}$ = 8.2, $^4J_{HH}$ = 1.4 Hz, H4), 8.34 (td, 1H, $^3J_{HH}$ = 7.8 Hz, $^4J_{HH}$ = 1.6 Hz, H3), 8.06 – 7.99 (m, 3H, H7-13), 7.57 – 7.44 (m, 4H, H2-8-17), 7.35 (dd, 2H, $^3J_{HH}$ = 7.8 Hz, $^4J_{HH}$ = 1.6 Hz, H18), 7.32 – 7.26 (m, 1H, H9), 7.24 (dd, 1H, $^3J_{HH}$ = 7.8 Hz, $^3J_{HH}$ = 1.5 Hz, H16), 6.95 (d, 1H, $^3J_{HH}$ = 7.9 Hz, H10), 3.05 (p, 2H, $^3J_{HH}$ = 6.7 Hz, H20), 2.89 (p, 2H, $^3J_{HH}$ = 6.7 Hz, H23), 1.45 (d, 6H, $^3J_{HH}$ = 6.6 Hz, H24), 1.27 (d, 6H, $^3J_{HH}$ = 6.7 Hz, H22), 1.13 (d, 6H, $^3J_{HH}$ = 6.8 Hz, H25), 0.72 (d, 6H, $^3J_{HH}$ = 6.7 Hz, H21). ^{13}C {^{1}H} NMR (101 MHz, $CDCl_3$, 298 K): δ(ppm) 163.80 (1C, C5), 149.20 (1C, C12), 148.46 (1C, C6), 147.26 (1C, C1), 147.20 (1C, C19), 144.93 (2C, C15), 144.43 (1C, C3), 143.40 (1C, C11), 132.58 (1C, C9), 132.50 (2C, C14), 132.21 (1C, C10), 131.98 (2C, C17), 130.02 (1C, C8), 128.67 (2C, C13), 127.59 (1C, C7), 125.16(2C, C16), 124.90 (2C, C18), 124.53 (1C, C2), 122.55 (1C, C4), 29.51 (2C, C23), 29.11 (2C, C20), 26.94 (2C, C25), 26.75 (2C, C22), 22.82 (2C, C21), 22.66 (2C, C24). ^{15}N (41 MHz, acetone-d_6, 298 K): δ(ppm) -147.7 (1N, N1), -189.8 (2N, N2). Anal. Calc. for $C_{38}H_{44}AuN_3Cl_2$ (MW: 810.66 g·mol^{-1}) C, 56.30; H, 5.47; Au, 24.30; N, 5.18, Cl, 8.75. Found: C, 56.1; H, 5.4; N 5.1.

3 [Chloro(phenylpyridin)(triphenylphosphin)gold(III)]triflate [(ppy)-Au-PPh_3-Cl]OTf

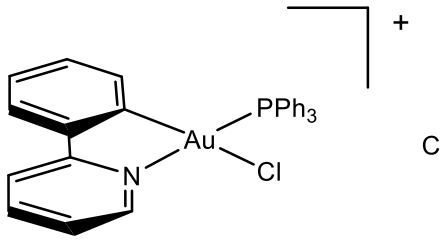

A solution of 9 mL of acetone containing **1** (105.5 mg, 0.25 mmol), triphenylphosphine (72.1 mg, 1.1 eq.) and $NaCF_3SO_3$ (172.06 mg, 4 eq.) was stirred overnight in a Schlenk flask. The solvent was removed under vacuum and replaced with dichloromethane. The solid was

removed via filtration through Celite®. The volume of the solution was reduced and the white solid was precipitated by addition of n-pentane. (yield 91.5%)

^{1}H NMR (400 MHz, CD_2Cl_2, 298 K): δ(ppm) 9.60 (br, 1H), 8.23 (br, 2H), 7.70 (m, 17H), 7.38 (br, 1H), 6.84 (m, 1H), 6.78 (m, 1H). ^{31}P {^{1}H} NMR (162 MHz, CD_2Cl_2, 298 K): δ(ppm) 43.46 (s). ^{19}F NMR (376 MHz, CD_2Cl_2, 298 K): δ(ppm) -78.88 (s). Anal. Calc. for $C_{30}H_{23}AuClF_3NO_3PS$ (MW: 797.97 g·mol^{-1}) C, 45.16; H, 2.91; Au, 24.68; Cl, 4.44; F, 7.14; N, 1.76 O, 6.02; P, 3.88; S, 4.02. Found: C, 45.1; H, 2.9; N 1.8.

[2-Cl]OTf **[(ppy)-Au-IPr-Cl]OTf**

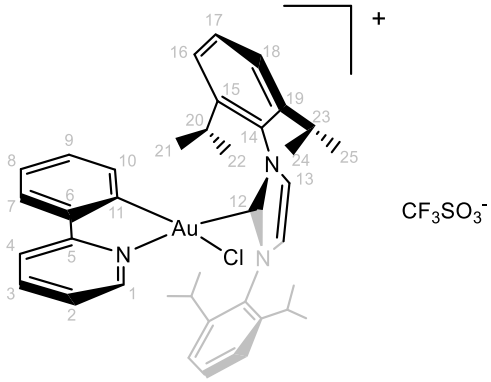

The complex [**2**-Cl]OTf was synthesized by adding in a Schlenk flask 1.1 eq. (17.4 mg, 0.07 mmol) of silver triflate to (50 mg, 0.06 mmol) [**2**-Cl]Cl in 2 mL of dichloromethane. The solution was filtered on Celite and the volume was reduced. The solution was filtered on Celite® and the volume was reduced. The final compound was crystallized with pentane. The complex was characterized by mono and bidimensional ^{1}H, ^{13}C, and ^{19}F NMR experiments. The assignment of all ^{1}H and ^{13}C resonances was made by means of bidimensional experiments, such as ^{1}H-^{1}H COSY, ^{1}H-^{13}C HSQC, ^{1}H-^{13}C HMBC, and ^{1}H-^{1}H NOESY.

^{1}H NMR (400 MHz, $CDCl_3$, 298 K): δ(ppm) = 9.27 (dd, 1H, $^{3}J_{HH}$ = 6.1, $^{4}J_{HH}$ = 1.5 Hz, H1), 8.21 (td, 1H, $^{3}J_{HH}$ = 7.8 Hz, $^{4}J_{HH}$ = 1.6 Hz, H3), 8.11 (dd, 1H, $^{3}J_{HH}$ = 8.3, $^{4}J_{HH}$ =1.6 Hz, H4), 7.88 (s, 2H, H13), 7.78 (dd, 1H, $^{3}J_{HH}$ = 7.9 Hz, $^{4}J_{HH}$ = 1.6 Hz, H7), 7.53 – 7.40 (m, 4H, H2-8-17), 7.38 – 7.29 (m, 3H, H9-18), 7.22 (dd, 2H, $^{3}J_{HH}$ = 7.8, $^{4}J_{HH}$ = 1.5 Hz, H16), 6.96 (d, 1H, $^{3}J_{HH}$ = 7.8 Hz, H10), 3.03 (hept, 2H, $^{3}J_{HH}$ = 6.7 Hz, H20), 2.86 (hept, 2H, $^{3}J_{HH}$ = 6.7 Hz, H23), 1.43 (d, 6H, $^{3}J_{HH}$ = 6.6 Hz, H24), 1.23 (d, 6H, $^{3}J_{HH}$ = 6.7 Hz, H22), 1.09 (d, 6H, $^{3}J_{HH}$ = 6.8 Hz, H25), 0.70 (d, 6H, $^{3}J_{HH}$ = 6.7 Hz, H21). ^{13}C{^{1}H} NMR (101 MHz, $CDCl_3$, 298 K) δ(ppm) = 163.79 (1C, C5), 148.67 (1C, C12), 148.53 (1C, C6), 147.40 (1C, C1), 147.21 (2C, C19), 145.04 (2C, C15), 144.14 (1C, C3), 143.19 (1C, C11), 132.89 (1C, C9), 132.53 (1C, C14), 132.47 (1C, C10), 131.91 (2C, C17), 129.87 (1C, C8), 128.66 (2C, C13), 126.96 (1C, C7), 125.13 (2C, C16), 124.83 (2C, C18), 124.56 (1C, C2), 121.88 (1C, C4), 29.49 (2C, C23), 29.06 (2C, C20), 26.79 (2C, C25), 26.56 (2C, C22), 22.80 (2C, C21), 22.66 (2C, C24). ^{19}F NMR (376 MHz, $CDCl_3$, 298 K): δ(ppm) = -78.08.

[2-Cl]BF_4 [(ppy)-Au-IPr-Cl]BF_4

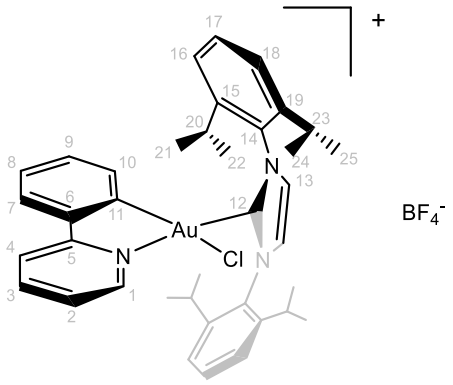

The complex [**2**-Cl]OTf was synthesized by adding in a Schlenk flask 1.1 eq. (13.6 mg, 0.07 mmol) of silver tetrafluoroborate to (50 mg, 0.06 mmol) [**2**-Cl]Cl in 2 mL of dichloromethane. The solution was filtered on Celite and the volume was reduced. The solution was filtered on Celite® and the volume was reduced. The final compound was crystallized with pentane. The complex was characterized by mono and bidimensional ^{1}H, ^{13}C, and ^{19}F NMR experiments.

^{1}H NMR (400 MHz, CD_2Cl_2, 298 K): δ(ppm) = 9.35 (dd, 1H, $^{3}J_{HH}$ = 6.1, $^{4}J_{HH}$ = 1.6 Hz, H1), 8.18 (td, 1H, $^{3}J_{HH}$ = 7.8, $^{4}J_{HH}$ = 1.6 Hz, H3), 7.98 (dt, 1H, $^{3}J_{HH}$ = 8.1, $^{4}J_{HH}$ = 1.1 Hz, H4), 7.80 (s, 2H, H13), 7.75 (dd, 1H, $^{3}J_{HH}$ = 7.9, $^{4}J_{HH}$ = 1.6 Hz, H7), 7.60 – 7.49 (m, 4H, H2-8-17), 7.41 (dd, 2H, $^{3}J_{HH}$ = 7.8, $^{4}J_{HH}$ = 1.5 Hz, H18), 7.36 (td, 1H, $^{3}J_{HH}$ = 7.7, $^{4}J_{HH}$ = 1.6 Hz, H9), 7.30 (dd, 2H, $^{3}J_{HH}$ = 7.8, $^{4}J_{HH}$ = 1.5 Hz, H16), 7.02 (dd, 1H, $^{3}J_{HH}$ = 7.8, $^{4}J_{HH}$ = 1.1 Hz, H10), 3.07 (hept, 2H, $^{3}J_{HH}$ = 6.7 Hz, H20), 2.92 (hept, 2H, $^{3}J_{HH}$ = 6.7 Hz, H23), 1.48 (d, 6H, $^{3}J_{HH}$ = 6.6 Hz, H24), 1.27 (d, 6H, $^{3}J_{HH}$ = 6.7 Hz ,H22), 1.15 (d, 6H, $^{3}J_{HH}$ = 6.8 Hz, H25), 0.79 (d, 6H, $^{3}J_{HH}$ = 6.7 Hz, H21). ^{19}F NMR (400 MHz, CD_2Cl_2, 298 K): δ = -152.98 – -153.09 (m).

[2-OTf]OTf [(ppy)-Au-IPr-OTf]OTf

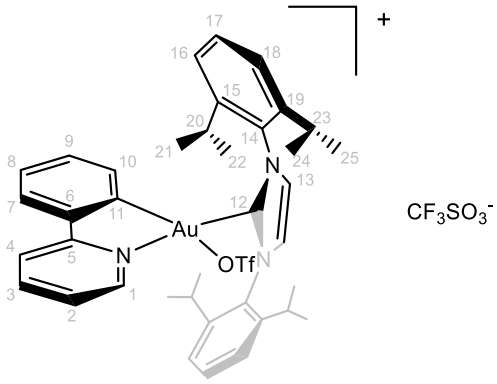

The complex [**2**-Cl]OTf was synthesized by adding in a Schlenk flask 2.5 eq. (34.8 mg, 0.14 mmol) of silver triflate to (50 mg, 0.06 mmol) [**2**-Cl]Cl in 2 mL of dichloromethane. The solution was filtered on Celite and the volume was reduced. The solution was filtered on Celite® and the volume was reduced. The final compound was crystallized with pentane. The complex was characterized by mono and bidimensional ^{1}H, ^{13}C, and ^{19}F NMR experiments.

^{1}H NMR (400 MHz, CD_2Cl_2, 298 K): δ (ppm)= 8.79 (d, 1H, $^{3}J_{HH}$ = 5.9 Hz, H1), 8.19 (t, 1H, $^{3}J_{HH}$ = 7.8 Hz, H3), 7.92 (d, 1H, $^{3}J_{HH}$ = 8.1 Hz,H4), 7.79 (s, 2H, H13), 7.71 (d, 1H, $^{3}J_{HH}$ = 7.79 Hz, H7), 7.67 – 7.59 (m, 2H, H17), 7.57 – 7.46 (m, 3H, H2-18), 7.36 (m, 3H, H8-16), 7.26 (td, 1H, $^{3}J_{HH}$ = 7.8, $^{4}J_{HH}$ = 1.7 Hz, H9), 6.72 (d, 1H, $^{3}J_{HH}$ = 8.1 Hz, H10), 2.96 (p, 2H, $^{3}J_{HH}$ = 6.7 Hz, H20), 2.66 (p, 2H, $^{3}J_{HH}$ = 6.7 Hz, H23), 1.52

(d, 7H, $^{3}J_{HH}$ = 6.4 Hz, H24), 1.29 (d, 8H, $^{3}J_{HH}$ = 6.4 Hz, H22), 1.15 (d, 8H, $^{3}J_{HH}$ = 6.5 Hz, H25), 0.85 (d, 6H, $^{3}J_{HH}$ = 6.7 Hz, H21). ^{19}F NMR (376 MHz, CD_2Cl_2, 298 K): δ(ppm) = -77.95.

[2-BF_4]BF_4 [(ppy)-Au-IPr-BF_4]BF_4

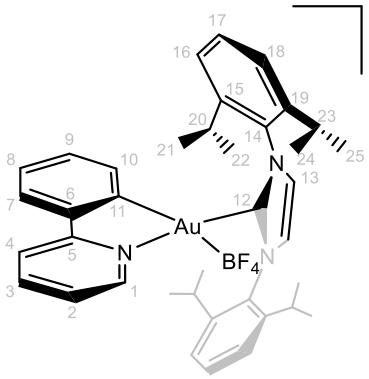

[**2**-BF_4]BF_4 was generated in a NMR tube by the reaction between [**2**-Cl]Cl (15 mg, 18.5 µmol) and 2 equiv (40 µmol) of $AgBF_4$ in 0.5 mL of CD_2Cl_2. The water complex [2-H_2O]$(BF_4)_2$ (48%) is also present in solution.

^{1}H NMR (400 MHz, CD_2Cl_2, 298 K): δ(ppm) = 8.55 (br, H1), 8.16 (br), 7.92 (d), 7.85-7.20 (m), 6.73 (d, 1H, $^{3}J_{HH}$ = 7.4 Hz, H10), 2.95 (br, H20), 2.65 (br, H23), 1.48 (H24), 1.30 (H22), 1.15 (d, $^{3}J_{HH}$ = 6.6 Hz, H25), 0.84 (H21). ^{19}F NMR (376 MHz, CD_2Cl_2, 298 K): δ(ppm) = -152.90 (d, *J* = 20.8 Hz).

[2-H_2O]$(OTf)_2$ [(ppy)-Au-IPr-H_2O]$(OTf)_2$

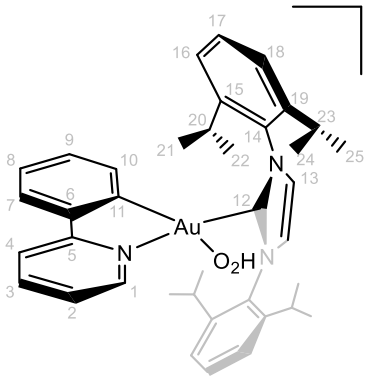

The complex [**2**-H_2O]$(OTf)_2$ was synthesized in an NMR tube by adding 5 eq of water to 15 mg (0.014 mmol) [**2**-OTf]OTf in 500 µL of deuterated dichloromethane. The complex was characterized by mono and bidimensional ^{1}H, ^{13}C and ^{19}F NMR experiments. The assignment of all ^{1}H, ^{13}C was made by means of bidimensional experiments such as ^{1}H-^{1}H COSY, ^{1}H-^{13}C HSQC, ^{1}H-^{13}C HMBC, and ^{1}H-^{1}H NOESY.

^{1}H NMR (400 MHz, CD_2Cl_2, 298 K): δ(ppm) = 8.75 (dt, 1H, $^{3}J_{HH}$ = 5.9, $^{4}J_{HH}$ = 2.0 Hz, H1), 8.18 (td, 1H, $^{3}J_{HH}$ = 7.9, $^{4}J_{HH}$ = 1.6 Hz, H3), 7.93 (dt, 1H, $^{3}J_{HH}$ = 8.2, $^{4}J_{HH}$ = 1.1 Hz, H4), 7.71 (s, 2H, H13), 7.66 (dt, 1H, $^{3}J_{HH}$ = 7.8, $^{4}J_{HH}$ = 1.8 Hz, H7), 7.61 – 7.52 (m, 3H, H2-17), 7.48 - 7.41 (m, 3H, H8-18), 7.32 (dd, 2H, $^{3}J_{HH}$ = 7.8, $^{4}J_{HH}$ = 1.5 Hz, H16), 7.25 (tt, 1H, $^{3}J_{HH}$ = 7.7, $^{4}J_{HH}$ = 1.8 Hz, H9), 6.98 (ddd, 1H, $^{3}J_{HH}$ = 7.9, $^{4}J_{HH}$ = 3.5 Hz, H10), 2.94 (m, 4H, H20-23), 1.46 (d, 6H, $^{3}J_{HH}$ = 6.6 Hz, H24), 1.33 (d, 6H, $^{3}J_{HH}$ = 6.7 Hz, H22), 1.13 (d, 6H, $^{3}J_{HH}$ = 6.8 Hz, H25), 0.94 (d, 6H, $^{3}J_{HH}$ = 6.8 Hz, H21). ^{19}F NMR (376 MHz, CD_2Cl_2, 298 K): δ(ppm) = -78.08.

[2-H_2O]$(BF_4)_2$ [(ppy)-Au-IPr-H_2O]$(BF_4)_2$

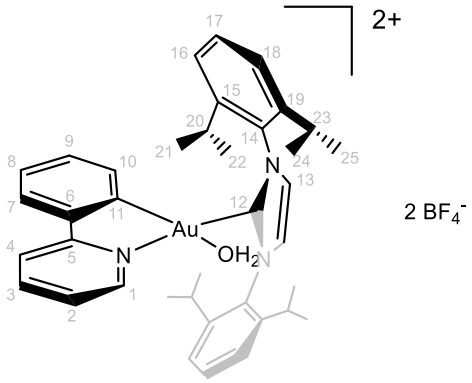

The complex [**2**-H_2O]$(BF_4)_2$ was synthesized in an NMR tube by adding an excess of silver tetrafluoroborate to 20 mg (0.025 mmol) [**2**-Cl]Cl in 500 µL of deuterated dichloromethane. To the solution was added 10 eq of water and the tube was shaken. The complex was characterized by mono and bidimensional ^{1}H, ^{13}C and ^{19}F NMR experiments. The assignment of all ^{1}H, ^{13}C was made by means of bidimensional experiments such as ^{1}H-^{1}H COSY, ^{1}H-^{13}C HSQC, ^{1}H-^{13}C HMBC, and ^{1}H-^{1}H NOESY.

^{1}H NMR (400 MHz, CD_2Cl_2, 298 K): δ(ppm) = 8.75 (dt, 1H, $^{3}J_{HH}$ = 5.9, $^{4}J_{HH}$ = 2.0 Hz, H1), 8.18 (td, 1H, $^{3}J_{HH}$ = 7.9, $^{4}J_{HH}$ = 1.6 Hz, H3), 7.93 (dt, 1H, $^{3}J_{HH}$ = 8.2, $^{4}J_{HH}$ = 1.1 Hz, H4), 7.71 (s, 2H, H13), 7.66 (dt, 1H, $^{3}J_{HH}$ = 7.8, $^{4}J_{HH}$ = 1.8 Hz, H7), 7.61 – 7.52 (m, 3H, H2-17), 7.48 - 7.41 (m, 3H, H8-18), 7.32 (dd, 2H, $^{3}J_{HH}$ = 7.8, $^{4}J_{HH}$ = 1.5 Hz, H16), 7.25 (tt, 1H, $^{3}J_{HH}$ = 7.7, $^{4}J_{HH}$ = 1.8 Hz, H9), 6.98 (ddd, 1H, $^{3}J_{HH}$ = 7.9, $^{4}J_{HH}$ = 3.5 Hz, H10), 2.94 (m, 4H, H20-23), 1.46 (d, 6H, $^{3}J_{HH}$ = 6.6 Hz, H24), 1.33 (d, 6H, $^{3}J_{HH}$ = 6.7 Hz, H22), 1.13 (d, 6H, $^{3}J_{HH}$ = 6.8 Hz, H25), 0.94 (d, 6H, $^{3}J_{HH}$ = 6.8 Hz, H21). ^{13}C {^{1}H} NMR (101 MHz, CD_2Cl_2, 298 K) δ(ppm) = 162.20 (1C, C5), 150.56 (1C, C12), 147.36 (1C, C19), 145.61 (d, 1C, C1), 144.91 (1C, C15), 144.16 (1C, C3), 143.05 (1C, C11), 134.70 (1C, C6), 133.32 (d, 1C, C10), 132.73 (1C, C9), 132.12 (2C, C14), 131.83(2C, C17), 129.52 (1C, C8), 127.14 (2C, C13), 126.47 (1C, C7), 124.99-124.96 (4C, C16-18), 124.42 (1C, C2), 120.97 (1C, C4), 29.22-29.17 (4C, C20-23), 26.31 (2C, C22), 26.18 (2C, C25), 22.68 (2C, C21), 22.16-22.10 (d, 2C, C24). ^{19}F NMR (376 MHz, CD_2Cl_2, 298 K): δ(ppm) = -152.74 (d, *J*=20.8 Hz).

4.3 Catalysis

4.3.1 Hydration of alkynes - Chapter 2.1.1

Hydration of 3-hexyne with L-Au-Cl (Table 3.1).

In a 2 mL glass screw-top vial were mixed L-Au-Cl (0.00175 mmol), AgOTf (0.45 mg, 0.00175 mmol), 3-hexyne (199 µL, 1.75 mmol), water (34.6 µL, 1.925 mmol), and NBu_4OTf (34.2mg, 0.0875 mmol). The vial was then placed in a bath oil at 30 °C with magnetic stirring. The progress of the reaction was checked by ^1H NMR.

Hydration of 3-hexyne with L-Au-OTf or L-Au-OTs (Table 3.1 and Table 3.2).

In a 2 mL glass screw-top vial were mixed L-Au-X (0.00175 mmol), 3-hexyne (199 µL, 1.75 mmol), water (34.6 µL, 1.925 mmol), and NBu_4OTf (0.0875 mmol). The vial was then placed in a bath oil at 30 °C with magnetic stirring. The progress of the reaction was checked by ^1H NMR.

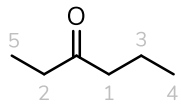

^1H NMR (200 MHz, $CDCl_3$, ppm): δ 2.49-2.32 (m, 4H, 2-1), 1.60 (m, 2H, 3), 1.05 (t, $^3J_{HH}$ = 7.3, 3H, 5), 0.89 (t, $^3J_{HH}$ = 7.4 Hz, 3H 4).

Hydration of diphenylacetylene (Table 3.3).

- With H_2O

In a 2 mL glass screw-top vial were mixed IPr-Au-X (from 0.01 to 0.1 mmol), diphenylacetylene (312 mg, 1.75 mmol), water (34.6 µL, 1.925 mmol) and NBu_4OTf (34.3 mg, 0.0875 mmol). The vial was then placed in a bath oil at a fixed temperature (60, 80 or 120 °C) with magnetic stirring. The progress of the reaction was checked by ^1H NMR.

- With D_2O

In a 2 mL glass screw-top vial were mixed IPr-Au-X (from 0.01 to 0.1 mmol), diphenylaceteylene (312 mg, 1.75 mmol), deuterium oxide (35 µL, 1.925 mmol) and NBu_4OTf (34.3 mg, 0.0875 mmol. The vial was then placed in a bath oil at 120°C with magnetic stirring. The progress of the reaction was checked by ^1H NMR.

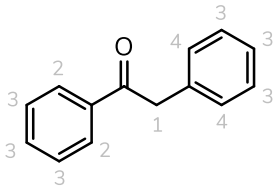

^1H NMR (200 MHz, $CDCl_3$, ppm): δ 8.01 (m, 2H, 2), 7.62-7.39 (m, 6H, 3), 7.31-7.27 (m, 2H, 4), 4.28 (s, 1H, 1).

Table 3.1: *L-Au-X (0.1 mol%) catalyzed hydration of 3-hexyne at 30 °C in the presence of NBu_4OTf[a,b]*

Entry	L[c]	X^-	AgOTf (mol%)	Conv. (%)[d]	Time[e] (h) (TOF[f])
1	IPr	OTf	-	10.6	0.5
				42.9	1
				77.5	1.5
				99.1	2 (495)
2	IPr	Cl^-	0.1	25.6	1
				66	1.5
				70	2
				70	2.5 (350)
3	BIAN	Cl^-	0.1	15.4	1
				67	1.5
				75.5	2 (380)
				75.5	2.5
4	NHC^{CH2}	Cl^-	0.1	16.1	1
				52.6	1.5
				75	2 (380)
				75	2.5
5	NAC	Cl^-	0.1	24	0
6	JPhos	Cl^-	0.1	18.3	1
				29.6	1.5
				46.9	2
				56.6	2.5
				66.9	3
				75.3	4 (188)
7	PCy_3	Cl^-	0.1	24	0
8	PAr^F	Cl^-	0.1	24	0
9	PPh_3	Cl^-	0.1	24	0
10	$P(OR)_3$	Cl^-	0.1	24	0
11	IPr	OTs^-	-	14.1	1
				77.7	2
				99.9	3 (285)
12	BIAN	OTs^-	-	2	1
				2.6	1.5
				18.1	2
				63.5	2.5
				93.8	3
				97.8	4 (248)
13	NHC^{CH2}	OTs^-	-	0	1
				0	2
				2	4

				26.9	6
				63.3	6.5
				86.6	7
				98.5	8 (122)
14	NAC	OTs^-	-	3	1
				4.8	2
				8.7	3
				9.0	4
				9.1	24 (4)
15	JPhos	OTs^-	-	19.5	1
				74.5	5 (148)
				85.3	24
16	PCy_3	OTs^-	-	0	1
				0	2
				2	6
				6	24 (3)
17	PAr^F	OTs^-	-	0	24
18	PPh_3	OTs^-	-	0	1
				0	2
				0	6
				3	24 (1)
19	$P(OR)_3$	OTs^-	-	0	1
				1.1	5
				17	24 (7)
20	BIAN	OTf^-	-	24.7	1
				94.3	1.5
				>99	2 (495)
21	NHC^{CH2}	OTf^-	-	0	1
				25.1	2
				73.7	3
				>99	4 (248)

[a] Catalytic conditions: 3-hexyne (1.75 mmol, 200 µL), 5% NBu_4OTf (0.087 mmol, 34.3 mg), H_2O (1.92 mmol, 35 µL), L-Au-X (0.00175 mmol) and AgOTf (0.00175 mmol, 0,45 mg) when indicated. [b] mol% = (moles of catalyst / moles of alkyne) x 100. [c] see text. [d] Determined by ^1H NMR, averaged value of three measurements. [e] Time necessary to reach the reported conversion. [f] TOF = ($n_{product}$ / $n_{catalyst}$) / t(h) at the reported conversion. [g] from reference [126].

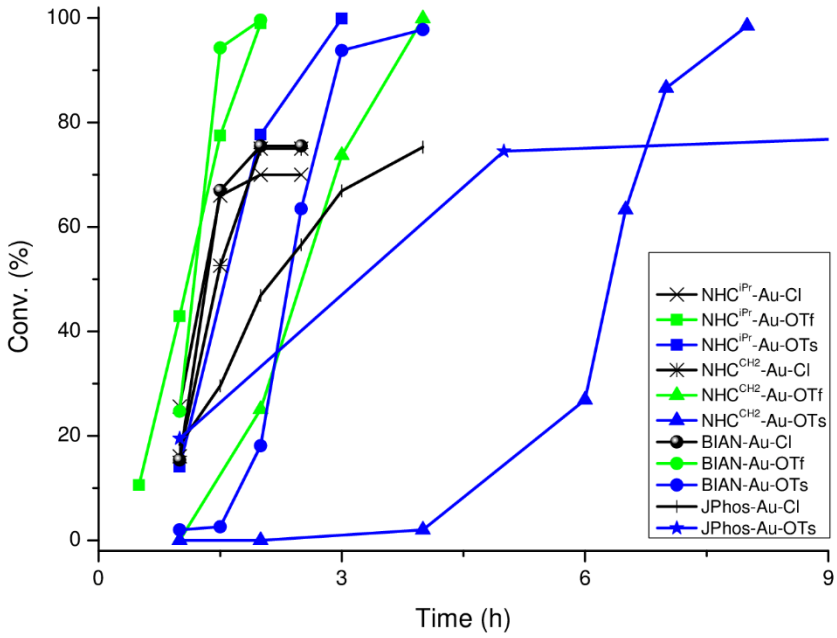

Figure 3.1: *Hydration of 3-hexyne with 0.1% cat. loading, at 30°C with 5% of NBu_4OTf*

Table 3.2: *IPr-Au-OTf catalyzed hydration of 3-hexyne*

entry	Loading (mol%)[b]	Additive	Conv.[c] (%)	Time[d] (h)
1	0.1	$(Bu)_2NH_2OTf$	0	2.5
			12.3	4
2		Aliquat-OTf	0	1
			2.4	2
			4.8	4
			41.9	6
			55.5	6.5
			68	7
			91.6	24
3		$(Me)_2(Et)(Dod)OTf$	5.03	0.5
			44.1	1
			76.9	1.5
			92.9	2.5

[a] Catalysis conditions: 3-hexyne (1.75 mmol, 200 µL) and H_2O (1.92 mmol, 35 µL) at 30 °C. [b] (moles of catalyst / moles of alkyne) x 100. [c] Determined by ^1H NMR, average value of three measurements; in brackets the products obtained (see below) with their molar ratio. [d] Time necessary to reach the reported conversion.

Table 3.3: *IPr-Au-X catalyzed hydration of diphenylacetylene*

entry	Catalyst loading (mol%)[b]	T (°C)	X^-	Conv.[c] (%)	Time[d] (h) (TOF[e])
1	0.1	60	OTf^-	26.3	2
				62.4	6
				72.8	7
				82.3	8 (102)
				88.9	24
2	0.05	80	OTf^-	7.5	2
				21.5	3
				27.1	4
				31.3	5
				35.0	6
				42,5	8 (105)
				56.2	24
				60.1	72
3	0.05	120	OTf^-	81.6	2
				94.1	4 (470)
				95.8	5
				96.0	8
				96.2	24
4	0.025	120	OTf^-	40.7	2
				67.2	4
				73.5	5
				84.6	8 (435)
				88..0	24
5	0.01	120	OTf^-	19.1	2
				27.4	4
				28.4	5 (560)
				28.4	8
				28.6	24
6[f]	0.05	120	OTf^-	47.0	2
				64.9	3
				75.7	4
				83.6	5
				86.0	6
				87.7	8 (220)
				89.7	24
7	0.05	120	OTs^-	1.4	2
				3.4	3
				4.1	4
				4.6	5
				6.9	6
				7.4	8 (17)

[a] Catalysis conditions: diphenylacetylene (1.75 mmol, 312 mg), 5% NBu_4OTf (0.087 mmol, 34.3 mg) and H_2O (1.92 mmol, 35 µL). [b] (moles of catalyst / moles of alkyne) x 100. [c] Determined by ^1H NMR; average value of three measurements. [d] Time necessary to reach the reported conversion. [e] TOF = ($n_{product}$ / $n_{catalyst}$) / t(h) at the reported conversion. [f] Using D_2O instead of H_2O.

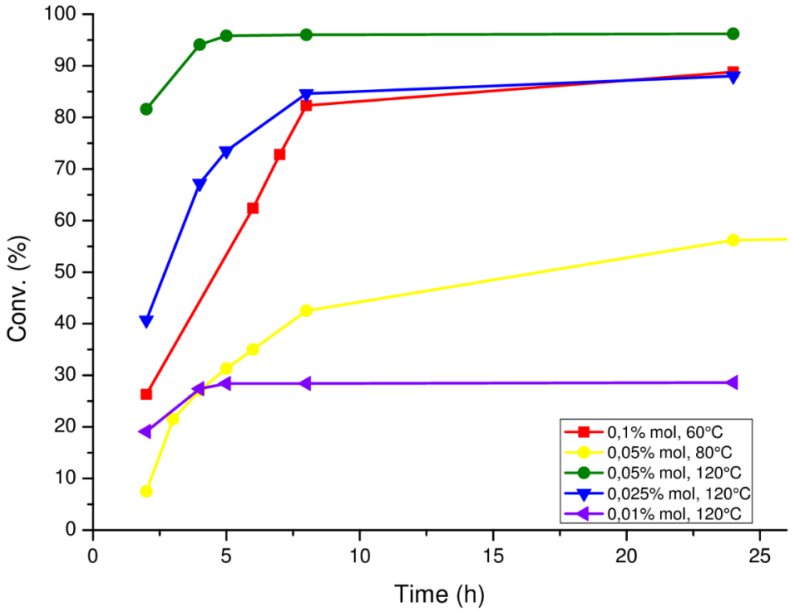

Figure 3.2: *Hydration of diphenylacetylene at different temperatures and catalyst loadings.*

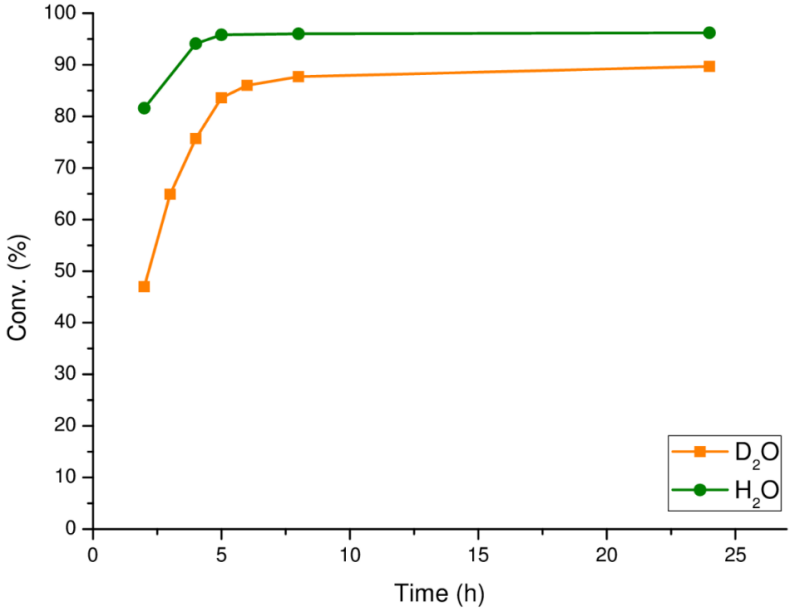

Figure 3.3: *Hydration of 3-hexyne with H_2O and D_2O at 120 °C using a 0.05 mol% catalyst loading. (**Table 3.3**)*

^{31}P NMR spectra for PPh_3-Au-OTs and JPhos-Au-OTs after 20 hours from the beginning of catalysis have been recorded to analyzed which species are present at the end of the hydration of 3-hexyne. The procedure written in section 2 was applied for the hydration. The reaction mixture was put in a NMR tube containing a capillary filled with D_2O. In **Table 3.4** are reported the chemical shifts of the possible P-containing species.[49,139]

Table 3.4: ^{31}P NMR chemical shifts

Ligand	Free	Oxide	Au-Cl	Au-OTf	Au-OTs	Au-η^2-hexyne	$[AuP_2]^+$
PPh_3	-5.4	31.6	33.8	29.4	27.9	37	45
JPhos	18.9	-	60.5	57.4	56.8	64.6	-

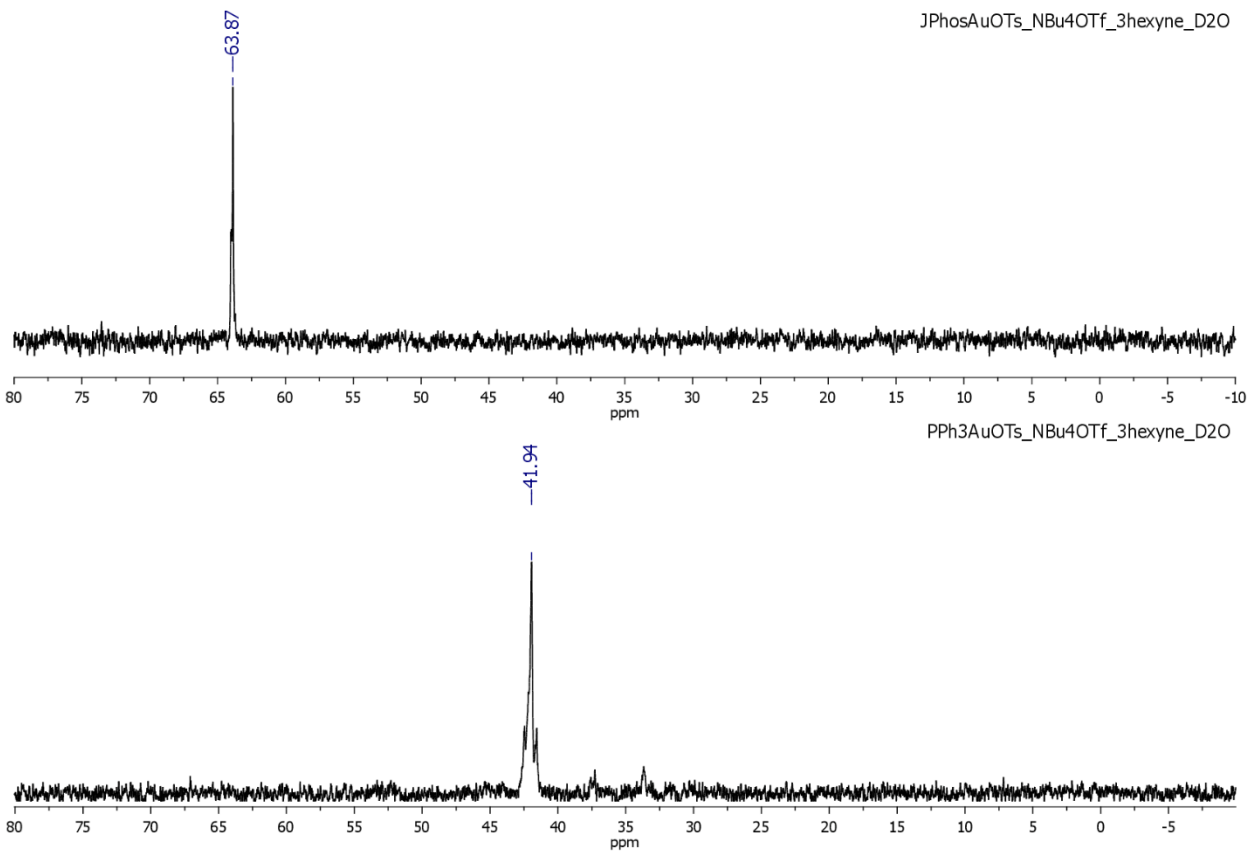

Figure 3.4: ^{31}P NMR spectra of PPh_3-Au-OTs (bottom) and JPhos-Au-OTs (top) in the hydration of 3-hexyne.

4.3.2 Meyer-Schuster - Chapter 2.1.2

Meyer-Schuster rearrangement of 1-phenyl-2-propyn-1-ol to cinnamaldehyde catalysed by IPr-Au-OTf (Table 3.5 and Table 3.6).

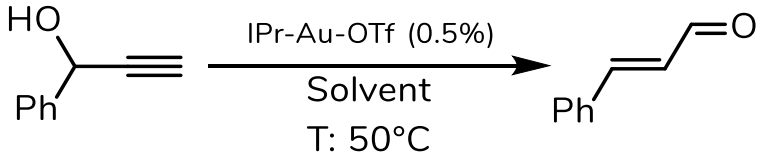

IPr-Au-OTf (1.8 mg, 0.0025 mmol), the appropriate solvent (200 µL), and 1-phenyl-2-propyn-1-ol (61 µL, 0.5 mmol) were added into a 2 mL glass screw-top vial. The vial was placed in a bath oil at 50°C with magnetic stirring. The reactions were checked by NMR: 10 µL of the reaction mixture was added to a 500 µL of non-anhydrous $CDCl_3$. The progress of the reaction was monitored integrating the signals of 1-phenyl-2-propyn-1-ol and cinnamaldehyde. Conversion was calculated from the integral intensities of the corresponding signals (conversion [%] = (n cinnamaldehyde) / (n 1-phenyl-2-propyn-1-ol + n cinnamaldehyde) x 100). Reported yields are an average of three runs.

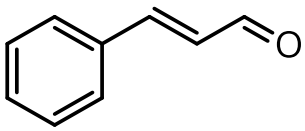

^{1}H NMR (400 MHz, $CDCl_3$, 298 K) δ(ppm): 9.74 (d, 1 H, $^3J_{HH}$ = 7.7 Hz), 7.60 (dd, 2H, $^3J_{HH}$ = 6.8, $^4J_{HH}$ = 2.9 Hz), 7.55 – 7.39 (m, 4H), 6.75 (dd, 1H, $^3J_{HH}$ = 15.9, $^4J_{HH}$ = 7.7Hz).

Stoichiometric reaction of 1-phenyl-2-propyn-1-ol with IPr-Au-OTf

3.6 µL (0.027mmol) of 1-phenyl-2-propyn-1-ol and 8.6 mg (0.0401 mmol) of protonsponge [1,8-Bis(dimethylamino)naphthalene] were added to 500 µL of $CDCl_3$. Then 20 mg (0.027 mmol) of IPr-Au-OTf was added in the NMR tube and the solution was shaken. The formation of sigma-bonded species was completely characterized by multinuclear NMR techniques.

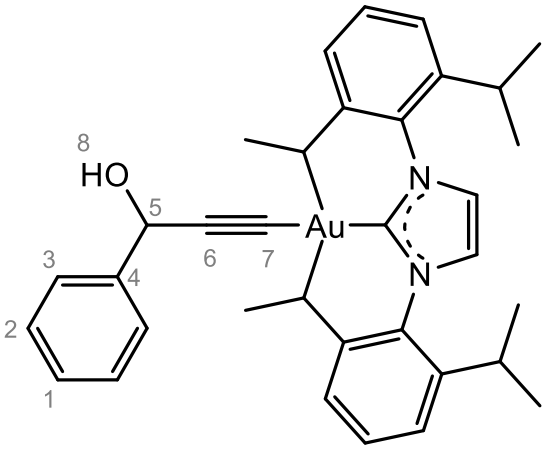

^{1}H NMR (400 MHz, $CDCl_3$, 298 K) δ(ppm): 7.50 (m), 7.26 (m), 5.41 (d, 1H, $^3J_{HH}$ = 5.5), 2.60 (hept, 4H, $^3J_{HH}$ = 6.8), 2.16 (d, 1H, $^3J_{HH}$ = 5.9, H8), 1.37 (d, 12H, $^3J_{HH}$ = 6.9), 1.24 (d, 12H, $^3J_{HH}$ = 6.8). ^{13}C{^{1}H} NMR (101 MHz, $CDCl_3$, 298 K) δ(ppm) = 190.77, 145.62, 142.58 (1C, C4), 134.26, 130.51 (2C, C2), 128.03, 127.35 (1C, C1), 127.03 (2C, C3), 125.43, 124.18, 123.22, 121.63, 102.97 (1C, C6), 65.32 (1C, C5), 28.81, 24.58, 24.03.

Table 3.5: *Catalyzed Meyer-Schuster rearrangement of 1-phenyl-2-propyn-1-ol to cinnamaldehyde at 50°C.*[a]

Entry	Solvent	Catalytic system	Conv.[b] (%)	TOF[c] (h^{-1})	ε_r[d]
	VOS				
1	Chloroform	IPr-Au-OTf	75	300	4.81
2	Dichloromethane	IPr-Au-OTf	12	53	8.93
3	Acetone	IPr-Au-OTf	13	50	21
	Green				
4	p-Cymene	IPr-Au-OTf	91	394	2.24
5	p-Cymene[e]	IPr-Au-Cl/ AgOTs	11	44	2.24
6	p-Cymene[f]	IPr-Au-Cl/ AgTFA	0.4	2	2.24
7	p-Cymene[g]	IPr-Au-Cl/$AgBF_4$	7	28	2.24
8	p-Cymene[h]	IPr-Au-Cl/AgOTf	30	115	2.24
9	p-Cymene[i]	IPr-Au-OTf/HOTf	100	400	2.24
10	p-Cymene[j]	IPr-Au-OTf/HOTs	93	371	2.24
11	p-Cymene[k]	IPr-Au-OTf/P.S.	0	0	2.24
12	Limonene	IPr-Au-OTf	67	246	2.4
13	Anisole	IPr-Au-OTf	85	368	4.3
14	Ethyl Lactate	IPr-Au-OTf	24	106	15.4
15	Furfuryl alcohol	IPr-Au-OTf	37	161	16.9
16	γ-Valerolactone	IPr-Au-OTf	23	105	36.9
17	DMSO	IPr-Au-OTf	0	0	46.7
18	Methyl levulinate	IPr-Au-OTf	17	74	-
19	-[l]	IPr-Au-OTf	74	296	-

[a]Catalysis conditions: IPr-Au-OTf (0.0025 mmol, 1.8 mg), 1-phenyl-2-propyn-1-ol (0.5 mmol, 61 µL), solvent (200 µL). [b]Determined by ^1H NMR; average value of three measurements after 30 minutes. [c]TOF = ($mol_{product}/mol_{catalyst}$)/t calculated after 30 minutes. [d]ε_r = dielectric constant. [e]IPr-Au-Cl (0.0025 mmol, 1.6 mg), 1.1 eq AgOTs. [f]IPr-Au-Cl (0.0025 mmol, 1.6 mg), 1.1 eq AgTFA. [g]IPr-Au-Cl (0.0025 mmol, 1.6 mg), 1.1 eq $AgBF_4$. [h]IPr-Au-Cl (0.0025 mmol, 1.6 mg), 1.1 eq AgOTf. [i]IPr-Au-OTf (0.0025 mmol, 1.8 mg), 10% (respect to substrate) HOTf. [j]IPr-Au-OTf (0.0025 mmol, 1.8 mg), 10% (respect to substrate) HOTs. [k]IPr-Au-OTf (0.0025 mmol, 1.8 mg), 10% (respect to substrate) proton sponge (1,8-Bis(dimethylamino)naphthalene). [l]no solvent was used.

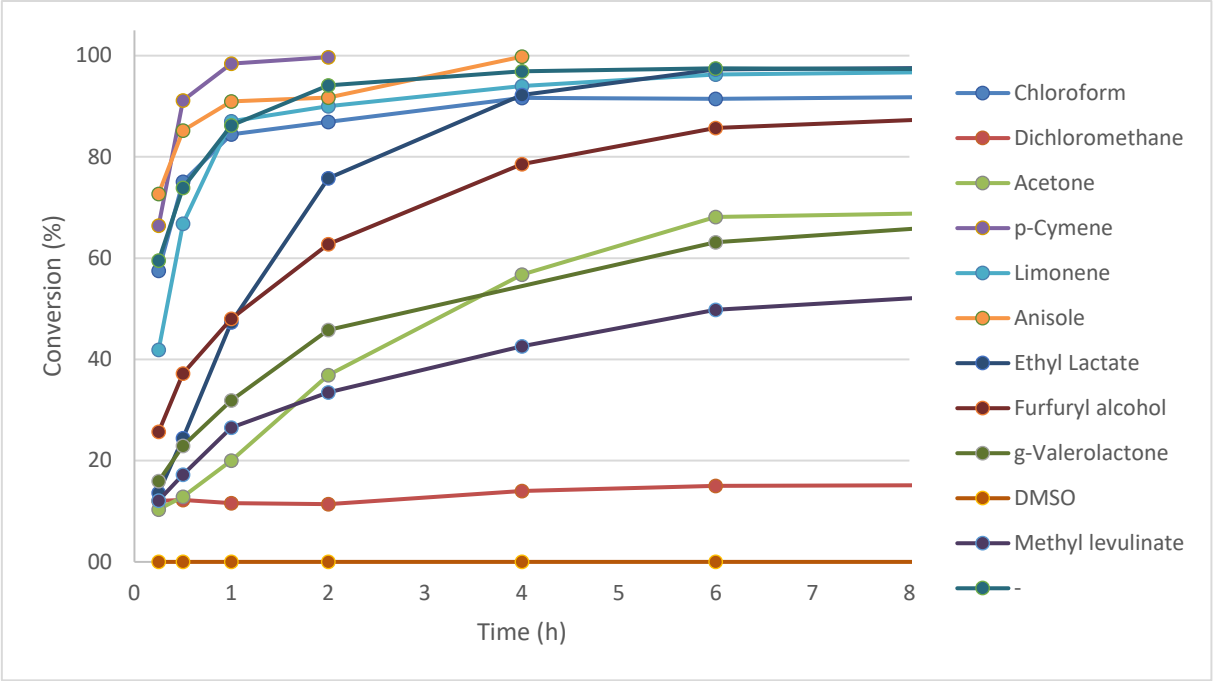

Figure 3.5: *Plot of conversion against time for IPr-Au-OTf catalyzed Meyer-Schuster rearrangement of 1-phenyl-2-propyn-1-ol to cinnamaldehyde at 50°C.*

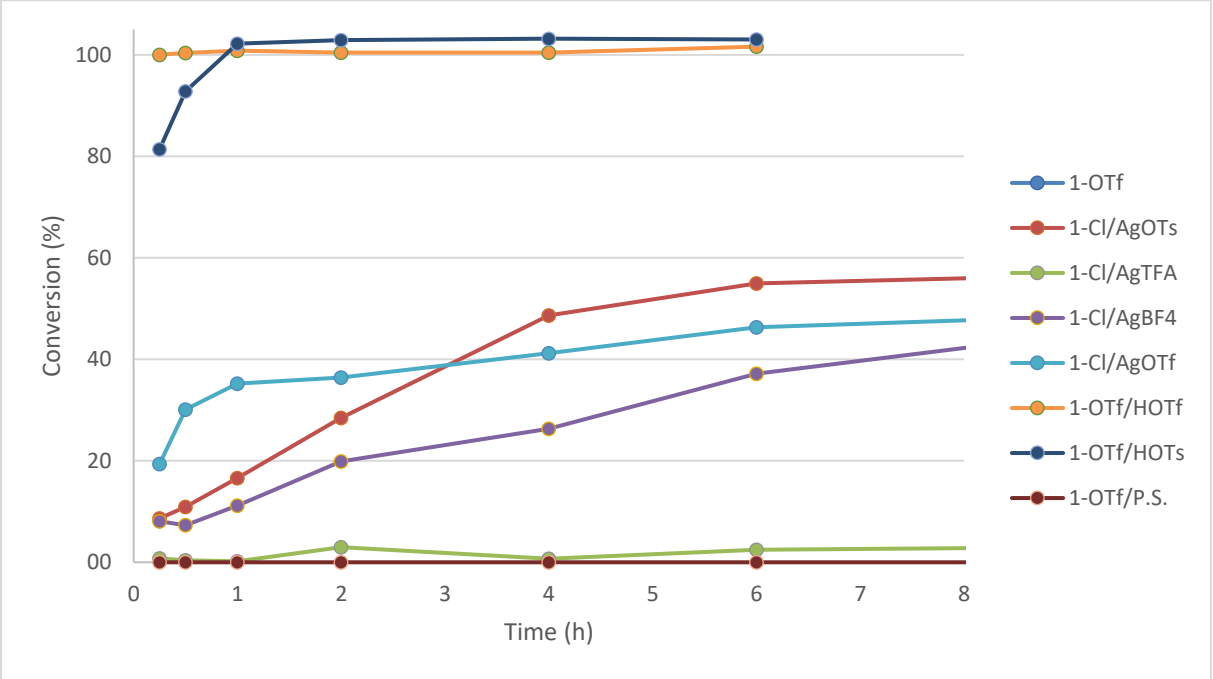

Figure 3.6: *Plot of conversion against time for IPr-Au-X catalyzed Meyer-Schuster rearrangement of 1-phenyl-2-propyn-1-ol to cinnamaldehyde at 50°C.*

Table 3.6: *catalyzed Meyer-Schuster rearrangement of 1-phenyl-2-propyn-1-ol to cinnamaldehyde at 50°C in different solvent.*

		TIME (h):	0.25		0.5		1		2		4		6		24	
ENTRY	SOLVENT	CAT	Conv. (%)	TOF (h^{-1})	Conv. (%)	TOF (h^{-1})	Conv. (%)	TOF (h^{-1})	Conv. (%)	TOF (h^{-1})	Conv. (%)	TOF (h^{-1})	Conv. (%)	TOF (h^{-1})	Conv. (%)	TOF (h^{-1})
1	Chloroform	1-OTf	57.5	460	75.1	300	84.4	169	86.9	87	91.7	46	91.5	30	94.3	8
2	Dichloromethane	1-OTf	12.1	104	12.3	53	11.6	25	11.4	12	14.0	6	15.0	1	16.0	0
3	Acetone	1-OTf	10.4	80	12.9	50	20.0	39	36.9	36	56.7	27	68.1	22	74.0	6
4	p-Cymene	1-OTf	66.4	574	91.1	394	98.4	213	99.7	108						
5	p-Cymene[e]	1-Cl/ AgOTs	8.6	69	10.9	44	16.6	33	28.4	28	48.7	24	55.0	18	64.0	5
6	p-Cymene[f]	1-Cl/ AgTFA	0.8	6	0.4	2	0.2	0	3.0	3	0.7	0	2.5	2	5.3	0
7	p-Cymene[g]	1-Cl/ $AgBF_4$	8.1	62	7.3	28	11.2	21	19.9	19	26.3	10	37.2	6	82.8	7
8	p-Cymene[h]	1-Cl/ AgOTf	19.4	149	30.1	115	35.2	67	36.4	35	41.2	20	46.3	10	58.6	5
9	p-Cymene[i]	1-OTf/ HOTf	100.0	800	100.4	402	100.8	202	100.4	100	100.5	50	101.6	34		
10	p-Cymene[j]	1-OTf/ HOTs	81.4	651	92.8	371	102.3	205	102.9	103	103.2	52	103.1	34		
11	p-Cymene[k]	1-OTf/ P.S.	0.0	0	0.0	0	0.0	0	0.0	0	0.0	0	0.0	0	0.0	0
12	Limonene	1-OTf	41.9	308	66.8	246	87.0	160	90.0	79	94.0		96.3	29	100.0	8
13	Anisole	1-OTf	72.7	628	85.2	368	91.0	197	91.7	99	99.8	50				
14	Ethyl Lactate	1-OTf	13.6	118	24.4	106	47.3	102	75.8	82	92.2	44	97.3	6	99.5	0
15	Furfuryl alcohol	1-OTf	25.7	222	37.2	161	48.0	104	62.7	68	78.6	9	85.7	2	99.6	0
16	γ-Valerolactone	1-OTf	16.0	147	22.9	105	31.9	73	45.8	53			63.2	24	86.7	8
17	DMSO	1-OTf	0.0	0	0.0	0	0.0	0	0.0	0	0.0		0.0		0.0	
18	Methyl levulinate	1-OTf	12.1	105	17.2	74	26.5	57	33.5	36	42.6	18	49.8	9	70.1	2
19	-	1-OTf	59.5	476	73.9	296	86.2	172	94.1	94	96.9	48	97.5	33	96.2	8

[a]Catalysis conditions: IPr-Au-OTf (0.0025 mmol, 1.8 mg), 1-phenyl-2-propyn-1-ol (0.5 mmol, 61 µL), solvent (200 µL). [b]Determined by 1H NMR; average value of three measurements after 30 minutes. [c]TOF = (molproduct/molcatalyst)/t calculated after 30 minutes. [d]ε_r = dielectric constant. [e]IPr-Au-Cl (0.0025 mmol, 1.6 mg), 1.1 eq AgOTs. [f]IPr-Au-Cl (0.0025 mmol, 1.6 mg), 1.1 eq AgTFA. [g]IPr-Au-Cl (0.0025 mmol, 1.6 mg), 1.1 eq AgBF4. [h]IPr-Au-Cl (0.0025 mmol, 1.6 mg), 1.1 eq AgOTf. [i]IPr-Au-OTf (0.0025 mmol, 1.8 mg), 10% (respect to substrate) HOTf. [j]IPr-Au-OTf (0.0025 mmol, 1.8 mg), 10% (respect to substrate) HOTs. [k]IPr-Au-OTf (0.0025 mmol, 1.8 mg), 10% (respect to substrate) proton sponge (1,8-Bis(dimethylamino)naphthalene). [l]no solvent was used.

4.3.3 Propargylamide - Chapter 2.1.3

IPr-Au-OTf (1.8 mg, 0.0025 mmol) or IPr-Au-Cl (0.0025 mmol, 1.6 mg) and 0.0027 mmol of AgX (X^- = BF_4^-, OTs^-, TFA^-), the appropriate solvent (200 µL), and N-(2-Propynyl)benzamide (79.6 mg, 0.5 mmol) were added into a 2 mL glass screw-top vial. The vial was placed in a bath oil at 50°C with magnetic stirring. The reactions were checked by NMR: 10 µL of the reaction mixture was added to a 500 µL of non-anhydrous $CDCl_3$. The progress of the reaction was monitored by following the signals of N-(2-Propynyl)benzamide and 2-phenyl-5-vinylidene-2-oxazoline. Conversion was calculated from the integral intensities of the corresponding signals (conversion [%] = (n 2-phenyl-5-vinylidene-2-oxazoline) / (n N-(2-Propynyl)benzamide + n 2-phenyl-5-vinylidene-2-oxazoline) x 100). Reported yields are an average of three runs.

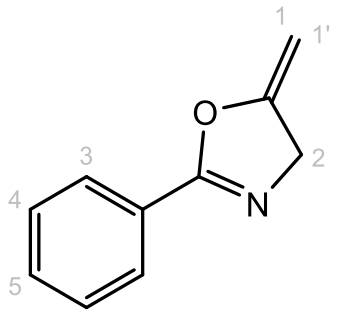

2-phenyl-5-vinylidene-2-oxazoline

^{1}H NMR ($CDCl_3$, 400 MHz, 298 K): δ (ppm) 8.01 – 7.93 (m, 2H, H3), 7.61 – 7.40 (m, 3H, H4,5), 4.82 (q, 1H, $^2J_{HH}$ = 3.1 Hz, $^4J_{HH}$ = 2.9 Hz, H1), 4.66 (t, 2H, $^4J_{HH}$ = 2.9 Hz, H2), 4.37 (q, 1H, $^2J_{HH}$ = 3.1 Hz, $^4J_{HH}$ = 2.9 Hz, H1').

Table 3.7: *IPr-Au-OTf catalyzed N-(2-propynyl)benzamide isomerization at 50 °C.*[a]

Entry	Solvent	Conv.[b] %	TOF[c](h^{-1})	ε_r[d]
	VOS			
1	Chloroform	90	354	4.81
2	Dichloromethane	89	406	8.93
3	Acetone [e]	10	43	21
4	3-Nitrotoluene	65	281	22.2
5	Nitromethane	67	274	35.87
	Green			
6	Cyclohexanone	47	206	2.02
7	p-Cymene	15	63	2.24
8	Limonene [e]	11	50	2.4
9a	Propionic acid	94	431	3.35
9b	Propionic acid [f]	16.7	65	3.35
9c	Propionic acid [g]	39.6	154	3.35
9d	Propionic acid [h]	90.9	354	3.35
10	Cyrene	23	94	3.4
11	Anisole [e]	13	56	4.3
12	Isopropyl acetate	49	223	6.3
13	MIBK	62	250	13.1
14	Ethyl Lactate	73	317	15.4
15	Furfuryl alcohol	39	148	16.85
16	Propionitrile [e]	12	50	27.7
17	g-Valerolactone	47	192	36.9
18	DMSO	5	21	46.7
19	Propylene carbonate	49	180	64
20	BMIM-OTf	28	120	-
21	Methyl levulinate	21	90	-

[a] Catalysis conditions: IPr-Au-OTf (0.0025 mmol, 1.8 mg), N-(2-Propynyl)benzamide (0.5 mmol, 79.6 mg), solvent (200 µL). [b] Determined by ^{1}H NMR; average value of three measurements after 30 minutes. [c] TOF = ($mol_{product}/mol_{catalyst}$)/t calculated after 30 minutes. [d] ε_r = dielectric constant. [e] slightly soluble or insoluble. [f] IPr-Au-Cl (0.0025 mmol, 1.6 mg), 1.1 equiv. AgOTs. [g] IPr-Au-Cl (0.0025 mmol, 1.6 mg), 1.1 equiv. AgTFA. [h] IPr-Au-Cl (0.0025 mmol, 1.6 mg), 1.1 equiv. $AgBF_4$.

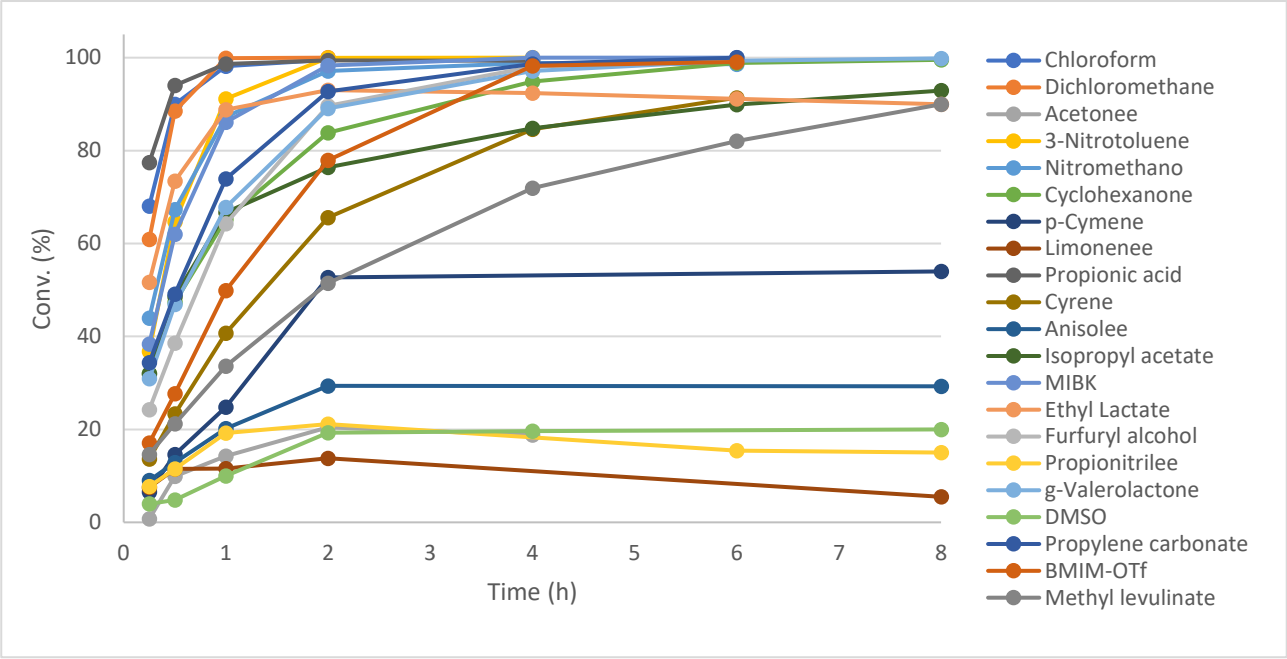

Figure 3.7: *Plot of conversion against time for IPr-Au-OTf catalyzed N-(2-propynyl)benzamide isomerization to 2-phenyl-5-vinylidene-2-oxazoline at 50 °C. See* ***Table 3.7*** *and* ***Table 3.8*** *for details.*

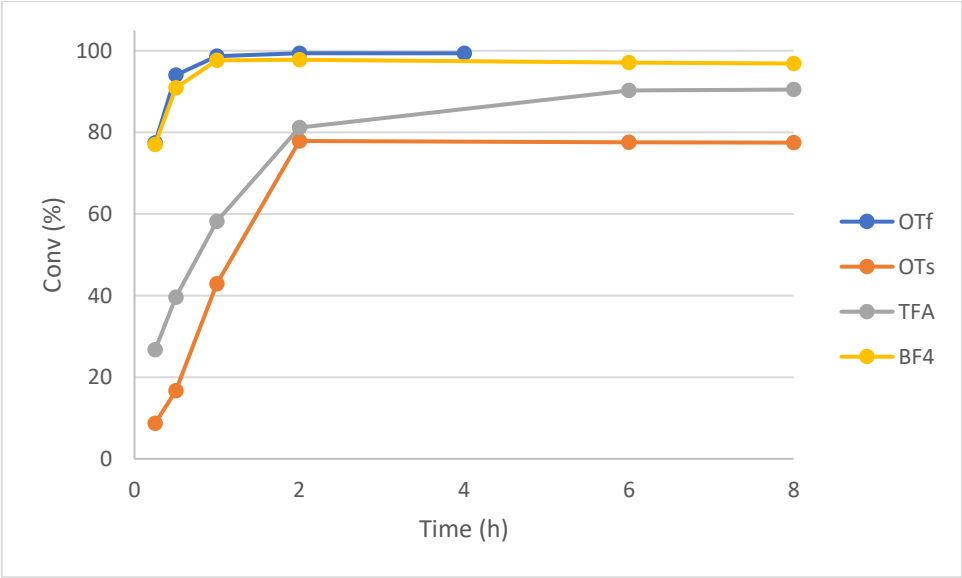

Figure 3.8: *Plot of conversion against time for IPr-Au-X catalyzed N-(2-propynyl)benzamide isomerization to 2-phenyl-5-vinylidene-2-oxazoline at 50 °C. See* ***Table 3.7*** *and* ***Table 3.8*** *for details.*

Table 3.8: *IPr-Au-OTf catalyzed N-(2-Propynyl)benzamide isomerization at 50 °C.[a] (see the text for details)*

	TIME (h):	0.25		0.5		1		2		4		6		8	
ENTRY	**SOLVENT**	Conv. (%)	TOF (h^{-1})	Conv. (%)	TOF (h^{-1})	Conv. (%)	TOF (h^{-1})	Conv. (%)	TOF (h^{-1})	Conv. (%)	TOF (h^{-1})	Conv. (%)	TOF (h^{-1})	Conv. (%)	TOF (h^{-1})
1	Chloroform	68	535	90	354	98	193	100	98	100	49				
2	Dichloromethane	61	558	89	406	100	229	100	115						
3	Acetone[e]	1	7	10	43	14	31	20	22					19	5
4	3-Nitrotoluene	37	319	65	281	91	198	100	108	100	54				
5	Nitromethano	44	358	67	274	87	178	97	99	99	50	99	33		
6	Cyclohexanone	32	278	47	206	65	142	84	91	95	52	99	36	100	27
7	p-Cymene	7	57	15	63	25	54	53	57					54	11
8	Limonene[e]	7	65	11	50	12	25	14	15					6	2
9a	Propionic acid	77	710	94	431	99	226	99	114	99	57				
9b	Propionic acid[f]	8.7	67	16.7	65	42.9	84	77.9	76			77.6	25	77.5	18
9c	Propionic acid[g]	26.7	208	39.6	154	58.2	113	81.2	79			90.3	29		
9d	Propionic acid[h]	77	600	90.9	354	97.7	190	97.8	95			97.1	32	97	21
10	Cyrene	14	109	23	94	41	82	66	66	85	42	91	31		
11	Anisole[e]	9	78	13	56	20	44	29	32					29	8
12	Isopropyl acetate	32	293	49	223	67	153	76	88	85	49	90	34	93	27
13	MIBK	38	309	62	250	86	174	98	99	100	50	100	34		
14	Ethyl Lactate	52	445	73	317	89	191	93	100	92	50	91	33	90	25
15	Furfuryl alcohol	24	186	39	148	64	123	90	86	98	47	100	32		
16	Propionitrile[e]	8	67	12	50	19	42	21	23			15	4	15	
17	g-Valerolactone	31	253	47	192	68	139	89	91	97	50	99	34	100	26
18	DMSO	4	34	5	21	10	22	19	21	20	5			20	4
19	Propylene carbonate	34	251	49	180	74	135	93	85	99	45	100	30		
20	BMIM-OTf	17	148	28	120	50	108	78	84	98	53	99	36		
21	Methyl levulinate	15	125	21	90	34	72	51	55	72	38	82	29	90	12

4.3.4 Gold(III) catalysis - Chapter 2.2.1

General procedure

A typical run was performed by mixing 100 µL of 3-hexyne (0.88 mmol), 18 µL of water, and 0.088 mmol of catalyst in 400 µL of γ-valerolactone in a 2 mL glass screw top vial. The mixture was stirred in a bath oil at 50 °C. The progress of the reaction was checked by NMR and the sample was prepared as follows: 10 µL of the reaction mixture was taken with a syringe and dissolved in 500 µL of non-anhydrous $CDCl_3$. Conversion was calculated from the integral areas of the corresponding signals (conversion [%] = (n 3-hexanone) / (n 3-hexyne + n 3-hexanone) x 100). Reported yields are an average of three runs.

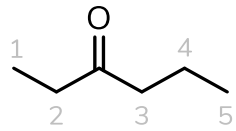

^{1}H NMR (400 MHz, $CDCl_3$, 298 K): δ(ppm) 2.36–2.39 (tq, 4H, $^3J_{HH}$ = 7.4 Hz, $^3J_{HH}$ = 7.3 Hz, H2,3), 1.58 (m, 2H, H4), 1.03 (t, 3H, $^3J_{HH}$ = 7.4 Hz, H1), 0.89 (t, 3H, $^3J_{HH}$ = 7.4 Hz, H5).

Ligand effect

Table 3.9: *Hydration of 3-hexyne in standard condition. IPr vs PPh_3[a]*

Entry	**1**		**2**		**3**		**4**	
Cat.	**1**		[**2**-Cl]Cl		[**3**-Cl]OTf		[**3**-Cl]OTf + AgOTf	
t (h)	Conv[b] (%)	TOF[c] (h^{-1})	Conv[b] (%)	TOF[c] (h^{-1})	Conv[b] (%)	TOF[c] (h^{-1})	Conv[b] (%)	TOF[c] (h^{-1})
0.5	0	0	0	0	0	0	12	23
1	0	0	0	0	0	0	23	23
2	0	0	0	0	0	0	38	19
4	0	0	0	0	0	0	58	14
6	-	-	-	-	-	-	71	12
8	-	-	-	-	-	-	80	10
24	0	0	0	0	0	0	95	4

[a] Catalytic conditions: 3-hexyne (0.88 mmol, 100 µL), H_2O (1.00 mmol, 18 µL), catalyst (0.0088 mmol, 1%) and AgX (0.0166 mmol) in γ-valerolactone (400 µL), T: 50 °C. [b] mol% = (moles of catalyst / moles of alkyne) x 100, determined by ^{1}H NMR averaged value of three measurements. [c] TOF = ($n_{product}$ / $n_{catalyst}$) / t(h) of conversion.

Anion effect

*Table 3.10: Hydration of 3-hexyne in standard condition. [**2**-Cl]Cl + 2 AgX[a]*

Entry	5		6		7		8		9		10	
X⁻	OTf⁻		TFA⁻		SbF_6^-		OTs⁻		BF_4^-		OAc⁻	
t (h)	Conv[b] (%)	TOF[c] (h^{-1})	Conv[b] (%)	TOF[c] (h^{-1})	Conv[b] (%)	TOF[c] (h^{-1})	Conv[b] (%)	TOF[c] (h^{-1})	Conv[b] (%)	TOF[c] (h^{-1})	Conv[b] (%)	TOF[c] (h^{-1})
0.5	3	7	11	22	2	3	2	3	6	13	1	2
1	7	7	1	1	6	6	5	5	5	5	1	1
2	15	8	0	0	19	9	10	5	14	7	1	1
4	49	12	4	1	60	15	20	5	44	11	2	0
6	72	12	6	1	84	14	31	5	60	15	2	0
8	95	12	9	1	94	12	42	5	94	12	3	0
24	94	4	27	1	95	4	92	3	94	3	5	0

[a] Catalytic conditions: 3-hexyne (0.88 mmol, 100 µL), H_2O (1.00 mmol, 18 µL), [**2**-Cl]Cl (0.0088 mmol, 1%) and AgX (0.0166 mmol) in γ-valerolactone (400 µL), T: 50 °C. [b]mol% = (moles of catalyst / moles of alkyne) x 100, determined by ^{1}H NMR averaged value of three measurements. [c] TOF = ($n_{product}$ / $n_{catalyst}$) / t(h).

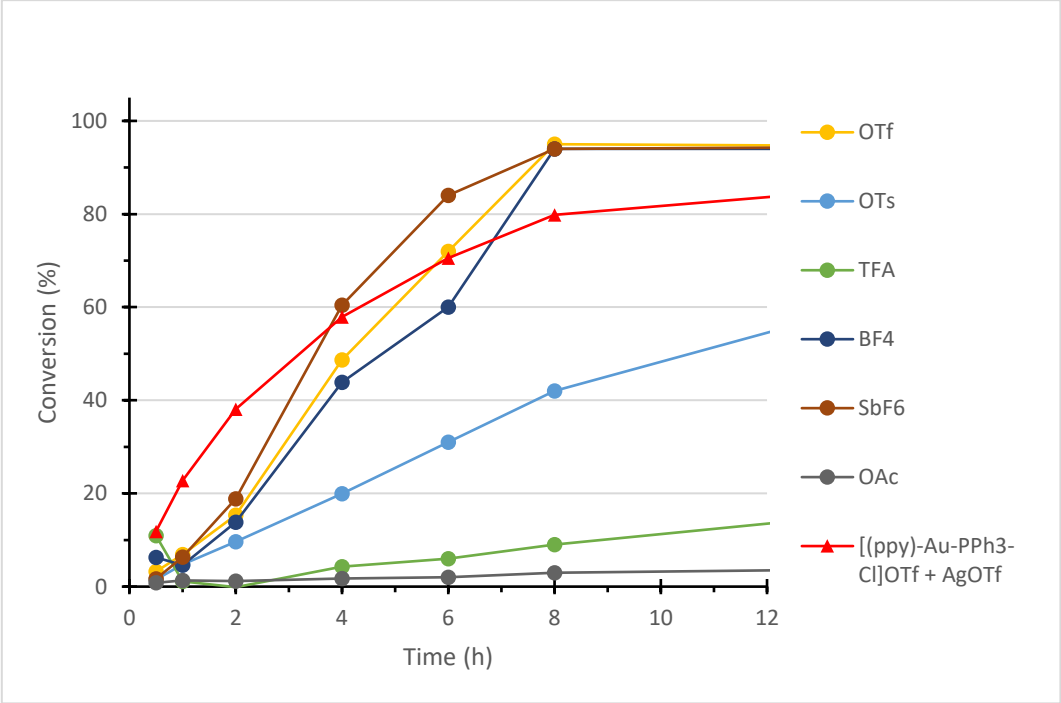

*Figure 3.9: Hydration of 3-hexyne with **2** bearing different anions and **3** with AgOTf.*

Acidic condition and KIE

Table 3.11: *Hydration of 3-hexyne in standard condition.[a] Acid and KIE*

	Reference		**HOTf 5%[b]**		**KIE study[c]**		
t (h)	Conv[d] (%)	TOF[e] (h^{-1})	Conv[d] (%)	TOF[e] (h^{-1})	Conv[d] (%)	TOF[e] (h^{-1})	H_2O/D_2O
0.5	6	11	9	19	4	9	1,27
1	14	14	18	19	10	10	1,36
2	31	15	33	17	17	9	1,78
4	66	17	58	15	46	12	1,44
6	90	15	74	13	70	12	1,29
8	89	11	85	11	88	11	1,01
24	90	4	95	4	91	4	0,99

[a] Catalytic conditions: 3-hexyne (0.88 mmol, 100 µL), H_2O (1.00 mmol, 18 µL), [**2**-Cl]Cl (0.0088 mmol, 1%) and AgOTf (0.0166 mmol) in γ-valerolactone (400 µL), T: 50 °C. [b]in the presence of HOTf (0.043 mmol, 3.8 µL). [c]D_2O instead of H_2O (1.10 mmol, 20 µL). [d]mol% = (moles of catalyst / moles of alkyne) x 100, determined by ^1H NMR averaged value of three measurements. [e] TOF = ($n_{product}$ / $n_{catalyst}$) / t(h).

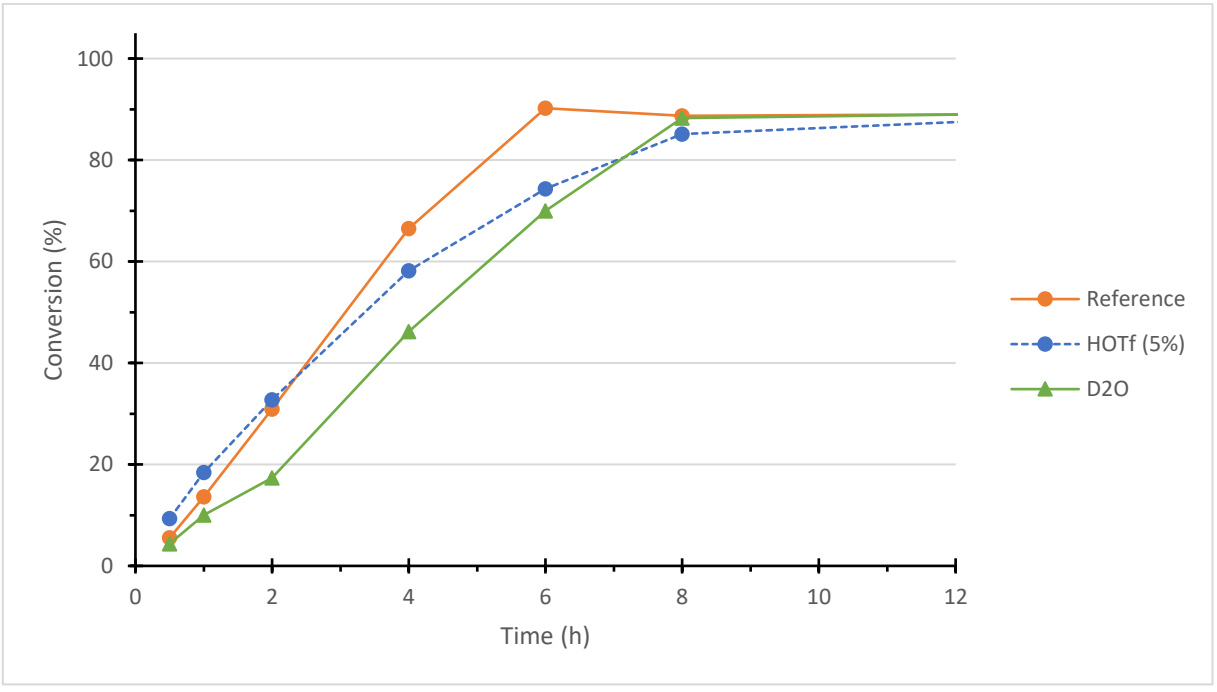

Figure 3.10*: Hydration of 3-hexyne in standard condition. Acid and KIE*

Temperature effect and activation energy

Table 3.12: Hydration of 3-hexyne in standard condition[a].

T	40 °C		50 °C		65 °C		80 °C		120 °C	
t (h)	Conv[b] (%)	TOF[c] (h^{-1})	Conv[b] (%)	TOF[c] (h^{-1})	Conv[b] (%)	TOF[c] (h^{-1})	Conv[b] (%)	TOF[c] (h^{-1})	Conv[b] (%)	TOF[c] (h^{-1})
0.17	-	-	-	-	-	-	-	-	46	289
0.5	4	8	6	11	16	32	32	64	83	172
1	7	7	14	14	32	32	60	60	88	92
2	14	7	31	15	65	33	89	45	-	-
4	28	7	66	17	90	22	93	23	-	-
6	44	7	90	15	90	15	-	-	-	-
8	62	8	89	11	-	-	-	-	-	-
24	93	4	90	4	-	-	95	4	-	-

[a] Catalytic conditions: 3-hexyne (0.88 mmol, 100 µL), H_2O (1.00 mmol, 18 µL), [**2**-Cl]Cl (0.0088 mmol, 1%) and AgOTf (0.0166 mmol) in γ-valerolactone (400 µL). [b]mol% = (moles of catalyst / moles of alkyne) x 100, determined by ^1H NMR averaged value of three measurements. [c] TOF = ($n_{product}$ / $n_{catalyst}$) / t(h).

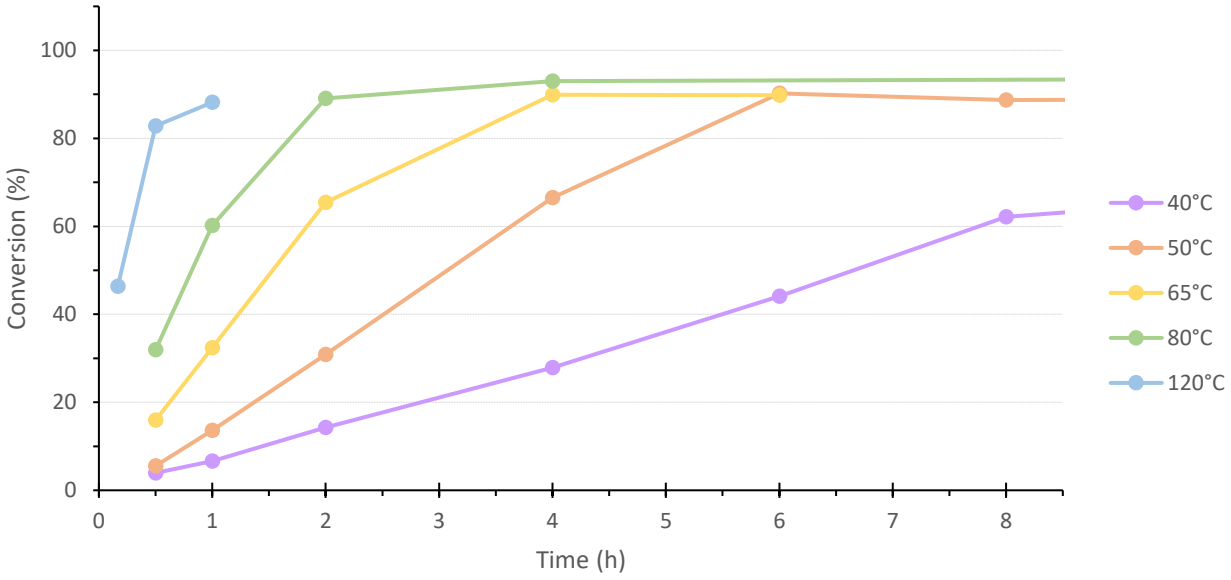

Figure 3.11: Hydration of 3-hexyne in standard condition.

Arrhenius equation

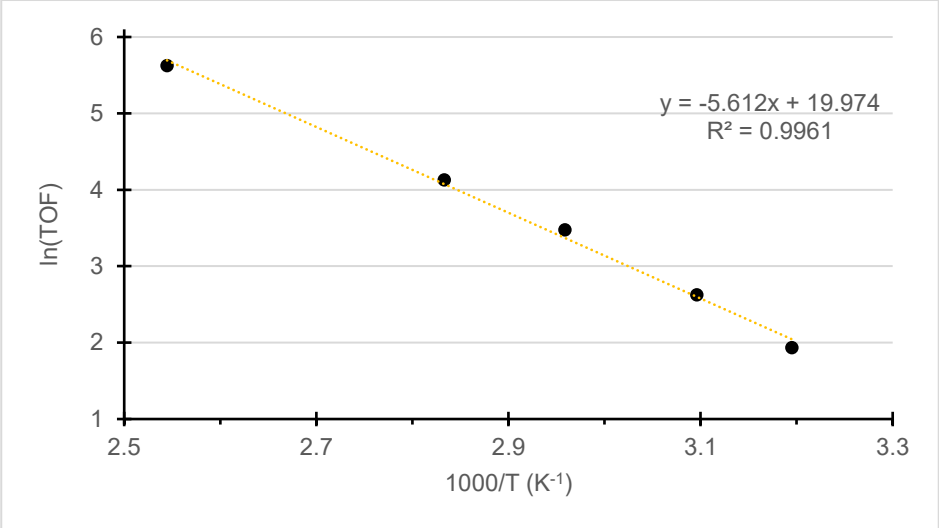

1/T (K^{-1})	ln(TOF)
0.0032	1.933
0.0031	2.625
0.0030	3.476
0.0028	4.127
0.0025	5.624

Figure 3.12: *Arrhenius plot with TOF calculated at 50% of conversion.*

$$k = Ae^{-\frac{E_a}{RT}} \rightarrow \ln(k) = \ln(A) - \frac{E_a}{R} \cdot \frac{1}{T}$$

$$\frac{E_a}{R} = 5.612 \cdot 10^3 \rightarrow E_a = 46\,660\,J = 11\,150\,cal$$

Concentration

Table 3.13*: Hydration of 3-hexyne catalyzed by [**2**-Cl]Cl in standard condition.*[a]

	0.1%		**0.2%**		**0.5%**		**1.0%**		**1.5%**		**2.0%**	
t (h)	Conv[b] (%)	TOF[c] (h^{-1})	Conv[b] (%)	TOF[c] (h^{-1})	Conv[b] (%)	TOF[c] (h^{-1})	Conv[b] (%)	TOF[c] (h^{-1})	Conv[b] (%)	TOF[c] (h^{-1})	Conv[b] (%)	TOF[c] (h^{-1})
05	3	58	2	16	3	13	5	10	9	12	9	9
1	0	2	3	17	6	12	13	13	17	11	22	11
2	-	-	3	8	13	13	28	14	30	10	44	11
4	1	3	10	13	24	12	60	15	70	11	85	11
6	0	1	12	10	35	12	87	15	88	10	89	7
8	-2	-2	21	13	58	15	92	12	87	7	90	6
24	25	10	75	16	91	8	92	4	87	2	90	2

[a] Catalytic conditions: 3-hexyne (0.88 mmol, 100 µL), H_2O (1.00 mmol, 18 µL), and AgOTf (twice the amount of catalyst) in γ-valerolactone (400 µL), T: 50 °C. [b]mol% = (moles of catalyst / moles of alkyne) x 100, determined by ^1H NMR averaged value of three measurements. [c]TOF = ($n_{product}$ / $n_{catalyst}$) / t(h).

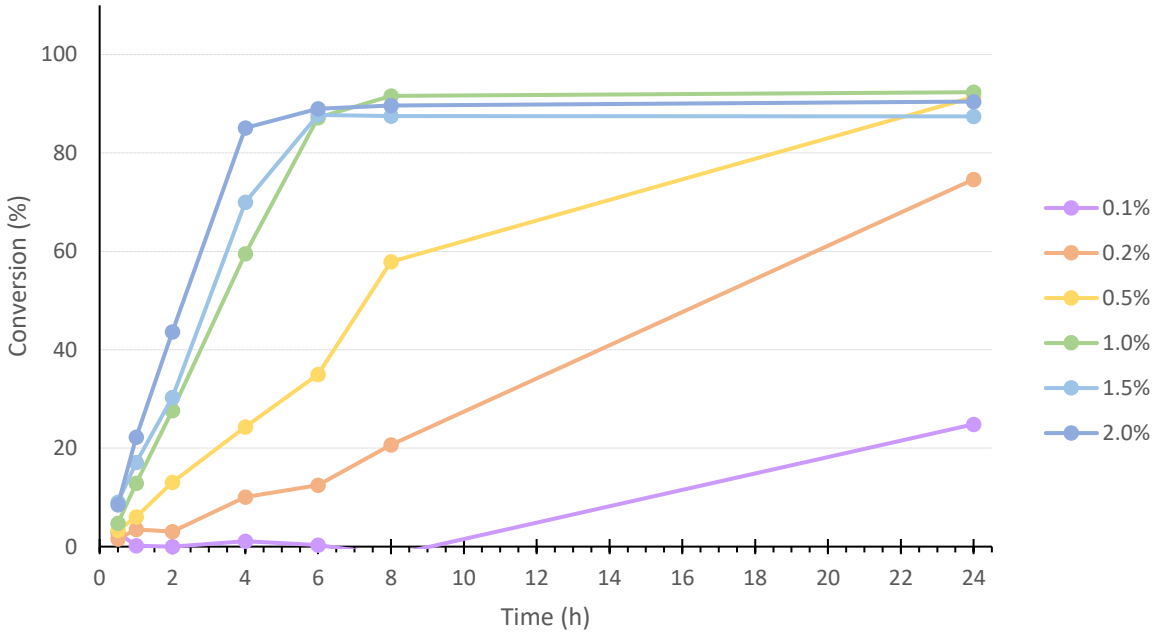

***Figure 3.13**: Hydration of 3-hexyne in standard condition as a function of catalyst [**2**-Cl]Cl concentration.*

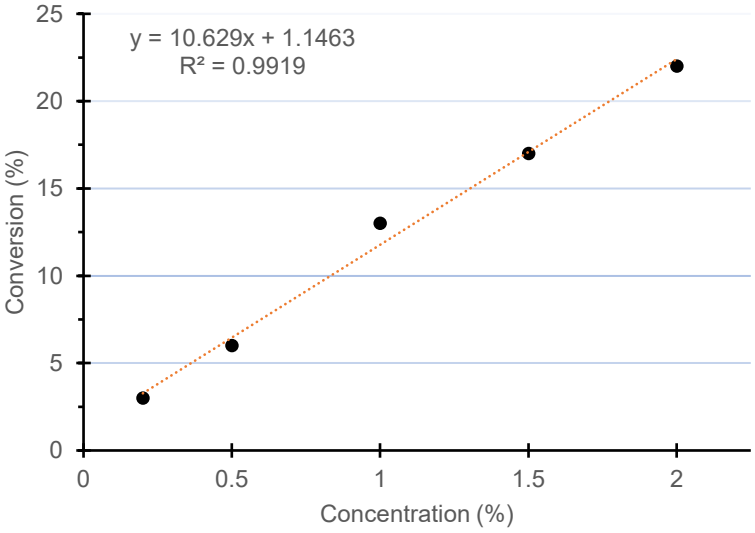

Catalyst conc. (%)	Conversion after 1h
0.1	-
0.2	3
0.5	6
1	13
1.5	17
2	22

***Figure 3.14:** Catalyst concentration vs conversion after 1 h.*

Table 3.14: Hydration of 3-hexyne with different substrates concentration[a].

	3-hexyne						H_2O					
Volume	**50 µL**		**100 µL**		**200 µL**		**18 µL**		**36 µL**		**54 µL**	
t (h)	Conv[b] (%)	TOF[c] (h^{-1})	Conv[b] (%)	TOF[c] (h^{-1})	Conv[b] (%)	TOF[c] (h^{-1})	Conv[b] (%)	TOF[c] (h^{-1})	Conv[b] (%)	TOF[c] (h^{-1})	Conv[b] (%)	TOF[c] (h^{-1})
0.5	13	13	6	11	4	16	6	11	1	1	1	3
1	28	14	14	14	10	21	14	14	9	9	10	10
2	59	15	31	15	24	24	31	15	25	12	25	12
4	90	11	66	17	36	18	66	17	60	15	62	15
6	91	8	90	15	42	14	90	15	86	14	87	14
8	92	6	89	11	44	11	89	11	88	11	89	11
24	90	2	90	4	49	4	90	4	88	4	88	4

[a]Catalytic conditions: [**2**-Cl]Cl (0.0088 mmol, 1%) and AgOTf (0.0166 mmol) in γ-valerolactone (400 µL), T: 50 °C. [b]mol% = (moles of catalyst / moles of alkyne) x 100, determined by ^{1}H NMR averaged value of three measurements. [c]TOF = ($n_{product}$ / $n_{catalyst}$) / t(h).

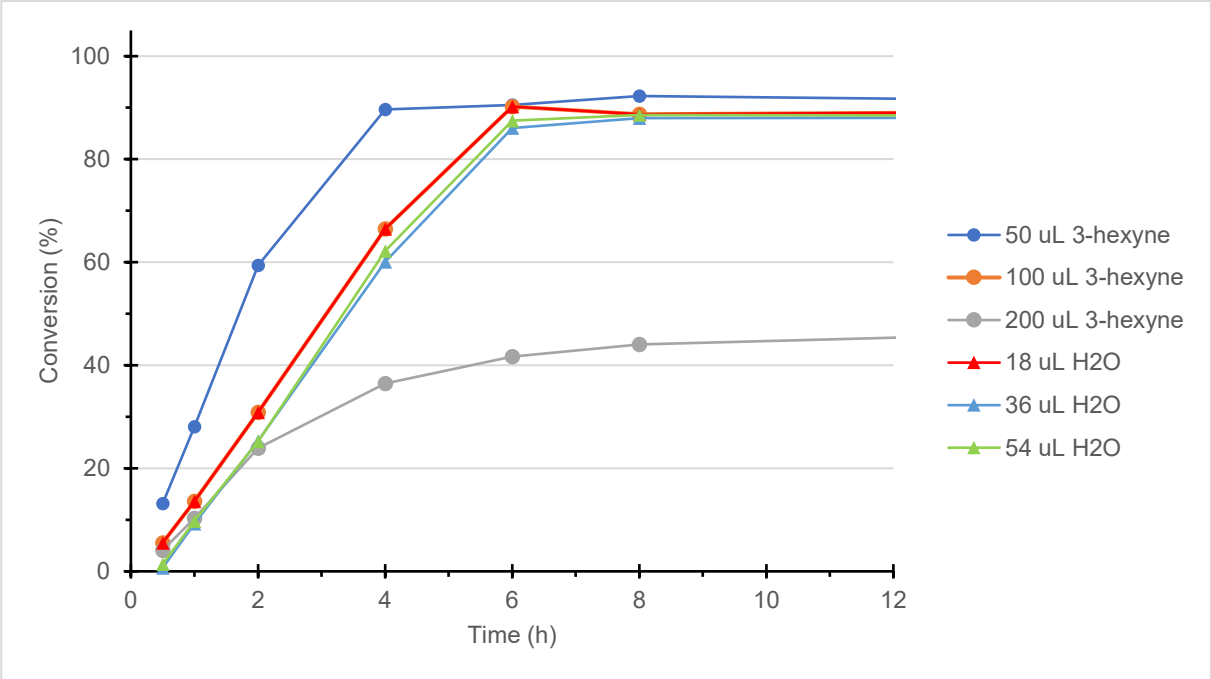

Figure 3.15: Hydration of 3-hexyne with different substrates concentration.

STABILITY STUDIES

In an NMR tube, the stability of [**3**-Cl]OTf and [**2**-Cl]Cl has been studied in a catalysis-like system, using acetone-d_6 as the solvent instead of GVL.

[3-Cl]OTf

The ^{1}H and ^{31}P spectra were recorded in this order:

1. [**3**-Cl]OTf (7 mg, 0.088 mmol) in 400 µL of acetone-d_6;
2. + 3-hexyne (100 µL, 0.88 mmol) + H_2O (18 µL, 1 mmol);
3. + 1.5 equivalent of AgOTf at 30 °C;
6. After 6h at 30 °C;
9. After 12h at 30 °C;

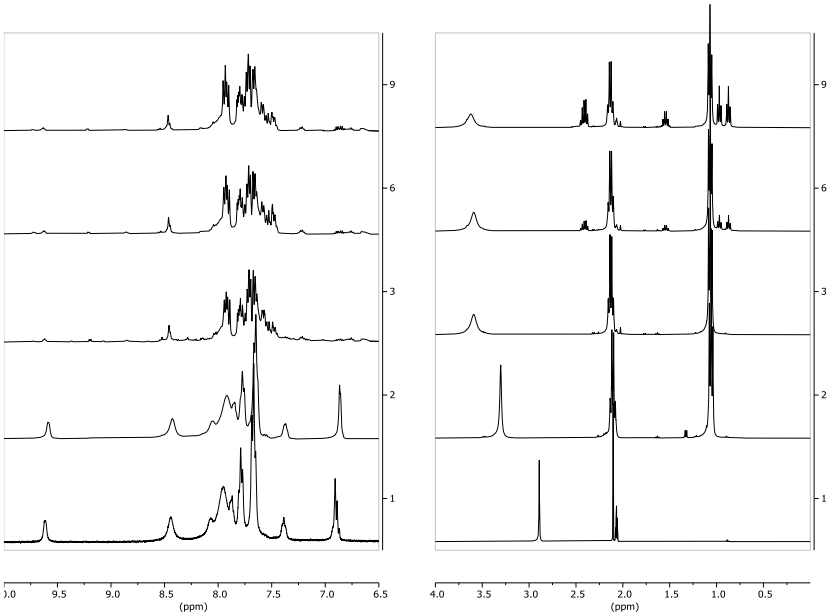

***Figure 3.16**: ^{1}H NMR in acetone-d_6 of catalysis mediated by [3-Cl]OTf.*

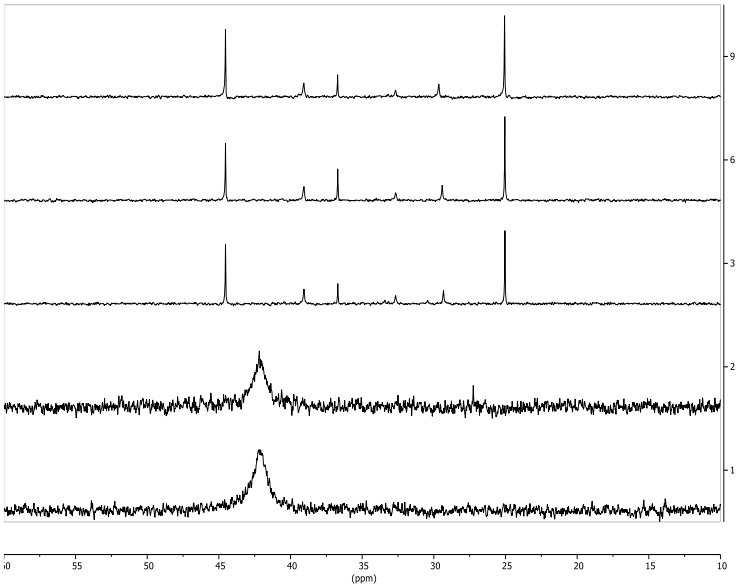

***Figure 3.17**: ^{31}P NMR in acetone-d_6 of catalysis mediated by [3-Cl]OTf.*

[2-Cl]Cl

The ^{1}H, ^{13}C DEPT, and ^{1}H-^{15}N HMBC spectra were recorded in this order:

^{1}H NMR in acetone-d_6

1. [**2**-Cl]Cl (20 mg, 0.025 mmol) in 450 µL of acetone-d_6;
2. Solution A: + $AgBF_4$ (1.5 eq.) + H_2O (4 µL, 0.247 mmol);
3. Solution B: + 3-hexyne (28 µL, 0.25 mmol) at 30% conversion

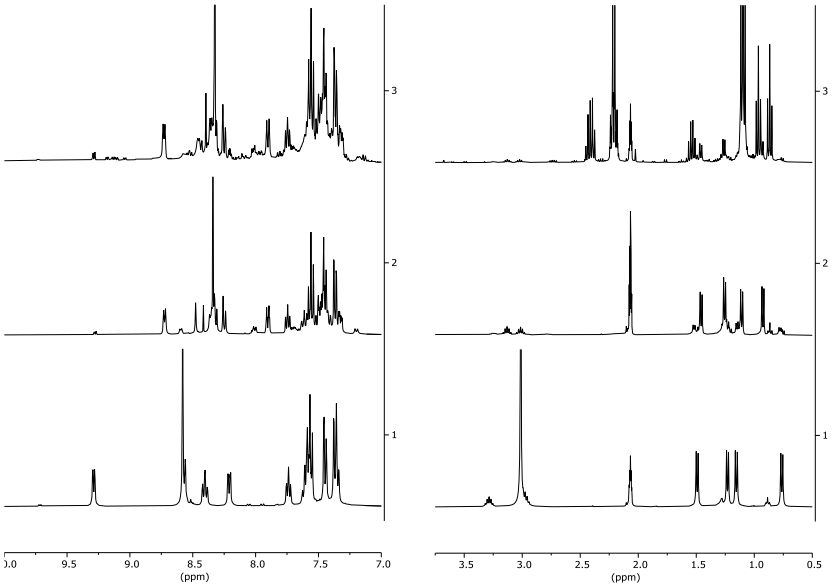

***Figure 3.18**: [1]H NMR in acetone-d_6 of catalysis mediated by [**2**-Cl]Cl.*

^{13}C NMR in acetone-d_6

1. Solution A
2. Solution B

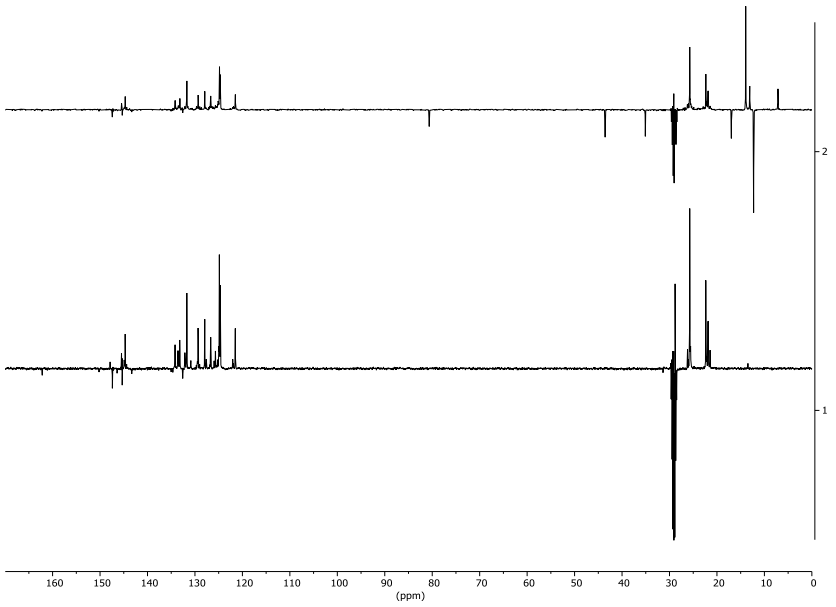

***Figure 3.19**: [13]C NMR in acetone-d_6.*

^{1}H-^{15}N HMBC in acetone-d_6

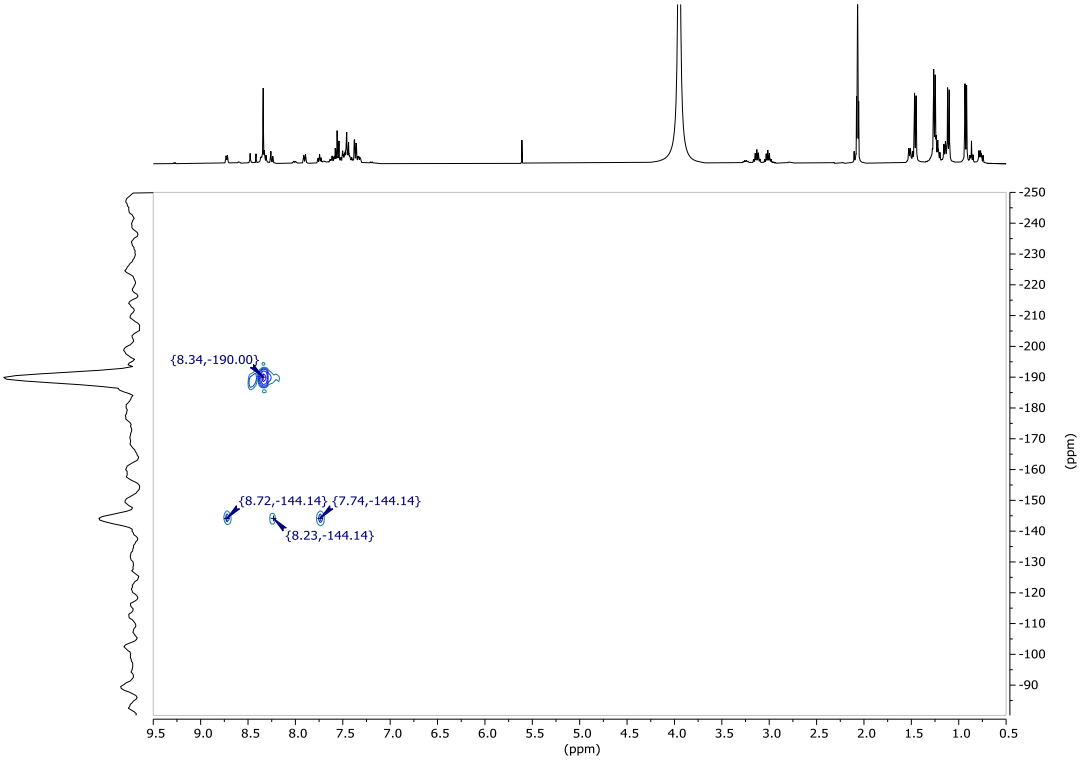

***Figure 3.20**: solution A.*

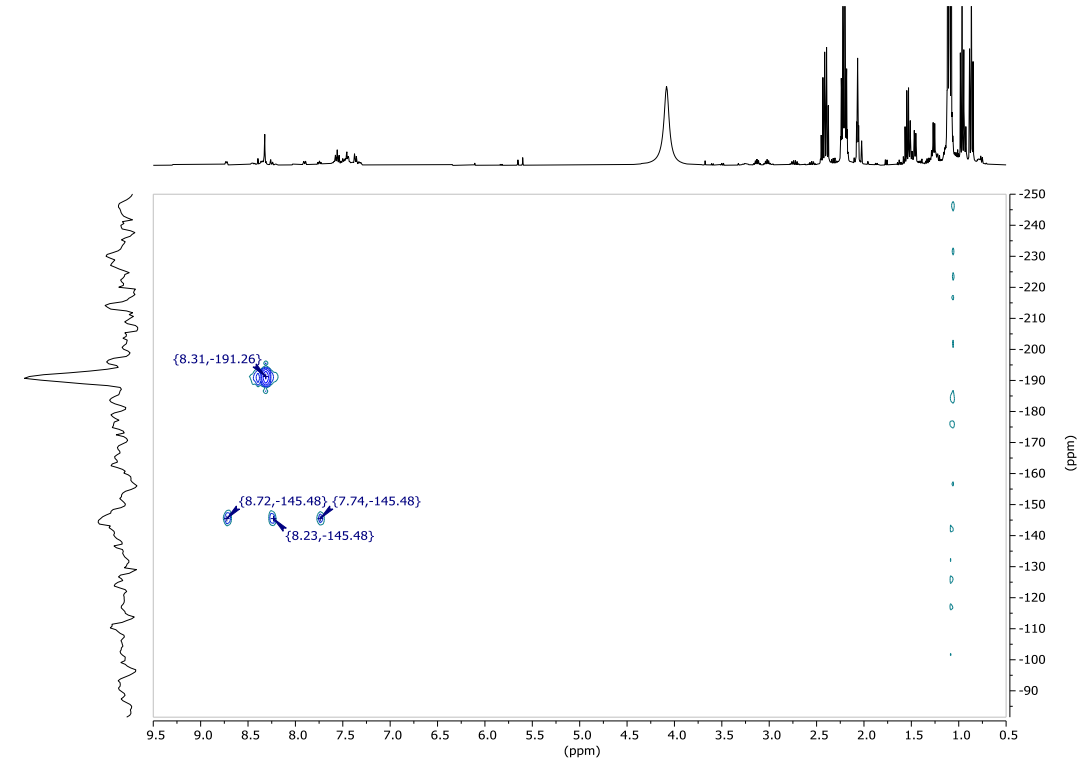

***Figure 3.21**: solution B.*

4.3.5 Gold(III) preequilibrium study - Chapter 2.2.2

General procedure

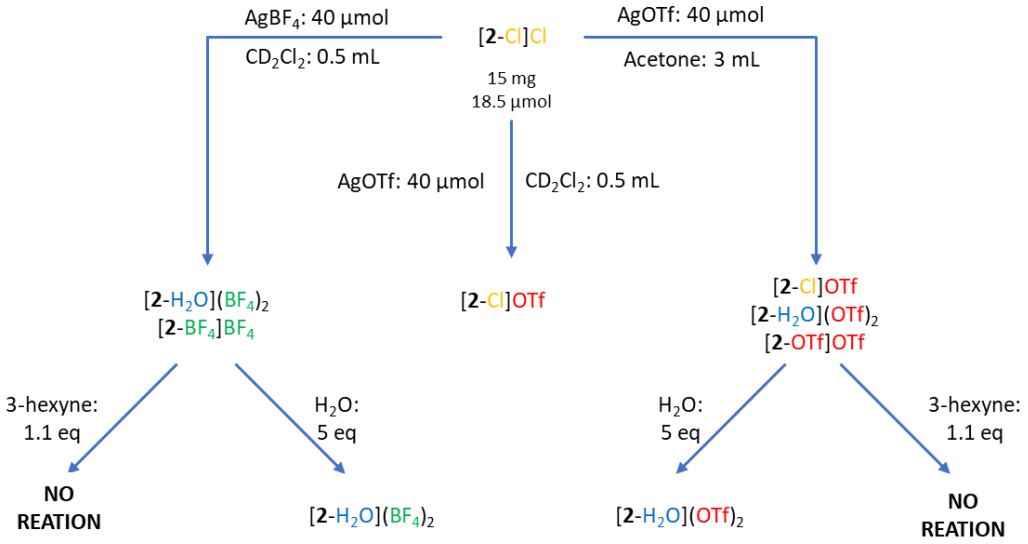

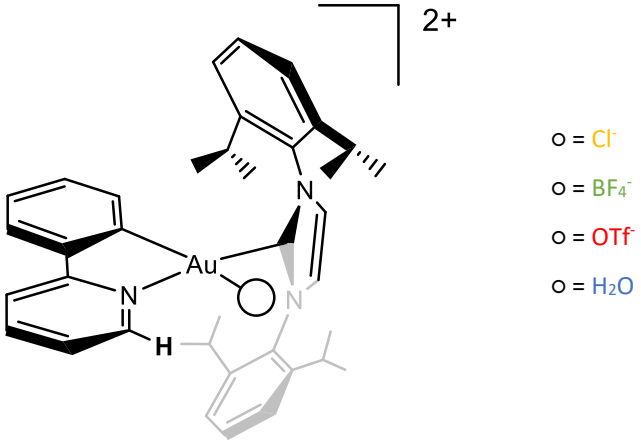

Scheme 3.1: *List of the reactions studied.*

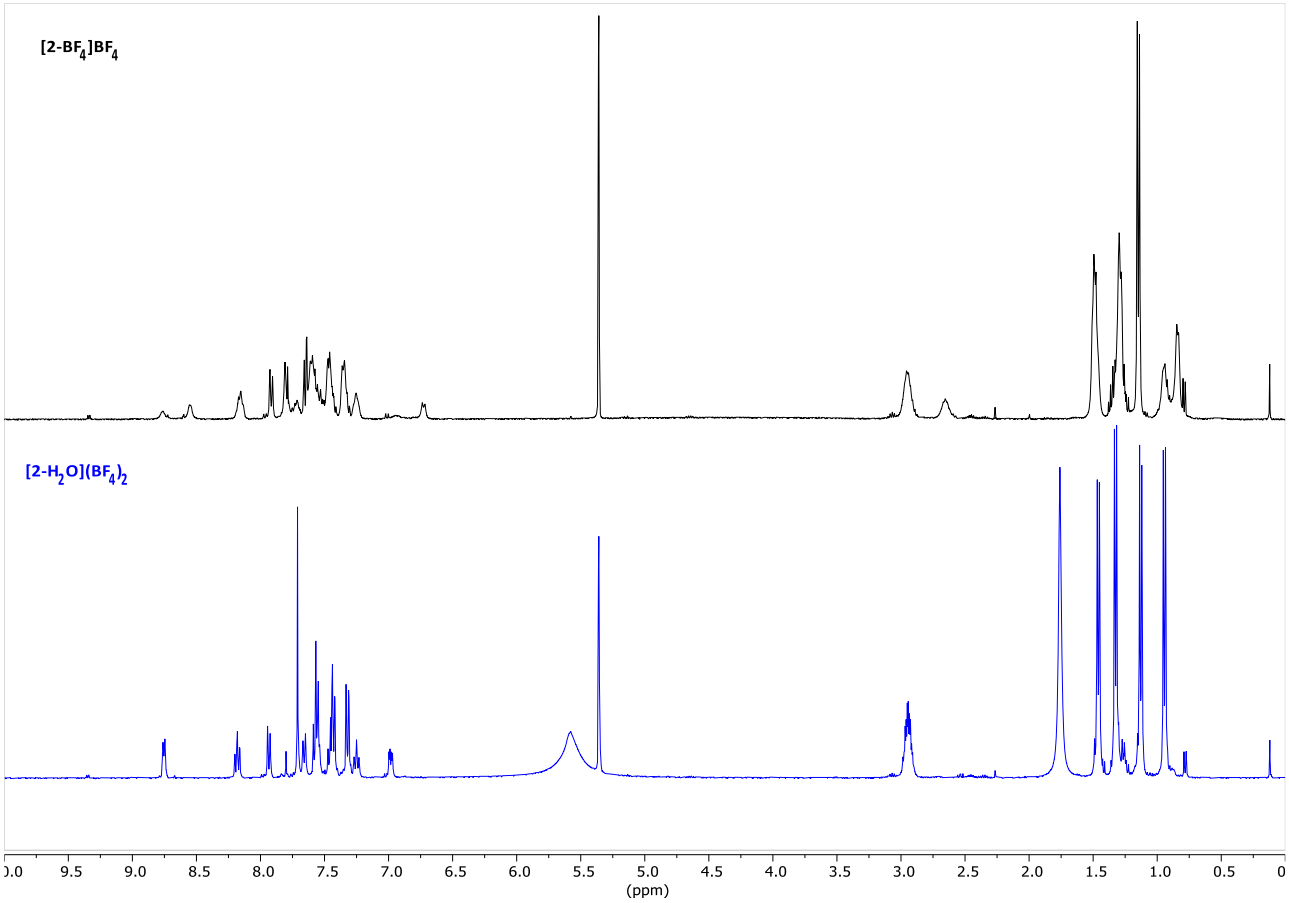

Figure 3.22: *^{1}H NMR spectra of the complexes [**2**-BF_4]BF_4 vs [**2**-H_2O]$(BF_4)_2$.*

4.4 Computational details

4.4.1 Meyer-Schuster - Chapter 2.1.2

Complexes NHC*-Au-X (NHC* = 1,3-dimethylimidazol-2-ylidene; X = OTf^- trifluoromethanesulfonate or triflate anion, OTs^- toluenesulfonyl or tosylate anion, BF_4^- tetrafluoroborate, TFA trifluoroacetate) and 1-phenyl-2-propyn-1-ol have been used in the calculations as a model for the catalyst and the substrate, respectively.

The computational analysis has been carried out with ADF related QUantum-regions Interconnected by Local Description (QUILD) program,[214] to identify reactant complexes, intermediates, product complexes and transition states of the carbene-gold(I) catalyzed Meyer-Schuster rearrangement of the 1-phenyl-2-propyn-1-ol, assisted by the OTf^-, OTs^-, BF_4^- and TFA^- counterions. A TZ2P basis set with the core small approximation, the GGA BP86 functional[215,216] and the scalar zeroth-order regular approximation ZORA Hamiltonian[203,217] for the inclusion of relativistic effects were used. This protocol is hereafter labeled as "BP86/ZORA".

The stationary points and transition states have also been optimized including Grimme's D3 dispersion correction,[218,219] in order to evaluate the effect of the dispersion on the geometries and, indirectly, on the reaction energies (this protocol is labeled as "BP86/ZORA/D3"). Frequency calculations have been carried out at the same level of theory in order to identify the stationary points (zero imaginary frequencies) and the transition states (one imaginary frequency). The same protocol (BP86/ZORA/D3) has been used for calculating the geometries of stationary points and transition states (with relative frequencies) for two model reactions that account for experimental conditions, i.e. traces of acid (where the OTf^- anion was protonated) and in presence of an explicit molecule of γ-valerolactone, in substitution of the anion.

With the BP86/ZORA protocol, other structures were optimized for modeling the preequilibrium step with the OTf^-. OTs^- and TFA^- counterions, a gold-hydroxy mechanism similar to the one reported in Ref. [154].

Final energies have been calculated at several levels of theory. For all optimized structures, final energies have been calculated with the same computational setup as that used for the optimizations, i.e. either "//BP86/ZORA" and "//BP86/ZORA/D3" when dispersion was included. In addition to this, single-point energy calculations were carried out using the ORCA program package[220] by single-point B2PLYP perturbatively corrected double hybrid functional[221] DFT calculations, with Ahlrich's def2-TZVP basis set[222] and an effective core potential (ECP) for gold,[223]

in order to account for relativistic effects. This setup is labeled as "//B2PLYP". The BP86/ZORA//B2PLYP protocol has been proven to be very accurate when analyzing reaction paths involving gold complexes as reactive species, as reported in previous benchmark studies.[164]

Nonetheless, for the reaction profiles of the intramolecular rearrangement of the substrate assisted by the three counterions (i.e. OTf^-, OTs^- and BF_4^-) and the acid- and γ-valerolactone-assisted reactions, we also calculated final energies using the DLPNO-CCSD(T) approach[162,163] (labelled as "//DLPNO-CCSD(T)"), which has been shown to yield very accurate results (comparable to the regular Coupled-Cluster approach[224]) by keeping the computational cost relatively low (it has been estimated that its computational cost is only two to four times the cost of DFT[225]). The calculations have been carried out with the ORCA program package, by using the def2-TZVP basis set and an effective core potential (ECP) for gold. The default "NormalPNO" DLPNO settings were used as recommended for obtaining a reasonable balance between computational cost and accuracy.[226]

The solvent effect has been taken into account for both the preequilibrium and the nucleophilic attack steps by using the Conductor-like Polarizable Continuum Model (CPCM)[227–229] as implemented in the ORCA package. Since the solvent used in the experiments (i.e. p-cymene) is not included in the list of solvents available for such model, we used toluene, since they have very similar dielectric constant (2.24 vs 2.38 for p-cymene and toluene, respectively) and dimension.

All the energies calculated with the methods described above are presented as electronic energy differences. However, for a full description of the mechanism of this reaction, enthalpies and Gibbs free energies have been calculated for the intramolecular rearrangement of the substrate assisted by the three counterions, in order to evaluate the effect of the entropic contributions on the energy profiles. These calculations have been carried out with the QUILD program, with the BP86/ZORA/D3//BP86/ZORA/D3 protocol.

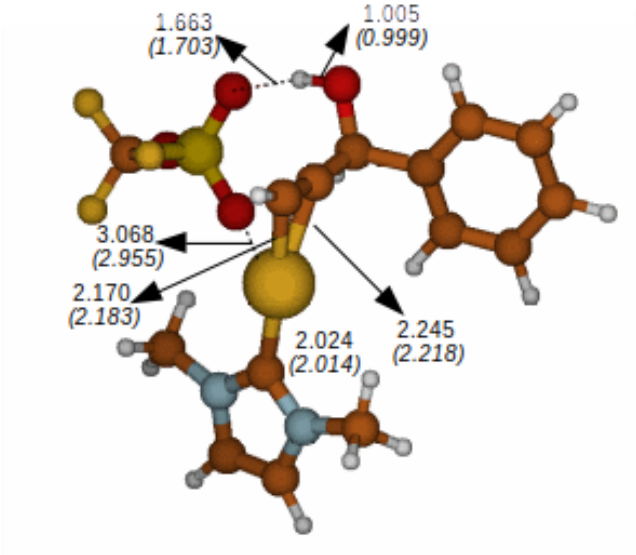

RC_OTf

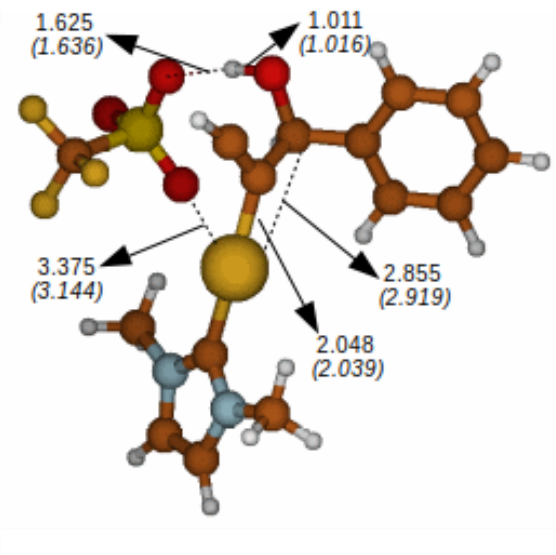

TS1_OTf

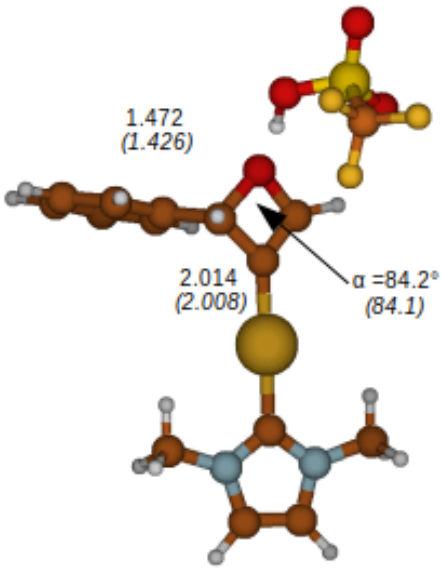

INT_OTf

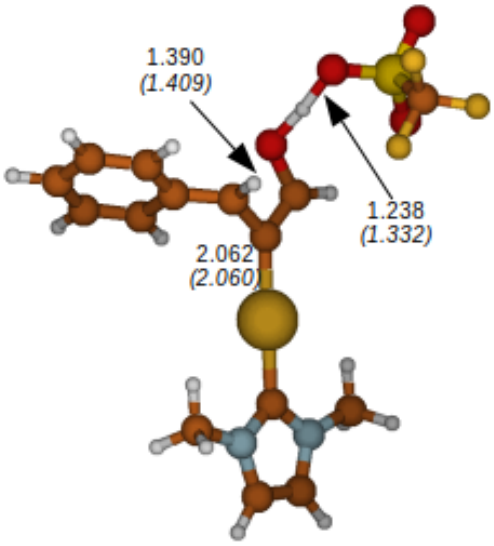

TS2_OTf

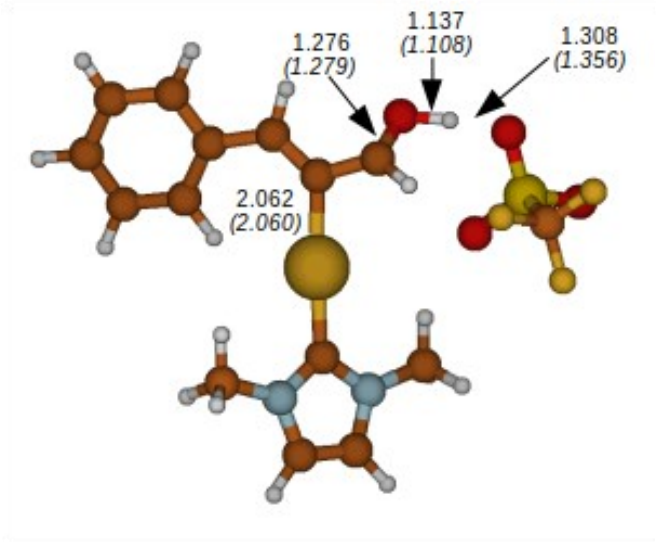

Figure 3.23: *Optimized geometries of stationary points for the intramolecular nucleophilic attack in the 1-phenyl-2-propyn-1-ol assisted by the OTf^- counterion. The most relevant bond lengths and angles at the BP86/ZORA level are reported (value in parenthesis refer to BP86/ZORA/D3 results).*

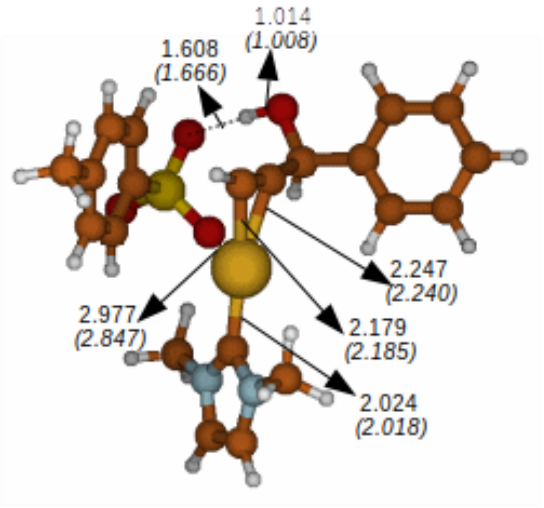

RC_OTs

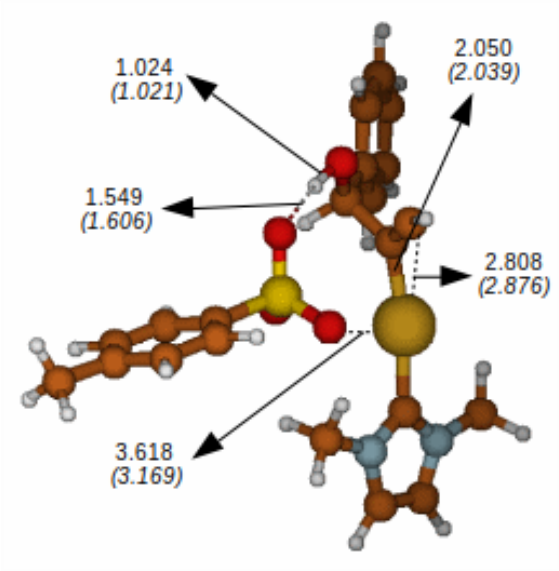

TS1_OTs

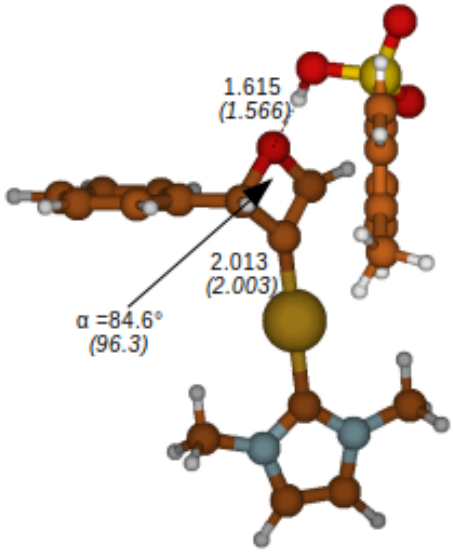

INT_OTs

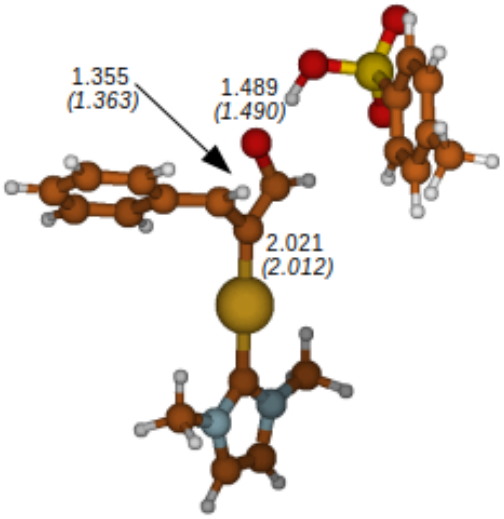

TS2_OTs

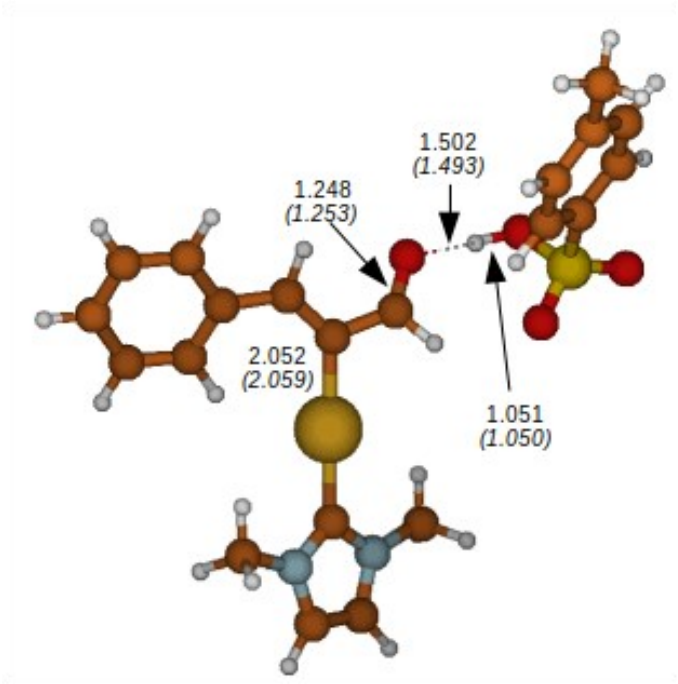

Figure 3.24: *Optimized geometries of stationary points for the intramolecular nucleophilic attack in the 1-phenyl-2-propyn-1-ol assisted by the OTs^- counterion. The most relevant bond lengths and angles at the BP86/ZORA level are reported (value in parenthesis refer to BP86/ZORA/D3 results).*

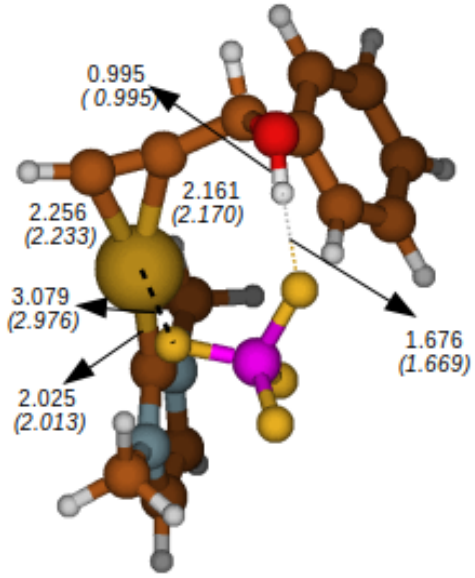

RC_{BF4}

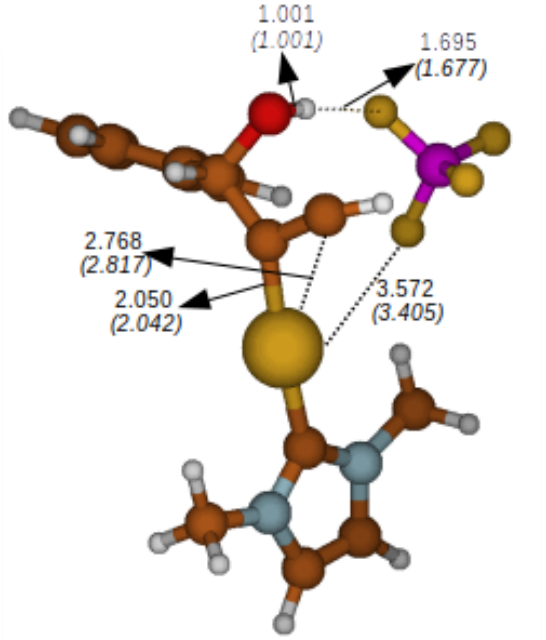

$TS1_{BF4}$

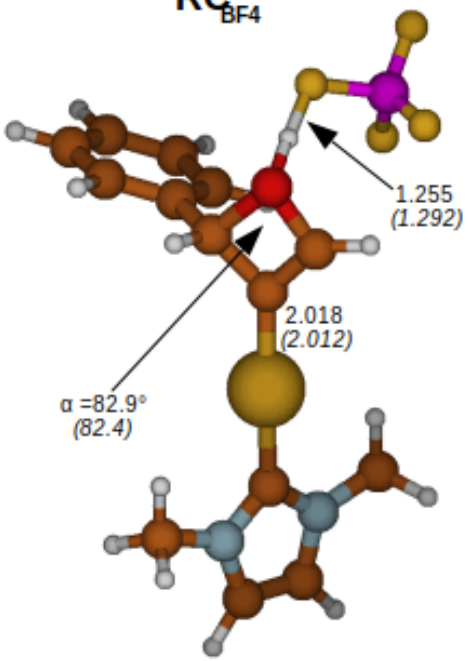

INT_{BF4}

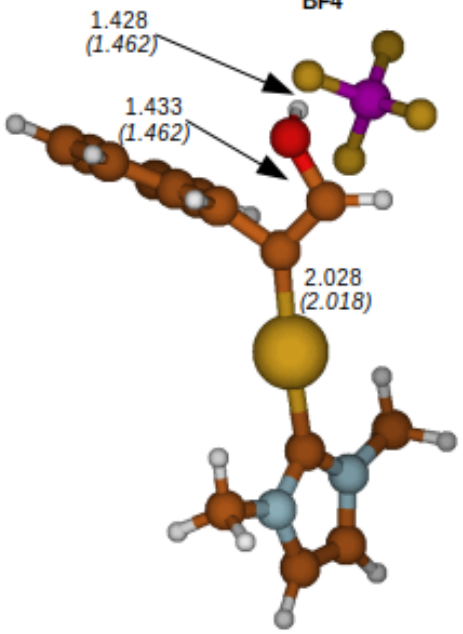

$TS2_{BF4}$

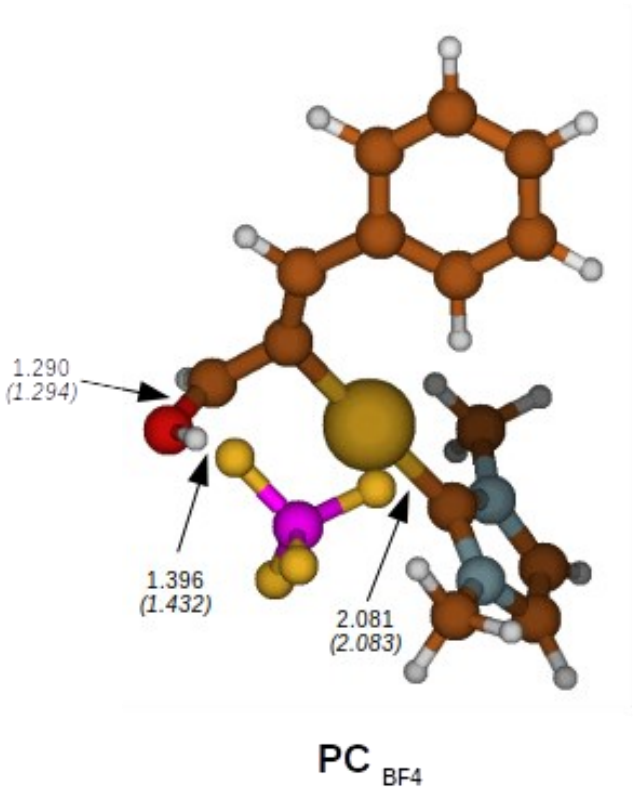

Figure 3.25: *Optimized geometries of stationary points for the intramolecular nucleophilic attack in the 1-phenyl-2-propyn-1-ol assisted by the BF_4^- counterion. The most relevant bond lengths and angles at the BP86/ZORA level are reported (value in parenthesis refer to BP86/ZORA/D3 results).*

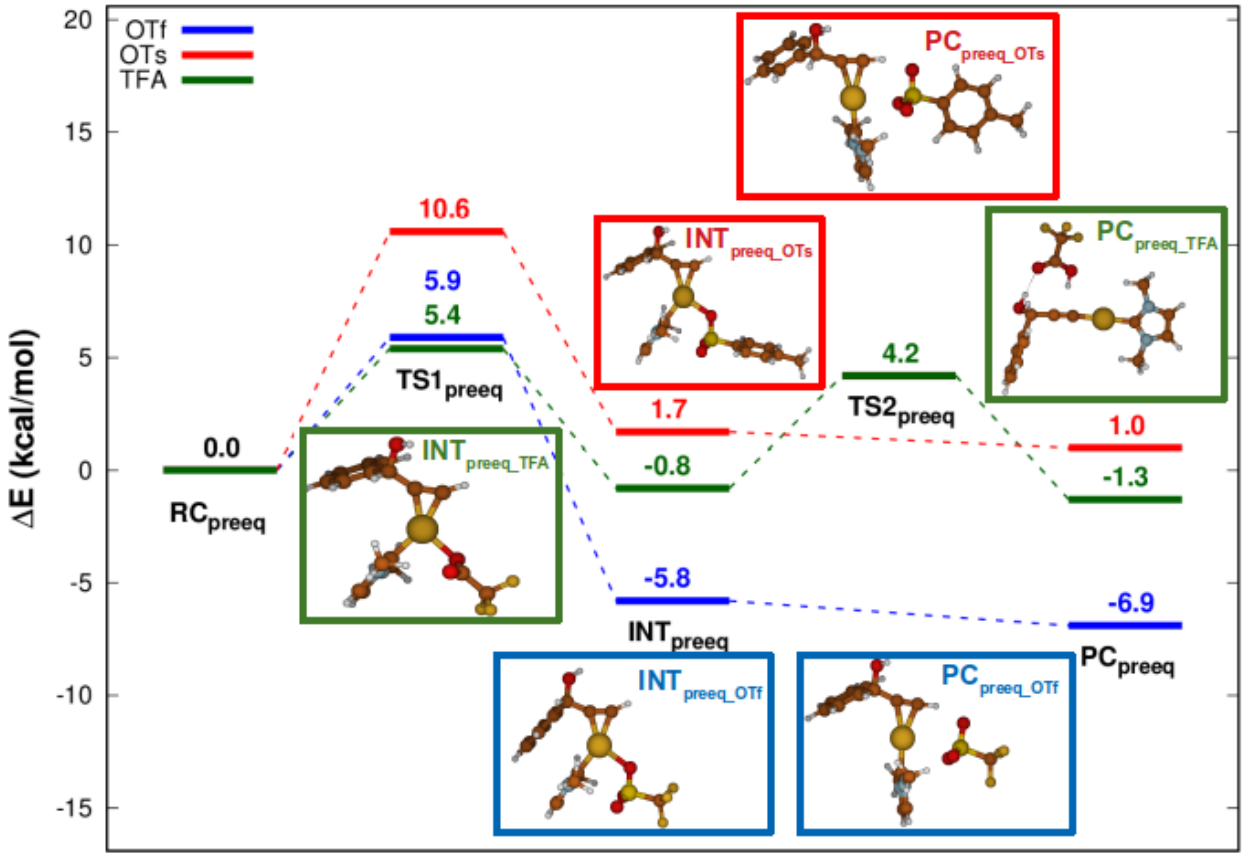

Figure 3.26: *Energy Energy profiles for the preequilibrium step with OTf^- (blue line), OTs^- (red line) and TFA^- (green line) counterions calculated at the BP86/ZORA//B2PLYP/CPCM level. Energies are reported with respect to the corresponding RC taken as zero reference energy.*

Figure 3.26 shows that the pre-equilibrium step occurs via formation of a tri-coordinated intermediate species (INT_{preeq_X}) where both the anion and the alkyne moiety are coordinated to the gold center, that is favored for OTf^- with an activation barrier of 5.9 kcal/mol (vs. 10.6 kcal/mol for OTs^-), as expected on the basis of their coordinating ability trend. Surprisingly, the calculated activation barrier for TFA^- is the lowest (5.4 kcal/mol), thus suggesting that coordination ability should not be the only important feature in this step. Indeed, upon de-coordination of the anion, the expected gold-alkyne complex (PC_{preeq_X}) (with the anion remaining in the first coordination sphere, simultaneously interacting with Au and the acidic hydrogen of the terminal alkyne moiety) is obtained in a barrierless and almost thermoneutral process for OTf^- and OTs^-, whereas for TFA^- a stable σ-bonded gold-alkynyl complex is formed through abstraction of the acidic hydrogen of the terminal alkyne by the anion with an energy barrier of 5.0 kcal/mol.

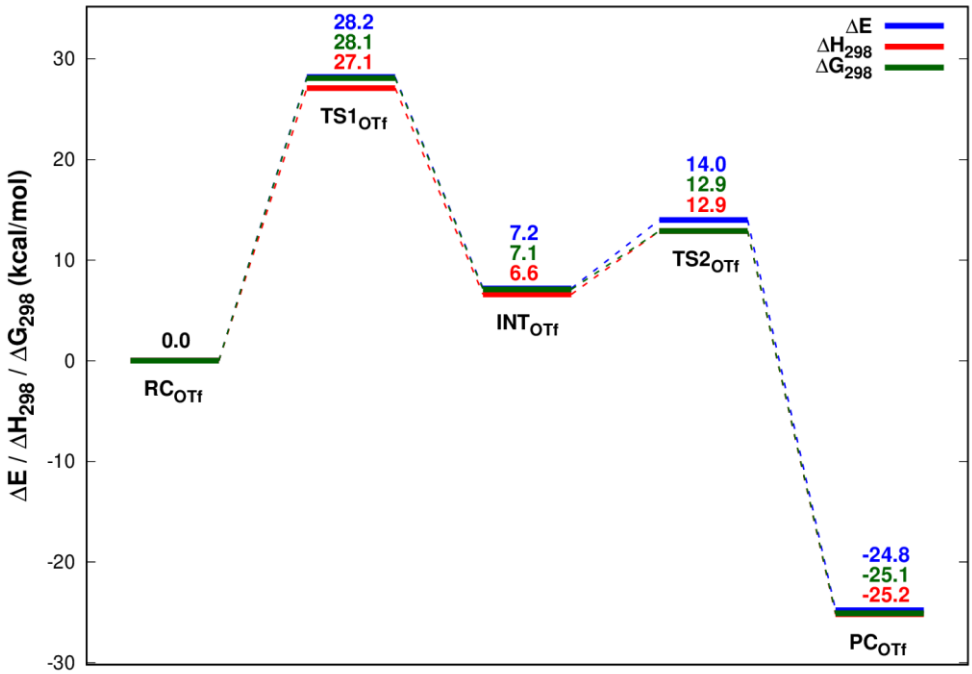

Figure 3.27: *Electronic energy (ΔE, in blue), enthalpy (ΔH_{298}, in red) and Gibbs' free energy (ΔG_{298}, in green) profiles at 298 K for the OTf⁻-assisted intramolecular nucleophilic attack in the 1-phenyl-2-propyn-1-ol calculated at the BP86/ZORA/D3//BP86/ZORA/D3 level. Energies are reported with respect to RC taken as zero reference energy.*

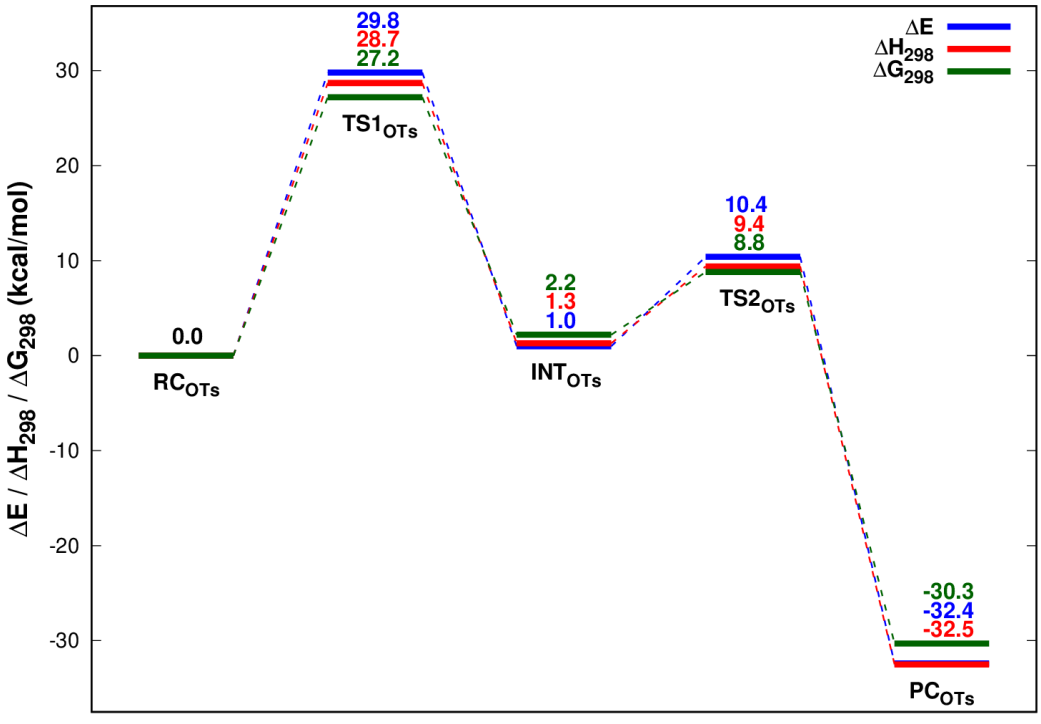

Figure 3.28: *Electronic energy (ΔE, in blue), enthalpy (ΔH_{298}, in red) and Gibbs' free energy (ΔG_{298}, in green) profiles at 298 K for the OTs⁻-assisted intramolecular nucleophilic attack in the 1-phenyl-2-propyn-1-ol calculated at the BP86/ZORA/D3//BP86/ZORA/D3 level. Energies are reported with respect to RC taken as zero reference energy.*

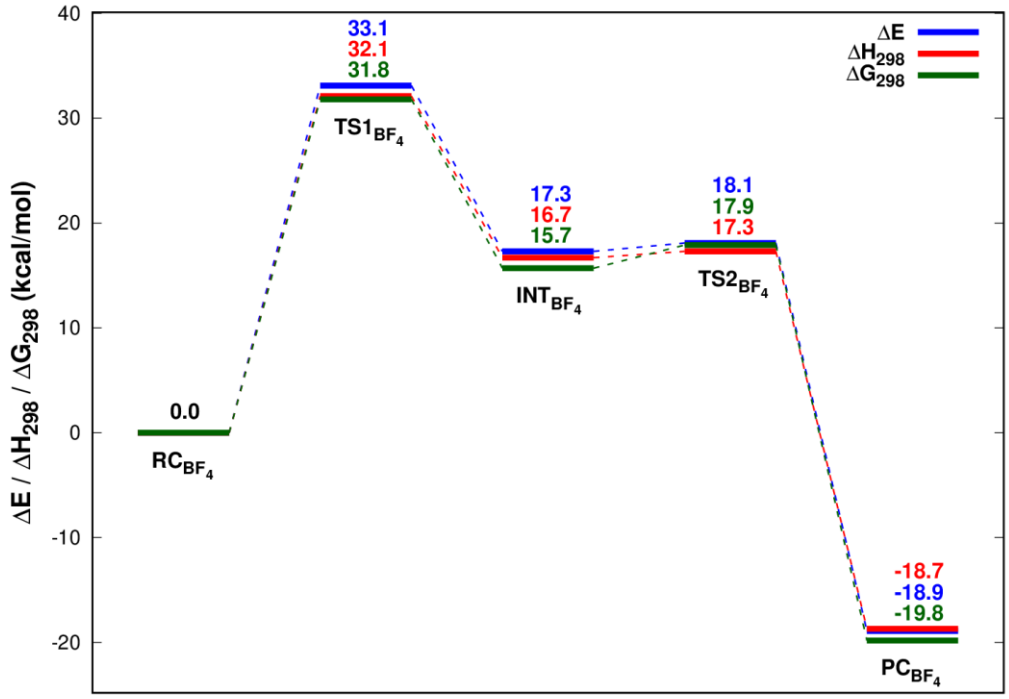

Figure 3.29: *Electronic energy (ΔE, in blue), enthalpy (ΔH_{298}, in red) and Gibbs' free energy (ΔG_{298}, in green) profiles at 298 K for the BF_4^--assisted intramolecular nucleophilic attack in the 1-phenyl-2-propyn-1-ol calculated at the BP86/ZORA/D3//BP86/ZORA/D3 level. Energies are reported with respect to RC taken as zero reference energy.*

As a general result, from **Figure 3.27** - **Figure *3.29*** we observe that electronic energies ΔEs can be considered a very good approximation to both reaction enthalpies ΔHs and Gibbs' free energies ΔGs.

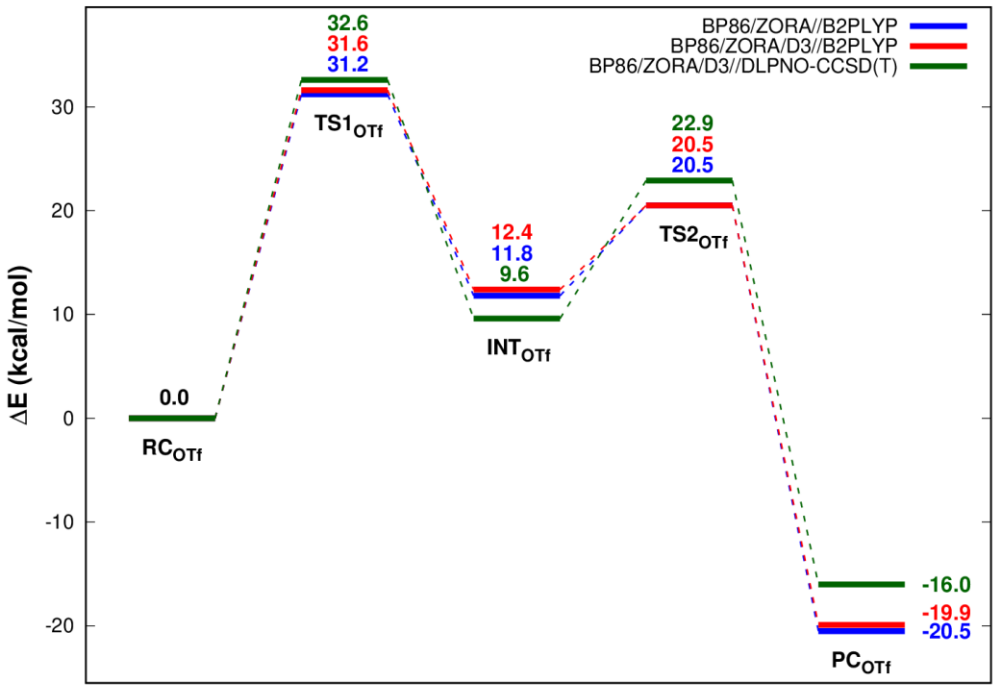

Figure 3.30: *Reaction profiles for the intramolecular nucleophilic attack in the 1-phenyl-2-propyn-1-ol assisted by the OTf^- counterion calculated with different computational protocols. In blue the BP86/ZORA//B2PLYP results, in red the BP86/ZORA/D3//B2PLYP results and in green the BP86/ZORA/D3//DLPNO-CCSD(T) results are shown. Energy are given with respect to the corresponding RC taken as zero reference energy.*

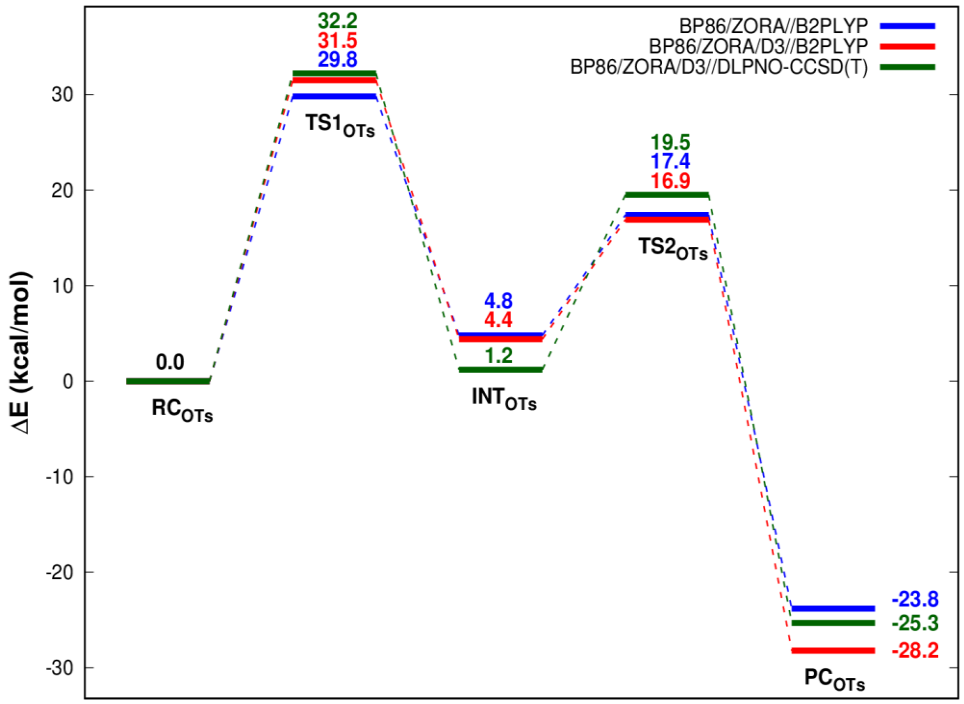

Figure 3.31: *Reaction profiles for the intramolecular nucleophilic attack in the 1-phenyl-2-propyn-1-ol assisted by the OTs^- counterion calculated with different computational protocols. In blue the BP86/ZORA//B2PLYP results, in red the*

BP86/ZORA/D3//B2PLYP results and in green the BP86/ZORA/D3//DLPNO-CCSD(T) results are shown. Energy are given with respect to the corresponding RC taken as zero reference energy.

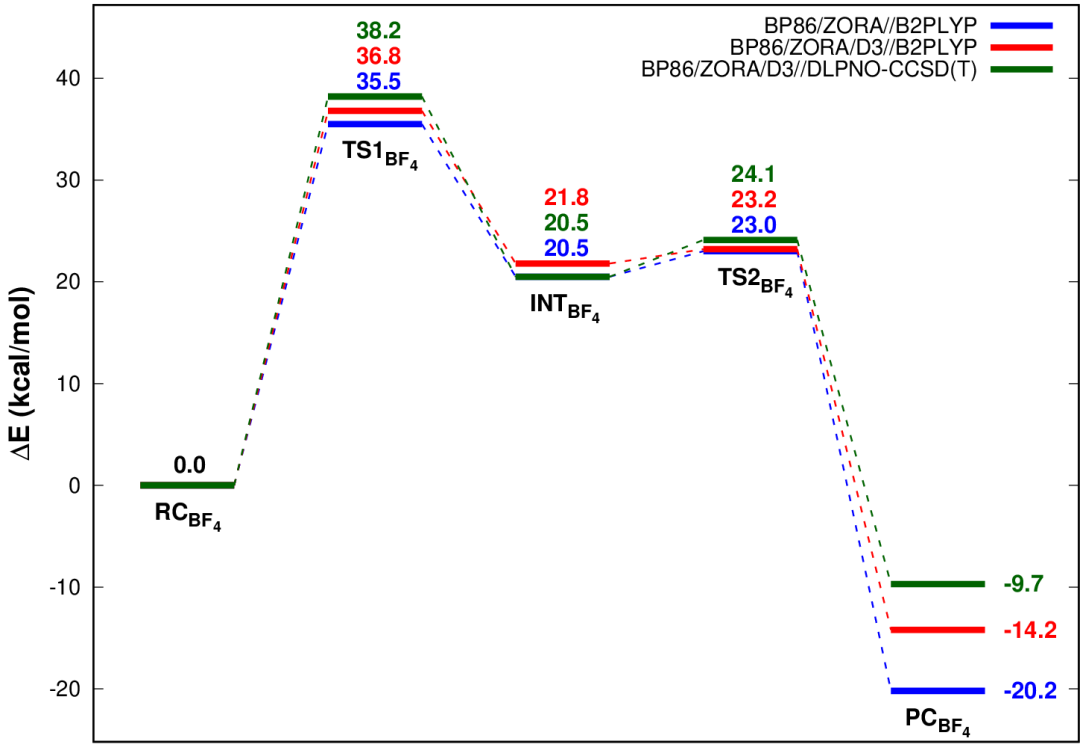

Figure 3.32: *Reaction profiles for the intramolecular nucleophilic attack in the 1-phenyl-2-propyn-1-ol assisted by the BF_4^- counterion calculated with different computational protocols. In blue the BP86/ZORA//B2PLYP results, in red the BP86/ZORA/D3//B2PLYP results and in green the BP86/ZORA/D3//DLPNO-CCSD(T) results are shown. Energy are given with respect to the corresponding RC taken as zero reference energy.*

The reaction profiles in **Figure 3.29** - **Figure *3.31*** highlight that: the BP86/ZORA//B2PLYP protocol, which is computationally less demanding, gives very similar results to those obtained with the BP86/ZORA/D3//B2PLYP setup for all the reaction profiles, indicating that the effect of the dispersion (included in the geometry optimization) on the energies is very small.

These results also allow to compare the performances of the DFT double-hybrid approach (BP86/ZORA/D3//B2PLYP) and the ab-initio one (BP86/ZORA/D3//DLPNO-CCSD(T)), highlighting that overall the reaction profiles are very similar, validating the very good accuracy of a protocol involving energy calculations performed at the B2PLYP level.

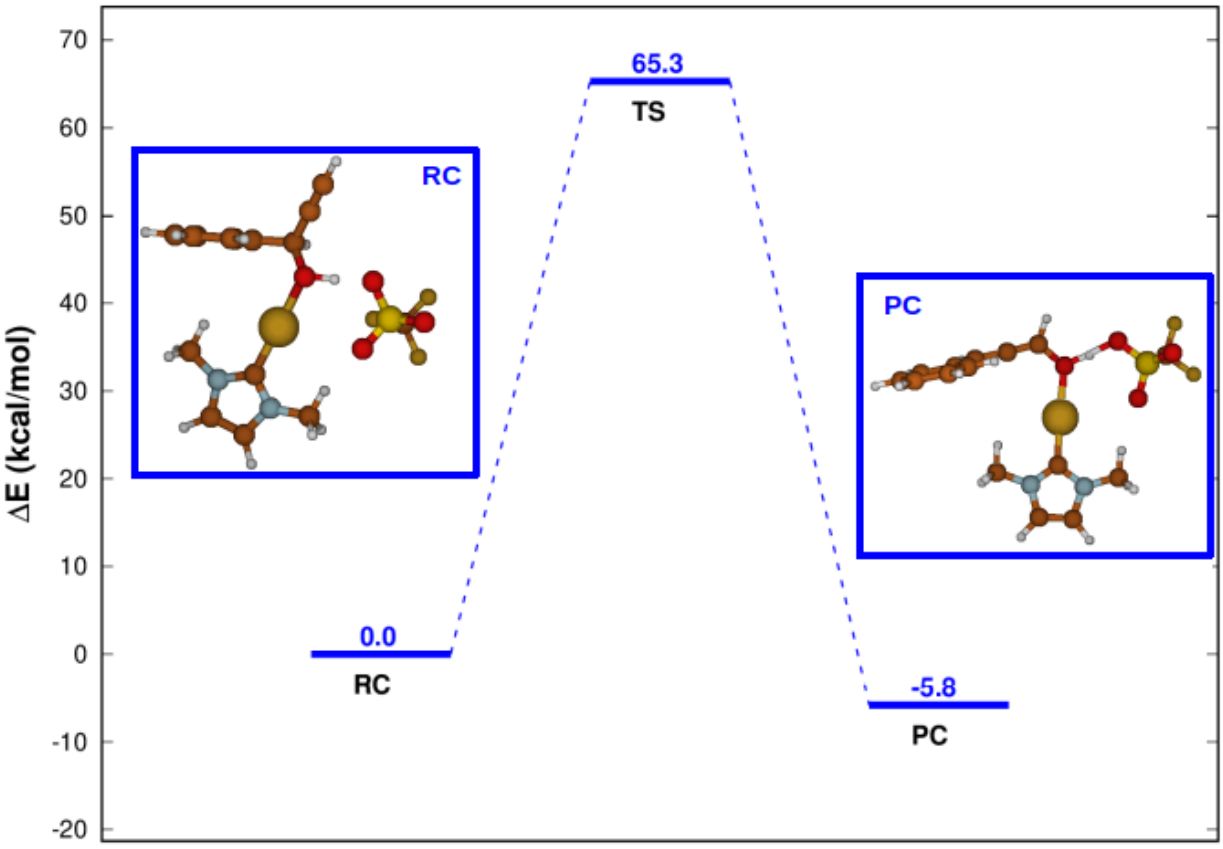

Figure 3.33: *Energy profile for the intramolecular nucleophilic attack in the 1-phenyl-2-propyn-1-ol assisted by the OTf counterion where the active catalytic species is a gold-hydroxo complex (RC). The profile has been calculated at the BP86/ZORA//B2PLYP level. Energies are given with respect to RC taken as zero reference energy.*

In Ref. 154, a mechanism for the gold-catalyzed Meyer-Schuster rearrangement of propargylic acetates has been proposed where a gold-hydroxo ([NHC(Au)OH]) complex is considered as the active catalytic species in solution. Here we model a similar mechanism for our reaction, to compare with the above calculated mechanism.

Considering that in our experimental conditions the solvent is p-cymene and water can be present only in traces, the formation of the active gold-hydroxo species can occur via:

1) Coordination of gold to the propargylic hydroxy group (RC in **Figure 3.31***).* By comparing the energy of this RC with respect to the one in which the gold fragment is coordinated to the alkyne triple-bond, the gold-hydroxo species is actually 11.4 kcal/mol more stable with respect to the former. However, as reported in **Figure 3.31**, the nucleophilic attack (which occurs without any intermediate) has an extremely high activation barrier (65.3 kcal/mol), almost two times as large as that of the gold-alkyne reactant complex rearranging to the gold-oxetene intermediate. Therefore,

this mechanism is unlikely to take place.

2) Formation of a gold-hydroxo complex via traces of water. The authors in Ref. 154 highlight that the high degree of water solvation of the precatalyst (i.e., a [NHC-Au-SbF_6] complex) makes the formation of the gold-hydroxo active species feasible. Moreover, they find that accounting for less than four water molecules in the simulation (which is the quantity that should model the solvation) makes the formation of the gold-hydroxo species unfavored (the reaction is endoergonic by 50 kcal/mol ca. with only one H_2O molecule in the simulation). In our experimental conditions, despite traces of water in solution can be present (that can be reasonably modelled by one explicit water molecule in the simulation), we expect, on the basis of the above results, that the formation of the gold-hydroxo species should be unfavored.

In general, we note that the mechanism we propose here (i.e., starting from the gold-alkyne reactant complex and forming a gold-oxetene intermediate) is energetically really similar to that reported with an active gold-hydroxo species. Both the mechanisms depict an overall exoergonic reaction by 30 kcal/mol ca., with an activation energy barrier for the rate-determining step of the reaction amounting to 32 kcal/mol ca in our mechanism.

Based on the above results and discussion, the presence of a catalytically active gold-hydroxo species is very unlikely in our specific case.

4.4.2 Propargylamide - Chapter 2.1.3

For the DFT study, the ADF2014.05[230–232] and the related Quantum-regions Interconnected by Local Descriptions (QUILD)[214] programs were used to identify the structures of reactant complexes, reaction intermediates, transition states and product complexes involved in the mechanism of the NHC*-Au-X (NHC* = 1,3-dimethylimidazol-2-ylidene; X^- = BF_4^-, OTf^-, OTs^-) - catalyzed cycloisomerization of N-(prop-2-ynyl)benzamide to 2-Phenyl-5-vinylidene-2-oxazoline reaction. Geometry optimization calculations were carried out using the GGA functional BP86[215,216] with Grimme 3 BJDAMP dispersion correction (BP86-D3).[219] All atoms were treated with a Slater-type TZ2P triple-ζ with two polarization functions quality basis set, using the frozen core approximation (core small). Relativistic effects were accounted for with the scalar zero-order regular approximation, ZORA model.[203,233,234] Frequency calculations have been also performed to identify all stationary points as minima (zero imaginary frequencies) or transition states (one imaginary frequency). Final energies have been computed using ORCA program package[220] by single point B2PLYP perturbatively corrected doubly hybrid functional[221] calculations performed on the optimized BP86-D3 gas phase structures in conjunction with a def2-TZVP basis set for all atoms and an ECP pseudopotential for gold to include relativistic effects. This computational set up has been proven to be very accurate in describing catalysis by gold-containing species in benchmark calculations.[164,235,236] Computational mechanistic analysis is presented in electron energies, since the entropic contribution to the reaction profile has been shown to be small (as reported in the Supporting Information of our previous works[48,126,127,158]). All calculations were carried out for the closed-shell singlet state.

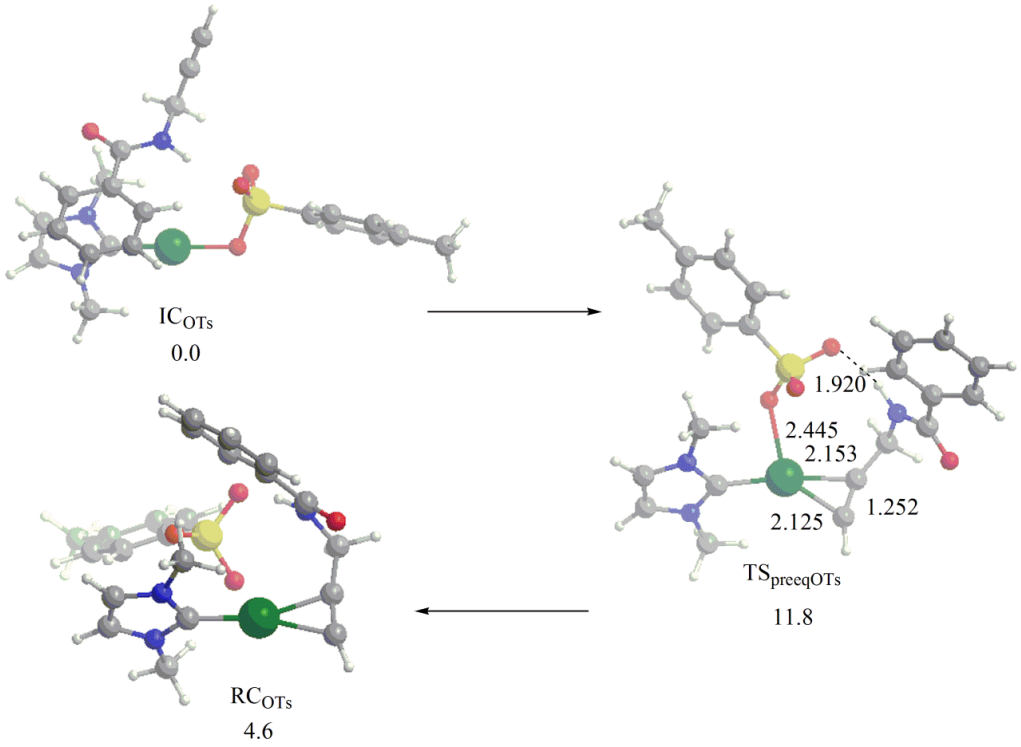

***Figure 3.34**: The pre-equilibrium step of the cycloisomerization of N- propargylcarboxamides reaction mechanism catalyzed by NHC*-Au-OTs. Bond lengths are in Å.*

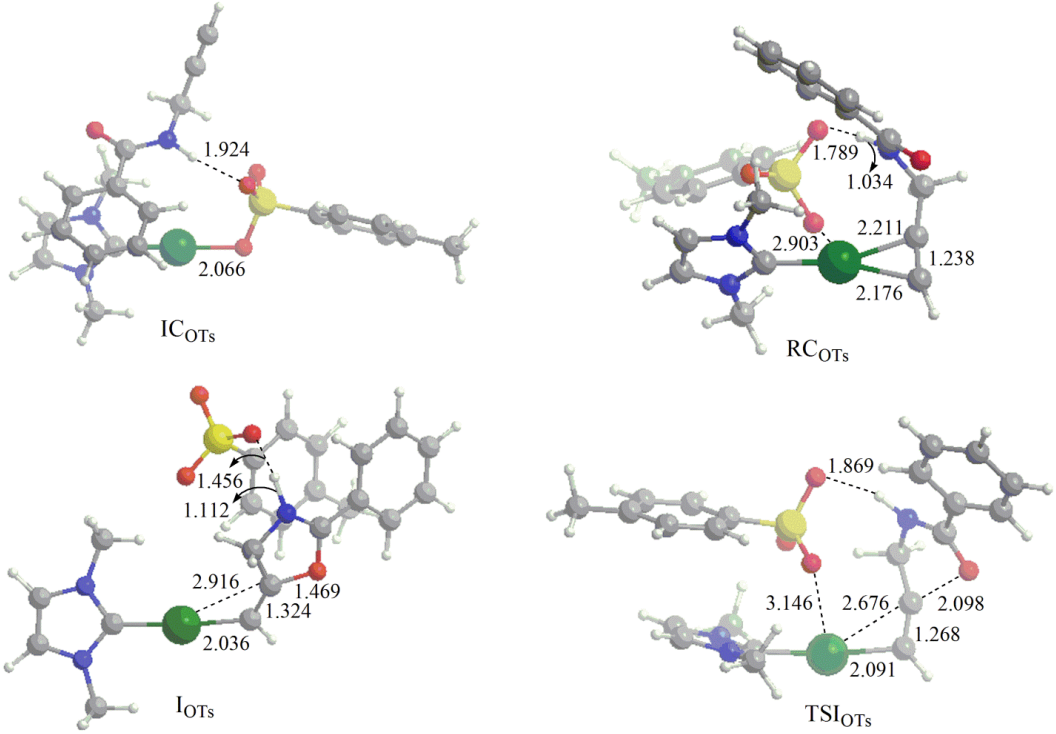

***Figure 3.35:** Initial complex IC$_{OTs}$, reactant complex RC$_{OTs}$, transition state TSI$_{OTs}$ and intermediate I$_{OTs}$ for the nucleophilic attack step of the cycloisomerization of N- propargylcarboxamides reaction mechanism catalyzed by NHC*-Au-OTs. Bond lengths are in Å.*

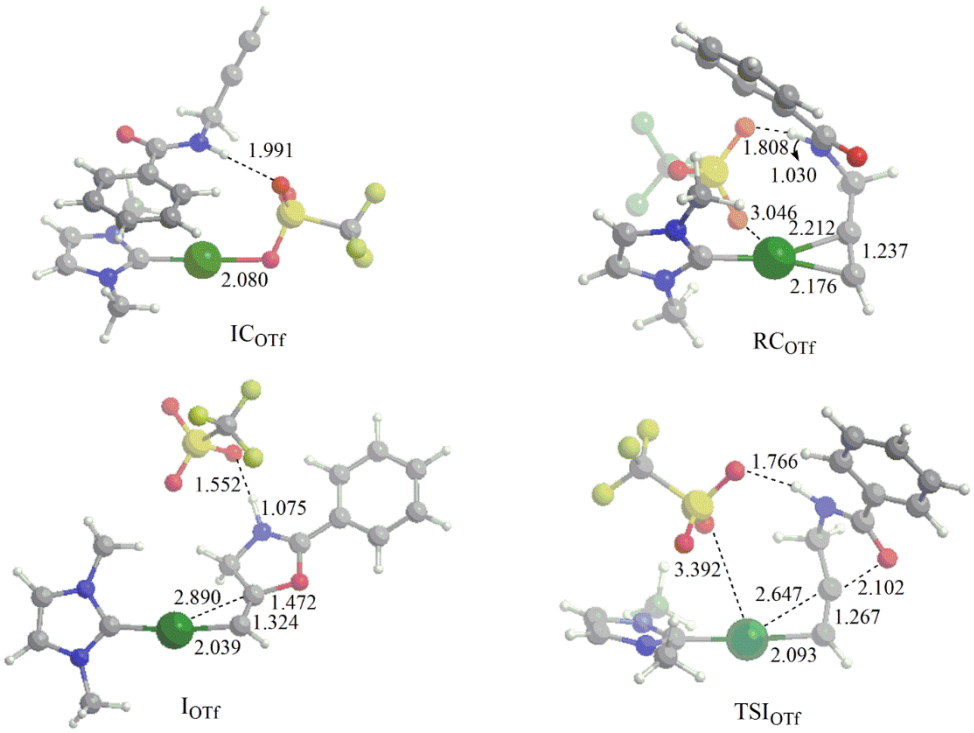

Figure 3.36: *Initial complex IC_{OTf}, reactant complex RC_{OTf}, transition state TSI_{OTf} and intermediate I_{OTf} for the nucleophilic attack step of the cycloisomerization of N- propargylcarboxamides reaction mechanism catalyzed by NHC*-Au-OTs. Bond lengths are in Å.*

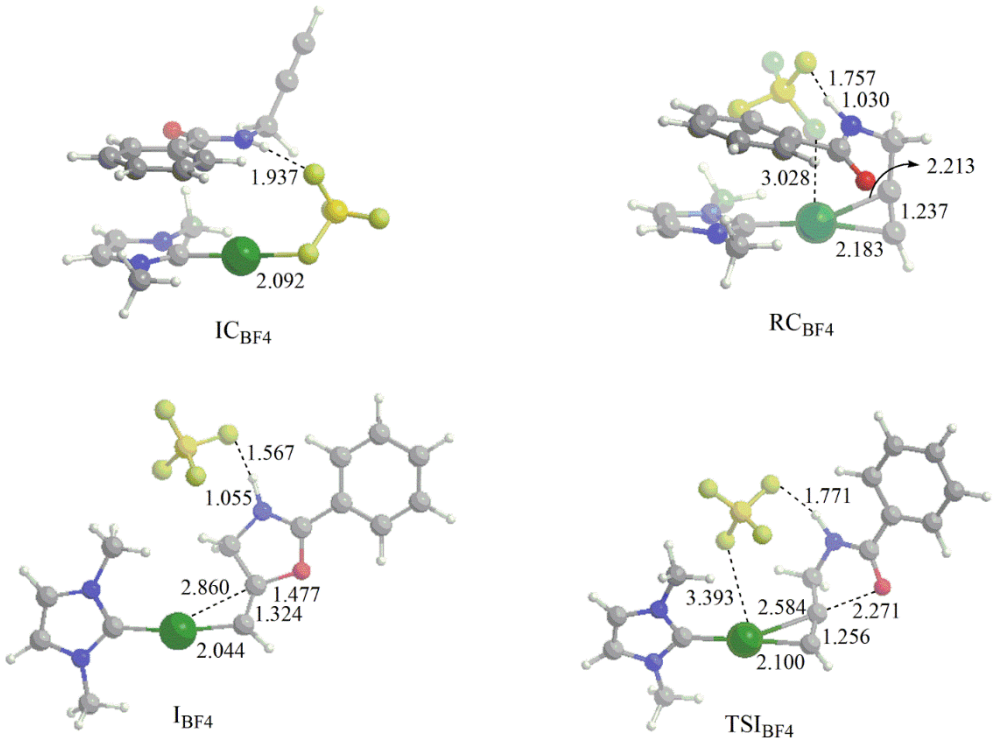

Figure 3.37: *Initial complex IC_{BF4}, reactant complex RC_{BF4}, transition state TSI_{BF4} and intermediate I_{BF4} for the nucleophilic attack step of the cycloisomerization of N- propargylcarboxamides reaction mechanism catalyzed by NHC*-Au-BF_4. Bond lengths are in Å.*

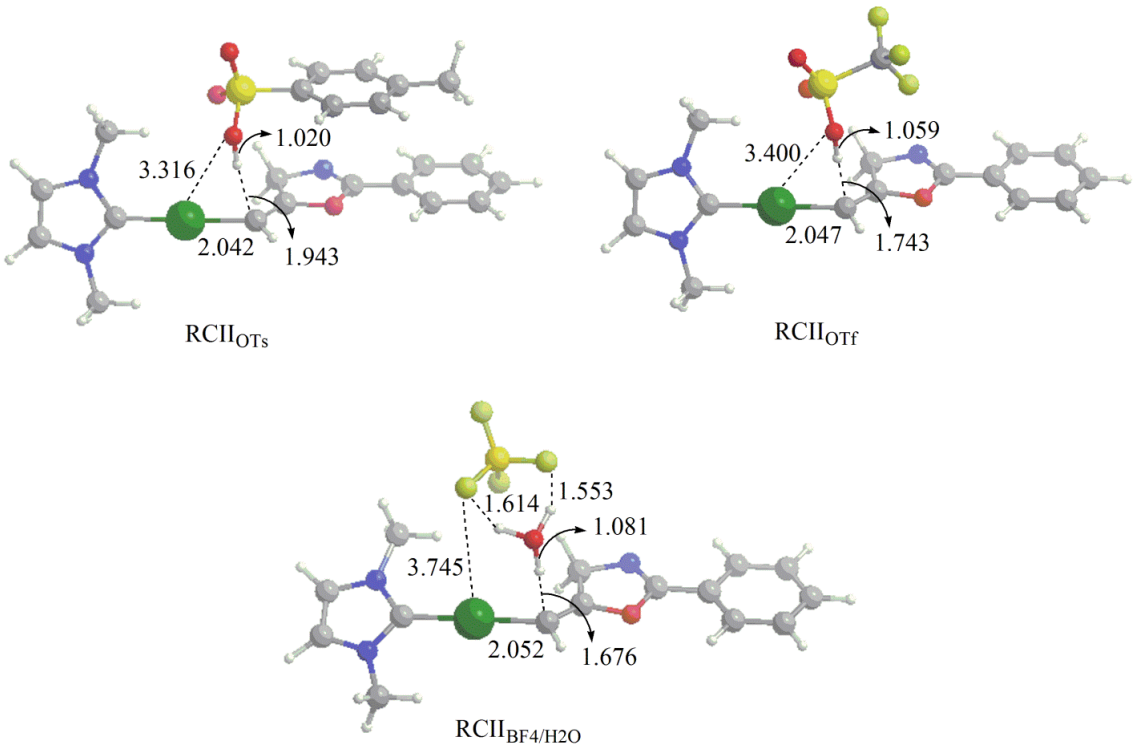

***Figure 3.38**: Reactant complex RCII$_X$ (X = OTs$^-$, OTf$^-$, and BF$_4^-$/H$_2$O) of the protodeauration step of the cycloisomerization of N- propargylcarboxamides reaction mechanism catalyzed by NHC*-Au-X. Bond lengths are in Å.*

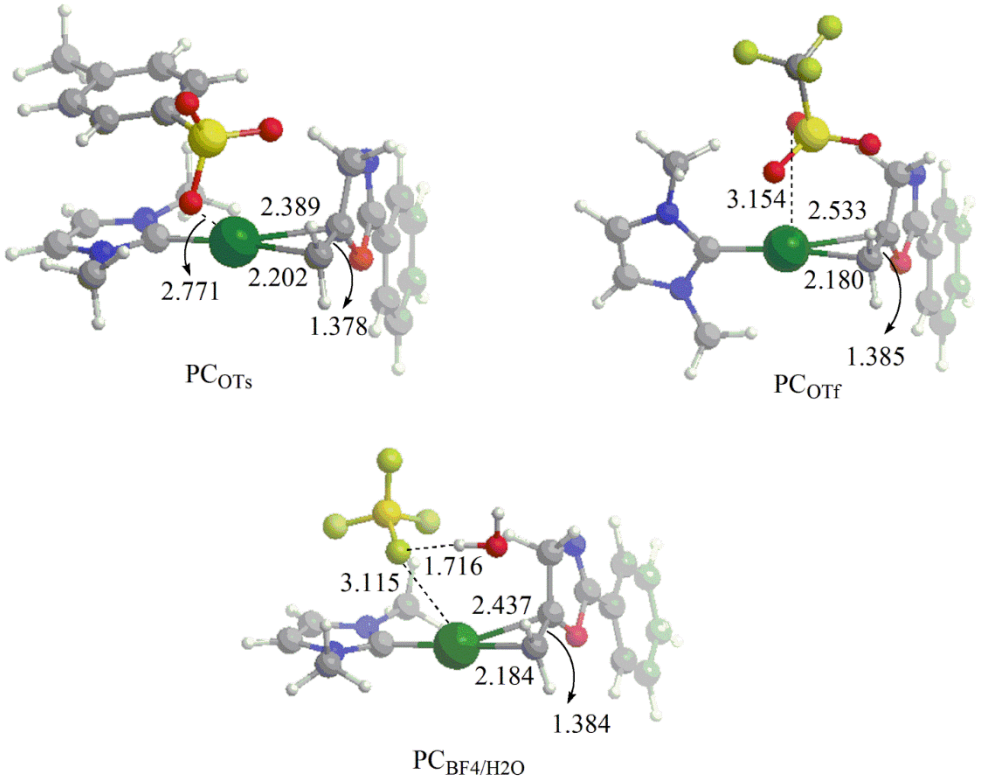

***Figure 3.39**: Product complex PC$_X$ (X = OTs$^-$, OTf$^-$, and BF$_4^-$/H$_2$O) of the protodeauration step of the cycloisomerization of N- propargylcarboxamides reaction mechanism catalyzed by NHC*-Au-X. Bond lengths are in Å.*

4.4.3 Gold(III) catalysis - Chapter 2.2.1

For the DFT study, the ADF2014.05[230–232] and the related Quantum-regions Interconnected by Local Descriptions (QUILD)[214] programs were used to identify the structures of reactant complexes, reaction intermediates, transition states and product complexes involved in the mechanism of the [(ppy)-Au-NHC*-$(OTf)_2$] - catalyzed addition of water to 2-butyne reaction. Geometry optimization calculations were carried out using the GGA functional BP86[215,216] (BP86). All atoms were treated with a Slater-type TZ2P triple-ς with two polarization functions quality basis set, using the frozen core approximation (core small). Relativistic effects were accounted for with the scalar zero-order regular approximation, ZORA model.[203,233,234] Frequency calculations have been also performed to identify all stationary points as minima (zero imaginary frequencies) or transition states (one imaginary frequency). Final energies have been computed using ORCA program package[220] by single point B2PLYP perturbatively corrected doubly hybrid functional[221] calculations performed on the optimized BP86 gas phase structures in conjunction with a def2-TZVP basis set for all atoms and an ECP pseudopotential for gold to include relativistic effects. This computational set up (referred as BP86/B2PLYP) has been proven to be very accurate in describing catalysis by gold-containing species in benchmark calculations.[164,235,236] Computational mechanistic analysis is presented in enthalpy energies, since both the entropic contribution to the reaction profile has been shown to be small (as reported in the Supporting Information of our previous works[48,126,127,158]) and in order to compare the present results with those previously obtained for gold(I) and gold(III) species.[193] All calculations were carried out for the closed-shell singlet state. Explicit dispersion effect has been evaluated by BP86 including Grimme's D3 dispersion correction[219] (BP86+D) single point calculations on optimized BP86 gas phase structures. Solvation has been taken into account by the Conductor like Screening Model COSMO[228,237,238] using nitromethane as solvent ($\varepsilon_{nitromethane} \sim \varepsilon_{valerolactone}$) by single point calculations (BP86+D/COSMO) on optimized BP86 gas phase structures for an estimate of the solvent effect on the activation energy barriers.

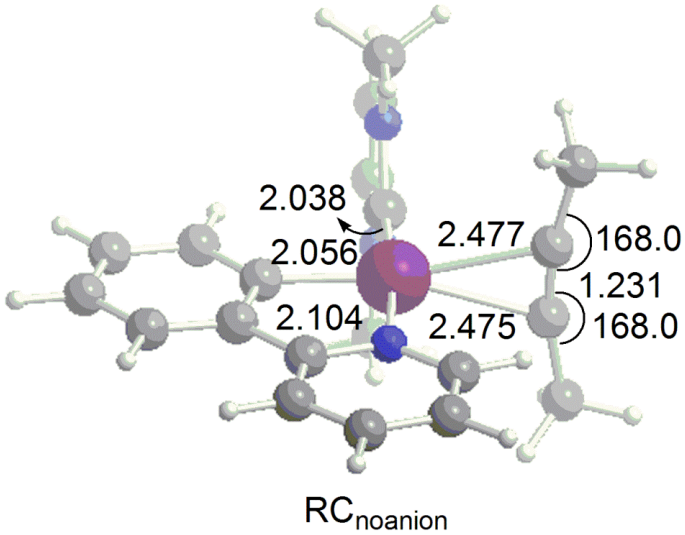

Figure 3.40: Optimized geometry of the reactant complex RC in the absence of both OTs^- anions. Distances are in Å.

4.4.4 Preequilibrium study - Chapter 2.2.2

Computational Details

DFT calculations have been performed using the Amsterdam Density Functional (ADF) (2016 version)[230–232] and the related Quantum-regions Interconnected by Local Descriptions (QUILD)[214] program packages. For geometry optimization the GGA BP86 functional[215,216] (DFT/BP86) and a Slater-type TZ2P triple zeta basis set with two polarization functions for all atoms, in the small frozen core approximation, were used. Relativistic effects were included by the scalar zero-order regular approximation ZORA Hamiltonian[203,233,234] The Grimme 3 BJDAMP dispersion correction[219] was included in BP86 single point calculation (BP86-D3) in analyses aimed at explicitly evaluating the dispersion forces contribution to the energy.

Unless otherwise specified, all final energies have been computed by single point B2PLYP perturbatively corrected doubly hybrid functional[221] calculations performed on the optimized BP86 gas phase structures in conjunction with a def2-TZVP basis set for all atoms and an ECP pseudopotential for gold to include relativistic effects. This computational set up (referred as to B2PLYP//BP86) has been shown to be very accurate in describing catalysis by gold-containing species in benchmark calculations,[164,235,236] with the B2PLYP functional, which includes also the dispersion terms of energy, using ORCA program.[220]

Frequency calculations have been also performed to identify all stationary points as minima (zero imaginary frequencies) or transition states (one imaginary frequency). Bonding energies and computational mechanistic analysis are presented in electronic energy values, ΔE, since both the entropic contribution has been shown to be small (as reported in the Supporting Information of our previous works[174,193]) and to compare the present results with those previously obtained for gold(I) and gold(III) species.[193] All calculations were carried out for the closed-shell singlet state. Solvation has been included by the Conductor like Screening Model COSMO,[228,237,238] using dichloromethane as the solvent, by single point BP86-D3 calculations on optimized BP86 gas phase structures.

Table 3.15: *X (X = Cl^-, BF_4^-, OTf^-, H_2O, 3-hexyne, 2-butyne) bonding electronic energies ΔE, bonding enthalpies ΔH and bonding Gibbs free energies ΔG (kcal/mol) to* ***2*** *(Au(III) model) complexes calculated at the BP86 including both the Grimme dispersion correction and solvent (ΔE(BP86-D3 solv)) level. Corresponding energy differences between coordination ability of OTf^- and BF_4^- (Δ OTf^-/BF_4^-), H_2O and 3-hexyne (Δ H_2O/3-hexyne) and H_2O and 2-butyne (Δ H_2O/2-butyne) are also reported.*

	(BP86-D3) solv Au(III) model		
	ΔE	ΔH	ΔG
$[Au(III)Cl]^+$	-60.2	-58.1	-59.2
$[Au(III)BF_4]^+$	-32.6	-30.9	-19.2
$[Au(III)OTf]^+$	-46.0	-44.2	-30.1
Δ OTf^-/BF_4^-	**-13.4**	**-13.3**	**-10.9**
$[Au(III)H_2O]^{2+}$	-20.9	-19.3	-8.5
$[Au(III)$3-hexyne$]^{2+}$	-32.8	-31.0	-17.6
Δ H_2O/3-hexyne	**-11.9**	**-11.7**	**-9.1**
$[Au(III)$2-butyne$]^{2+}$	-31.3	-29.6	-18.5
Δ H_2O/2-butyne	**-10.4**	**-10.3**	**-10.0**

In **Table 3.15** bonding electronic energies ΔE, bonding enthalpies ΔH and bonding Gibbs free energies ΔG (kcal/mol) of all the considered ligands X (X = Cl^-, BF_4^-, OTf^-, H_2O, 3-hexyne, 2-butyne) to the **2** (Au(III) model) complex calculated at the BP86 level including both Grimme dispersion correction and solvent (BP86-D3 X (X = Cl^-, BF_4^-, OTf^-, H_2O, 3-hexyne, 2-butyne) solv) are compared. Results show that electronic bonding energies are a good approximation to the bonding enthalpy values and a reasonable approximation for the bonding free energies. Notably, energy differences between coordination ability of OTf^- and BF_4^- (Δ OTf^-/BF_4^-), H_2O and 3-hexyne (Δ H_2O/3-hexyne) and H_2O and 2-butyne (Δ H_2O/2-butyne) are very close in terms of ΔE, ΔH and ΔG.

5. References

(1) Vronsky, I. M. History of Gold.

(2) Bishop, P. “Modern Supramolecular Gold Chemistry”, Edited Antonio Laguna. *Gold Bull.* **2009**, *42* (1), 74.

(3) Niece, S. L. *Gold*; Harvard University Press, 2009.

(4) Gopher, A.; Tsuk, T.; Shalev, S.; Gophna, R. Earliest Gold Artifacts in the Levant. *Curr. Anthropol.* **1990**, *31* (4), 436–443.

(5) Klemm, R.; Klemm, D. *Gold and Gold Mining in Ancient Egypt and Nubia*; Springer-Verlag, Ed.; Berlin Heidelberg, 2013.

(6) Providentmetals.com. How Precious Metals Were Used in Ancient Egypt https://blog.providentmetals.com/how-precious-metals-were-used-in-ancient-egypt.htm#.X1OTO3kzZEY.

(7) Cartwright, M. Minoan Jewellery https://www.ancient.eu/article/449/minoan-jewellery/.

(8) Aldenderfer, M.; Craig, N. M.; Speakman, R. J.; Popelka-Filcoff, R. Four-Thousand-Year-Old Gold Artifacts from the Lake Titicaca Basin, Southern Peru. *Proc. Natl. Acad. Sci. U. S. A.* **2008**, *105* (13), 5002–5005.

(9) https://it.wikipedia.org/wiki/Maschera_funeraria_di_Tutankhamon#/media/File:TUT-Ausstellung_FFM_2012_47_(7117819557).jpg.

(10) Yamamura, K. Minoan “Master of the Animals” Pendant https://www.ancient.eu/image/887/minoan-master-of-the-animals-pendant/.

(11) Pricker, S. P. Medical Uses of Gold Compounds: Past, Present and Future. *Gold Bull.* **1996**, *29* (2), 53–60.

(12) IUPAC. Compendium of Chemical Terminology, 2nd Ed. (the “Gold Book”). Compiled by A. D. McNaught and A. Wilkinson. Blackwell Scientific Publications, Oxford (1997).

(13) Schmidbaur, H.; Cronje, S.; Djordjevic, B.; Schuster, O. Understanding Gold Chemistry through Relativity. *Chem. Phys.* **2005**, *311* (1–2), 151–161.

(14) Hashmi, A. S. K.; Toste, F. D. *Modern Gold Catalyzed Synthesis*; WILEY-VCH Verlag GmbH & Co. KGaA: Weinheim, Germany, 2012.

(15) Pearson, R. G. Hard and Soft Acids and Bases. *J. Am. Chem. Soc.* **1963**, *85* (22), 3533–3539.

(16) Crabtree, R. D. *The Organometallic Chemistry of the Transition Metals, 6th Edition*; Whiley: Weinheim, Germany, 2014.

(17) MedlinePlus. Auranofin https://medlineplus.gov/druginfo/meds/a685038.html.

(18) Lewis, M. G.; DaFonseca, S.; Chomont, N.; Palamara, A. T.; Tardugno, M.; Mai, A.; Collins, M.; Wagner, W. L.; Yalley-Ogunro, J.; Greenhouse, J.; et al. Gold Drug Auranofin Restricts the Viral Reservoir in the Monkey AIDS Model and Induces Containment of Viral Load Following ART Suspension. *AIDS* **2011**, *25* (11).

(19) Rothan, H. A.; Stone, S.; Natekar, J.; Kumari, P.; Arora, K.; Kumar, M. The FDA-Approved Gold Drug Auranofin Inhibits Novel Coronavirus (SARS-COV-2) Replication and Attenuates Inflammation in Human Cells. *Virology* **2020**, *547*, 7–11.

(20) Forward, J. M.; Bohmann, D.; Fackler, J. P.; Staples, R. J. Luminescence Studies of Gold(I) Thiolate Complexes. *Inorg. Chem.* **1995**, *34* (25), 6330–6336.

(21) Yam, V. W.-W.; Wong, K. M.-C. Luminescent Metal Complexes of D6, D8 and D10 Transition Metal Centres. *Chem. Commun.* **2011**, *47* (42), 11579–11592.

(22) Luengo, A.; Marzo, I.; Reback, M.; Daubit, I. M.; Fernández-Moreira, V.; Metzler-Nolte, N.; Gimeno, M. C. Luminescent Bimetallic IrIII/AuI Peptide Bioconjugates as Potential Theranostic Agents. *Chem. – A Eur. J.* **2020**.

(23) Bindoli, A.; Rigobello, M. P.; Scutari, G.; Gabbiani, C.; Casini, A.; Messori, L. Thioredoxin Reductase: A Target for Gold Compounds Acting as Potential Anticancer Drugs. *Coord. Chem. Rev.* **2009**, *253* (11), 1692–1707.

(24) Yam, V. W.-W.; Wong, K. M.-C.; Hung, L.-L.; Zhu, N. Luminescent Gold(III) Alkynyl Complexes: Synthesis, Structural Characterization, and Luminescence Properties. *Angew. Chemie Int. Ed.* **2005**, *44* (20), 3107–3110.

(25) Eichelbaum, M.; Rademann, K. Plasmonic Enhancement or Energy Transfer? On the Luminescence of Gold-, Silver-, and Lanthanide-Doped Silicate Glasses and Its Potential for Light-Emitting Devices. *Adv. Funct. Mater.* **2009**, *19* (13), 2045–2052.

(26) To, W.-P.; Tong, G. S.-M.; Lu, W.; Ma, C.; Liu, J.; Chow, A. L.-F.; Che, C.-M. Luminescent Organogold(III) Complexes with Long-Lived Triplet Excited States for Light-Induced Oxidative C□H Bond Functionalization and Hydrogen Production. *Angew. Chemie Int. Ed.* **2012**, *51* (11), 2654–2657.

(27) Daniel, M. C.; Astruc, D. Gold Nanoparticles: Assembly, Supramolecular Chemistry, Quantum-Size-Related Properties, and Applications Toward Biology, Catalysis, and Nanotechnology. *Chem. Rev.* **2004**, *104* (1), 293–346.

(28) Bond, G. C.; Sermon, P. A. Gold Catalysts for Olefin Hydrogenation. *Gold Bull.* **1973**, *6* (4), 102–105.

(29) Bond, G. C.; Sermon, P. A.; Webb, G.; Buchanan, D. A.; Wells, P. B. Hydrogenation over Supported Gold Catalysts. *J. Chem. Soc. Chem. Commun.* **1973**, No. 13, 444b – 445.

(30) Hutchings, G. J. Nanocrystalline Gold and Gold Palladium Alloy Catalysts for Chemical Synthesis. *Chem. Commun.* **2008**, No. 10, 1148–1164.

(31) Das, M.; Shim, K. H.; An, S. S. A.; Yi, D. K. Review on Gold Nanoparticles and Their Applications. *Toxicol. Environ. Health Sci.* **2011**, *3* (4), 193–205.

(32) Frens, G. Controlled Nucleation for the Regulation of the Particle Size in Monodisperse Gold Suspensions. *Nat. Phys. Sci.* **1973**, *241* (105), 20–22.

(33) Carabineiro, S. A. C. Supported Gold Nanoparticles as Catalysts for the Oxidation of Alcohols and Alkanes . *Frontiers in Chemistry* . 2019, p 702.

(34) Grisel, R.; Weststrate, K.-J.; Gluhoi, A.; Nieuwenhuys, B. E. Catalysis by Gold Nanoparticles. *Gold Bull.* **2002**, *35* (2), 39–45.

(35) Hashmi, A. S. K. Gold-Catalyzed Organic Reactions. *Chem. Rev* **2007**, *107*, 3180–3211.

(36) Teles, J. H.; Brode, S.; Chabanas, M. Cationic Gold(I) Complexes: Highly Efficient Catalysts for the Addition of Alcohols to Alkynes. *Angew. Chemie Int. Ed.* **1998**, *37* (10), 1415–1418.

(37) Wang, W.; Hammond, G. B.; Xu, B. Ligand Effects and Ligand Design in Homogeneous Gold (I) Catalysis. *J. Am. Chem. Soc.* **2012**, *134* (I), 5697−5705.

(38) Schneider, S. K.; Herrmann, W. A.; Herdtweck, E. Synthesis of the First Gold(I) Carbene Complex with a Gold-Oxygen Bond — First Catalytic Application of Gold(I) Complexes Bearing N-Heterocyclic Carbenes. *Zeitschrift für Anorg. und Allg. Chemie* **2003**, *629* (12-13), 2363–2370.

(39) Marion, N.; Ramon, R. S.; Nolan, S. P. [(NHC)AuI]-Catalyzed Acid-Free Alkyne Hydration at Part-per-Million Catalyst Loadings. *J. Am. Chem. Soc.* **2009**, *131* (2), 448–449.

(40) Nevado, C.; Echavarren, A. M. Intramolecular Hydroarylation of Alkynes Catalyzed by Platinum or Gold: Mechanism and Endo Selectivity. *Chem. – A Eur. J.* **2005**, *11* (10), 3155–3164.

(41) Li, H.; Widenhoefer, R. A. Gold(I)-Catalyzed Intramolecular Dihydroamination of Allenes with N,N'-Disubstituted Ureas To Form Bicyclic Imidazolidin-2-Ones. *Org. Lett.* **2009**, *11* (12), 2671–2674.

(42) Wang, D.; Cai, R.; Sharma, S.; Jirak, J.; Thummanapelli, S. K.; Akhmedov, N. G.; Zhang, H.; Liu, X.; Petersen, J. L.; Shi, X. "Silver Effect" in Gold(I) Catalysis: An Overlooked Important Factor. *J. Am. Chem. Soc.* **2012**, *134* (21), 9012–9019.

(43) Shen, H. C. Recent Advances in Syntheses of Heterocycles and Carbocycles via Homogeneous Gold Catalysis. Part 1: Heteroatom Addition and Hydroarylation Reactions of Alkynes, Allenes, and Alkenes. *Tetrahedron* **2008**, *64* (18), 3885–3903.

(44) Mizushima, E.; Hayashi, T.; Tanaka, M. Au(I)-Catalyzed Highly Efficient Intermolecular Hydroamination of Alkynes. *Org. Lett.* **2003**, *5* (18), 3349–3352.

(45) Brouwer, C.; He, C. Efficient Gold-Catalyzed Hydroamination of 1,3-Dienes. *Angew. Chemie Int. Ed.* **2006**, *45* (11), 1744–1747.

(46) Zhdanko, A.; Ströbele, M.; Maier, M. E. Coordination Chemistry of Gold Catalysts in Solution: A Detailed NMR Study. *Chem. – A Eur. J.* **2012**, *18* (46), 14732–14744.

(47) Zhdanko, A.; Maier, M. E. Explanation of Counterion E Ff Ects in Gold(I)-Catalyzed Hydroalkoxylation of Alkynes. *ACS Catal.* **2014**, *4* (I), 2770–2775.

(48) Biasiolo, L.; Trinchillo, M.; Belanzoni, P.; Belpassi, L.; Busico, V.; Ciancaleoni, G.; D'Amora, A.; Macchioni, A.; Tarantelli, F.; Zuccaccia, D. Unexpected Anion Effect in the Alkoxylation of Alkynes Catalyzed by N-Heterocyclic Carbene (NHC) Cationic Gold Complexes. *Chem. Eur. J.* **2014**, *20* (45), 14594–14598.

(49) Biasiolo, L.; Del Zotto, A.; Zuccaccia, D. Toward Optimizing the Performance of Homogeneous L-Au-X Catalysts through Appropriate Matching of the Ligand (L) and Counterion (X^-). *Organometallics* **2015**, *34* (9), 1759–1765.

(50) D'Amore, L.; Ciancaleoni, G.; Belpassi, L.; Tarantelli, F.; Zuccaccia, D.; Belanzoni, P. Unraveling the Anion/Ligand Interplay in the Reaction Mechanism of Gold(I)-Catalyzed Alkoxylation of Alkynes. *Organometallics* **2017**, *36* (12), 2364–2376.

(51) Jia, M.; Bandini, M. Counterion Effects in Homogeneous Gold Catalysis. *ACS Catal.* **2015**, *5* (3), 1638–1652.

(52) Schießl, J.; Schulmeister, J.; Doppiu, A.; Wörner, E.; Rudolph, M.; Karch, R.; Hashmi, A. S. K. An Industrial Perspective on Counter Anions in Gold Catalysis: Underestimated with Respect to "Ligand Effects." *Adv. Synth. Catal.* **2018**, *360* (13), 2493–2502.

(53) Obradors, C.; Echavarren, A. M. Intriguing Mechanistic Labyrinths in Gold(i) Catalysis. *Chem. Commun.* **2014**, *50* (1), 16–28.

(54) Wang, Y.-M.; Lackner, A. D.; Toste, F. D. Development of Catalysts and Ligands for Enantioselective Gold Catalysis. *Acc. Chem. Res.* **2014**, *47* (3), 889–901.

(55) Dorel, R.; Echavarren, A. M. Gold(I)-Catalyzed Activation of Alkynes for the Construction of Molecular Complexity. *Chem. Rev.* **2015**, *115* (17), 9028–9072.

(56) Hashmi, A. S. K. Dual Gold Catalysis. *Acc. Chem. Res.* **2014**, *47* (3), 864–876.

(57) Yeom, H.-S.; Shin, S. Catalytic Access to $α$-Oxo Gold Carbenes by N–O Bond Oxidants. *Acc. Chem. Res.* **2014**, *47* (3), 966–977.

(58) Zhang, L. A Non-Diazo Approach to $α$-Oxo Gold Carbenes via Gold-Catalyzed Alkyne Oxidation. *Acc. Chem. Res.* **2014**, *47* (3), 877–888.

(59) Qian, D.; Zhang, J. Gold-Catalyzed Cyclopropanation Reactions Using a Carbenoid Precursor Toolbox. *Chem. Soc. Rev.* **2015**, *44* (3), 677–698.

(60) Pflästerer, D.; Hashmi, A. S. K. Gold Catalysis in Total Synthesis – Recent Achievements. *Chem. Soc. Rev.* **2016**, *45* (5), 1331–1367.

(61) Alyabyev, S. B.; Beletskaya, I. P. Gold as a Catalyst. Part I. Nucleophilic Addition to the Triple Bond. *Russ. Chem. Rev.* **2017**, *86* (8), 689–749.

(62) Alyabyev, S. B.; Beletskaya, I. P. Gold as a Catalyst. Part II. Alkynes in the Reactions of Carbon–Carbon Bond Formation. *Russ. Chem. Rev.* **2018**, *87* (10), 984–1047.

(63) Nijamudheen, A.; Datta, A. Gold-Catalyzed Cross-Coupling Reactions: An Overview of Design Strategies, Mechanistic Studies, and Applications. *Chem. Eur. J.* **2020**, *26* (7), 1442–1487.

(64) Barber, D. M.; Sanganee, H.; Dixon, D. J. One-Pot Nitro-Mannich/Hydroamination Cascades for the Direct Synthesis of 2,5-Disubstituted Pyrroles Using Base and Gold Catalysis. *Chem. Commun.* **2011**, *47* (15), 4379–4381.

(65) Borsini, E.; Broggini, G.; Fasana, A.; Baldassarri, C.; Manzo, A. M.; Perboni, A. D. Access to Pyrrolo-Pyridines by Gold-Catalyzed Hydroarylation of Pyrroles Tethered to Terminal Alkynes. *Beilstein J. Org. Chem.* **2011**, *7*, 1468–1474.

(66) Hossein Bagi, A.; Khaledi, Y.; Ghari, H.; Arndt, S.; Hashmi, A. S. K.; Yates, B. F.; Ariafard, A. A Mechanistic Investigation of the Gold(III)-Catalyzed Hydrofurylation of C–C Multiple Bonds. *J. Am. Chem. Soc.* **2016**, *138* (44), 14599–14608.

(67) Shaikh, A. C.; Ranade, D. S.; Rajamohanan, P. R.; Kulkarni, P. P.; Patil, N. T. Oxidative Intramolecular 1,2-Amino-Oxygenation of Alkynes under AuI/AuIII Catalysis: Discovery of a Pyridinium-Oxazole Dyad as an Ionic Fluorophore. *Angew. Chemie Int. Ed.* **2017**, *56* (3), 757–761.

(68) Yang, Y.; Shen, Y.; Wang, X.; Zhang, Y.; Wang, D.; Shi, X. Triazole Acetyl Gold(III) Catalyzed Meyer–Schuster Rearrangement of Propargyl Alcohols. *Tetrahedron Lett.* **2016**, *57* (21), 2280–2282.

(69) Hashmi, A. S. K.; Ding, L.; Bats, J. W.; Fischer, P.; Frey, W. Gold Catalysis: Efficient Synthesis

and Structural Assignment of Jungianol and Epi-Jungianol. *Chem. – A Eur. J.* **2003**, *9* (18), 4339–4345.

(70) Abdelkhalik, A. M.; Paul, N. K.; Jha, A. Concise Synthesis of 12a-Methyl-11-Aryl-1,2-Dihydrobenzo[f]Pyrrolo[1,2-a]Quinolin-3(12aH)-Ones as Racemic 14-Azaestrogen Analogs. *Steroids* **2015**, *98*, 107–113.

(71) Pažický, M.; Loos, A.; Ferreira, M. J.; Serra, D.; Vinokurov, N.; Rominger, F.; Jäkel, C.; Hashmi, A. S. K.; Limbach, M. Synthesis, Reactivity, and Electrochemical Studies of Gold(I) and Gold(III) Complexes Supported by N-Heterocyclic Carbenes and Their Application in Catalysis. *Organometallics* **2010**, *29* (20), 4448–4458.

(72) Wang, D.; Yang, Y.; Huang, R.; Wang, L.; Wan, H. Synthesis of Allenes through Triazole Gold(III) Catalysed Rearrangement of Propargyl Vinyl Ethers. *J. Chem. Res.* **2016**, *40* (11), 645–647.

(73) Wong, K.-F.; Deng, J.-R.; Wei, X.-Q.; Shao, S.-P.; Xiang, D.-P.; Wong, M.-K. Visual Detection of Formaldehyde by Highly Selective Fluorophore Labeling via Gold(Iii) Complex-Mediated Three-Component Coupling Reaction. *Org. Biomol. Chem.* **2015**, *13* (27), 7408–7411.

(74) Hui, T.-W.; Cui, J.-F.; Wong, M.-K. Modular Synthesis of Propargylamine Modified Cyclodextrins by a Gold(Iii)-Catalyzed Three-Component Coupling Reaction. *RSC Adv.* **2017**, *7* (24), 14477–14480.

(75) Lee, J. S.; Kapustin, E. A.; Pei, X.; Llopis, S.; Yaghi, O. M.; Toste, F. D. Architectural Stabilization of a Gold(III) Catalyst in Metal-Organic Frameworks. *Chem* **2020**, *6* (1), 142–152.

(76) Tian, X.; Song, L.; Farshadfar, K.; Rudolph, M.; Rominger, F.; Oeser, T.; Ariafard, A.; Hashmi, A. S. K. Acyl Migration versus Epoxidation in Gold Catalysis: Facile, Switchable, and Atom-Economic Synthesis of Acylindoles and Quinoline Derivatives. *Angew. Chemie Int. Ed.* **2020**, *59* (1), 471–478.

(77) Jiang, J.-J.; Cui, J.-F.; Yang, B.; Ning, Y.; Lai, N. C.-H.; Wong, M.-K. Chiral Cyclometalated Oxazoline Gold(III) Complex-Catalyzed Asymmetric Carboalkoxylation of Alkynes. *Org. Lett.* **2019**, *21* (16), 6289–6294.

(78) O'Neill, J. A. T.; Rosair, G. M.; Lee, A.-L. Gold(III)–Oxo Complexes as Catalysts in Intramolecular Hydroamination. *Catal. Sci. Technol.* **2012**, *2* (9), 1818–1821.

(79) Wang, G.; Liu, X.; Chen, Y.; Yang, J.; Li, J.; Lin, L.; Feng, X. Diastereoselective and Enantioselective Alleno-Aldol Reaction of Allenoates with Isatins to Synthesis of Carbinol

Allenoates Catalyzed by Gold. *ACS Catal.* **2016**, *6* (4), 2482–2486.

(80) Montanel-Pérez, S.; Herrera, R. P.; Laguna, A.; Villacampa, M. D.; Gimeno, M. C. The Fluxional Amine Gold(III) Complex as an Excellent Catalyst and Precursor of Biologically Active Acyclic Carbenes. *Dalt. Trans.* **2015**, *44* (19), 9052–9062.

(81) Wu, C.-Y.; Horibe, T.; Jacobsen, C. B.; Toste, F. D. Stable Gold(III) Catalysts by Oxidative Addition of a Carbon–Carbon Bond. *Nature* **2015**, *517* (7535), 449–454.

(82) Cui, J. F.; Ko, H. M.; Shing, K. P.; Deng, J. R.; Lai, N. C. H.; Wong, M. K. C,O-Chelated BINOL/Gold(III) Complexes: Synthesis and Catalysis with Tunable Product Profiles. *Angew. Chemie - Int. Ed.* **2017**, *56* (11), 3074–3079.

(83) Rekhroukh, F.; Blons, C.; Estévez, L.; Mallet-Ladeira, S.; Miqueu, K.; Amgoune, A.; Bourissou, D. Gold(III)–Arene Complexes by Insertion of Olefins into Gold–Aryl Bonds. *Chem. Sci.* **2017**, *8* (6), 4539–4545.

(84) Teci, M.; Hueber, D.; Pale, P.; Toupet, L.; Blanc, A.; Brenner, E.; Matt, D. Metal Confinement through N-(9-Alkyl)Fluorenyl-Substituted N-Heterocyclic Carbenes and Its Consequences in Gold-Catalysed Reactions Involving Enynes. *Chem. – A Eur. J.* **2017**, *23* (32), 7809–7818.

(85) Blons, C.; Mallet-ladeira, S.; Amgoune, A.; Bourissou, D. (P , C) Cyclometalated Gold (III) Complexes : Highly Active Catalysts for the Hydroarylation of Alkynes. *Angew. Chem. Int. Ed.* **2018**, *57*, 11732–11736.

(86) Lo, V. K.-Y.; Kung, K. K.-Y.; Wong, M.-K.; Che, C.-M. Gold(III) (C^N) Complex-Catalyzed Synthesis of Propargylamines via a Three-Component Coupling Reaction of Aldehydes, Amines and Alkynes. *J. Organomet. Chem.* **2009**, *694* (4), 583–591.

(87) Li, G.; Zhang, L. Gold-Catalyzed Intramolecular Redox Reaction of Sulfinyl Alkynes: Efficient Generation of α-Oxo Gold Carbenoids and Application in Insertion into R□CO Bonds. *Angew. Chemie Int. Ed.* **2007**, *46* (27), 5156–5159.

(88) Shaw, M.; Thakur, R.; Kumar, A. Gold(III)-Catalyzed Glycosylation Using Phenylpropiolate Glycosides: Phenylpropiolic Acid, An Easily Separable and Reusable Leaving Group. *J. Org. Chem.* **2019**, *84* (2), 589–605.

(89) Hikawa, H.; Matsumoto, M.; Tawara, S.; Kikkawa, S.; Azumaya, I. Gold(III)/Sodium Diphenylphosphinobenzene-3-Sulfonate (TPPMS) Catalyzed Dehydrative N-Benzylation of Electron-Deficient Anilines in Water. *Synthesis (Stuttg).* **2019**, *51* (13), 2729–2736.

(90) Xie, J.; Li, H.; Zhou, J.; Cheng, Y.; Zhu, C. A Highly Efficient Gold-Catalyzed Oxidative C□C Coupling from C□H Bonds Using Air as Oxidant. *Angew. Chemie Int. Ed.* **2012**, *51* (5), 1252–

1255.

(91) Chipman, A.; Gouranourimi, A.; Farshadfar, K.; Olding, A.; Yates, B. F.; Ariafard, A. A Computational Mechanistic Investigation into Reduction of Gold(III) Complexes by Amino Acid Glycine: A New Variant for Amine Oxidation. *Chem. – A Eur. J.* **2018**, *24* (33), 8361–8368.

(92) Aguilar, D.; Contel, M.; Urriolabeitia, E. P. Mechanistic Insights into the One-Pot Synthesis of Propargylamines from Terminal Alkynes and Amines in Chlorinated Solvents Catalyzed by Gold Compounds and Nanoparticles. *Chem. – A Eur. J.* **2010**, *16* (30), 9287–9296.

(93) Oliver-Meseguer, J.; Cabrero-Antonino, J. R.; Domínguez, I.; Leyva-Pérez, A.; Corma, A. Small Gold Clusters Formed in Solution Give Reaction Turnover Numbers of 107 at Room Temperature. *Science (80-.).* **2012**, *338* (6113), 1452–1455.

(94) Reiersølmoen, A. C.; Csókás, D.; Øien-Ødegaard, S.; Vanderkooy, A.; Gupta, A. K.; Carlsson, A.-C. C.; Orthaber, A.; Fiksdahl, A.; Pápai, I.; Erdélyi, M. Catalytic Activity of Trans-Bis(Pyridine)Gold Complexes. *J. Am. Chem. Soc.* **2020**, *142* (13), 6439–6446.

(95) Casado, R.; Contel, M.; Laguna, M.; Romero, P.; Sanz, S. Organometallic Gold(II) Compounds as Catalysts for the Addition of Water and Methanol to Terminal Alkynes. *J. Am. Chem. Soc.* **2003**, *125* (Iii), 11925–11935.

(96) Cordón, J.; Jiménez-Osés, G.; López-de-Luzuriaga, J. M.; Monge, M.; Olmos, M. E.; Pascual, D. Experimental and Theoretical Study of Gold(III)-Catalyzed Hydration of Alkynes. *Organometallics* **2014**, *33* (14), 3823–3830.

(97) Yang, Y.; Qin, A.; Zhao, K.; Wang, D.; Shi, X. Design and Synthesis of Alanine Triazole Ligands and Application in Promotion of Hydration, Allene Synthesis and Borrowing Hydrogen Reactions. *Adv. Synth. Catal.* **2016**, *358* (9), 1433–1439.

(98) Xing, Y.; Zhang, M.; Ciccarelli, S.; Lee, J.; Catano, B. AuIII-Catalyzed Formation of α-Halomethyl Ketones from Terminal Alkynes. *European J. Org. Chem.* **2017**, *2017* (4), 781–785.

(99) Chen, T.; Cai, C. Catalytic Hydration of Alkynes to Ketones by a Salen–Gold(III) Complex. *Catal. Commun.* **2015**, *65*, 102–104.

(100) Lein, M.; Rudolph, M.; Hashmi, S. K.; Schwerdtfeger, P. Homogeneous Gold Catalysis: Mechanism and Relativistic Effects of the Addition of Water to Propyne. *Organometallics* **2010**, *29* (10), 2206–2210.

(101) Trost, B. The Atom Economy--a Search for Synthetic Efficiency. *Science (80-.).* **1991**, *254*

(5037), 1471–1477.

(102) Sheldon, R. A.; Arends, I. W. C.; Hanefeld, U. *Green Chemistry and Catalysis*; Wiley Online Books; 2007.

(103) Anastas, P.; Warner, J. *Green Chemistry: Theory and Practice*; Inc, O. U. P., Ed.; 2000.

(104) Anastas, P. T.; Kirchhoff, M. M. Origins, Current Status, and Future Challenges of Green Chemistry. *Acc. Chem. Res.* **2002**, *35* (9), 686–694.

(105) Anastas, P.; Eghbali, N. Green Chemistry: Principles and Practice. *Chem. Soc. Rev.* **2010**, *39* (1), 301–312.

(106) Doble, M.; Kruthiventi, A. K. CHAPTER 5 - Alternate Solvents; Doble, M., Kruthiventi, A. K. B. T.-G. C. and E., Eds.; Academic Press: Burlington, 2007; pp 93–104.

(107) Hudlicky, T.; A. Frey, D.; Koroniak, L.; D. Claeboe, C.; E. Brammer Jr., L. Toward a 'Reagent-Free' Synthesis. *Green Chem.* **1999**, *1* (2), 57–59.

(108) Eckert, M.; Fleischmann, G.; Jira, R.; Bolt, H. M.; Golka, K. Acetaldehyde. *Ullmann's Encyclopedia of Industrial Chemistry*. December 15, 2006.

(109) Xi, Y.; Wang, D.; Ye, X.; Akhmedov, N. G.; Petersen, J. L.; Shi, X. Synergistic Au/Ga Catalysis in Ambient Nakamura Reaction. *Org. Lett.* **2014**, *16* (1), 306–309.

(110) Blanco Jaimes, M. C.; Böhling, C. R. N.; Serrano-Becerra, J. M.; Hashmi, A. S. K. Highly Active Mononuclear NAC–Gold(I) Catalysts. *Angew. Chemie Int. Ed.* **2013**, *52* (31), 7963–7966.

(111) Canseco-Gonzalez, D.; Petronilho, A.; Mueller-Bunz, H.; Ohmatsu, K.; Ooi, T.; Albrecht, M. Carbene Transfer from Triazolylidene Gold Complexes as a Potent Strategy for Inducing High Catalytic Activity. *J. Am. Chem. Soc.* **2013**, *135* (35), 13193–13203.

(112) Gómez-Suárez, A.; Oonishi, Y.; Meiries, S.; Nolan, S. P. [{Au(NHC)}2(μ-OH)][BF4]: Silver-Free and Acid-Free Catalysts for Water-Inclusive Gold-Mediated Organic Transformations. *Organometallics* **2013**, *32* (4), 1106–1111.

(113) Blanco Jaimes, M. C.; Rominger, F.; Pereira, M. M.; Carrilho, R. M. B.; Carabineiro, S. A. C.; Hashmi, A. S. K. Highly Active Phosphite Gold(i) Catalysts for Intramolecular Hydroalkoxylation, Enyne Cyclization and Furanyne Cyclization. *Chem. Commun.* **2014**, *50* (38), 4937–4940.

(114) Veenboer, R. M. P.; Dupuy, S.; Nolan, S. P. Stereoselective Gold(I)-Catalyzed Intermolecular Hydroalkoxlation of Alkynes. *ACS Catal.* **2015**, *5* (2), 1330–1334.

(115) Shu, X.-Z.; Nguyen, S. C.; He, Y.; Oba, F.; Zhang, Q.; Canlas, C.; Somorjai, G. A.; Alivisatos, A. P.; Toste, F. D. Silica-Supported Cationic Gold(I) Complexes as Heterogeneous Catalysts for

Regio- and Enantioselective Lactonization Reactions. *J. Am. Chem. Soc.* **2015**, *137* (22), 7083–7086.

(116) Vriamont, C.; Devillers, M.; Riant, O.; Hermans, S. A Covalently Anchored Homogeneous Gold Complex on Carbon Nanotubes: A Reusable Catalyst. *Chem. Commun.* **2013**, *49* (89), 10504–10506.

(117) Dupuy, S.; Gasperini, D.; Nolan, S. P. Highly Efficient Gold(I)-Catalyzed Regio- and Stereoselective Hydrocarboxylation of Internal Alkynes. *ACS Catal.* **2015**, *5* (11), 6918–6921.

(118) Ebule, R. E.; Malhotra, D.; Hammond, G. B.; Xu, B. Ligand Effects in the Gold Catalyzed Hydration of Alkynes. *Adv. Synth. Catal.* **2016**, *358*, 1478–1481.

(119) Hintermann, L. Expedient Syntheses of the N-Heterocyclic Carbene Precursor Imidazolium Salts IPr ·HCl , IMes ·HCl and IXy ·HCl. *Beilstein J. Org. Chem.* **2007**, *3* (22), 2–6.

(120) Alonso, F.; Beletskaya, I. P.; Yus, M. Transition-Metal-Catalyzed Addition of Heteroatom−Hydrogen Bonds to Alkynes. *Chem. Rev.* **2004**, *104* (6), 3079–3160.

(121) Schrore. No Title. *Chem. Ber.* **1875**, *8*, 367.

(122) Mizushima, E.; Sato, K.; Hayashi, T.; Tanaka, M. Highly Efficient AuI-Catalyzed Hydration of Alkynes. *Angew. Chem. Int. Ed. Engl.* **2002**, *41* (23), 4563–4565.

(123) 1, N. Only for the Hydration of 1-Octyne Hayashi and Tanaka Reported Low Catalyst Loadings (100 Ppm) and Low Amounts of Acid Promoter (4 Mol %). All Other Alkynes Catalyst Loadings Range from 0.2 to 1 Mol %and Acid from 25 to 50 Mol %.

(124) Xu, Y.; Hu, X.; Shao, J.; Yang, G.; Wu, Y.; Zhang, Z. Hydration of Alkynes at Room Temperature Catalyzed by Gold(i) Isocyanide Compounds. *Green Chem.* **2015**, *17* (1), 532–537.

(125) Wang, W.; Zheng, A.; Zhao, P.; Xia, C.; Li, F. Au-NHC@Porous Organic Polymers: Synthetic Control and Its Catalytic Application in Alkyne Hydration Reactions. *ACS Catal.* **2014**, *4* (1), 321–327.

(126) Gatto, M.; Belanzoni, P.; Belpassi, L.; Biasiolo, L.; Del Zotto, A.; Tarantelli, F.; Zuccaccia, D. Solvent-, Silver-, and Acid-Free NHC-Au-X Catalyzed Hydration of Alkynes. The Pivotal Role of the Counterion. *ACS Catal.* **2016**, *6* (11), 7363–7376.

(127) Gatto, M.; Baratta, W.; Belanzoni, P.; Belpassi, L.; Del Zotto, A.; Tarantelli, F.; Zuccaccia, D. Hydration and Alkoxylation of Alkynes Catalyzed by NHC-Au-OTf. *Green Chem.* **2018**, *20* (9), 2125–2134.

(128) Kerton, F.; Marriott, R. *Alternative Solvents for Green Chemistry*; Green Chemistry Series;

The Royal Society of Chemistry, 2013.

(129) Clarke, C. J.; Tu, W.-C.; Levers, O.; Bröhl, A.; Hallett, J. P. Green and Sustainable Solvents in Chemical Processes. *Chem. Rev.* **2018**, *118* (2), 747–800.

(130) Alder, C. M.; Hayler, J. D.; Henderson, R. K.; Redman, A. M.; Shukla, L.; Shuster, L. E.; Sneddon, H. F. Updating and Further Expanding GSK's Solvent Sustainability Guide. *Green Chem.* **2016**, *18* (13), 3879–3890.

(131) Hashmi, A. S. K. Homogeneous Gold Catalysis Beyond Assumptions and Proposals—Characterized Intermediates. *Angew. Chemie Int. Ed.* **2010**, *49* (31), 5232–5241.

(132) Attar, S.; Bearden, W. H.; Alcock, N. W.; Alyea, E. C.; Nelson, J. H. Phosphole Complexes of Gold(I) Halides: Comparison of Solution and Solid-State Structures by a Combination of Solution and CP/MAS Phosphorus-31 NMR Spectroscopy and x-Ray Crystallography. *Inorg. Chem.* **1990**, *29* (3), 425–433.

(133) Zuccaccia, D.; Belpassi, L.; Rocchigiani, L.; Tarantelli, F.; Macchioni, A. A Phosphine Gold(I) $π$-Alkyne Complex: Tuning the Metal−Alkyne Bond Character and Counterion Position by the Choice of the Ancillary Ligand. *Inorg. Chem.* **2010**, *49* (7), 3080–3082.

(134) Zuccaccia, D.; Belpassi, L. Ion Pairing in Cationic Olefin− Gold (I) Complexes. *J. …* **2009**, No. 131, 3170–3171.

(135) Cordón, J.; López-de-Luzuriaga, J. M.; Monge, M. Experimental and Theoretical Study of the Effectiveness and Stability of Gold(I) Catalysts Used in the Synthesis of Cyclic Acetals. *Organometallics* **2016**, *35* (5), 732–740.

(136) Kumar, M.; Jasinski, J.; Hammond, G. B.; Xu, B. Alkyne/Alkene/Allene-Induced Disproportionation of Cationic Gold(I) Catalyst. *Chem. – A Eur. J.* **2014**, *20* (11), 3113–3119.

(137) Lu, Z.; Han, J.; Hammond, G. B.; Xu, B. Revisiting the Influence of Silver in Cationic Gold Catalysis: A Practical Guide. *Org. Lett.* **2015**, *17* (18), 4534–4537.

(138) Preisenberger, M.; Schier, A.; Schmidbaur, H. (Phosphine)Gold(I) Trifluoromethanesulfonates, Trifluoroacetates and Trichlorothioacetates †. *J. Chem. Soc. Dalt. Trans.* **1999**, No. 10, 1645–1650.

(139) Ciancaleoni, G.; Belpassi, L.; Tarantelli, F.; Zuccaccia, D.; Macchioni, A. A Combined NMR/DFT Study on the Ion Pair Structure of [(PR12R2)Au(H2-3-Hexyne)]BF4 Complexes. *Dalt. Trans.* **2013**, *42* (12), 4122–4131.

(140) Makosza, M. Phase-Transfer Catalysis. A General Green Methodology in Organic Synthesis. *Pure Appl. Chem.* **2000**, *72* (7), 1399–1403.

(141) Leyva, A.; Corma, A. Isolable Gold(I) Complexes Having One Low-Coordinating Ligand as Catalysts for the Selective Hydration of Substituted Alkynes at Room Temperature without Acidic Promoters. *J. Org. Chem.* **2009**, *74* (5), 2067–2074.

(142) Gaillard, S.; Bosson, J.; Ramón, R. S.; Nun, P.; Slawin, A. M. Z.; Nolan, S. P. Development of Versatile and Silver-Free Protocols for Gold(I) Catalysis. *Chem. – A Eur. J.* **2010**, *16* (46), 13729–13740.

(143) Nun, P.; Ramón, R. S.; Gaillard, S.; Nolan, S. P. Efficient Silver-Free Gold(I)-Catalyzed Hydration of Alkynes at Low Catalyst Loading. *J. Organomet. Chem.* **2011**, *696* (1), 7–11.

(144) Weerasiri, K. C.; Chen, D.; Wozniak, D. I.; Dobereiner, G. E. Internal Alkyne Regio- and Chemoselectivity Using a Zwitterionic N-Heterocyclic Carbene Gold Catalyst in a Silver-Free Alkyne Hydration Reaction. *Adv. Synth. Catal.* **2016**, *358* (24), 4106–4113.

(145) Collado, A.; Patrick, S. R.; Gasperini, D.; Meiries, S.; Nolan, S. P. Influence of Bulky yet Flexible N-Heterocyclic Carbene Ligands in Gold Catalysis. *Beilstein J. Org. Chem.* **2015**, *11*, 1809–1814.

(146) Brill, M.; Nahra, F.; Gómez-Herrera, A.; Zinser, C.; Cordes, D. B.; Slawin, A. M. Z.; Nolan, S. P. Gold- N-Heterocyclic Carbene Complexes of Mineral Acids. *ChemCatChem* **2017**, *9* (1), 117–120.

(147) Zhang, B.; Wang, T. Gold-Catalyzed Transformations of Propargyl Alcohols and Propargyl Amines. *Asian J. Org. Chem.* **2018**, *7* (9), 1758–1783.

(148) Meyer, K. H.; Schuster, K. Umlagerung Tertiärer Äthinyl-Carbinole in Ungesättigte Ketone. *Berichte der Dtsch. Chem. Gesellschaft (A B Ser.* **1922**, *55* (4), 819–823.

(149) Swaminathan, S.; Narayanan, K. V. Rupe and Meyer-Schuster Rearrangements. *Chem. Rev.* **1971**, *71* (5), 429–438.

(150) Georgy, M.; Boucard, V.; Campagne, J. M. Gold(III)-Catalyzed Nucleophilic Substitution of Propargylic Alcohols. *J. Am. Chem. Soc.* **2005**, *127* (41), 14180–14181.

(151) Lopez, S. S.; Engel, D. A.; Dudley, G. B. The Meyer-Schuster Rearrangement of Ethoxyalkynyl Carbinols. *Synlett* **2007**, *2007* (06), 949–953.

(152) Lee, S. I.; Baek, J. Y.; Sim, S. H.; Chung, Y. K. Gold(I)-Catalyzed Rearrangement of Propargylic Alcohols to α,β-Unsaturated Ketones. *Synthesis (Stuttg).* **2007**, *2007* (14), 2107–2114.

(153) Engel, D. A.; Lopez, S. S.; Dudley, G. B. Lewis Acid-Catalyzed Meyer–Schuster Reactions: Methodology for the Olefination of Aldehydes and Ketones. *Tetrahedron* **2008**, *64* (29), 6988–6996.

(154) Marion, N.; Carlqvist, P.; Gealageas, R.; de Frémont, P.; Maseras, F.; Nolan, S. P. [(NHC)AuI]-Catalyzed Formation of Conjugated Enones and Enals: An Experimental and Computational Study. *Chemistry* **2007**, *13* (22), 6437–6451.

(155) Zuccaccia, D.; Belpassi, L.; Macchioni, A.; Tarantelli, F. Ligand Effects on Bonding and Ion Pairing in Cationic Gold(I) Catalysts Bearing Unsaturated Hydrocarbons. *Eur. J. Inorg. Chem.* **2013**, No. 24, 4121–4135.

(156) Zuccaccia, D.; Zotto, A. Del; Baratta, W. The Pivotal Role of the Counterion in Gold Catalyzed Hydration and Alkoxylation of Alkynes. *Coord. Chem. Rev.* **2019**, *396*, 103–116.

(157) Gatto, M.; Del Zotto, A.; Segato, J.; Zuccaccia, D. Hydration of Alkynes Catalyzed by L–Au–X under Solvent- and Acid-Free Conditions: New Insights into an Efficient, General, and Green Methodology. *Organometallics* **2018**, *37* (24), 4685–4691.

(158) Ciancaleoni, G.; Belpassi, L.; Zuccaccia, D.; Tarantelli, F.; Belanzoni, P. Counterion Effect in the Reaction Mechanism of NHC Gold(I)-Catalyzed Alkoxylation of Alkynes: Computational Insight into Experiment. *ACS Catal.* **2015**, *5* (2), 803–814.

(159) Schießl, J.; Schulmeister, J.; Doppiu, A.; Wörner, E.; Rudolph, M.; Karch, R.; Hashmi, A. S. K. An Industrial Perspective on Counter Anions in Gold Catalysis: On Alternative Counter Anions. *Adv. Synth. Catal.* **2018**, *360* (20), 3949–3959.

(160) Zhdanko, A.; Maier, M. E. Explanation of “Silver Effects” in Gold(I)-Catalyzed Hydroalkoxylation of Alkynes. *ACS Catal.* **2015**, *5* (10), 5994–6004.

(161) Lauterbach, T.; Asiri, A. M.; Hashmi, A. S. K. Chapter Five - Organometallic Intermediates of Gold Catalysis; Pérez, P. J. B. T.-A. in O. C., Ed.; Academic Press, 2014; Vol. 62, pp 261–297.

(162) Riplinger, C.; Sandhoefer, B.; Hansen, A.; Neese, F. Natural Triple Excitations in Local Coupled Cluster Calculations with Pair Natural Orbitals. *J. Chem. Phys.* **2013**, *139* (13), 134101.

(163) Riplinger, C.; Neese, F. An Efficient and near Linear Scaling Pair Natural Orbital Based Local Coupled Cluster Method. *J. Chem. Phys.* **2013**, *138* (3), 34106.

(164) Ciancaleoni, G.; Rampino, S.; Zuccaccia, D.; Tarantelli, F.; Belanzoni, P.; Belpassi, L. An Ab Initio Benchmark and DFT Validation Study on Gold(I)-Catalyzed Hydroamination of Alkynes. *J. Chem. Theory Comput.* **2014**, *10* (3), 1021–1034.

(165) Bistoni, G.; Belanzoni, P.; Belpassi, L.; Tarantelli, F. π Activation of Alkynes in Homogeneous and Heterogeneous Gold Catalysis. *J. Phys. Chem. A* **2016**, *120* (27), 5239–5247.

(166) Alabugin, I. V; Gilmore, K.; Manoharan, M. Rules for Anionic and Radical Ring Closure of

Alkynes. *J. Am. Chem. Soc.* **2011**, *133* (32), 12608–12623.

(167) Alcaide, B.; Almendros, P.; del Campo, T. M.; Fernández, I. Fascinating Reactivity in Gold Catalysis: Synthesis of Oxetenes through Rare 4-Exo-Dig Allene Cyclization and Infrequent β-Hydride Elimination. *Chem. Commun.* **2011**, *47* (32), 9054–9056.

(168) Renault, J.; Qian, Z.; Uriac, P.; Gouault, N. Electrophilic Carbon Transfer in Gold Catalysis: Synthesis of Substituted Chromones. *Tetrahedron Lett.* **2011**, *52* (19), 2476–2479.

(169) Kazem Shiroodi, R.; Soltani, M.; Gevorgyan, V. Gold-Catalyzed 1,3-Transposition of Ynones. *J. Am. Chem. Soc.* **2014**, *136* (28), 9882–9885.

(170) Badrieh, Y.; Kayyal, A.; Blum, J. Rearrangement, Hydrochlorination and Hydration of Conjugated Alkynones by Platinum(IV) Compounds under Homogeneous and under Biphasic Conditions. *J. Mol. Catal.* **1992**, *75* (2), 161–167.

(171) Johnston, P.; Carthey, N.; Hutchings, G. J. Discovery, Development, and Commercialization of Gold Catalysts for Acetylene Hydrochlorination. *J. Am. Chem. Soc.* **2015**, *137* (46), 14548–14557.

(172) Janzen, D. E.; Doherty, S. R.; Vanderveer, D. G.; Hinkle, L. M.; Benefield, D. A.; Vashi, H. M.; Grant, G. J. Cyclometallated Gold(III) Complexes with a Trithiacrown Ligand: Solventless Au(III) Cyclometallation, Intramolecular Gold-Sulfur Interactions, and Fluxional Behavior in 1,4,7-Trithiacyclononane Au(III) Complexes. *J. Organomet. Chem.* **2014**, *755*, 47–57.

(173) Zuccaccia, D.; Belpassi, L.; Ciancaleoni, G.; Biasiolo, L.; Bistoni, G.; Macchioni, A.; Tarantelli, F. NHC-Gold-Alkyne Complexes: Influence of the Carbene Backbone on the Ion Pair Structure. *Organometallics* **2013**, *32*, 4444–4447.

(174) Tlahuext-Aca, A.; Hopkinson, M. N.; Daniliuc, C. G.; Glorius, F. Oxidative Addition to Gold(I) by Photoredox Catalysis: Straightforward Access to Diverse (C,N)-Cyclometalated Gold(III) Complexes. *Chem. Eur. J.* **2016**, *22* (33), 11587–11592.

(175) Lin, J. C. Y.; Huang, R. T. W.; Lee, C. S.; Bhattacharyya, A.; Hwang, W. S.; Lin, I. J. B. Coinage Metal−N-Heterocyclic Carbene Complexes. *Chem. Rev.* **2009**, *109* (8), 3561–3598.

(176) Fuchita, Y.; Ieda, H.; Tsunemune, Y.; Kinoshita-Nagaoka, J.; Kawano, H. Synthesis, Structure and Reactivity of a New Six-Membered Cycloaurated Complex of 2-Benzoylpyridine [AuCl2(Pcp-C 1,N)] [Pcp = 2-(2-Pyridylcarbonyl)Phenyl]. Comparison with the Cycloaurated Complex Derived from 2-Benzylpyridine. *J. Chem. Soc. Dalt. Trans.* **1998**, No. 5, 791–796.

(177) Zhdanko, A.; Maier, M. E. The Mechanism of Gold(I)-Catalyzed Hydroalkoxylation of Alkynes: An Extensive Experimental Study. *Chem. – A Eur. J.* **2014**, *20* (7), 1918–1930.

(178) Roithová, J.; Janková, Š.; Jašíková, L.; Váňa, J.; Hybelbauerová, S. Gold–Gold Cooperation in the Addition of Methanol to Alkynes. *Angew. Chemie Int. Ed.* **2012**, *51* (33), 8378–8382.

(179) Oonishi, Y.; Gómez-Suárez, A.; Martin, A. R.; Nolan, S. P. Hydrophenoxylation of Alkynes by Cooperative Gold Catalysis. *Angew. Chemie Int. Ed.* **2013**, *52* (37), 9767–9771.

(180) Krauter, C. M.; Hashmi, A. S. K.; Pernpointner, M. A New Insight into Gold(I)-Catalyzed Hydration of Alkynes: Proton Transfer. *ChemCatChem* **2010**, *2* (10), 1226–1230.

(181) Faza, O. N.; López, C. S. Computational Approaches to Homogeneous Gold Catalysis. *Top. Curr. Chem.* **2015**, *357*, 213–283.

(182) Jiménez-Núñez, E.; Echavarren, A. M. Gold-Catalyzed Cycloisomerizations of Enynes: A Mechanistic Perspective. *Chem. Rev.* **2008**, *108* (8), 3326–3350.

(183) Zuccaccia, D.; Belpassi, L.; Rocchigiani, L.; Tarantelli, F.; Macchioni, A. Ion Pairing in Cationic Olefin− Gold (I) Complexes. *Inorg. Chem.* **2010**, *49* (131), 3170–3171.

(184) Pazderski, L.; Pawlak, T.; Sitkowski, J.; Kozerski, L.; Szłyk, E. 1H, 13C, 15N and 195Pt NMR Studies of Au(III) and Pt(II) Chloride Organometallics with 2-Phenylpyridine. *Magn. Reson. Chem.* **2009**, *47* (11), 932–941.

(185) Rubbiani, R.; Can, S.; Kitanovic, I.; Alborzinia, H.; Stefanopoulou, M.; Kokoschka, M.; Mönchgesang, S.; Sheldrick, W. S.; Wölfl, S.; Ott, I. Comparative in Vitro Evaluation of N-Heterocyclic Carbene Gold(I) Complexes of the Benzimidazolylidene Type. *J. Med. Chem.* **2011**, *54* (24), 8646–8657.

(186) Marchione, D.; Belpassi, L.; Bistoni, G.; Macchioni, A.; Tarantelli, F.; Zuccaccia, D. The Chemical Bond in Gold(I) Complexes with N-Heterocyclic Carbenes. *Organometallics* **2014**, *33* (16), 4200–4208.

(187) Schwerdtfeger, P.; Hermann, H. L.; Schmidbaur, H. Stability of the Gold(I)−Phosphine Bond. A Comparison with Other Group 11 Elements. *Inorg. Chem.* **2003**, *42* (4), 1334–1342.

(188) Rocchigiani, L.; Fernandez-Cestau, J.; Agonigi, G.; Chambrier, I.; Budzelaar, P. H. M.; Bochmann, M. Gold(III) Alkyne Complexes: Bonding and Reaction Pathways. *Angew. Chemie - Int. Ed.* **2017**, *56* (44), 13861–13865.

(189) 3-hexanone, the catalysis conducted with 0. 1. mol of 1/AgOTf shows no conversion to 3-hexanone. No Title.

(190) Biasiolo, L.; Ciancaleoni, G.; Belpassi, L.; Bistoni, G.; Macchioni, A.; Tarantelli, F.; Zuccaccia, D. Relationship between the Anion/Cation Relative Orientation and the Catalytic Activity of Nitrogen Acyclic Carbene–Gold Catalysts. *Catal. Sci. Technol.* **2015**, *5* (3), 1558–1567.

(191) Trinchillo, M.; Belanzoni, P.; Belpassi, L.; Biasiolo, L.; Busico, V.; D'Amora, A.; D'Amore, L.; Del Zotto, A.; Tarantelli, F.; Tuzi, A.; et al. Extensive Experimental and Computational Study of Counterion Effect in the Reaction Mechanism of NHC-Gold(I)-Catalyzed Alkoxylation of Alkynes. *Organometallics* **2016**, *35* (5), 641–654.

(192) Kumar, R.; Krieger, J. P.; Gómez-Bengoa, E.; Fox, T.; Linden, A.; Nevado, C. The First Gold(III) Formate: Evidence for $β$-Hydride Elimination. *Angew. Chemie - Int. Ed.* **2017**, *56* (42), 12862–12865.

(193) Gregori, L.; Sorbelli, D.; Belpassi, L.; Tarantelli, F.; Belanzoni, P. Alkyne Activation with Gold(III) Complexes: A Quantitative Assessment of the Ligand Effect by Charge-Displacement Analysis. *Inorg. Chem.* **2019**, *58* (5), 3115–3129.

(194) Đurović, M. D.; Bugarčić, Ž. D.; van Eldik, R. Stability and Reactivity of Gold Compounds – From Fundamental Aspects to Applications. *Coord. Chem. Rev.* **2017**, *338*, 186–206.

(195) Yepes, D.; Neese, F.; List, B.; Bistoni, G. Unveiling the Delicate Balance of Steric and Dispersion Interactions in Organocatalysis Using High-Level Computational Methods. *J. Am. Chem. Soc.* **2020**, *142* (7), 3613–3625.

(196) Bistoni, G.; Auer, A. A.; Neese, F. Understanding the Role of Dispersion in Frustrated Lewis Pairs and Classical Lewis Adducts: A Domain-Based Local Pair Natural Orbital Coupled Cluster Study. *Chem. – A Eur. J.* **2017**, *23* (4), 865–873.

(197) Sromek, A. W.; Rubina, M.; Gevorgyan, V. 1,2-Halogen Migration in Haloallenyl Ketones: Regiodivergent Synthesis of Halofurans. *J. Am. Chem. Soc.* **2005**, *127* (30), 10500–10501.

(198) Morita, N.; Yasuda, A.; Shibata, M.; Ban, S.; Hashimoto, Y.; Okamoto, I.; Tamura, O. Gold(I)/(III)-Catalyzed Synthesis of Cyclic Ethers; Valency-Controlled Cyclization Modes. *Org. Lett.* **2015**, *17* (11), 2668–2671.

(199) Crabtree, R. H. *The Organometallic Chemistry of the Transition Metals, 6*; WILEY, 2014.

(200) Chambrier, I.; Rocchigiani, L.; Hughes, D. L.; Budzelaar, P. M. H.; Bochmann, M. Thermally Stable Gold(III) Alkene and Alkyne Complexes: Synthesis, Structures, and Assessment of the Trans-Influence on Gold–Ligand Bond Enthalpies. *Chem. – A Eur. J.* **2018**, *24* (44), 11467–11474.

(201) Kumar, R.; Nevado, C. Cyclometalated Gold(III) Complexes: Synthesis, Reactivity, and Physicochemical Properties. *Angew. Chemie - Int. Ed.* **2017**, *56* (8), 1994–2015.

(202) Sorbelli, D.; Belpassi, L.; Tarantelli, F.; Belanzoni, P. Ligand Effect on Bonding in Gold(III) Carbonyl Complexes. *Inorg. Chem.* **2018**, *57* (10), 6161–6175.

(203) van Lenthe, E.; Baerends, E. J.; Snijders, J. G. Relativistic Total Energy Using Regular Approximations. *J. Chem. Phys.* **1994**, *101* (11), 9783–9792.

(204) Segato, J.; Del Zotto, A.; Belpassi, L.; Belanzoni, P.; Zuccaccia, D. Hydration of Alkynes Catalyzed by [Au(X)(L)(Ppy)]X in the Green Solvent γ-Valerolactone under Acid-Free Conditions: The Importance of the Pre-Equilibrium Step. *Catal. Sci. Technol.* **2020**, *10*, 7757–7767.

(205) Macchioni, A. Ion Pairing in Transition-Metal Organometallic Chemistry. *Chem. Rev.* **2005**, *105* (6), 2039–2073.

(206) Arduengo, A. J.; Craig, H. A.; Goerlich, J. R.; Marshall, W. J.; Unverzagt, M. Imidazolylidenes , Imidazolinylidenes and Imidazolidines. *Tetrahedron* **1999**, *55* (99), 14523–14534.

(207) Hintermann, L. Expedient Syntheses of the N-Heterocyclic Carbene Precursor Imidazolium Salts IPr · HCl , IMes · HCl and IXy · HCl. *Beilstein J. Org. Chem.* **2007**, *3* (22), 2–6.

(208) Paulovicova, A.; El-Ayaan, U.; Shibayama, K.; Morita, T.; Fukuda, Y. Mixed-Ligand Copper(II) Complexes with the Rigid Bidentate Bis(N-Arylimino)Acenaphthene Ligand: Synthesis, Spectroscopic-, and X-Ray Structural Characterization. *Eur. J. Inorg. Chem.* **2001**, *2001* (10), 2641–2646.

(209) Vasudevan, K. V; Butorac, R. R.; Abernethy, C. D.; Cowley, A. H. Synthesis and Coordination Compounds of a Bis(Imino)Acenaphthene (BIAN)-Supported N-Heterocyclic Carbene. *Dalt. Trans.* **2010**, *39* (31), 7401–7408.

(210) Uson, R.; Laguna, A.; Laguna, M.; Briggs, D. A.; Murray, H. H.; Fackler Jr., J. P. (Tetrahydrothiophene)Gold(I) or Gold(III) Complexes. In *Inorganic Syntheses*; John Wiley & Sons, Ltd, 2007; pp 85–91.

(211) Müller, T. E.; Green, J. C.; Mingos, D. M. P.; McPartlin, C. M.; Whittingham, C.; Williams, D. J.; Woodroffe, T. M. Complexes of Gold(I) and Platinum(II) with Polyaromatic Phosphine Ligands1Dedicated to Professor Peter Maitlis on the Occasion of His 65th Birthday.1. *J. Organomet. Chem.* **1998**, *551* (1), 313–330.

(212) Hashmi, A. S. K.; Hengst, T.; Lothschütz, C.; Rominger, F. New and Easily Accessible Nitrogen Acyclic Gold(I) Carbenes: Structure and Application in the Gold-Catalyzed Phenol Synthesis as Well as the Hydration of Alkynes. *Adv. Synth. Catal.* **2010**, *352* (8), 1315–1337.

(213) Collado, A.; Gómez-Suárez, A.; Martin, A. R.; Slawin, A. M. Z.; Nolan, S. P. Straightforward Synthesis of [Au(NHC)X] (NHC = N-Heterocyclic Carbene{,} X = Cl{,} Br{,} I) Complexes. *Chem. Commun.* **2013**, *49* (49), 5541–5543.

(214) Swart, M.; Bickelhaupt, F. M. QUILD: QUantum-Regions Interconnected by Local Descriptions. *J. Comput. Chem.* **2008**, *29* (5), 724–734.

(215) Perdew, J. P. Density-Functional Approximation for the Correlation Energy of the Inhomogeneous Electron Gas. *Phys. Rev. B* **1986**, *33* (12), 8822–8824.

(216) Becke, A. D. Density-Functional Exchange-Energy Approximation with Correct Asymptotic Behavior. *Phys. Rev. A* **1988**, *38* (6), 3098–3100.

(217) van Lenthe, E.; van Leeuwen, R.; Baerends, E. J.; Snijders, J. G. Relativistic Regular Two-Component Hamiltonians. *Int. J. Quantum Chem.* **1996**, *57* (3), 281–293.

(218) Grimme, S.; Antony, J.; Ehrlich, S.; Krieg, H. A Consistent and Accurate Ab Initio Parametrization of Density Functional Dispersion Correction (DFT-D) for the 94 Elements H-Pu. *J. Chem. Phys.* **2010**, *132* (15), 154104.

(219) Grimme, S.; Ehrlich, S.; Goerigk, L. Effect of the Damping Function in Dispersion Corrected Density Functional Theory. *J. Comput. Chem.* **2011**, *32* (7), 1456–1465.

(220) Neese, F. The ORCA Program System. *WIREs Comput. Mol. Sci.* **2012**, *2* (1), 73–78.

(221) Grimme, S. Semiempirical Hybrid Density Functional with Perturbative Second-Order Correlation. *J. Chem. Phys.* **2006**, *124* (3), 34108.

(222) Weigend, F.; Ahlrichs, R. Balanced Basis Sets of Split Valence, Triple Zeta Valence and Quadruple Zeta Valence Quality for H to Rn: Design and Assessment of Accuracy. *Phys. Chem. Chem. Phys.* **2005**, *7* (18), 3297–3305.

(223) Andrae, D.; Häußermann, U.; Dolg, M.; Stoll, H.; Preuß, H. Energy-Adjustedab Initio Pseudopotentials for the Second and Third Row Transition Elements. *Theor. Chim. Acta* **1990**, *77* (2), 123–141.

(224) Riplinger, C.; Pinski, P.; Becker, U.; Valeev, E. F.; Neese, F. Sparse Maps—A Systematic Infrastructure for Reduced-Scaling Electronic Structure Methods. II. Linear Scaling Domain Based Pair Natural Orbital Coupled Cluster Theory. *J. Chem. Phys.* **2016**, *144* (2), 24109.

(225) Liakos, D. G.; Neese, F. Is It Possible To Obtain Coupled Cluster Quality Energies at near Density Functional Theory Cost? Domain-Based Local Pair Natural Orbital Coupled Cluster vs Modern Density Functional Theory. *J. Chem. Theory Comput.* **2015**, *11* (9), 4054–4063.

(226) Liakos, D. G.; Sparta, M.; Kesharwani, M. K.; Martin, J. M. L.; Neese, F. Exploring the Accuracy Limits of Local Pair Natural Orbital Coupled-Cluster Theory. *J. Chem. Theory Comput.* **2015**, *11* (4), 1525–1539.

(227) Tomasi, J.; Persico, M. Molecular Interactions in Solution: An Overview of Methods Based

on Continuous Distributions of the Solvent. *Chem. Rev.* **1994**, *94* (7), 2027–2094.

(228) Klamt, A. Conductor-like Screening Model for Real Solvents: A New Approach to the Quantitative Calculation of Solvation Phenomena. *J. Phys. Chem.* **1995**, *99* (7), 2224–2235.

(229) Cramer, C. J.; Truhlar, D. G. Implicit Solvation Models: Equilibria, Structure, Spectra, and Dynamics. *Chem. Rev.* **1999**, *99* (8), 2161–2200.

(230) Universiteit, V. *SMC, Theoretical Chemistry*; Amsterdam, The Netherlands, 2014.

(231) Fonseca Guerra, C.; Snijders, J. G.; te Velde, G.; Baerends, E. J. Towards an Order-N DFT Method. *Theor. Chem. Acc.* **1998**, *99* (6), 391–403.

(232) te Velde, G.; Bickelhaupt, F. M.; Baerends, E. J.; Fonseca Guerra, C.; van Gisbergen, S. J. A.; Snijders, J. G.; Ziegler, T. Chemistry with ADF. *J. Comput. Chem.* **2001**, *22* (9), 931–967.

(233) Lenthe, E. van; Baerends, E. J.; Snijders, J. G. Relativistic Regular Two-component Hamiltonians. *J. Chem. Phys.* **1993**, *99* (6), 4597–4610.

(234) van Lenthe, E.; Ehlers, A.; Baerends, E.-J. Geometry Optimizations in the Zero Order Regular Approximation for Relativistic Effects. *J. Chem. Phys.* **1999**, *110* (18), 8943–8953.

(235) Kang, R.; Chen, H.; Shaik, S.; Yao, J. Assessment of Theoretical Methods for Complexes of Gold(I) and Gold(III) with Unsaturated Aliphatic Hydrocarbon: Which Density Functional Should We Choose? *J. Chem. Theory Comput.* **2011**, *7* (12), 4002–4011.

(236) Kang, R.; Lai, W.; Yao, J.; Shaik, S.; Chen, H. How Accurate Can a Local Coupled Cluster Approach Be in Computing the Activation Energies of Late-Transition-Metal-Catalyzed Reactions with Au, Pt, and Ir? *J. Chem. Theory Comput.* **2012**, *8* (9), 3119–3127.

(237) Klamt, A.; Schüürmann, G. COSMO: A New Approach to Dielectric Screening in Solvents with Explicit Expressions for the Screening Energy and Its Gradient. *J. Chem. Soc. Perkin Trans. 2* **1993**, No. 5, 799–805.

(238) Klamt, A.; Jonas, V. Treatment of the Outlying Charge in Continuum Solvation Models. *J. Chem. Phys.* **1996**, *105* (22), 9972–9981.